Astrocytic channels interplay: modulation of potassium currents and its importance for astrocytic functions

Liliya Vadimovna Andrianova, B.Sc.

A thesis submitted for the degree of
Doctor of Philosophy

School of Life Sciences
University of Warwick

August 2016

THE UNIVERSITY OF
WARWICK

i Abstract

A healthy cognition rests on a balanced interaction of neuronal and glial cell populations. Astrocytes are most numerous glial cells in the brain. Their functions include modulation of signalling and plasticity at the tripartite synapse and homeostasis of the brain, in particularly the control of potassium and glutamate in the extracellular space. This project aimed at bridging the two pools of astrocytic functions, by investigating molecular links between ionotropic channels and potassium currents of astrocytes. Whole-cell potassium currents were recorded in the acutely isolated astrocytes of somatosensory cortex layer II/III in young and old mice, and both the **capacitance** and the **current density of the voltage-gated** but not of inwardly rectifying **potassium currents increased with age**. The modulation of potassium currents by other ionic channels, including $P2X_{1/5}$, NMDARs and PAR-1 receptors was established. Activation of these channels was found to **potentiate outward potassium current** by 15 - 35%, and this mechanism was found to be calcium-dependent. The addition of 4-aminopyridine blocked this facilitation, whereas barium chloride did not. This effect was explored in Light Transmittance experiments where tissue swelling was measured. Activation of this mechanism increased the extent of tissue swelling during neuronal activity in young adult mice. This modulation was found to diminish with age, as the effect dramatically reduced in group II mice. It is believed that this could be an important step in the initiation of potassium buffering in the cortex. The data contributes to the current understanding of the molecular processes linking signalling and physiological functions of astrocytes.

ii Acknowledgements

Firstly, I would like to express my sincere gratitude to my supervisor, Dr. Yuriy Pankratov for granting me this opportunity to take up this project as well as for his guidance, caring and patience throughout my research project, and for fostering my independence as a researcher. I would like to thank Dr. Lalo for her kindness and advice, Dr. Palygin for showing me the laboratory and giving me an opportunity to learn electrophysiology and Dr. Rasooli-Nejad for teaching me the laboratory practices and his friendship and support. I am grateful to have worked in this laboratory.

I would also like to thank my advisory committee, Dr. Wall and Dr. Pires da Silva for providing their support and guidance throughout my project. Special thanks go to members of the office: Jessicka, Greta, Lucy, Eric, Matei, Tommy, Michael and Lorenzo. Thank you guys for making this a joyful and easy environment to be working in. I'd like to thank my friends, for always providing a positive outlook when I needed it. I want to thank Anna separately, for always being there for me.

I'd like to thank my partner, Jonathan, for being my better other half. For your never-ceasing love, support and continuous belief in me, as well as for putting up with me during the bad days – I am very grateful. Thank you for being my friend, my confidence and my therapist at times – I could not ask for a better soul mate. I also want to thank your families for welcoming me in and for their love and care. I am grateful for you all being there for me, and for giving me a home away from home.

Lastly, I want to express my utmost gratitude to my family, for granting me this opportunity to pursue my ambitions and supporting me both financially and emotionally every minute of my project. I am thankful to my parents, Vadim and Zoya Andrianovi, for allowing me to realize my full potential and reach for the opportunities. I thank you both for supporting my choices and your ever-excellent advice. Thank you to my siblings, Alina and Dimitry, for their endless support and humour. I'd like to also thank my brother-in-law, Abdulaziz, for his encouragement and support. Everything I have achieved is because of you all and I feel incredibly lucky to have such an exceptional family.

Thank you all for your support, I could not do this without you.

For my family

iii List of abbreviations

4-AP – 4-Aminopyridine
AA – amino acids
αβATP - αβ-methylene ATP
aCSF – artificial cerebrospinal fluid
AD – Alzheimer's disease
AHP – after hyperpolarisation
AP – action potential
AQPR4 - aquaporin-4
ATP – adenosine 5′ – triphosphate
Ba – barium chloride
BK – big conductance potassium channel
BOLD- blood oxygen level-dependent method
Ca^{2+}_I – cytoplasmic free Ca^{2+} concentration
GCAMP – genetically encoded calcium indicator
cDNA – complementary DNA
CNS – central nervous system
DCT – distal convoluted tubule
ECM – extra cellular matrix
ECS – extracellular space
EGTA - ethylene glycol-bis(β-aminoethyl ether)-N,N,N',N'-tetraacetic acid
E_K – equilibrium potential (K^+)
E_M – membrane potential
ER – endoplasmic reticulum
fEPSP – field excitatory postsynaptic potential
GABA – γ-aminobutyric acid
GBM – glioblastoma multiform
Gβγ – a component of heteromeric G protein
GFAP – glial fibrillary acidic protein
GFP – green fluorescent protein
GLAST – glutamate aspartate transporter
GLT-1 – glutamate transporter 1
GPCRs – G-protein coupled receptors
HFS – high frequency stimulation
IK – intermediate conductance potassium channel
InsP3R – inositol 1,4,5 triphosphate (InsP3)-gated Ca^{2+} channel/receptor
K_A – A-type potassium current
K-ATP – ATP-sensitive potassium channels
K_{CA} – calcium-activated potassium channels
KCC - K^+, Cl^- co-transporter
K_D – D-type potassium current
K_G – GPCR potassium channel

Kir – inwardly rectifying potassium channels
KO – knock - out (mice)
K_V – voltage-gated potassium channels
K2P – two-pore domain background potassium channels
LT – light transmittance
LTP – long-term potentiation
mGluR – metabotropic glutamate receptor
mRNA – messenger RNA
Na^+_I – cytoplasmic Na+ concentration
NKA - Na^+, K^+-ATPase
NKCC1 - Na^+, K^+, Cl- co-transporter
NMDA – N-methyl D-aspartate
P2X – ionotropic purinoreceptors
PAP – perisynaptic astrocytic process
PAR-1 – protease-activated receptor
PCT – proximal convoluted tubule
PIP2 – phosphatidylinositol 4,5-bisphosphate
PKA – protein kinase A
PKC – protein kinase C
PLC – phospholipase C
RPE – retinal pigment epithelium
ROI – region of interest
ROS – reactive oxygen species
S4 – voltage sensor sequence
SEM – standard error of mean
SGK – serine/threonine kinases
sIPSP - slow inhibitory postsynaptic potential
SK – small conductance potassium channels
STP – short-term potentiation
SUR – sulfonylurea receptors
TBS – theta burst stimulation
TM – trans-membrane domain
TREK-1 – two-pore potassium channel (K2p1.1)
TTX - tetrodotoxin

iii List of figures

Table of Contents

Chapter 1 - Introduction

Astrocytes – from 'brain glue'' to active players in brain functioning

1.1 Current aims of neuroscience

The importance of neuroscience cannot easily be overestimated. In the last century and a half, a great progress in studying the brain has been achieved. Partially, this is due to the development of a whole new range of techniques, making it possible to intricately investigate the processes taking place in the brain within a set of physiological conditions, such as development of various electrophysiological techniques (Verkhratsky, Krishtal, and Petersen 2006) and, more recently, optogenetics (Boyden et al. 2005).

With the global population higher than ever before and still on the rise (it is projected to reach 9.7 billion people by 2050)(United Nations 2015), the number of people of all ages is increasing. Coupled with improved healthcare and current knowledge of disease prevention and prophylaxes the average lifespan has increased significantly in the last 100 years. This means that the proportion of people whose brains is undergoing to the process of senility will keep on rising too. Therefore, understanding the processes underlying the ageing phenomenon in the human brain is a chief task that science is currently faced with. It is only through having a detailed understanding of age-related diseases and conditions that their devastating consequences may be averted.

However, before going any further, it is important to discuss what is meant by the term 'senescent brain' and how it is different from dementia and other age-related conditions. In 1924 Lhermitte and Nicolas proposed the term "psychic senescence" referring to the physiological state of brain in healthy old age: "The outstanding features include diminished acuity of memory, or better a loss of adherence to

recent events; impaired faculty of rapid evocation of events; loss of fluidity; and weakness of creative imagination" (Critchley 1931).

It is widely believed that healthy cognition rests on a balanced interaction of two populations of cells – electrically active neurones and passive glial cells (J. Martin and Gorenstein 2010). Historically, quite distinct roles of these two cell types were assigned: signalling and metabolic support were considered to be neuronal and glial functions respectively (Henn, Haljamae, and Hamberger 1972). In the last 20 years, however, a vast amount of evidence has been collected to show that glial involvement in brain function is omnipresent and crucial (Bezzi and Volterra 2001; Allen and Barres 2005). Neuroscience has been more closely focused on investigating the structures and functions of neurones, hence the name of the field, despite glial cells being the more numerous cell type (Pelvig et al. 2008). This project set out to investigate the functions of astrocytes, with the specific focus on the potassium channels. In this chapter first the evolution of the field of glial science will be covered, following the review on the recent progress in the field. The objectives of this project will be explained in the context of current knowledge, with the overall aim being to propagate the understanding of the molecular mechanisms taking place in astrocytes and their respective functions.

1.2 Evolution of the view on the roles of glia

Historically, neuroscience has always expressed a very neurocentric view, with the excitable cells carrying out the vital processes, underlying the functioning of the brain. Non-excitable, or glial cells, despite being the most numerous cell type in the organ (Herculano-Houzel 2014), for a long time were considered to only be responsible for metabolic and supportive functions for the organ. Quoting Rudolf Virchow - the neuroscientist that put forward the concept of neuroglia first, back in 1858:

> *"Hitherto, gentlemen, in considering the nervous system, I have only spoken of the really nervous parts of it. But if we would study the nervous system in its real relations in the body, it is extremely important to have a knowledge of that substance also which lies between the proper nervous parts, holds them together and gives the whole its form in a greater or lesser degree"* (Taylor 1895).

The 19th century was the golden era for histology, with many different types of glial cells having been described as a result of these studies. The most famous histologist, whose drawings remain the most recognisable depictions of astrocytes, was the 1906 Nobel Prize laureate Ramon y Cajal. Figure 1.1 shows an example of Cajal's histological preparations and drawings of glial cells (Garcia-Lopez 2010). Cajals preparations clearly suggested the heterogeneity of glial cells and a whole range of distinct functions, although these were laid uncovered for the bigger half of the 20th century, as the view of glia as a support structure persisted. This distinct functional division between glia and neurons is still a view of many neuroscientists (Kettenmann and Verkhratsky 2008).

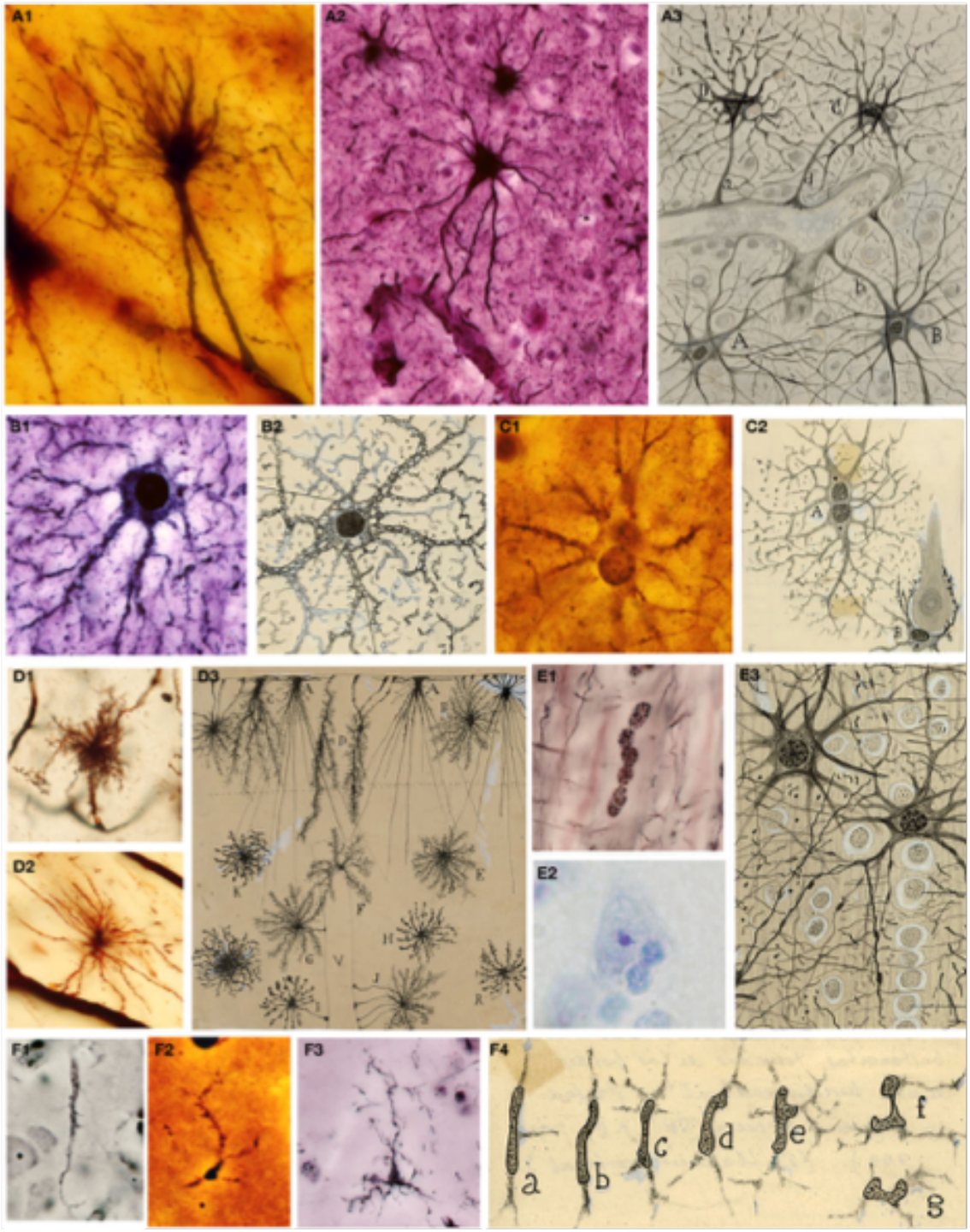

Figure 1.1: **Cajal's histological preparations and drawings**. A – Fibrous astrocyte in the white matter of adult brain (formalin-uranium nitrate and gold-sublimated chloride); B – Protoplasmic astrocyte in an adult brain (silver carbonate (del Rio) and formalin-uranium nitrate); C- Twin astrocytes in the human hippocampus (formalin-uranium nitrate); D – Fibrous astrocytes from the white substance of adult brain (Golgi methods); E – Oligodendrocytes (ammoniacal silver oxide and Nissl); F – Microglial cells (ammonical silver oxide, reduced silver nitrate and silver carbonate (del Rio) methods). (Drawings reproduced with the permission of the Inheritor of Santiago Ramon y Cajal) (Garcia-Lopez 2010).

Despite the persistence of this view of glia as a "space not occupied by neurons" (Taylor 1895); glia's function was being further investigated into. Throughout the second half of the 20th century glial and specifically astrocytic functions were investigated, with the main focus on neurovascular control by the astrocytes. The specific structural peculiarity – the fact that the endfeet of astrocytic cells wrap around the blood vessels of the brain, suggested the probable function in blood flow regulation. Golgi observed this phenomenon first, and so proposed a nutritional role for astrocytes (Oberheim, Goldman, and Nedergaard 2011). This eventually developed into a separate research field with specialised methodologies.

At present, a separate research field is devoted to studying neuronal-glial-vascular unit (Hirase 2005; Verkhratsky and Toescu 2008). The studies of the connections between metabolism and neuronal functioning are using neuroimaging techniques, with the increasing amount of data generated through *in vivo* imaging techniques (2008). Magnetic resonance being one of the most commonly used technique that uses deoxyhemoglobin in venous blood (BOLD – blood oxygen level dependent), yielding in vivo images of the amount of oxygen carried in the microvasculature of the brain (Ogawa et al. 1990). However, it has been recently suggested that the haemodynamic responses of blood vessels are not directly linked to the local energy need of the brain but neurotransmitter-related signalling; evidence was gathered to show that most brain energy is used to power postsynaptic currents and action potentials rather than presynaptic or glial activity (J. Larson and Munkácsy 2014; Attwell et al. 2010).

As metabolic functions of astrocytes were researched into, their function of sustaining metabolism started to include control of the cerebral blood flow. Previously, the main hypothesis included a local negative-feedback system, depending on the neural activity. If an increased supply of oxygen is demanded, a

signal, such as production of CO_2 or lack of O_2, could cause the greater blood flow (Sofroniew and Vinters 2009). However, changes in the O_2 levels experimentally proved against this hypothesis (Lynch et al. 2008). Similarly, it was shown that accumulation of CO_2 in the blood causes initial pH to rise, as expected. Increased blood flow takes the CO_2 away rapidly and higher neuronal activity causes Ca^{2+}, H^+, - ATPase pump to alkalinize the extracellular space (Makani and Chesler 2010). Current hypothesis includes both neurons and astrocytes acting simultaneously to control the blood flow of the brain. Neurons can use neurotransmitters to implement changes in the local blood flow, as can gliotransmitters as well as metabolic agents (Malenka 1994; Kuo and Dringenberg 2012). One of the key players in this regulation is glutamate (Rasooli-Nejad et al. 2014).

Apart from controlling cerebral blood flow glial cells were found to be participating in other aspects of the brain functioning on the control levels. Starting with Carl Ludwig Schleich in 1898(Lalo et al. 2014) suggesting that glial cells control neuronal communication, it is known that some glial cells are able to rapidly grow and retrieve their processes in relevant situations (Ma, Mufti, and Leung 2015). Furthermore, in 1970s several studies have shown that neuroactive substances can be released from nerve endings by cells other than neurons (Talantova et al. 2013). A couple of decades later it was confirmed that astrocytes are able to release a list of chemical, some of which have neuroactive properties (Ahmed et al. 2004). Within the next few years multiple laboratories have reported that astrocytes not only respond to various stimuli by elevating intracellular calcium concentrations, but also that these so called ''calcium waves'' propagate along the glial syncytium(Corner-Bell et al. 1990; Parpura et al. 1994). It was proposed by Araque et al. (1999) that astrocytes are an active participant in synaptic signalling. In particular astrocytes and perisynaptic Schwann cells,

should "be viewed as integral modulatory elements of tripartite synapse"(Araque et al. 1999).

Tripartite synapse (Figure 1.2) is a term used to describe a synapse that consists of three parts: pre and post synaptic neurons and an astrocyte, enveloping the synapse, thus being in the position to actively participate in the signalling process. Astrocytes were also shown to activate following certain stimuli, such as glutamate, aspartate and gamma-aminobutyric acid (Kettenmann, Backus, and Schachner 1984) via corresponding ion channels and neurotransmitter receptors (Verkhratsky and Steinhäuser 2000).

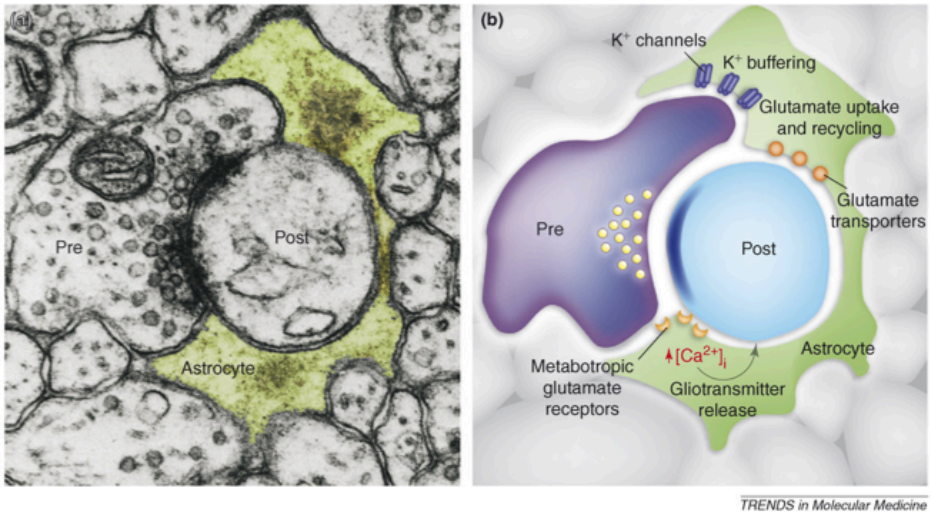

Figure 1.2: **An EM image (left) and a diagram representation showing the structure of a tripartite synapse.** Synaptic vesicles can be seen on both pre- and postsynaptic neurons as well as astrocytes (Halassa, Fellin, and Haydon 2007)**.**

Numerous studies done in this field have shown that astrocytes are capable of feeding back to neurones using a whole range of transmitters, named gliotransmitters, including glutamate (Parpura et al. 1994; Bezzi et al. 1998), D-serine (Mothet et al. 2000), ATP (Coco et al. 2003; Pankratov et al. 2007), and many others (Benz, Grima, and Do 2004; Mongin 2004; Krzan et al. 2003). This evolution of understanding of glial cells has been scrupulously depicted at every stage (Steinhäuser and Gallo 1996; Volterra and Meldolesi 2005; Allen and Barres 2005;

Parpura and Verkhratsky 2012), and historical overviews are also available, such as Kettenmann and Verkhratsky's and Hatton's reviews in 2008 and 2004, respectively (Kettenmann and Verkhratsky 2008; Hatton 2004). There are studies debating the mechanisms of gliotransmission, for example Li et al. 2013 argues that there is a lack of evidence supporting the vesicular glutamate transport hypothesis as proposed by Montana et al. 2004 (Dongdong Li et al. 2013; Montana 2004).

A vast amount of research on the roles of glial cells has unearthed that glial cells are in fact an active key players in bi-directional glial-neural communication. This discovery, however, split the neuroscience community into two camps, one supporting the neurocentric view, and tripartite synapse supporters. With such a large number of laboratories around the world and study models from several study models including robust *in vitro* techniques and an increasing number of *in vivo* techniques there is no doubt the neuroscience community will be expecting tremendous progress in this field in the foreseeable future. A thorough understanding of glial-neuronal interactions will pave the way to investigating the age-related changes and potentially developing prophylaxis for dementia and other numerous diseases linked to senility.

1.3 Age-related changes and non pathological ageing

As stated above, the subject of ageing in respect to human brain has interested scientific community for a long time. Non-pathological or normal ageing is generally considered to be a slow accumulation of changes in the brain parenchyma without development of clinical symptoms of dementia. Normal ageing – just like normality itself is of course a very hard concept to define and it varies immensely with time, place and many other variables. For instance, in the study by Silver et al. 2002, brains of centenarians that participated in the cognitive

test assessment were then assessed postmortem for the deposition of neuritic amyloid plaques. For some cases it was found hard to distinguish between the two states of brain functioning (pathological and non-pathological), especially with the high degree of variation between the extents to which different individuals may be affected. Such, some subjects showed no dementia but upon examination showed to have enough of the plaques deposition to be considered a possible case of AD (Alzheimer's Disease) and *vice versa* (Silver et al. 2002).

Since the flourishing of molecular biology and neuroimaging, it is now generally agreed that normal brain ageing consists of small functional and morphological alterations, and that these changes are incredibly varied in different brain regions. The process of ageing is very similar across mammalian species, which makes rodents a good study model for ageing. It has been established that with age multiple brain areas shrink in size, and there are alterations on all levels from molecular to structural changes in tissue: protein synthesis and degradation processes undergo changes, various channels undergo remodeling, dendritic spines reduce in numbers, and various different cell types have different patterns of age-related changes (Scheibel et al. 1975; Sloane et al. 2000; Shimada et al. 2006; Staff et al. 2006; Hayakawa et al. 2008; Pelvig et al. 2008; Stephens et al. 2011; Lalo, Palygin, et al. 2011; Kremsky et al. 2012). Alterations in the vascular landscape of the brain and in the metabolism was found to differ between young and older rodents (A. J. Martin et al. 1991; Meltzer et al. 2000). Synaptic changes in different regions of the brain, including hippocampus and cortex were examined and after a large number of studies it was concluded that there is no large scale decrease in the number of synapses (Morrison and Baxter 2012). Instead, more subtle morphological changes take place (Brunso-Bechtold, Linville, and Sonntag 2000; Mostany et al. 2013); often these changes vary across the different brain regions (Petralia, Mattson, and Yao 2014). A decrease in the amounts of pre and post-synaptic proteins were found to take place (VanGuilder et al. 2010), as well as

higher levels of expression of pro-inflammatory genes and proteins fighting oxidative stress (Lee, Weindruch, and Prolla 2000).

Age-related changes occur in both neurons and glial cells; for instance, the levels of expression of GFAP (glial fibrillary acidic protein) in the astrocytes of mice were found to increase with age in some brain regions (Nichols et al. 1993). Increased production of GFAP has been linked to a rise in reactive astrocytes population – first step towards astrogliosis and degeneration (Kamphuis et al. 2014; Le Prince et al. 1993; Jalenques et al. 1995). Since astrocytes carry out multiple functions, such as control of vascular tone and metabolism, mediation of signaling via the tripartite synapse and the calcium signaling changes due to age will have drastic consequences on these processes. One of the main characteristics of astrocytes is the expression of a list of potassium channels - they are involved in the vast majority of astrocytic functions. This makes potassium channels a good meeting point of integration of messengers from various functions. Astrocytic functions are discussed in the next section.

1.4 Functions of astrocytes

Various functions of astrocytes can roughly be divided into two major categories: the sustainment of metabolic functioning, such as cerebral blood flow and nutrient exchange control and the participation in signalling in the brain. Below the descriptions of the current understanding and the future questions posing in the context of these functions are discussed.

1.4.1 Metabolic

Astrocytic potassium channels are known to be involved in the clearance of excess extracellular potassium (Walz 2000). During neuronal activity the amount of potassium ions in the extracellular matrix rises, making the membrane more susceptible to further depolarization after the refractory period. In non-pathological scenarios the concentration of potassium fluctuates between 3mM at rest and up to 8 mM (in a pathological condition, however, this value can be greater). The excess potassium is cleared away, however it is still a matter of debate, which exact mechanism takes place or if more than one pathway is involved, how does each of the multiple mechanisms contribute to the overall function (Kofuji and Newman 2004). The neuronal reuptake of potassium is too slow to prevent the build up of excess potassium ion and thus alter the kinetics of the synapses involved and those nearby. Idea first put forward by Hertz (1965), of astrocytes removing potassium from the areas of extracellular space with higher concentration, had two main mechanisms that were thought to be mutually exclusive: uptake of the excess potassium followed by its accumulation and then release into other area of extracellular space (Hertz 1965) and the removal of excess potassium without its subsequent accumulation, but instead a simultaneous release of potassium at a distant area of the astrocytic syncytium (Kuffler, Nicholls, and Orkand 1966).

It is now believed that both net uptake of potassium as well as ''buffering'' takes place in the brain (Kofuji and Newman 2004). The influx of potassium ions into the astrocytic syncytium may also be a metabolic signal that can subsequently control the glial energy metabolism. According to a recent review by MacAulay and Zeuthen (2012), main candidates for the role of key transporters of potassium ions are the Na^+, K^+-ATPase (NKA), the Na^+, K^+, Cl- co-transporter (NKCC1), the K^+, Cl^- co-transporter (KCC), and the inwardly rectifying K^+ channel, Kir 4.1 is capable of

conducting both inward or outward current, depending on the equilibrium potential of the ion and the membrane potential (Butt and Kalsi 2006). This channel subtype is expressed in astrocytes, with more dense presence on the membrane around the perisynaptic feet (Higashi et al. 2001). Kir4.1 channel is closely co-expressed with Aquaporin-4 (AQPR4) – a water channel that is highly expressed in the CNS (Amiry-Moghaddam, Frydenlund, and Ottersen 2004). Both of these channels are perfectly located around the blood vessels and the brain blood barrier to make them primary candidates for controlling the water fluxes in the brain (Nagelhus, Mathiisen, and Ottersen 2004). It is also known that Kir 4.1 channel type can be affected by external cations, which can trigger the process of buffering (Edvinsson, Shah, and Palmer 2011). Kir 4.1 is thought to be the major glial subtype of potassium channel and its down regulation causes malfunctioning of astrocytic resting potential as well as the uptake of glutamate by astrocytes (Djukic et al. 2007; Y. V. Kucheryavykh et al. 2006). However, different groups conclude the opposing results from this finding. Such, Haj-Yasein argues a key role for Kir 4.1 in the mechanism of potassium buffering, whereas Chever propose this channel to have little importance in the matter (Haj-Yasein et al. 2011; Chever et al. 2010).

It has been shown that potassium fluctuations may well be involved in the control of cerebral blood flow. Schielke et al. demonstrate that an increase in the extracellular concentration of potassium ($[K_o]$) may stimulate transport across the cerebral capillary, yet have little effect on Na, K-pump activity in neurons (Schielke, Moises, and Betz 1990). It is also unfortunate that the subcellular localization of potassium channels has only been assessed in a few brain regions, and primarily in neurons (Vacher, Mohapatra, and Trimmer 2008; Trimmer 2015). This is due to technical morphological peculiarities of astrocytes: having a relatively small cell body and a large volume of fine branches and projections,

ensures that imaging protein expression becomes unclear(Sofroniew and Vinters 2009).

1.4.2 Signalling

The concept of tripartite synapse has already been introduced above. It has been shown that astrocytes are not only located near chemical synapses, and often enwrap them (Ventura and Harris 1999); astrocytes release a long list of gliotransmitters and the mechanisms of the release are varied and are still a subject of debate (Lalo et al. 2014; Dongdong Li et al. 2013; Pankratov et al. 2007; Coco et al. 2003; Parpura and Zorec 2010). It is now widely accepted that astrocytes signal to each other via calcium waves, but the complexity and lack of universality of these signals leads to a question: are there multiple types of calcium signalling (Agulhon et al. 2008; Nedergaard and Verkhratsky 2012; Rusakov 2015). More precise methods for studying calcium signalling (e.g. GCAMP calcium indicator (Nakai, Ohkura, and Imoto 2001)) have determined that there are some very local increases in intracellular calcium, and the concentration within a single cell varies enormously (Zheng et al. 2015). One of the main tasks in this are of research is the disentanglement of calcium signalling in astrocytes and finding a true understanding: what exactly is the function of gliotransmission and how it affect plasticity (Rusakov et al. 2014; Volterra, Liaudet, and Savtchouk 2014; Araque et al. 2014; Rusakov 2015; Covelo and Araque 2016)?

1.4.3 Glutamate uptake and recycling

The glutamate-glutamine cycle is a well-known cellular mechanism that consists of transfer of glutamine to neurons and glutamate from neurons to astrocytes. Astrocytes uptake and recycle glutamate using an enzyme called glutamine synthetase. Glutamine synthetase is expressed exclusively in astrocytes(Norenberg and Martinez-Hernandez 1979). Since glutamate is considered to be the major neurotransmitter, its concentration must be tightly controlled, providing a high

signal-to-noise ratio for quicker detection of increasing concentration of glutamate(Danbolt 2001). Failure to remove synaptic glutamate effectively could cause increased levels of extracellular glutamate, which in turn begins the process of excitotoxicity.

Glutamate is taken up by astrocytes via glutamate transporters (GLAST and GLT-1) by an electrogenic process. The expression of these transporters near the synaptic cleft and the high affinity to the substrate ensures a rapid clearance of glutamate from the extracellular matrix. Glutamate transporters utilise the energy from the exchange of Na^+ and K^+ ions (3 Na^+ in: 2K^+ out), which increases the extracellular concentration of potassium(Diniz et al. 2010; Vandenberg and Ryan 2013). This tight coupling of potassium and glutamate homeostasis introduces limitations into experimental set ups and the conclusion, that can be drawn from the data acquired (See Chapter 6). Once glutamate is taken up by astrocytes, and subsequently detoxified into glutamine, it can be transported to glutamatergic or GABAergic neurons. There it can be used converted into neurotransmitter glutamate or GABA, respectively(Walls et al. 2014). Many diseases, including age-related Alzheimer's and others are linked to misbalance in glutamate uptake and as a consequence – in potassium homeostasis (Liévens et al. 2001; Scott et al. 2011; Rivera-Aponte et al. 2015).

1.5 Astrocytic channels

> *''Electricity plays an unavoidable role in biology. Whenever solutes like phosphate compounds, amino acids, or inorganic ions are transported across membranes, the movement of their charge constitutes an electrical current that produces a voltage difference across the membrane. Beyond managing to keep this accumulation of charge from getting too far out of balance, all living cells have developed the ability to exploit a transmembrane electrical potential as an intermediate in the storage of energy and the synthesis of ATP.'' (Yellen 2002)*

Astrocytes express a great number of both ionotropic and metabotropic receptors, but due to space constraints of this introduction only channels, directly relevant to this project are discussed below. For more information on glial channels see the following reviews (Bradley and Challiss 2012; Barbara A Barres et al. 1990; Verkhratsky and Steinhäuser 2000).

1.5.1 Potassium channels

Potassium channels are the most ubiquitous channels that can be found in virtually every living cell of both prokaryotes and eukaryotes. Potassium channels are tetrameric integral membrane proteins that form aqueous channels allowing the passage of K^+ ions. There are normally 30-100 K^+ genes in each living organism and some possess mechanisms of alternative splicing. Many super families of potassium channels vary on their mechanisms of gating and the function they carry out in the body (Miller 2000). As one of the most abundant channels types, potassium channels are present in every cell type. More specifically, in astrocytes potassium channels are by far the most dominantly expressed channel type. Classification of potassium channels utilises their functions and hallmark properties. Figure 1.3 summarises the subclasses of potassium channels. Here, the potassium channels are classified based on their structure.

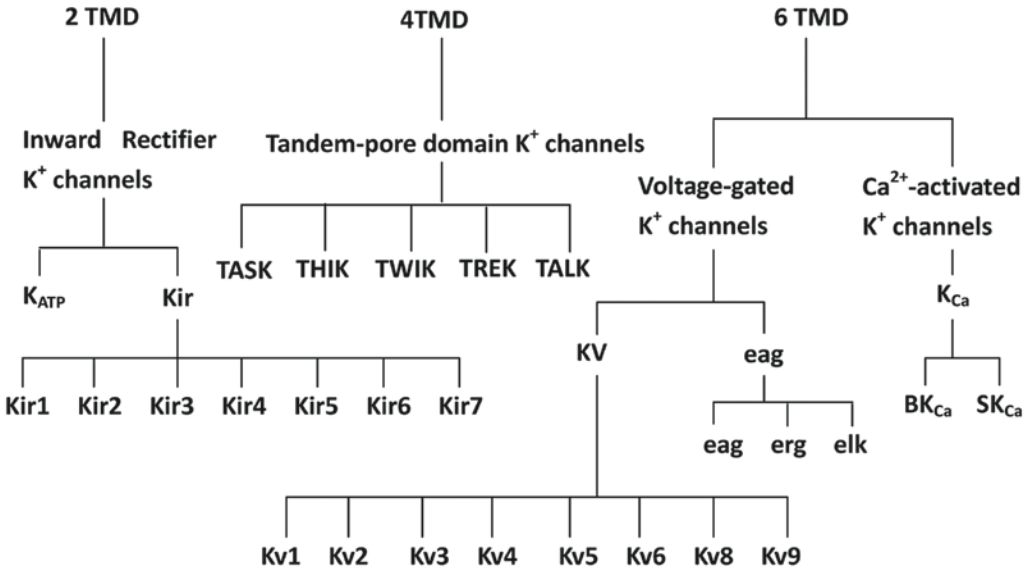

Figure 1.3: **Classification of potassium ion channels.** TMD, trans-membrane domain; K_{ATP}, ATP-sensitive K^+ channel; Kir, inward-rectifier channel; TASK, tandem- pore domain K^+ channel; KV, voltage-gated K^+ channel; EAG, ether-á-go-go channel; K_{Ca}, Ca^{2+}-activated channel; BK_{Ca}, large conductance K_{Ca} channel; SK_{Ca}, small conductance K_{Ca} channel (W. M. Liu 2013).

Current knowledge of potassium channels in astrocytes remains rather irregular, partially due to a great degree of variation in the structure, stoichiometry and expression of potassium channels in various tissues. Below the three classes of potassium channels are discussed in more details.

Inwardly rectifying channels

Inward rectifying potassium channels were first identified in skeletal muscles (L. Y. Jan and Yan 1994). The voltage relationship of these potassium channels did not fit Hodgkin – Huxley kinetics and was therefore named the ''anomalous'' potassium channel (Hodgkin and Huxley 1952; Hibino et al. 2010). These channels are much more likely to allow the influx of potassium ions than the voltage-gated potassium channels (Guo et al. 2003). Being voltage-independent channels, Kir channels are lacking the S4 voltage sensor sequence, whereas in other types of K^+, Na^+, and Ca^{2+} channels this feature is conserved (Guo et al. 2003). Main elements of control of the activity of the inward rectifying potassium channels are therefore said to be the membrane potential (E_M) and the equilibrium potential for

potassium ions, or E_K. Under permitting E_M and E_K, and also absence of any mechanism of the blockage of potassium channels, such as ATP blocking K-ATP channels; inwardly rectifying potassium channels will be active at all voltage steps. There are 15 genes encoding various potassium channel subtypes classified as inward rectifiers. These are divided into 7 families: Kir 1.x to Kir 7.x. They are further classified by their function. Thus, there are said to be 4 classes of inwardly rectifying potassium channels (Figure 1.4).

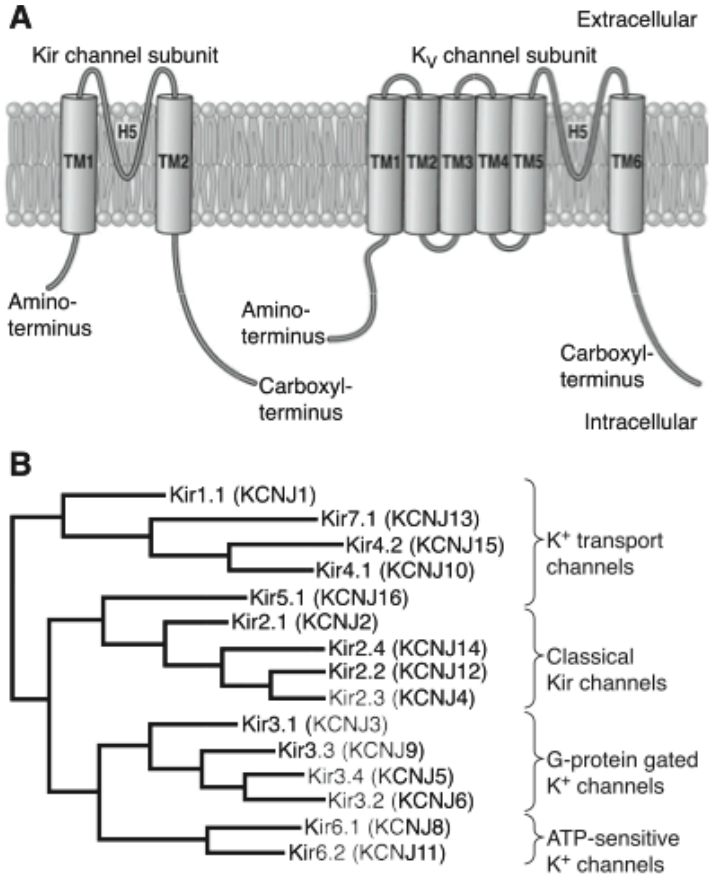

Figure 1.4: **Diversity of potassium channels**. A - Comparison of the structure of inwardly rectifying (left) and voltage-gated (right) potassium channels. B - Classification of inward rectifiers based on sequence identity and function (Hibino et al. 2010).

Classical Kir channels

Potassium channels found in both skeletal and cardiac muscle types belong to the Kir2.x channel family. They determine and sustain a highly negative E_M and contribute to the action potential plateau in various cells. Starting from Kir 2.1, three other subunits were cloned, Kir2.2, Kir2.3 and Kir2.4 (Kubo et al. 1993;

Topert et al. 1998). Kir2.1 subtype, expressed in mouse brain has 70, 61 and 63% identity with the three respective channel subtypes. Conserved sequences constitute predominantly to the two membrane spanning regions and H5 region also. Despite historical opinion of Kir2.x channel types being strictly homomeric (Tinker, Jan, and Jan 1996), it has been shown with the use of electrophysiological experiments that each of the four subtypes can assemble with any other subtype and that the heteromers have distinct properties to their respective homomeric channels (Preisig-Muller et al. 2002). The Kir2.1/2.4 channel is expressed in the brain (Schram et al. 2004).

Using techniques such as immune-histochemistry and in situ hybridization, the localization of Classical Kir channels was studied. Kir2.1 is expressed in the entire brain, although quite weakly. Kir 2.2 is expressed strongly in cerebellum and temperately within the whole brain (Horio et al. 1996). Forebrain and olfactory bulb express Kir2.3 and Kir2.4 is located exclusively in the cranial nerve motor nuclei in the midbrain, pons and medulla, but the expression is mainly limited to the dendrites and soma (Karschin et al. 1996; Topert et al. 1998; Prüss et al. 2005). Using electrophysiological techniques it was established that different heteromers of Kir2.x channel subtypes are present in neurons in several brain regions, such as hippocampus and spinal motor neurons (Brown et al. 1990; Takahashi 1990). These channels are involved with the E_M and the control of neuronal excitability; hence the Ba^{2+} block of Kir2.x channels in neurons causes depolarization and initiated action potential firing (Day et al. 2005). In Schwann cells surrounding the peripheral nerve fibers, specifically in the microvilli of these cells, both Kir 2.1 and Kir 2.3 were detected, using immune-histochemical analysis (Wilson and Chiu 1990; Mi et al. 1996). These channels may be involved with maintaining the $[K^+]_O$ by collecting the excess K^+ released from the nearby axons. This function of peripheral Schwann cells is similar to the K^+ buffering of the excess extracellular potassium ions by the astrocytes in the central nervous system (Hibino et al. 2010).

G-protein gated Kir channels (Kir3.x)

There are thousands of GPCRs in the human genome; they are target to various signaling molecules and in response to stimulation two effector molecules (Gα and G$\beta\gamma$) dissociate and can pass on the signal inside the cell. There are four subunit types: Kir 3.1 – Kir 3.4. They can also form various homo- or heteromers and their functions are defined by the exact cellular localisations, nearby protein complexes and a range of signalling substances (Lesage et al. 1995; Jelacic et al. 2000).

Kir 3.1 (GIRK1) was the first cDNA to be isolated and it is 39 and 42% identical to the Kir 1.1 and Kir2.1 channel subtypes respectively (Kubo et al. 1993). Kir3.2 channel subtype possesses at least four different isoforms, due to alternative splicing of the GIRK2 gene. These isoforms are named Kir3.2a – Kir3.2d respectively. It is suggested that Kir3.2 isoforms usually form heteromers with other subunits, for example Kir3.1 or Kir3.3. Kir 3.3 channel subtype is expressed in the mouse brain, in at least two variants (17 AAs length difference) (Lesage et al. 1995; Jelacic, Sims, and Clapham 1999). The rat and human Kir3.3 subunits are nearly matching the longer variant of the mouse Kir3.3 (Jelacic, Sims, and Clapham 1999). Studies of various heteromeric combinations of all the K_G channels are numerous and sometimes conflicting. Some heteromers are expressed in some species but not others and the combinations may vary depending on tissue and cell type and intracellular localization. Most K_G channels (Kir3.1, Kir3.2 and Kir3.3) are evenly expressed throughout the brain (Hibino et al. 2010). Kir3.1 and Kir3.2 are localized in both post- and pre-synaptic regions, as shown by electron microscopy. Kir3.3 and Kir3.4, however, have only been detected in the axons of neurons (Iizuka et al. 1997; Grosse et al. 2003). This localization hints at K_G channels' involvement with not only the post-synaptic but also presynaptic modulation of neuronal activity. Homomeric complexes of Kir3.2 isoforms were

found in dopaminergic neurons of the substantia nigra (Inanobe et al. 1999). These homomers thus could potentially be involved in the age-related degeneration process in the dopaminergic neurons. Once activated by any of the known GPCRs at either post- or presynaptic site, the K_G channels produce a slow inhibitory postsynaptic potential (sIPSP) and thus suppress the cells excitability (Thompson and Gahwiller 1992; Muller and Misgeld 1989). This function of potassium channels in hippocampal and cerebral neurons comprise of Kir3.2 channels, as shown by the knockout experiments where KO mice had spontaneous seizures and were generally more susceptible to induced seizures (Signorini et al. 1997; Luscher et al. 1997). This phenotype seems to be related to the lack of Kir3.2 function in providing IPSPs. If the Kir3.2 was knocked out, there was a clear reduction in the Kir3.1 expression levels as well (Signorini et al. 1997). In a study in the hippocampus, a null Kir3.4 channel resulted in a decrease in spatial learning and memory task test, despite localization experiments demonstrating that Kir3.4 is expressed weakly in the hippocampus (Wickman et al. 2000). K_G could be similarly involved in a negative feedback loop, set to control neuronal excitability. Trafficking of these channels can be affected by neuronal activity of the cell. A study by Chung et al 2009 illustrated how Kir3.1/3.2 heteromers are present predominantly in the cytoplasmic regions, until the stimulation of NMDA receptors by glutamate. The number of Kir3.1/3.2 channels on the soma, dendrites and dendritic spines membranes doubles on a time scale of 15 minutes (H. J. Chung et al. 2009).

K-ATP channels (Kir6.x/SURx)

K-ATP is a type of inwardly rectifying potassium channels that can be blocked by the internal ATP. These channels are only weak inward rectifiers. It is believed that K-ATP might provide a link between the metabolic state of the cells and the excitability. When expression cloning isolated both, a classic Kir 2.1 and K-ATP 1.1 (Kubo et al. 1993), the conserved features present in these types were the TM1 and

TM2 membrane-spanning regions and the H5 extracellular loop that forms the pore of the channel (see Figure 1.4). Functional K-ATP channels comprise of four Kir subunits forming the pore as well as four auxiliary proteins, the SUR or sulfonylurea receptors. These SUR subunits are susceptible to inhibitory agents such as sulfonylureas (tolbutamide and glibenclamide) that are used for treating type II diabetes. K-ATP channels play a vital role in pathogenesis of type II diabetes: they are present in the β-cells of the pancreas and are a key player in the insulin secretion into the ducts. K-ATP channels are expressed throughout the organism, participating in the control and regulation of glucose level inside and outside of the cells. Kir6.1 channel subtype was found in the mitochondrial membrane of rat liver and it was blocked by ATP application to the luminal matrix face as well as 4-AP and glibenclamide (Inoue et al. 1991). Other studies also identified Kir6.1, Kir6.2 and SUR2A subunits in the mitochondria of both heart and brain (Lacza 2003; Lacza et al. 2003). These channels are also expressed moderately in the brain, however the main focus of investigation of these channels remains metabolic and blood glucose regulation (Minami et al. 2004; Dongliang Li et al. 2013).

As well as carrying out this important function of facilitating the insulin secretion in the pancreas, these ATP-sensitive channels play another significant role in the brain, by protecting neurons against ischemic damage. The vulnerability to stroke is varied among distinct regions of the brain, and this is one of the higher causes of death in the UK (152,000 strokes a year according to Stroke Association, UK (stroke.org.uk 2016)). A recent study has compared the Kir6.2 knockout with the wild-type mouse and concluded that Kir6.2 channels provide a protection from neuronal death following a 15-minute induction of ischemia in vivo. This result suggests that cortical K-ATP channels are part of a specific mechanism aimed at limiting the damage of neurons that can be caused by a cerebral ischemic stroke (Sun et al. 2007). These channels were also investigated in the hypothalamus, in

the so-called "glucose-sensitive" neurons. For instance, orexin neurons can be inhibited by an increase in glucose concentration thus affected regulation of wakefulness, locomotor activity and appetite; whereas neurons, concentrating melanin hormone are excited upon an increase in the glucose level (R. Wang et al. 2004). The details of the mechanisms of inhibition and stimulation of neuronal activity are elusive and still being debated (Karnani and Burdakov 2011; De Backer et al. 2016).

K-transport channels (Kir1.1, Kir4.x, Kir5.x and Kir7.x)

Kir1.1 channel subtype possesses an ER retention signal in its - COOH terminus (D. Ma et al. 2001). Several proteins, including PKA and SGK, are involved with Kir1.1 channels trafficking to and from the surface membrane. This channel subtype plays a vital role in the nephron of kidneys, which will be described later. In situ hybridization has also shown that Kir1.1 is expressed in neurons of both cortex and hippocampus, however, its physiological function remains unknown (Kenna et al. 1994). Another type of transport potassium channel is Kir4.1 channel (KCNJ10), which has 53, 43 and 43% amino acid sequence identity with Kir1.1, Kir2.1, and Kir3.1 channels (for Kir5.1 it is 39, 50 and 40% identity respectively) (Hibino et al. 2010). Kir4.1 subtype can form both hetero- and homomers, unlike Kir5.1 channel that is only fully functional if co-expressed with Kir4.1 (Butt and Kalsi 2006). Pessia et al. 1996 has shown that a homo-tetrameric Kir4.1 channel can produce potassium current. Biophysical properties, such as pH sensitivity, of Kir4.1/4.1 are distinct to those of Kir4.1/5.1 (Pessia et al. 2001). Kir4.2 (KCNJ15) was first isolated from a human kidney cDNA library (Pearson et al. 2004). This channel subtype possesses a 62% identity to Kir4.1, but it is lacking an ATP-binging cassette in its' COOH terminus (Takumi et al. 1995). Kir4.2 can form a homomer as well as co-express with Kir5.1. This heteromer produces a different single channel conductance and is present on a greater cell surface (Pearson et al. 1999; Pessia et al. 2001). Three groups identified channel subtype Kir7.1

simultaneously (Derst et al. 1998; Krapivinsky et al. 1998; Partiseti et al. 1998). To date there are no reports of any heteromeric combinations of Kir7.1 channel. In general, there is a fair degree of variation within the four classes of Kir channels. Their sequences are quite distinct from one another, and hence the behavior, such as formation of homo- or heteromers and the existence of alternative splice forms, varies from transport potassium channels to ATP-sensitive potassium channels.

In situ hybridization indicated that Kir4.1 is predominantly expressed in astrocytes (Takumi et al. 1995). It is said to be involved in the "potassium buffering" by astrocytes, thus regulating the neuronal excitability and carrying out a neuroprotective function. As well as being expressed in astrocytes Kir 4.1 is present in oligodendrocytes and is linked to the vital process of myelination of the developing nervous system (Neusch et al. 2001). The gene expressing Kir 4.1 is located on chromosome 1. Kir4.1 forms both homomeric and heteromeric (with Kir5.1) channels in astrocytes that appear to have distinct localization patterns; perisynaptic processes both types of channels, unlike the endfeet projections, that only contain the heteromers. Another type of glial cells that expresses Kir4.1 channels is the satellite cells (Hibino et al. 1999). These cells wrap around ganglion neurons in the peripheral nervous system. In fibrocytes of cochlea, a non-functional homomer of Kir5.1 and a fully functional Kir4.1 channels are present (Hibino, Higashi-Shingai, et al. 2004). Kir4.1 in astroglial cells constitutes to the basal conductance of potassium ions in brain, spinal cord and retina (T. M. Ishii et al. 1997; Kaiser et al. 2006; Neusch 2006; Olsen, Campbell, and Sontheimer 2007). A knockout in the Kir4.1 gene causes a decrease in potassium conductance, depolarization of E_M in astrocytes (Neusch 2006). Homomeric Kir4.1 and Kir4.1/5.1 have different location configurations in astrocytes (M. Ishii et al. 2003; Hibino, Fujita, et al. 2004). On the perisynaptic projections of the astrocytes both homo- and heteromeric Kir channels are present, whereas the endfeet of astrocytes only show presence of the heteromeric Kir4.1/5.1. Since astrocytes are believed to expel

potassium ions onto the blood vessels one may assume that this is done via the heteromeric Kir4.1/5.1 channels. Homomeric Kir4.1 channels may then be responsible for taking up the potassium ions into the cell. The main difference between the Kir4.1 homomer and the Kir4.1/5.1 channel is their sensitivity to pH. Within the physiological pH range (6.5-8) the homomeric Kir4.1 channel is inhibited by acidification with a pKa of 6 (Pessia et al. 2001). Dissimilarly to that, the heteromeric channel is suppressed by only a slight acidification of the pH and its activity is heightened by alkalization (Zhenjiang Yang et al. 2000). During the developmental stage Kir4.1 is expressed in both astrocytes and oligodendrocytes, however 10-20 days after birth the expression of this channel subtype only proceeds in the astrocytes (Kaiser et al. 2006; Neusch et al. 2001). There is a suggestion that Kir4.1 is functionally coupled to glutamate transporters, since GLT-1 and GLAST transporters are also expressed in astrocytes and the knockout experiments with Kir4.1 lead to an impaired glutamate uptake by astrocytes (Olsen, Campbell, and Sontheimer 2007; Djukic et al. 2007).

Kir 4.2, also called Kir1.3, is important in development of kidney, lung, heart, thymus and thyroid, is located on chromosome 21 in humans. This means that Kir4.2 channel may play a role in the pathogenesis of the Down's syndrome. Often Kir4.2 forms a hetero-channel with Kir 5.1 (works in kidney and pancreas). Kir4.2 has been found in mouse liver, where its function is unknown (Pearson et al. 1999); and as a part of the heteromeric Kir4.2/5.1 in the renal epithelial cells (Pessia et al. 2001). The Kir4.2 channels are largely internalised if expressed alone in heterologous systems, and so only produce small potassium current (Pearson et al. 1999).

Kir7.1 channel type is widely expressed in different epithelial cells, for instance in DCT, PCT and the collecting duct of kidney. In these cells this channel is expressed on the basolateral membrane (Nakamura et al. 1999; Kusaka et al. 2001).

However, in the choroid plexus Kir7.1 channels are present on the apical membrane of the cell only (Nakamura et al. 1999). Some of the mechanisms underlying the targeting and expression of each of the potassium channel subtypes are not clear yet. Choroid plexus and RPE (Retinal Pigment Epithelium) have a strong polarity, produced by the activity of Na^+-K^+- ATPase on their apical membrane (0kami et al. 1990). Kir7.1 homomers seem to aid maintain this polarity. In thyroid follicular cells and renal epithelial cells Kir channels are located on the basolateral membrane, close to the Na^+-K^+-ATPase pump, thus suggesting that the function of these Kir7.1 channels is to provide the potassium ions for their respective pumps. Kir7.1 are the least heavily researched into channels and many physiological functions of this channel are still not proven or in some cases unknown.

Kir4.x and Kir5.1 channels participate in potassium recycling in the basolateral membrane of kidneys and stomach epithelium. Providing potassium ions to the extracellular site of Na^+, K^+-ATPase helps to maintain its activity. This process can be blocked by the addition of Ba^{2+} (Schafer and Troutman 1987). Either Kir4.1 or Kir4.2 can affect Ca^{2+} sensing receptors in the basolateral membrane of DCT, resulting in a decreased current produced by the subunits (Huang et al. 2007). These channels are involved in Calcium and Magnesium homeostasis (Blaine, Chonchol, and Levi 2015). A homomer of Kir4.1 is co-localized with the H^+-K^+-ATPase at the apical membrane of gastric parietal cells. Kir4.1 is presumably aiding to maintain the activity of the pump, by delivering potassium ions for the pump. Another tissue where Kir4.1 is expressed is the endolymph of the cochlea of the inner ear. It contains an approximate concentration of 150mM K^+ and has a very positive membrane potential of +80 mV relative to that of blood. These unique conditions are essential for hearing to take place. Kir4.1 knockout mice are deaf, providing more evidence for the importance of this channel subtype in the

cochlea. Application of Ba^{2+} to the membrane suppressed the endocochlear potential (Marcus et al. 2002; Chen and Zhao 2014).

Voltage-gated potassium channels

There are more than 40 genes encoding subunits for voltage-gated potassium channels. Voltage-gated potassium channels are homo-tetrameric, with each of the alpha subunits possessing a voltage sensor (S4) and six trans-membrane domains (S1-S6), with both termini located on the intracellular side of the membrane (Yellen 2002). These 6 domains contribute to alpha subunits, of which there are 20 types described to date. These alpha subunits are classified into 6 subfamilies Kv1 (Shaker), Kv2 (Shab), Kv3 (Shaw), Kv4 (Shal), KyLOT and EAG. Since the pore domain (H5) is highly conserved, potassium channels are able to preferentially conduct K+ ions over Na+ ions (over 1000 fold preference), despite these two ions being of similar size (MacKinnon 2003). Voltage gated potassium channels can form channels from alpha subunits from the same subfamily as well as other subfamilies (Christie et al. 1990; Shahidullah et al. 1995). For instance, Kv1.2 and Kv1.4 co-precipitate together from extract of the brain, they appear to form functional multi-heteromers on the terminals of neurons and produce A-type (rapidly inactivating) current (H. Wang et al. 1993). There is an immense potential for variation of all the possible multi-heteromers that can be build from the alpha subunits. Some of the subfamilies, however, do not express currents by themselves (Kv5, Kv6, Kv8 and Kv9) (Coetzee et al. 2002).

Another subfamily of voltage gated potassium channels is the Calcium dependent voltage-gated potassium channels, containing three members: SK (Small), IK (Intermediate) and BK (Big) conductance – termed so based on the extent of the conductance of potassium ions. An increase in the intracellular calcium reduced the conductance of these channels. These channel types are involved in multiple processes in the brain, including response to injury (Armstead 2005), sensing

osmotic changes in the paraventricular nucleus (Feetham et al. 2015), cerebral blood flow regulation (Philip and Armstead 2004), synaptic activity modulation (Carlson 2014) and many more. KCa3.1 expression is up-regulated in glioblastoma multiform (GBM) and was shown to play a pro-invasive role in a malignant glioma (Turner et al. 2014).

Voltage-gated potassium channels carry a great importance in neurons in the brain, where they lead the repolarisation process of the action potential (Pathak, Guan, and Foehring 2016). Since voltage gated potassium channels may underlie both the sub-threshold and larger currents during spikes, thus producing even more complexity for studying the individual roles of these channels. Any mutations in voltage-gated potassium channels can lead to devastating consequences; many channel impairments are involved in epilepsy – termed 'channelepsy' (D'Adamo et al. 2013; Simons et al. 2014). Even single base mutations can give rise to severe phenotypes, such as 'shaker' in Drosophila. These diseases are called channelopathies (Lehmann, Bette, and Engele 2009).

In astrocytes, as in other glial cells, high densities of potassium channels are expressed, which is expected due to their function of controlling K^+ homeostasis. Surprisingly though, both types of outward potassium current, rapidly inactivating and delayed rectifier are also present. Some propose that these channels are important for regulating glial proliferation. However, high densities of these channels persist in mature age as well. Their relevance is yet to be fully understood (Verkhratsky and Steinhäuser 2000). According to Expression Atlas database, which stores both microarray and RNA-sequencing data, two most prominently expressed voltage-gated potassium channels are Kv1.2 and Kv3.4 (Petryszak et al. 2016). They correspond to K_D and K_A types of currents respectively (Smith, Rosenheimer, and Kalil 2008; Angulo et al. 2004).

Leak potassium channels

A third subfamily of potassium channels is the two pore or ''leaky'' potassium channels. They contain four trans-membrane domains and two pore domains (Coetzee et al. 2002). The structure of leak channels is similar to a doubled up Kir subunit conformation. Unlike the other two classes, 4 domain potassium channels form dimers, thus keeping the symmetry of the central pore. Two-pore potassium channels largely lack any time- and voltage dependence (Verkhratsky and Steinhäuser 2000). The first gene (KCNK0) encoding a two-pore subunit was cloned from *Drosophila melanogaster* in 1996, and since then at least 14 subunits have been cloned and formally studied (Goldstein et al. 1998; Goldstein et al. 2001). Since two-pore potassium channels are subjects to both physical (stretching, temperature and pH fluctuations) and chemical (a vast number of signalling molecules, e.g. lipids) regulation, it is said to be a high controlled class of channels. Coupled with their distribution in the central nervous system, this makes these channels, such as TREK-1, a potential therapeutic target (Vivier et al. 2016). A further regulatory mechanism of the 2 - pore channels has recently been described – a non-traditional voltage gating mechanism, where the sensitivity arises from the interaction of 3-4 potassium ions with the electric field of the selectivity filter, which act similar to a ''check valve'' (Schewe et al. 2016).

It was reported that two isoforms of two-pore potassium channels were expressed in astrocytes of the mouse forebrain: TWIK-1 ($K_{2P}1.1$) and TREK-1 ($K_{2P}2.1$) (Cahoy et al. 2008). In a heterologous system, TWIK-1 shows a weakly inward rectification, whereas TREK-1 conducts an outwardly rectifying current (Lesage et al. 1996; Fink et al. 1996). These two channel subtypes are believed to conduct a large proportion of the overall astrocytic potassium current, and to be mildly sensitive to blockage by barium chloride (Zhou et al. 2009).

1.5.2 P2X receptors

ATP is a universal energy-providing molecule. However, in the central nervous system it also acts as a signalling molecule – both a neuro- and gliotransmitter, with it's own set of receptors (Abbracchio et al. 2009). ATP can be both released and received as a messenger from multiple locations in the brain, and both neuronal and glial cells. The release mechanisms include exocytosis and transport via channels and pumps (Verkhratsky et al. 2012). There are seven subtypes of ionotropic purinoceptors: P2X1-P2X7; they form functional channels out of three subunits. Most of the P2X receptor subunits are able to form both homo- and heteromeric channels, with some combinations being far more typical than others(Jiang et al. 2003). Common heteromers include $P2X_{1/2}$, $P2X_{1/4}$, $P2X_{1/5}$, $P2X_{2/3}$, $P2X_{2/6}$ and $P2X_{4/6}$ (North 2002; Surprenant and North 2009). Since the currents conducted by the seven subunits vary to a large degree, existence of multiple patterns for heteromeric channels introduces a great variation in the functioning of these channels. Figure 1.5 shows the desensitization of the seven homomeric P2X receptors in rat (North 2002).

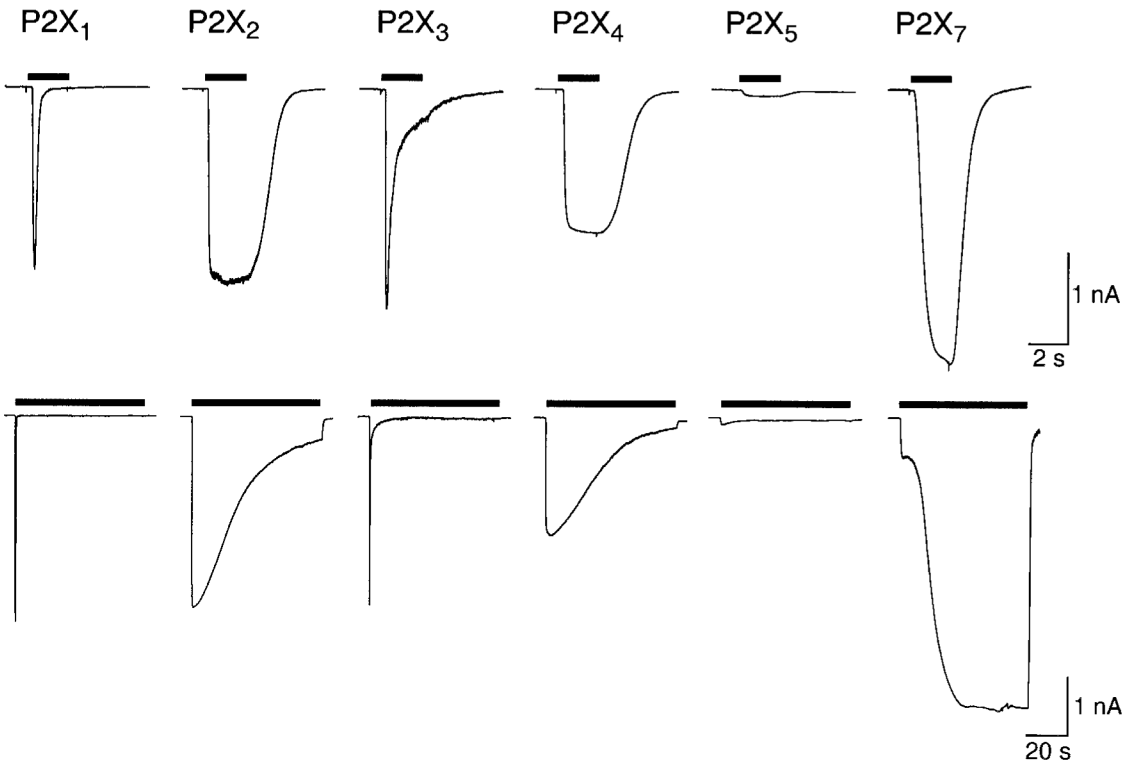

Figure 1.5: **Fast (top) and slow (bottom) desensitization compared for homomeric rat P2X receptors.** Fast desensitization is only noted in $P2X_1$ and $P2X_3$ channel subtypes, following a brief application (2s) of 30 μM ATP (except $P2X_7$, where 1mM was used). Slow desensitization was observed in $P2X_2$ and P2X4, following a 60s application of ATP. HEK293 cells were transfected with 1 μg/ml cDNA 48h prior to the recordings being made. In all cases a single application yielded the response showing, except $P2X_7$, which required a 2min application. Figure taken from North et al. (2002).

Although all seven P2X subunits were found in astrocytes on a transcriptional level (Verkhrasky, Krishtal, and Burnstock 2009), when acutely isolated cortical astrocytes (from mouse) were tested for the mRNA levels, only $P2X_1$ and $P2X_5$ subunits were identified (Lalo et al. 2008). These subunits were shown to form functional heteromers, which were extremely sensitive to ATP (K_D approximately 50 nM) and have intermediate Ca^{2+} permeability ($P_{Ca}/P_{monovalent}$ – 2.2). Activation of these heteromers by either exogenous or synaptically derived ATP can trigger calcium signals (Palygin et al. 2010). The expression of $P2X_{1/5}$ channels in astrocytes varies with age, reaching it's peak around 3-6 months old mice (Lalo, Palygin, et al. 2011).

1.5.3 Other relevant astrocytic channels

NMDA receptors are a type of ionotropic glutamate receptor that is very abundant in the central nervous system. The name of this channel comes from the selective agonist N-methyl-D-aspartate. Functional channels are formed by hetero-tetrameric composition of GluN1 and GluN2 subunit types. Properties of the subunit types are different, thus introducing an increased variation in regulation of these channels. NMDARs are expressed on both neurons and glial cells (Conti et al. 1997). One of the hallmark properties of neuronal NMDARs is the presence of Mg^{+} ion block in the channel pore, thus requiring two events to take place before the channel can be activated. In astrocytes mRNA for both NR1 and NR2A/B subunits were detected in the past with various methods (Conti et al. 1997; Schipke et al. 2001). Recently, it was shown by our laboratory that astrocytes express NMDA receptors that are devoid of this magnesium ion block and that these channels can mediate the transmission from glia to neurons (Lalo et al. 2006). It was then also shown that both $P2X_{1/5}$ and NMDA receptors expressed in cortical astrocytes are permeable to calcium (P_{Ca}/P_{K} was 2.2 and 3.1 respectively); these influxes of calcium are consecutively capable of triggering Ca^{2+} signals when stimulated (Palygin et al. 2010).

Another receptor type involved in this project is the astrocytic PAR-1 receptor. Protease-activated receptor is a subfamily of related GPCRs that are highly expressed on platelets and are vital for the process of blood clotting, as well as being involved in control of vascular tone, immune response (T-cells) and many other. Activation of PAR-1 receptors propagate signals via many G-proteins, including G_i, G_q, and $G_{12/13}$ and can lead to profound consequences in the cells, such as proliferation (Traynelis and Trejo 2007). In the CNS PAR-1 receptors are expressed in plural cell types, but the highest expression was found in glial cells (Junge et al. 2004). Activating astrocytes via the addition of agonist to PAR-1

receptor (e.g. specific peptide agonist TFLLR) was found to increase the exocytosis of ATP from astrocytes, thus down-regulating the inhibitory synaptic currents in the neocortex. In essence this means that by activating PAR-1 receptors in astrocytes the synaptic plasticity balance shifts towards potentiation (Lalo et al. 2014).

Having discussed several types of channels, their similarities and differences in structure, cellular localization and functions, it is clear that despite a great deal of research has been carried out there are still many areas in which further work is needed. Put together with the demand for more investigations into the age-related changes in glial cells, especially in astrocytes, exploring the functions and potential links between these channels may yield progress in the understanding of the ageing process of astrocytes. Since functions of astrocytes include neuroprotection as well as signaling, learning about the ways in which astrocytic functions degenerate with time, is one of the areas of neuroscience where more investigations should be undertaken.

1.6 Hypothesis

Two pools of astrocytic functions were described above: the signalling and metabolic functions. These functions are performed by the same set of glial cells (although there likely are discrepancies in regional location, cell subtypes and subcellular compartments involved in each of the functions). An emerging field of the heterogeneity of glia is focusing on these differences (Matyash and Kettenmann 2010). Overall, it is thought that a single astrocyte should be able to carry out multiple functions simultaneously within its domain (Bushong et al. 2002). It is therefore possible that a mechanism of linking these two sets of functions exists. Potassium channels would make a perfect candidate for this role, due to their abundant expression levels and involvement in both types of

processes: Kir4.1 channels have been implicated in the process of potassium buffering after synaptic activity and control of osmotic balance.

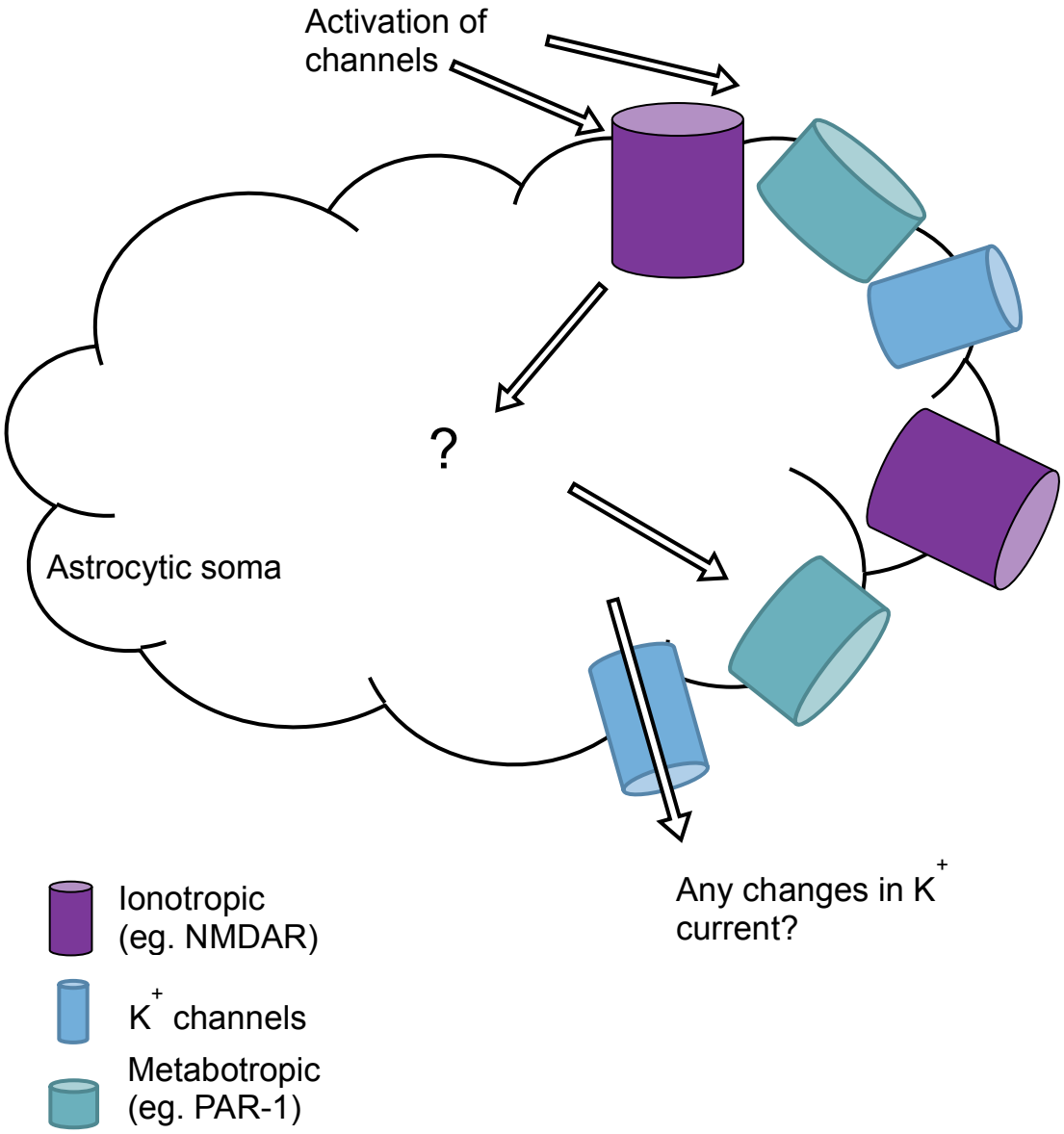

Figure 1.6: **A schematic of the hypothesis**. A diagram of a single isolated astrocytic soma, with typical channels found displayed on the cell surface, depicts the hypothesis. Activation of certain astrocytic channels allows the calcium influx into the cell, where the signal can increase through transduction pathway via the IP_3 channels on the ER. This can then lead to a local change in the conductance of potassium channels.

Firstly, the current densities of potassium currents in astrocytes from the neocortex were to be determined; the changes in current density or susceptibility to blockers during the process of non-pathological ageing were compared to those obtained from young adult mice (to exclude developmental changes). Astrocytes were isolated from the slice preparation to exclude the secondary network and

neuronal effects. Since activation of astrocytes can be achieved by overspill of neurotransmitters in the synaptic and extra synaptic spaces, some agonists of iono- and metabotropic channels, expressed in astrocytes were applied to acutely isolated cortical astrocytes (see Methods and Materials chapter for details of isolation). Potassium currents before, during and after the application of these agonists were measured and some potassium blockers were used to determine which potassium currents were affected, if any. It was expected that activating an astrocyte would result in the up-regulation of the inwardly rectifying potassium channel conductance. Once a relationship, if any, between the stimulated astrocytic channels (in thus study agonists to $P2X_{1/5}$, NMDARs and PAR-1 were used) and the potassium current has been established in isolated astrocytes, it was tested if the same mechanism takes place in slices. Finally, it was investigated whether altering this relationship in slices can affect one of the astrocytic functions – control of concentration of ions in the extracellular space. For this the extent of tissue swelling under various conditions was studied in young adult and older mice, to account for any age-related changes. Some LTP (Long Term Potentiation) experiments were conducted simultaneously with LT (Light Transmittance) experiments to test the signalling function of astrocytes, and if it can also be affected by the same mechanism.

Overall, the aim of this study was to explore any potential links between various channels expressed in neocortical astrocytes as well as finding out how these links can affect both signalling and potassium buffering functions of astrocytes. Collecting these data will help understanding the role of astrocytes and how they perform their roles in a healthy young brain versus a non-pathologically ageing brain. Working with the tissue derived from mice can provide an insight on the processes underlying healthy cognition in humans, thus hoping to improve the current understanding of normal brain functioning as well as bringing closer the

time when it is possible to prevent senility and a myriad of age-related conditions that come as a consequence.

1.7 Nomenclature statement

In this study the potassium channels were explored based on their functionality, as oppose to expression. Therefore, the following jargon was used to refer to specific potassium currents:

- Generic or total potassium current – potassium currents recorded upon the stimulation of astrocyte (with a series of depolarizing voltage steps from holding potential of -80 mV)
- Inwardly rectifying potassium current – current recorded at -130 and -110 mV steps (from holding potential of -50mV), where the dominant potassium current is expected to be the conducted via inwardly rectifying potassium channels (Kir4.1, which are highly expressed in astrocytes (Higashi et al. 2001))
- Steady state voltage gated potassium current or K_D – slowly inactivating delayed rectifying potassium current (Smart, Bosma, and Tempel 1997)
- Rapidly inactivating or K_A current – transient outward potassium current (Gordon, Kocsis, and Waxman 1988)

Chapter 2: Materials and Methods

2.1 Solutions and Drugs used in the project

Name/Abbreviation	Concentration	Activity/Function	Source
KREBS **cutting** solution/aCSF:			
Sodium Chloride/NaCl	130 mM	Used for dissection and slicing the brain.	Sigma Aldrich biochemical (Dorset, UK)
Potassium Chloride/KCl	2.7 mM		
Sodium Bicarbonate/ $NaHCO_3$	18 mM	Continuously perfused with 95% O_2/5% CO_2 to keep the pH at 7.4	
Sodium Dihydrogen monophosphate/ NaH_2PO_4	1 mM		
Glucose/$C_6H_{12}O_6$	10 mM		
Calcium Chloride/ $CaCl_2$	0.5 mM		
Magnesium Chloride/$MgCl_2$	3 mM		
KREBS **experimental** solution/aCSF:			
Sodium Chloride/NaCl	130 mM	Used for recovery chamber, field and LT recordings.	Sigma Aldrich biochemical (Dorset, UK)
Potassium Chloride/KCl	2.7 mM		
Sodium Bicarbonate/ $NaHCO_3$	18 mM	Continuously perfused with 95% O_2/5% CO_2 to keep the pH at 7.4	
Sodium Dihydrogen monophosphate/ NaH_2PO_4	1 mM		
Glucose/$C_6H_{12}O_6$	10 mM		
Calcium Chloride/ $CaCl_2$	2.5 mM		
Magnesium Chloride/$MgCl_2$	1 mM		

New Ringer solution/NR2: Sodium Chloride/NaCl Potassium Chloride/KCl Sodium Dihydrogen monophosphate/ NaH_2PO_4 4-(2-Hydroxyethyl) piperazine-1-ethanesulfonic acid/HEPES Glucose/$C_6H_{12}O_6$ Calcium Chloride/ $CaCl_2$ Magnesium Chloride/$MgCl_2$	 135 mM 2.7 mM 1 mM 10 mM 15 mM 2.5 mM 1 mM	Used for vibro-dissociation[1] preparation of isolated cells and whole cell patch clamping experiments. HEPES regulates the pH, keeping it constant at 7.3 (adjusted with NaOH).	Sigma Aldrich biochemical (Dorset, UK)
Intracellular patch solution: Sodium Chloride/ NaCl 4-(2-Hydroxyethyl) piperazine-1-ethanesulfonic acid /HEPES Potassium Chloride/KCl Ethylene glycol-bis (β-aminoethyl ether) – N,N,N′,N′- tetraacetic acid tetrasodium salt /EGTA Guanosine -5′-triphosphate/GTP Adenosine-5′-triphosphate magnesium salt/mgATP Calcium Chloride/ $CaCl_2$	 12 mM 10 mM 110 mM 0.1 or 10 mM 0.5 mM 5 mM 1 mM	Used for whole cell patch clamping experiments. HEPES regulates the pH, keeping it constant at 7.35 (adjusted with NaOH).	Sigma Aldrich biochemical (Dorset, UK)
4-Aminopyridine/ 4-AP	40 μM	Non-specific voltage-gated K^+ channel blocker	Sigma Aldrich biochemical (Dorset, UK)
Aβ-Methylene	10 μM	Specific $P2X_1$ and $P2X_3$	Sigma Aldrich

[1] See Chapter 2.4 Vibrodissociation

adenosine -5' triphosphate lithium salt/ Aβme-ATP		agonist (at selected concentration)	biochemical (Dorset, UK)
Adenosine triphosphate/ ATP	10 μM	P2 receptors agonist	Sigma Aldrich biochemical (Dorset, UK)
Barium / Ba	100 μM	Specific inwardly rectifying potassium channel inhibitor	Sigma Aldrich biochemical (Dorset, UK)
3,5-Dimethyl-tricyclo [3.3.1.13,7] decan-1-amine hydrochloride / Memantine	3 μM	An antagonist to NMDA receptor	Tocris Bioscience (Bristol, UK)
N-methyl-D-aspartic acid/NMDA	10 μM	Prototypic NMDA receptor agonist	Tocris Bioscience (Bristol, UK)
Thr-Phe-Leu-Leu-Arg-NH_2 /TFLLR	10 μM	PAR-1 selective agonist	Tocris Bioscience (Bristol, UK)

Table 1: **Solutions and drugs used in the project.**

2.2 Animals

Animal work was approved by AWERB and carried out in accordance with UK legislation and adhering to the '3R strategy''. Animals used were GFAP-EGFP$^{+/+}$ (Nolte et al. 2001) and their littermates, kept in Standard Housing conditions (1989). Mice were divided into 4 groups based on their age:

Group I	1-3 months PN (Post Natal)
Group II	6-9 months PN
Group III	9-12 months PN
Group IV	12-24 months PN

The groups refer to these ages unless otherwise stated.

2.3 Slice preparation

Mice were anaesthetised with sufficient IsoFluorane to induce unconsciousness, followed by cardiac arrest and death (Schedule 1 procedure)(1989). Upon the confirmation of death the animals were decapitated and the brain was removed rapidly (typically in under 1 minute), and placed in the ice-cold aCSF (see Table 1 for solution details) in the vibratome chamber for slicing. Coronal slices of 300 μm thicknesses were cut from the somato-sensory cortex and placed into recovery chamber with aCSF gassed with 95% O_2 and 5% CO_2 at room temperature for 2-2.5 hours to recover prior to the experiments.

2.4 Vibrodissociation

For experiments with isolated astrocytes and neurons a technique called vibrodissociation (Vorobjev 1991) was used. A micro capillary ending with glass ball 200 μm in diameter was moved across the surface of the neocortical slice, vibrating at 100 Hz (lateral displacement 20-30 μm). This process mechanically dissociates the cells out of the slice, leaving them viable. The benefit of using this technique compared to enzymatic restriction is that vibrodissociation does not cause any chemical changes to the cell membranes, leaving them intact. This method is therefore an effective tool for studying cellular mechanisms in the brain by taking integral cells out of the slice. Figure 2.1 illustrates the set up of the vibrodissociation technique. The vibrating ball was moved across the slice over layers II/III of somatosensory cortex multiple times to increase the number of dissociated cells. The slices were discarded after about 5 minutes of

vibrodissociation.

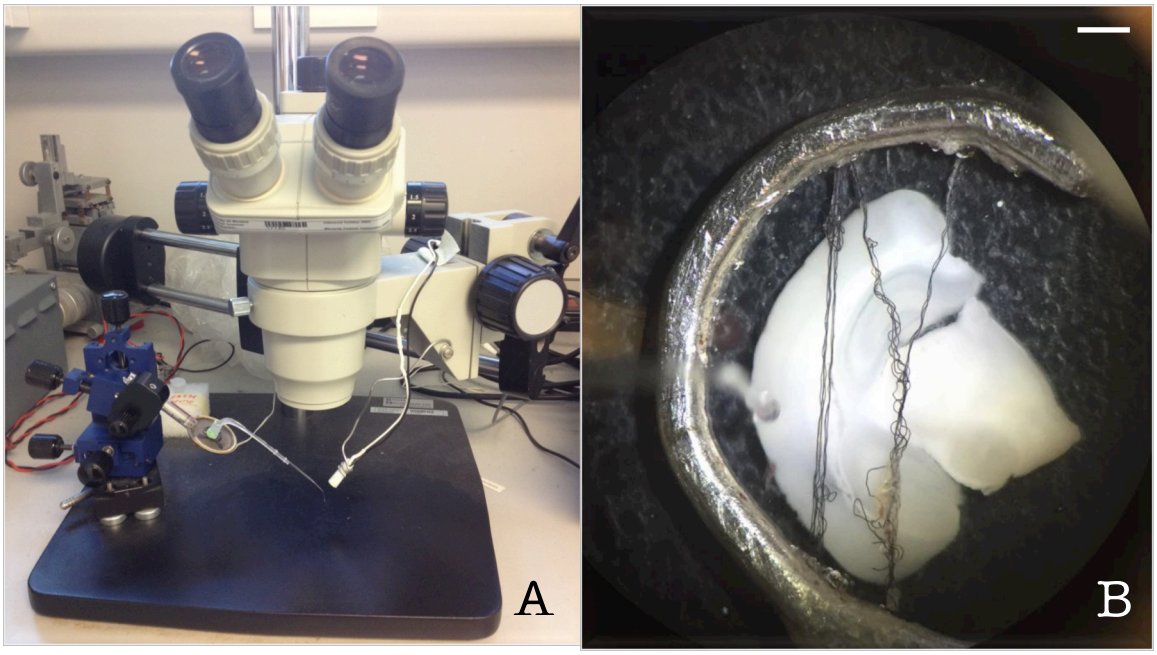

Figure 2.1: **Acute vibrodissociation set up**. A – Microscope and micro capillary with a vibrating glass ball on the end, B - the view through the objective (20X magnification) of the coronal slice with typical position of glass ball. Scale bar, 1 mm.

2.5 Whole-cell patch clamping isolated cells

The preparation of isolated cells was kept in the recording chamber for the cells to settle to the bottom of the recording chamber, where they adhere to the glass surface. Unhealthy cells float and therefore are lost during the perfusion. Electrophysiological recordings were made from isolated cells suspended in the New Ringer solution being perfused through the bath chamber (see Figure 1 for composition) at 1.5-2 ml/min. Patch pipette were made of borosilicate glass capillaries of 1.5 mm diameter (World Precision Instruments, USA), pulled with a laser micro pipette puller (Sutton Instrument P-2000). Pipettes were differential sizes for neurons (4-5 MΩ) and astrocytes (6-8 MΩ) and filled with intracellular solution (see Figure 1 for solution composition). The AxoPatch200B patch-clamp amplifier (Axon Instruments, USA) was used to observe the currents and those were filtered at 2 kHz and digitized at 4 kHz. To control the experiments the data acquisition board PCI-6229 (NI, USA) was used. Cells with input resistance of 500-

1100 MΩ and 50-150 MΩ for neurons and astrocytes respectively, with less than 20% variation throughout recordings, were used for the analysis (Pankratov et al. 2007; Pankratov et al. 2009).

2.5.1 Cell identification: astrocytes *vs* neurons

Astrocytes and neurons were distinguished by their corresponding morphology and input resistances. Figure 2.2 shows examples of the typical morphologies displayed by astrocytes and neurons (A and B respectively) and the currents evoked from a series of voltage steps (C and D). Morphologically, the neuronal cell body is much larger than that of a cortical astrocyte. Upon the isolation process neurons normally keep their axons intact, whereas astrocytes tend to lose their fine projections and are left mostly with the soma.

Electrophysiologically, the main difference between neurons and astrocytes is the inward sodium current, which is absent in astrocytes (Perea and Araque 2010). Astrocytes can also be distinguished from oligodendrocytes for the same reason – oligodendrocytes display a small inward sodium current (Fields 2008). Compared to published data, the currents recorded in isolated astrocytes are smaller than reported values (Bekar 2004). This is most likely due to the loss of fine projections that contain a high number of channels, and thus correspond to the overall current. Currents recorded from slices, however were similar in size to the published values (Pannicke et al. 2000).

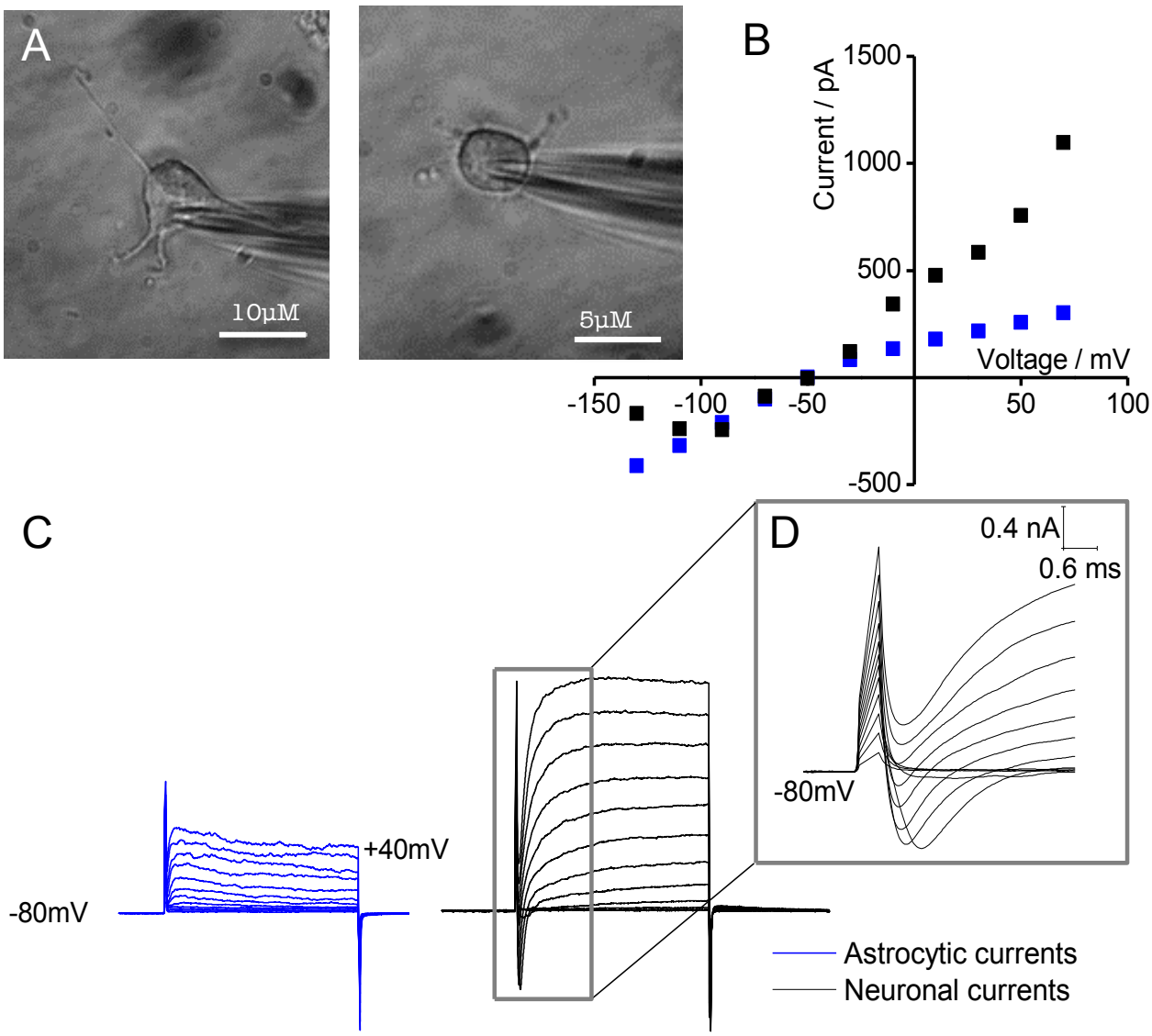

Figure 2.2: **Isolated neurones and astrocytes have distinctive electrophysiological and morphological properties.** A- Isolated astrocyte (right) and neurone (left), B – typical I/V curves from isolated neurone (black) and astrocyte (blue), C – typical currents of astrocyte and neurones in response to depolarising voltage steps from holding potential -80 mV, D - Inward sodium current of an isolated neurone.

2.5.2 Patch clamping in slice

WinFlour software (Strathclyde University, UK) was used to record the currents from layers II/III of somatosensory cortical astrocytes in coronal slices. A protocol with 9 consecutive voltage steps, from -130 mV to +30 mV, from a holding potential of -50 mV, was used to record both the inwardly rectifying potassium current, which is most prominent at the lowest 2-3 steps of this protocol and the voltage gated potassium current, which is considered to be the dominant subtype

of current at the highest voltage steps of this protocol. Another protocol, with one voltage step from the holding potential of -80 mV to -70 mV was used for calculating the capacitance and for controlling the health of the patched cell.

2.5.3 Patch clamping isolated cells

For isolated cells WinWCP (Strathclyde University, UK) was used to record from isolated neurons and astrocytes. Four protocols were used to gather electrical currents from cells.

Firstly, to watch the health of the experimental cell, a single 10 mV step protocol (from a holding potential of -80 mV to -70 mV) was recorded throughout the experiment. The capacitance of the cell and input resistance was calculated at the start of the experiment. As stated above, the cells with greater variation than 20% from the normal range (50-150 MΩ for astrocytes and 500-1100 MΩ for neurons) were not used for data analysis. The experimental leak was also estimated from this protocol; any experiments with abrupt leak changes were excluded from the data collected.

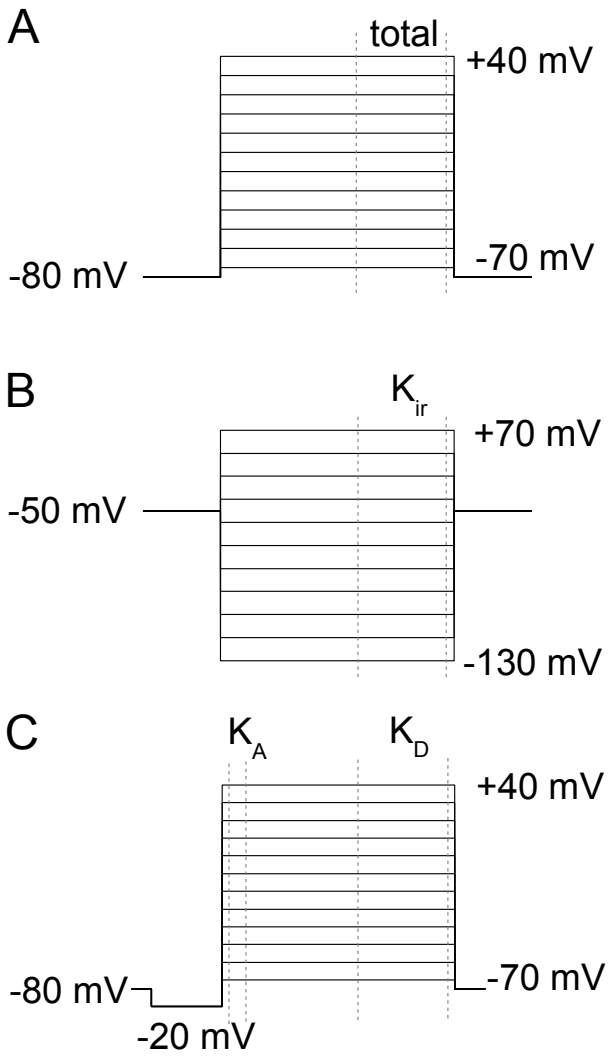

Figure 2.3: Voltage protocol used in the study. A – Protocol to record sodium current in neurones and total potassium current in astrocytes. B – Protocol to record inwardly rectifying potassium current. C – Protocol with a pre step to deactivate inwardly rectifying potassium current and measure voltage-gated current.

Figure 2.3 illustrates structure of protocols, used to record currents in this study. A series of voltage steps were used to record sodium current in neurons were also utilised to test for the absence of a sodium current in astrocytes: the holding potential was kept at -80 mV, to keep the glial cell healthy, and 12 voltage steps were recorded from -70 mV to +40 mV. The current recorded at the highest voltage steps of this protocol is referred to as total potassium current throughout this thesis.

Thirdly, a protocol that recorded both inwardly rectifying and voltage gated potassium currents consisted of 11 voltage steps from -130 mV to +70 mV from a holding potential of -50 mV. At lowest voltage steps the majority of the current is conducted through the inwardly rectifying potassium channels, whereas the highest voltage steps display mainly the voltage sensitive potassium current. To exclude the influence of the inwardly rectifying potassium channel, another protocol with a deactivating pre-step was devised. The holding potential was -80 mV and again 12 voltage steps were recorded from -70 mV to +40 mV but with a -20 mV pre-step.

2.6 Field recording

The fEPSPs were measured in cortical slices; the recording electrode was placed in layer 2/3 of the somatosensory cortex. A thin walled glass pipette with resistance of 1-2 MΩ was filled with the same aCSF used for perfusion of brain slices. To induce fEPSPs, the concentric bipolar microelectrode with 127 μm thick core diameter and 4 μm thick tip diameter (World Precision Instruments, USA) was used as stimulation. The stimulating electrode was placed atop layers IV/V, parallel to the recording electrode. A constant current stimulator isolator (A.M.P.I. ISO-Flex Instrumentation Canada Inc.) was used. In order to measure synaptic plasticity, either LTP (Long Term Potentiation) or STP (Short Term Potentiation) was recorded. Theta Burst Stimulation (TBS) was applied to the slice to produce a change in synaptic plasticity. Each TBS is made of ten repetitions of High Frequency Stimulation (HFS) trains with 200 ms intervals between bursts; each burst consisted of 5 pulses at 100 Hz. Different combinations of one, two or five TBS were applied to slices to induce synaptic plasticity. Before the onset of TBS, a control fEPSPs were recorded for approximately 10-15 minutes to establish a steady baseline with stimulation that caused a response of 30-50% of maximal intensity.

To analyse recordings, the slope of the post-synaptic component of the fEPSP was calculated as a difference in amplitude between t_1 and t_2 (see Figure 2.3B). Slope values were then normalised to t_0 – the last slope measurement prior to TBS stimulation. Figure 2.4 shows the region of the recording where the post-synaptic slope was measured. The slopes were then presented as percentage of baseline (t_0) fEPSP.

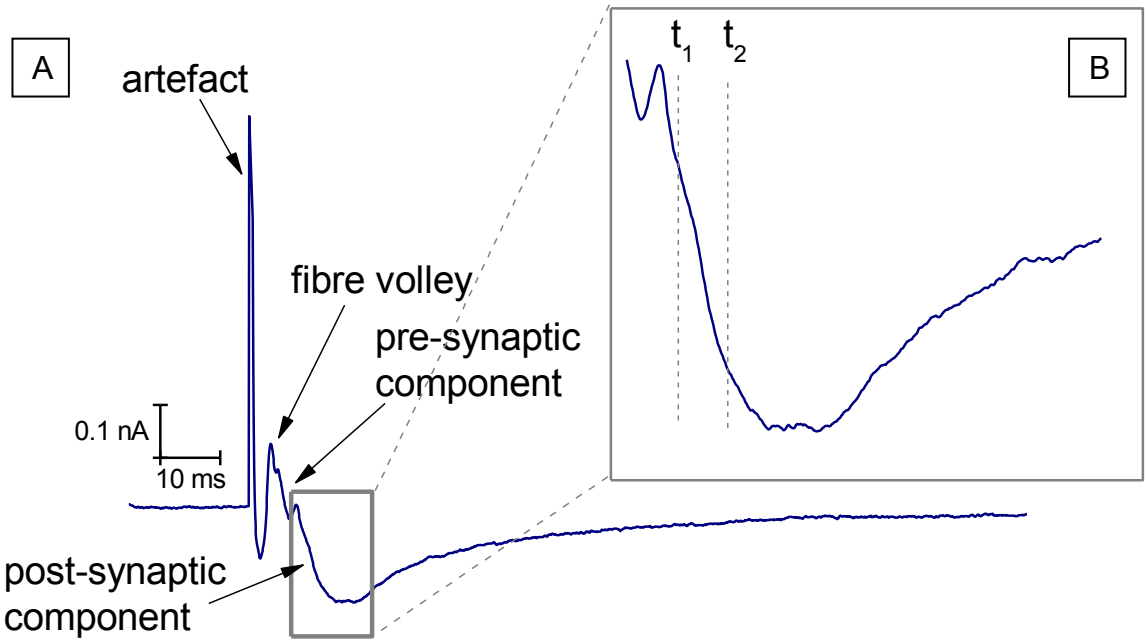

Figure 2.4: **Slope analysis of a fEPSP (panel A).** Typical trace recorded during field recording experiments. Slope of post-synaptic component is measured between points t_1 and t_2, shown on panel B; note the artefact of the recording is clipped.

2.7 Light Transmittance (LT) experiments

The coronal slices were placed into the recording chamber, where they were perfused at with KREBS aCSF (see Table 1 for details on composition) at 2.5-3.5 ml/min rate and whilst being oxygenated with 95% O_2 and 5% CO_2. Simultaneously with field recording, the video frames of light trans illuminated slice were obtained at 0.3 Hz for short experiments (20 minutes long) and at 0.1 Hz for long experiments (20 minutes with 0.3 Hz frequency followed by 50 minutes at 0.1 Hz). The fEPSP data was analysed using WinWCP software (Strathclyde

University, UK), whilst the corresponding LT data was analysed using ImageJ software (National Institutes of Health, NIH).

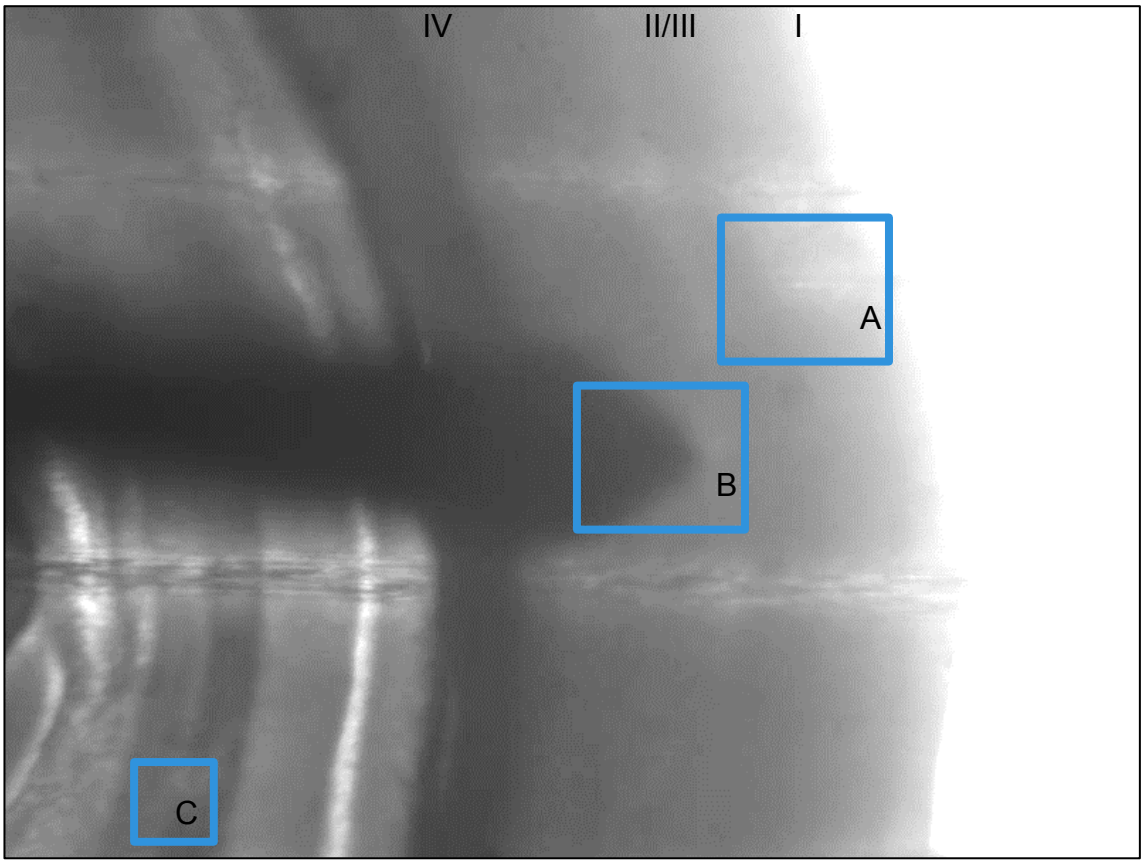

Figure 2.5: **Experimental set up for LT experiments**. A coronal slice of somatosensory cortex with recording (box A) and stimulating (box B) electrodes positioned in layers II/III and IV/V, respectively. Box C shows control region of slice, used to monitor health of tissue and signal quality of recordings.

2.8 Data analysis

2.8.1 Whole cell recordings

Cells accepted for analysis had to pass two criteria: cell input resistance should be within the respective ranges and vary less than by 20% throughout the experiment (input resistance for neurons 500-1100 MΩ and 50-150 MΩ for astrocytes).

Capacitances of astrocytes were calculated from a 10 mV step from holding potential -80 mV to -70 mV by multiplying the artefact of the recording by the $\tau_{(decay)}$. Since the soma of the astrocytic cell is close to round in shape, and following vibrodissociation the cell body takes up a more round form, this was a

close approximation to the true size of the cell patched. Current densities of astrocytes were also calculated for different age groups to look for any potential changes that take place in cortical astrocytes during the process of ageing. These results can be found in Chapter 3.

To find the effect of the drugs a ratio was calculated, where the current under the drug application was divided by the average of current in control and washout parts of recording. The same process was undertaken for all drugs used. For experiments where potassium current blockers were added prior to the application of the drug, the average between the currents measured under the blocker and after the washout of the drug (still under the influence of the potassium current blocker) was used as control for analysis. Examples of representative recordings with three currents: control, current under the application of the drug and the washout current, were constructed as well as single ratios of currents (described above) plotted as bar charts. This was done for every experimental condition to build a full representative illustration of the data gathered throughout the project.

2.8.2 Field recording

In order to analyze synaptic plasticity, alterations in the slope of the fEPSPs were compared throughout the recording. To compare the changes in the slope of the fEPSP, a time zero (T_0) was defined as the last point before the TBS was given to the slice. The average current from T_{-5}–T_0 was used as 100% value against which the consecutive fEPSPs were measured. Figure 2.5 illustrates a typical fEPSP recorded in the coronal slice with stimulation located in layer IV/V and post-synaptic response recorded in layer II/III of the somatosensory cortex. As stated above, STP and LTP were calculated at 20-30 and 50-60 minutes respectively. Experiments were represented as both typical examples of time courses and average single value for STP and/or LTP in bar charts.

2.8.3 Light Transmittance (LT) experiments

Regions of interest (ROI) were chosen to calculate any differences in the light transmittance of the brain slice. A typical selection of ROIs is shown on Figure 2.5: one control area to measure background noise, and two ROIs near the recording electrode to measure the change in light transmittance due to activity of the tissue. A time zero (T_0) was defined as the last time point before the TBS was given to the slice. Similarly to the fEPSP analysis, the average of 5 time points before the T_0 was set as the 100% of the response. The following points were represented as T_t/T_0 ratio. Similarly to the field recordings, LT experiments were plotted against the time to show typical time courses of the experiments and the highest peaks (ratios of T_t/T_0) during the activity of the tissue were plotted in bar charts for each of the experimental conditions.

All data are presented as Mean±SEM unless otherwise stated.

Chapter 3 – Age differences in astrocytes

Electrophysiological characteristics of cortical astrocytes with specific focus on Potassium currents

3.1 Aim and hypothesis of the chapter

The aim of this part of the project was to gain an insight into the electrophysiological changes that occur in astrocytes with age. There are multitudes of subtypes of glial cells in the brain, all with their specific electrophysiological characteristics and functions (Matyash and Kettenmann 2010; Rose and Kirchhoff 2015; Oberheim, Goldman, and Nedergaard 2011). It is therefore vital to study the individual types of astrocytes, to avoid the differences in subtypes of glial cells in the brain based on their location (in this case layer II/III of somatosensory cortex). Cortical astrocytes were chosen because of their abundance and well-studied functions: participating in the plasticity of the brain as well as keeping certain metabolic characteristics constant (Kimelberg and Nedergaard 2010).

To find out if there is any electrophysiological differences between the young adult mice of group I (1-3 months postnatal). This includes comparing the size of the cell bodies of astrocytes, the current densities for total potassium current, inwardly rectifying and voltage-gated potassium currents; and the proportions of the current that is blocked by the addition of specific potassium current blockers: 4-aminopyridine (4-AP) and barium (Ba). Two methods were used for this latter test: a combined effect of addition both of the blockers and addition of the blockers separately in different experiments. The null hypothesis was that **there is no difference** between any of the above-mentioned characteristics of the **astrocytes in groups I and III** (1-3 and 9-12 months postnatal). If the null hypothesis was correct, the conclusion to follow should be that the age introduces

no change in the electrophysiological properties of cortical astrocytes in the somatosensory cortex of mice.

3.2 Capacitance of cortical astrocytes

The capacitances of the astrocytes were calculated from the tau decay (T_{dec}) and the artefact height of the +10 mV step from holding potential of -80 mV. This is a characteristic, proportional to the size of the spherical cell body of the astrocytes, that remains after the Vibrodissociation process (see Methods chapter for details) (Vorobjev 1991). It is assumed that proportion of cellular extensions lost during the dissociation process is similar in both Group I and Group III and that therefore, the isolation method does not introduce any differences in cell size.

Capacitances were plotted for young adult and old mice, as distributions and linear regression of capacitances and current density, as can be seen on Figure 3.1 (panels B and D, respectively). There is a clear right shift that is consistent with large sample size and small error, which leads to believe that there is a tendency for the capacitance of the cell to increase with age. From the frequency distribution (see Figure 3.1) of capacitance it can be seen that there is a shift in the distribution towards the increase when comparing astrocytes from old mice to those of young adult mice. This positive shift in the capacitances of the astrocytic cells with regards to age signifies a shift in the cell size. Since the capacitance is a measure of the ability to hold the electrical charge, in a round body it is proportional to the size of this body. Therefore the positive shift in the capacitances distribution displays the positive shift in the cell body sizes of the astrocytes of old mice. Since there is no sharp increase in the numbers of cells with the highest capacitances; instead the shift appears rather gradual and small changes appear on majority of cells, not a handful of extremely large cells. These data supports the idea that astrocytes increase in size with age (Schipper 1998). This could be potentially due to increased number of reactive astrocytes in age group III (9-12 months) that

corresponds with enhanced production of GFAP (Hayakawa, Kato, and Araki 2007).

A weak positive correlation was found between current density and capacitance size (panel D, Figure 3.1). The R numbers were 0.39 and 0.41 for groups I and III respectively. This shows a correlation between the size of the capacitance – which in itself is a measure of volume of isolated astrocytic soma and the current density that is measured in each cell. An existing correlation allows some assumptions about the size of the cells to be made from measuring the current density. However, because this correlation is weak, current density cannot substitute the classic I/V measurement. Therefore, the data for current/voltage relationship is presented as current and not current density, thus providing a better representation of current measured.

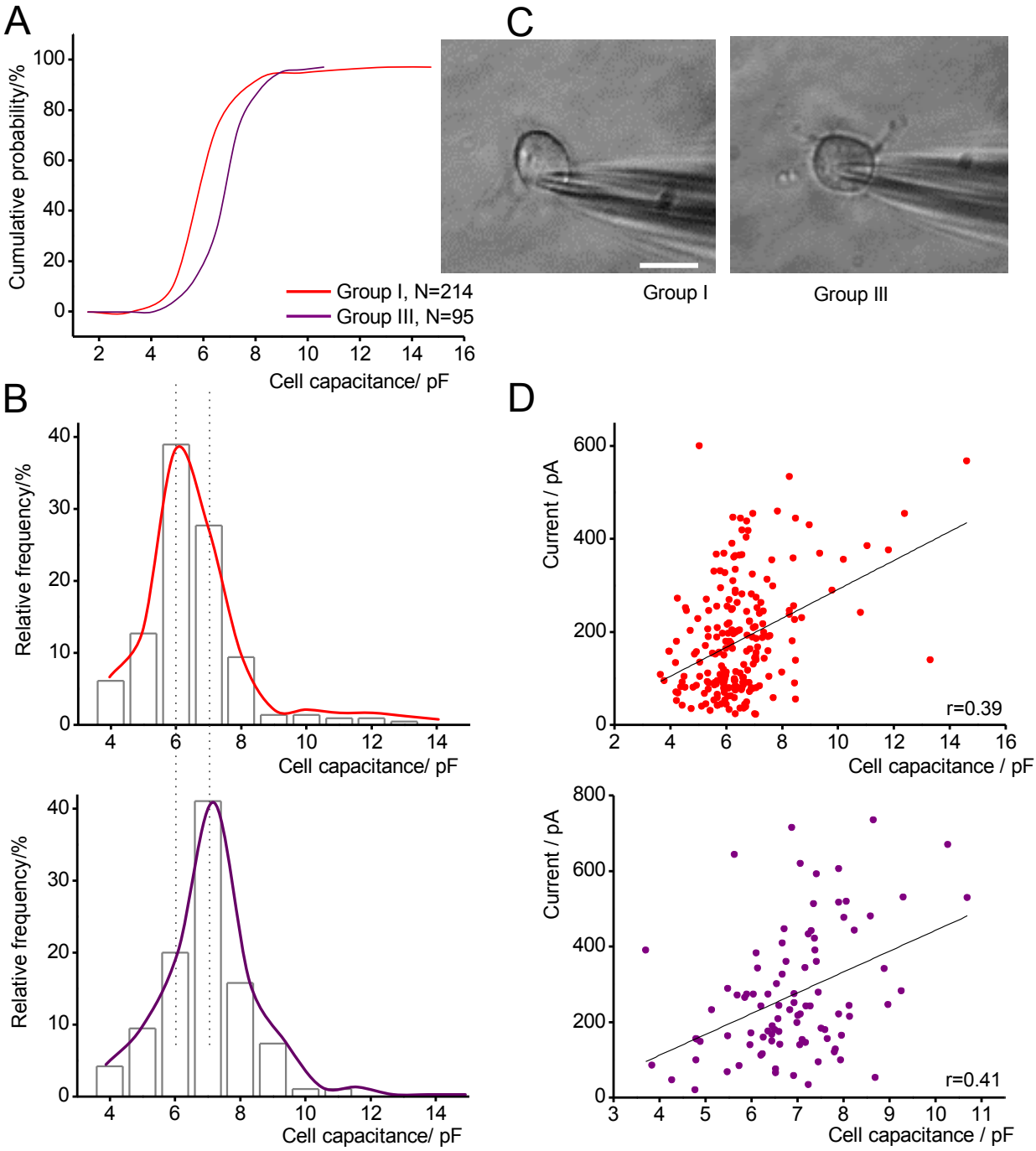

Figure 3.1: **Cell capacitance significantly increases with age**. A – Probability distribution of cell capacitances of astrocytes from young adult and old mice (1-3 months and 9-12 months old, respectively). B – Relative distribution of cell capacitances in young (red) and old (purple) mice. C- Representative isolated cells from group I (left) and group III (right). D – Current/cell capacitances linear regression relationships in groups I and III (voltage step +30mV). Cell capacitances of young mice was significantly lower than old mice ($p<0.01$).

3.3 Current densities of cortical astrocytes

Current densities were calculated for young adult and old mice. This was done by normalising the current evoked at +40 mV from -80 mV holding potential, at -130 mV step from holding potential -50 mV and +40 mV from holding -80 mV with a deactivating pre-step of -20 mV (both the steady state and the rapidly desensitizing potassium current). These current densities are corresponding to total potassium current, inwardly rectifying and steady state and rapidly deactivating voltage-dependent potassium currents respectively. Measuring the current density can help take into the account the size of the astrocytic cell body and thus provides a better electrophysiological description of the astrocyte. This measurement can help in investigating whether the astrocytic cells experience and increase or decrease in number of potassium channels present on the cellular membranes, as the mouse grows older. The limitation of this measurement is that only the channels present on the membrane of the cell body were measured, as finer astrocytic projections were lost during the cell isolation process. The results were differential, and are illustrated and described below.

3.3.1 Total potassium current densities

To compare total or combined potassium current produced by the cortical astrocytes in young adult and old mice, a current was evoked by a voltage step from holding potential of -80mV to +40 mV, thus imitating a stimulation of the glial cell. Astrocytes do not exhibit voltage-dependent sodium channels and therefore the entire current that is evoked is attributed to the opening of the potassium channels present in the surface of the cell body of the isolated glial cell. The findings below are presented as current density, which as explained above is the amount of current conducted per unit of capacitance. Figure 3.2 shows the distributions and the mean current densities of two pools of astrocytes: from young adult and old mice. It is clear that there is a shift to the right from the young to old mice, with an increased number of cells with very high current

densities. A handful of cells with current densities of 100 pA/pF or above appear in Group III that were not present in Group I. As well as a few cells with very high current densities, the proportion of cells with the lowest densities is significantly diminished in the older group of cells. Therefore, not only the clear shift for an increased current density at +40mV is apparent but also the appearance of some cells with very high current densities. The cells with extremely high current densities could potentially be those astrocytes that have been activated and are part of the reactive gliosis of the brain – an event that can take place in older brain tissue (Hablitz et al. 2000). The mean current density almost doubles going from young adult to old mice.

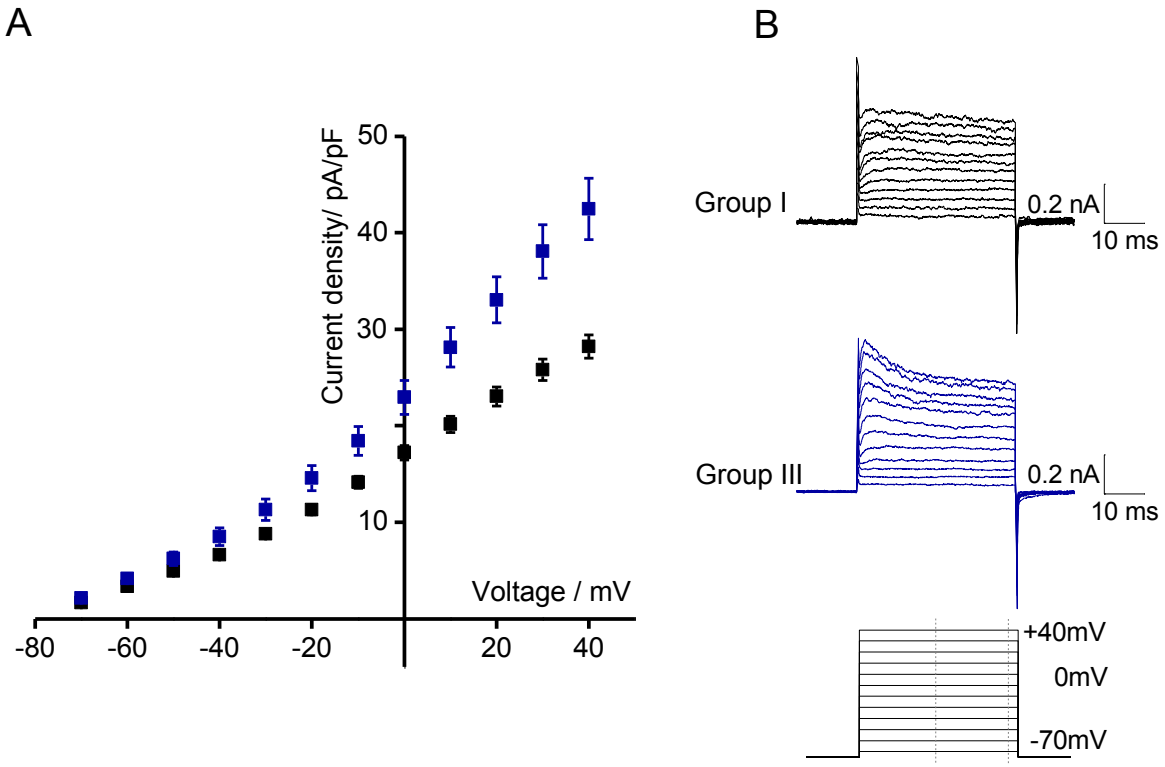

Figure 3.2: **Current density of total potassium current decreases with age.** A – Current/voltage relationship of cells from young (black) and old (navy) mice. B – Representative traces from cell derived from mice group I and III (1-3 and 9-12 months old, black and navy, respectively), recorded in response to a set of depolarising voltage steps from holding potential -80mV. The average current density was calculated to be 25.9±1.0 pA/pF and 42.5±3.2 pA/pF for astrocytes from young adult and old mice respectively. Two sample t test showed that the average current density is greater in the old astrocytic cells than in young adult ($p=0.1*10^{\wedge-6}$ when current densities for total potassium currents evoked at +40mV in young adult and old mice were compared).

3.3.2 Inwardly rectifying potassium current densities

In order to compare the inwardly rectifying potassium current of old and young adult astrocytic cells of mice, the following protocol was used: a series of voltage steps from -130 mV to +70 mV with holding potential of -50 mV was recorded. The inwardly rectifying potassium current is conducted mainly through the Kir4.1 potassium channel subtype (Verkhratsky and Steinhäuser 2000; Higashi et al. 2001). This subtype has an equilibrium potential of -90 mV, thus making the two lowest voltage steps, -130 mV and -110 mV displays predominantly the current conducted by K_{ir} channel in astrocytes (Butt and Kalsi 2006). As can be seen from Figure 3.3, there is no significant shift in the distribution of the current densities due to age of the animal used. Mean current density also does not change between young adult and old mice. Thus, it can be concluded that there is no significant change in the current density of the inwardly rectifying potassium current due to the process of ageing.

Currents evoked on depolarising voltage steps (-30 mV and above) show a higher current density in older mice. As can be seen from Figure 3.3, the current/voltage relationship is different between two groups. For example, the mean current density of the +70 mV step of old mice is much greater than that of the young adult mice, 34 pA/pF against 20 pA/pF. Since the repolarising voltage steps do not display such a pattern, this change therefore arises from other potassium channel subtypes, perhaps such as delayed rectifier potassium channel (Hablitz et al. 2000).

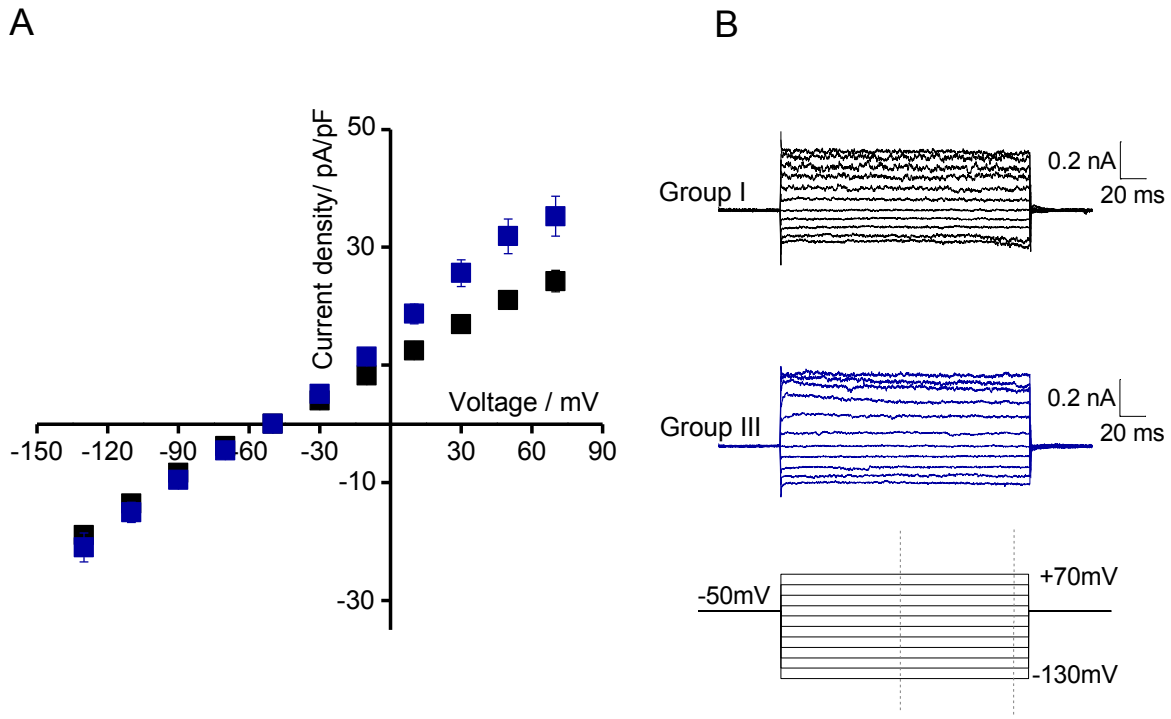

Figure 3.3: **Current densities of inwardly rectifying potassium current do not change with age.** A – Current/voltage relationships of cells from young (black) and old (navy) mice. B – Representative traces from cell derived from mice group I and III (1-3 and 9-12 months old, black and navy, respectively), recorded in response to a set of repolarising and depolarising voltage steps from holding potential -50 mV. The two-sample student t-test found no significant difference between the current density of the inwardly rectifying potassium channel in young and the old astrocytes (p=0.8). At repolarising voltage steps the difference between current densities of young and old mice is significant ($p=4.1*10^{-9}$).

3.3.3 Voltage gated potassium current densities

A third protocol, with a deactivating pre step of -20 mV was recorded. This was done to exclude other potassium currents except for the voltage gated potassium currents. The currents evoked had two segments: the rapidly desensitizing potassium current, measured at the start of the recording and immediately after the artefact (Tokimasa and Nishimura 2013); and the steady state potassium current (slowly inactivating potassium current), measured across the second half of the evoked current (Bordey and Sontheimer 1999). Figure 3.4 below shows the steady state and rapidly desensitizing potassium current densities respectively. The current densities for the steady state potassium current display a similar positive shift as the total potassium currents. The proportion of cells with very low current density is halved in the astrocytes of old mice when compared to young adult mice. The frequency of cells with higher current densities is increased in the old astrocytes as well. Also the mean current density is higher by approximately 40% in old astrocytic cells (96 pA/pF in young adult astrocytes compared to 152 pA/pF in old astrocytic cells).

When the current densities were calculated for the rapidly inactivating part of the current, a different distribution was acquired. In astrocytes of young adult mice there were very few cells with the lowest current density, whereas in the steady state segment of the current this was a frequent density. This shows that overall; in the young astrocytes the rapidly desensitizing potassium current displays greater current density than the steady state potassium current. There were a higher number of cells that exhibit a rather large current density of 100 pA/pF and above for the rapidly desensitizing compared to the steady state potassium current. However, there is still a clear shift for the increase of the current density for the rapidly desensitizing potassium current from the cortical astrocytes from young adult mice to old mice. The number of cells that have the lowest current density

decreases, and the cells with higher current densities become more abundant. The mean current density was calculated to be 111pA/pF for the astrocytes from young adult mice and 167 pA/pF for the astrocytes isolated from the slices of old mice.

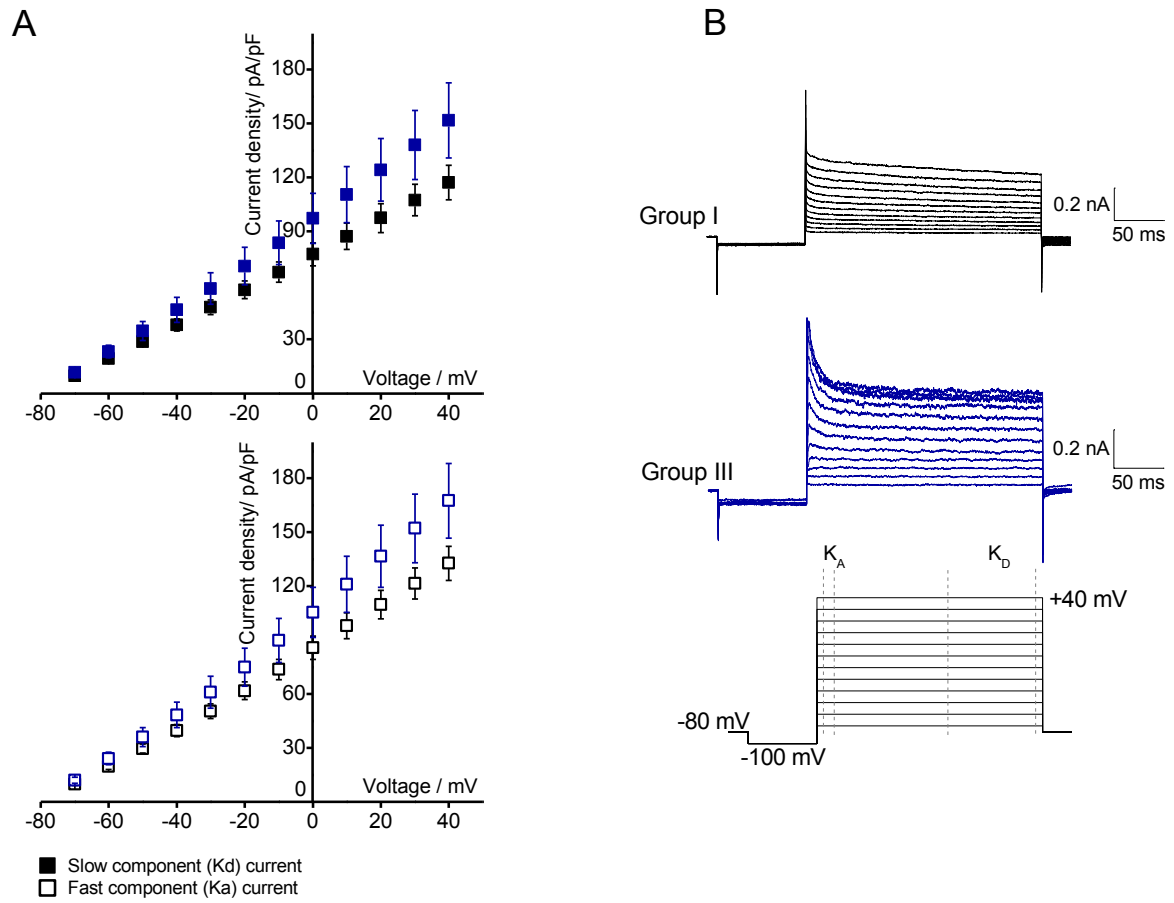

Figure 3.4: **Current densities of steady state and rapidly inactivating voltage gated potassium current are higher in astrocytes isolated from old mice.** A – Current/voltage relationship in young (black) and old (navy) astrocytic cells. B – Representative traces from cell derived from mice group I and III (1-3 and 9-12 months old, black and navy, respectively), recorded in response to a set of depolarising voltage steps from holding potential -80 mV with a deactivating pre-step of -20 mV. Young adult cells have the average steady state current density 94.7±6.2 pA/pF compared to the average current density 151.7±20.9 pA/pF for astrocytes of old mice. Rapidly inactivating current density is 110.8±6.1 pA/pF and 167.5±20.8 pA/pF for young and old mice, respectively. Two-sample student t test showed that current densities are significantly greater in older mice for both current components ($p = 0.0004$ for K_D and K_A).

3.3.4 Conclusions for comparing capacitances and current densities of astrocytes

The data presented above illustrates the difference in capacitance and current densities of acutely isolated cortical astrocytes of young mature and old mice. It was shown that the mean capacitance increases with age, thus complying with the notion that astrocytes increase in size, but not numbers during the process of ageing (Amenta et al. 1998; Finch 2003). Total potassium current as well as both delayed rectifier (also referred to as steady state potassium current) and rapidly desensitizing potassium current all increase their respective current densities by 41%, 37% and 34% respectively. When measuring the current densities of astrocytes of young adult and old mice, it was found that inwardly rectifying potassium current it the only subtype of potassium currents that does not increase in its' density with age. These differential age-related changes in the current density of potassium currents

3.4 Blocking differential potassium currents with 4-aminopyridine and barium

To investigate the average electrophysiological profile of cortical astrocytes a number of potassium channel blockers was used; namely 4-aminopyridine and barium, at 40 and 100 μM concentrations respectively (Bordey and Sontheimer 1999; Hibino et al. 2010). Two methods were implemented: in some experiments either of the blocker was used and the total amount of current blocked was added up from multiple recordings, whereas in other experiments both of the blockers were used in the same recording in increments.

The proportions of the total potassium current of astrocytes may change with age, which could give rise to consequent greater alterations or disturbances of the astrocytic function. Any alterations of the proportions of potassium current due to age demonstrate the changes in either the quantity or quality of the potassium channel subtypes. As has already been shown, the current densities of potassium

channel subtypes do indeed change as a result of age, and more importantly change they change differentially; that leads to expectations of more prominent changes in the potassium channel subtypes fractions in the total potassium current measured in the isolated astrocytes.

3.4.1 Individual blockers for separate experiments

Recordings were conducted in a following manner: for each cell the control current was recorded before the addition of the blocker and its' consecutive washout. All of the results are presented as percentage ratios of the potassium current inhibited by the addition of the blocker over the average current (average between the control and washout currents). Similarly to current densities, multiple ratios were calculated for different current subtypes and for multiple voltage steps, i.e. two highest and two lowest steps of the recording protocol.

3.4.1.1 Proportion of total potassium current sensitive to 4-aminopyridine blocker in young and old mice

The fractions of the potassium current in astrocytes from young adult and old mice that is susceptible to blockage by a non-selective voltage-dependent blocker called 4-aminopyrimidine at 40 μM was calculated. This blocker is widely used in research as an anti-convulsant as it aids the generation of seizures in animal models of epilepsy (Avoli and Jefferys 2016; Frenguelli and Wall 2016). This blocker inhibits both Kv1.1 and Kv1.2 potassium channel subtypes at the concentration used (Bordey and Sontheimer 1999). By comparing the fractions of the overall current that can be blocked by the bath addition of 4-aminopyridine in different age groups, one can find out whether the composition of the potassium current produced by the astrocytes alters depending on age. The data were collected for all three protocols used in the electrophysiological recordings of isolated astrocytes, and are presented below as bar charts of the current that was sensitive to the 4-aminopyridine block (as percentage of the overall current of the experiment).

Figure 3.5 illustrates the proportion of total potassium current that is sensitive to 4-aminopyridine. The fraction appears to be fairly similar in lowest and highest voltage steps of the recording protocol; it fluctuates around the 25 per cent mark of the total potassium current, with the lowest being 23.5 per cent and the highest 29.4 per cent. When comparing the different age groups to each other there appears to be little difference between proportions of the current that is sensitive to this blocker. Taken together with the results obtained for the current density of the total potassium current, it seems that although the current density of the total potassium current increases with age by 41 per cent (for +40 mV step in this protocol with holding potential -80 mV), the fraction of the current that is sensitive to voltage-gated potassium current blocker does not change. It is therefore possible to suggest that the increase in the current density does not take place due to voltage-gated potassium channel subtypes.

A similar result illustrated on Figure 3.6 was obtained with the second experimental protocol, which consisted of 11 voltage steps from (-130 mV to +70 mV) the rest potential of -50 mV. The proportion of the current blocked by 4-aminopyridine was within the range established from the data from the protocol recording the total potassium current, i.e. 23.5-29.4 per cent of the total current was blocked by the addition of 40 μM 4-aminopyridine. At lower voltage steps, where the inwardly rectifying potassium current is most prominent, there is no change in proportion of current that is susceptible to 4-aminopyridine.

Figures 3.7 and 3.8 show the fractions of the overall potassium current that are blocked by 4-aminopyridine in steady state and rapidly desensitizing potassium currents respectively. The data for both Figures was gathered in a single protocol, with a deactivating -20 mV pre step and a series of voltage steps from holding potential of -80 mV. None of the voltage steps display a significant change due to

age in the proportion of the potassium current that is susceptible to 4-aminopyridine, as tested with the two-sample t test. However, in the steady state current, at high voltage steps there seems to be a trend for a decrease in the 4-aminopyridine sensitive current.

Altogether the comparison of the effect of 4-aminopyridine on potassium currents in astrocytes from different age groups shows no significant alteration due to age. This means that the functioning of the voltage-gated potassium currents remains the same throughout the lifespan of mice, granted the lack of development of any pathological conditions.

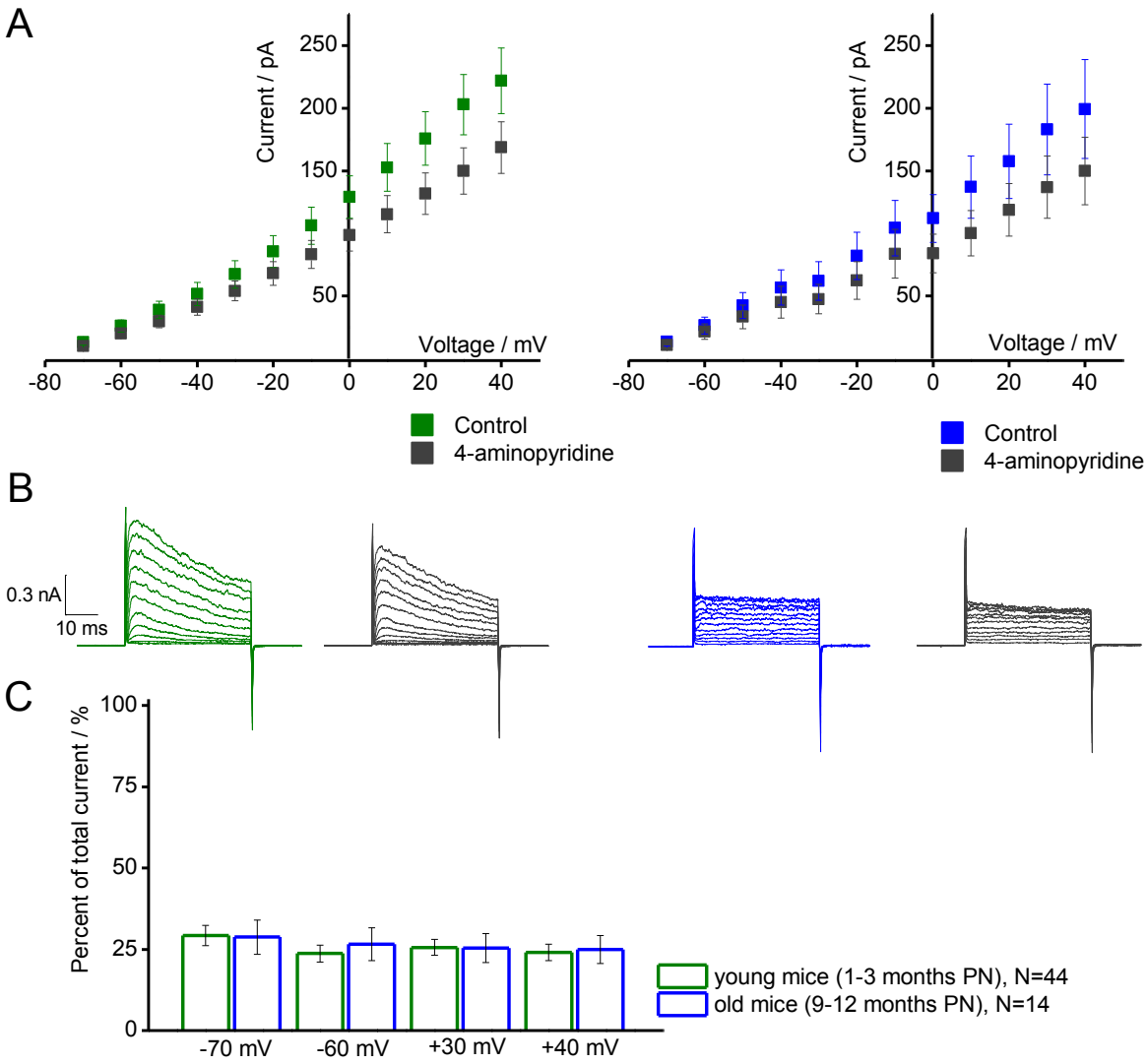

Figure 3.5: **Fractions of the 4-AP sensitive currents in total potassium current do not change with age.** The ratios of 4-AP sensitive currents were 29.3±3.1 and 25.6±2.4 per cent of control currents (in Group I at -70 mV and -60 mV voltage steps) and 23.7±2.6 and 24.1±2.5 per cent (in Group III at -70 mV and -60 mV steps); two highest voltage steps of astrocytes from Group I show 28.8±5.3 and 25.4±4.4 per cent of the current are susceptible to 4-aminopyridine; 26.6±5.0 and 25.0±4.3 (Group III). Two-sample t-test showed no significant differences between two age groups.

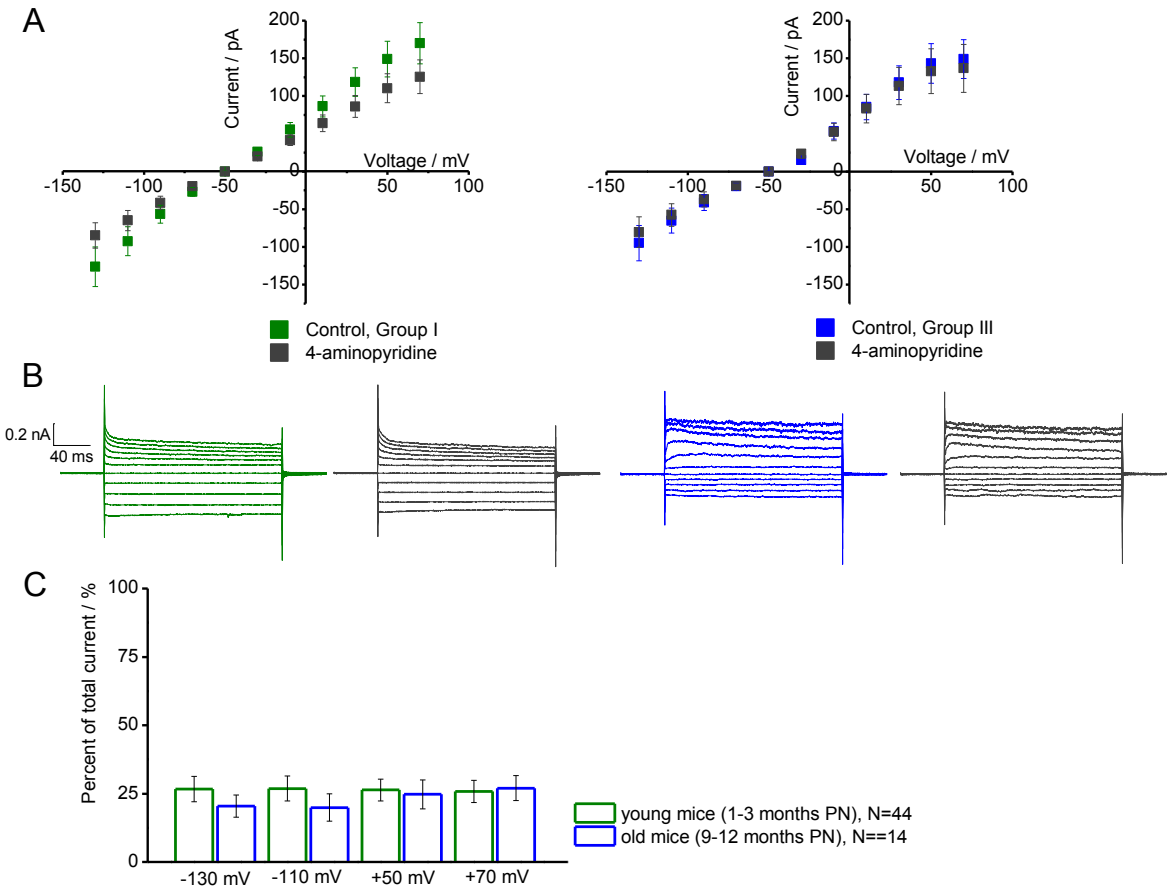

Figure 3.6: **Fractions of the 4-AP sensitive currents in inwardly rectifying and total potassium current do not change with age.** The ratios of 4-AP sensitive current portion in inwardly rectifying potassium current display a trend towards decreasing in astrocytes of old mice. For the total potassium current (two highest voltage steps) the ratio of 4-AP sensitive current was 20.5±4.1 and 24.8±5.3 % in Group I and 19.9±5.0 and 27.0±4.6 per cent range of total potassium current. At two lowest voltage steps the ratios measured in young astrocytes were 26.6±4.6 and 26.3±4.0, and in Group III the corresponding voltage steps yielded 26.9±4.5 and 25.8±4.0 per cent of the control current. Two-sample t-test showed no significant differences between any voltage steps of the two age groups.

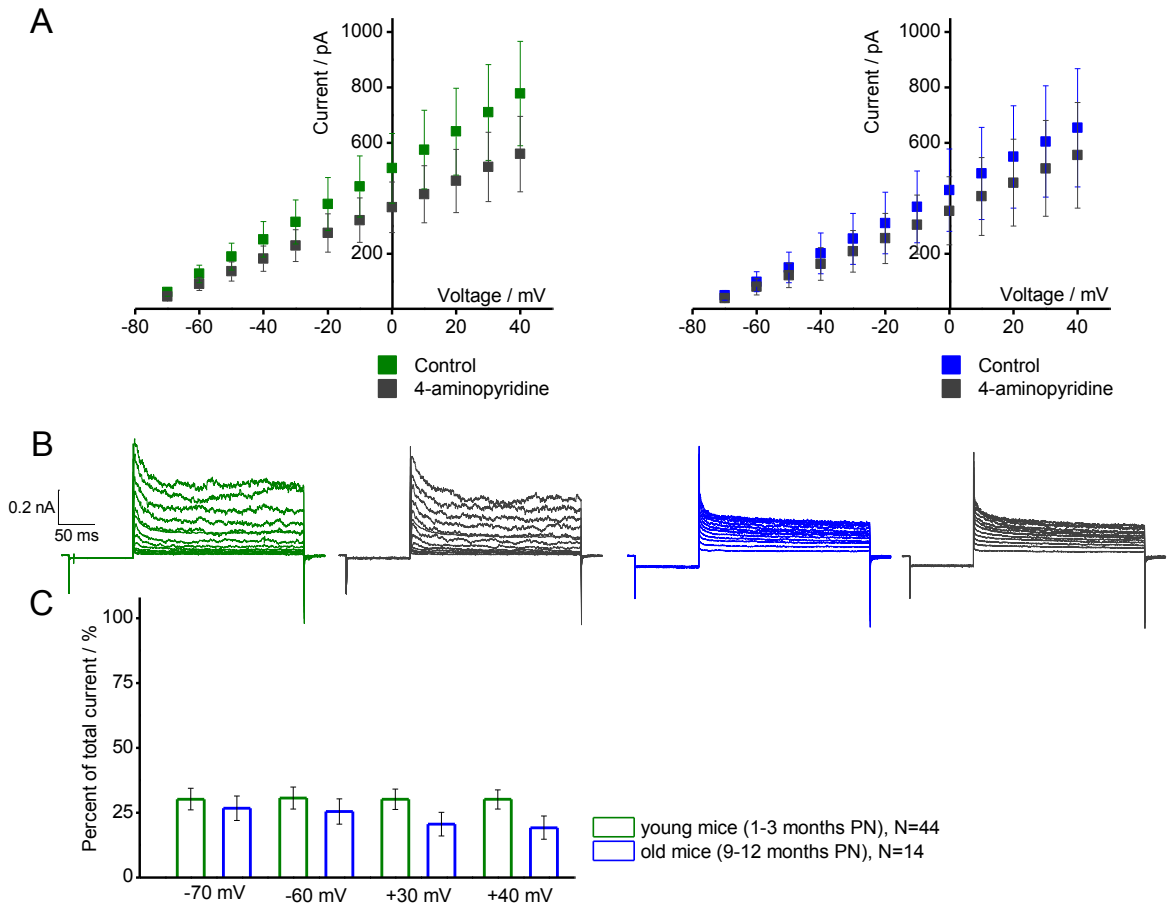

Figure 3.7: **Fractions of the 4-AP sensitive currents in steady state potassium current do not change with age.** The ratios of 4-AP sensitive current portion in steady state or delayed rectifier potassium current display a trend towards decreasing in astrocytes of old mice. The 4-aminopyridine sensitive current in Group I were 30.2±4.2, 30.2±3.9, 26.8±4.8 and 20.6±4.6 per cent for the voltage steps from -70 mV to +40 mV. Group III displayed the following proportions of current: 30.6±4.2, 30.2±3.7, 25.5±4.9 and 19.2±4.4 per cent of control current. Two-sample t-test showed no significant differences between two age groups.

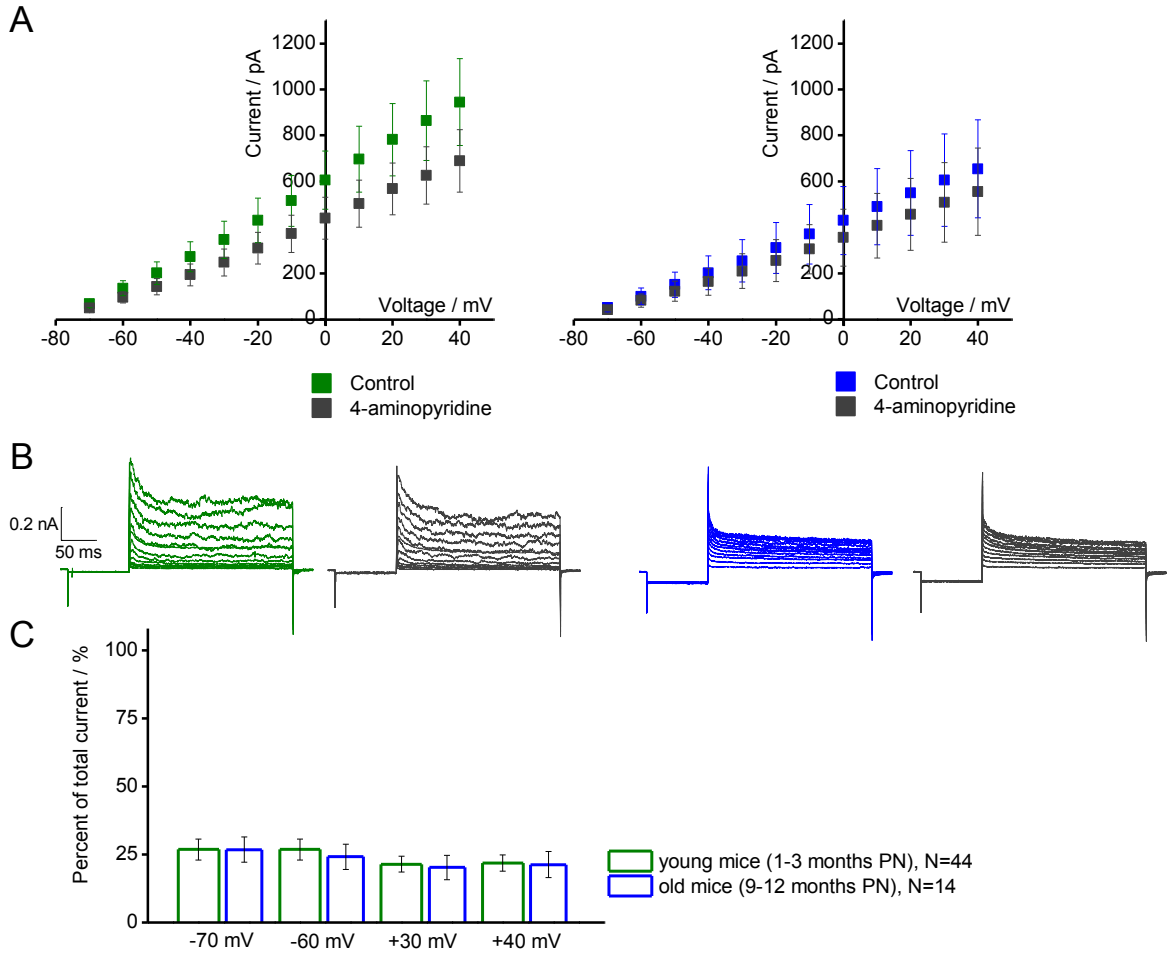

Figure 3.8: **Fractions of the 4-AP sensitive currents in rapidly inactivating potassium current do not change with age.** The ratios of 4-AP sensitive current portion in rapidly inactivating potassium current display very little difference between the two groups of cells. The ratios of 4-AP sensitive current for Group I were 26.8±3.8, 21.4±3.0, 26.8±4.6 and 20.2±4.5 per cent of the total potassium current. Group III displayed the following proportions of 4-aminopyridine sensitive current: 26.8±3.8, 21.9, 24.2±4.6 and 21.3±4.8 per cent for voltage steps in order of increase. Two-sample t-test showed no significant differences between two age groups.

3.4.1.2 Proportion of total potassium current sensitive to Barium blocker in young and old mice

The second blocker used was barium chloride, used at 100 μM concentration to block the inwardly rectifying potassium current (Hibino et al. 2010). Inwardly rectifying potassium current is mainly conducted via the Kir4.1 potassium channel subunit in the glial cells (Higashi et al. 2001; Seifert et al. 2009). This potassium current subtype helps astrocytes carry out one of their main functions: homeostatic control of the concentration of potassium ions in the CSF. However, Kir4.1 channels are located in highest density near the areas of greatest K^+ perturbations: perisynaptic feet and at the tripartite synapses (Higashi et al. 2001). During this project the fraction of the overall potassium current that is sensitive to blockage by bath addition of barium chloride dihydride was measured in isolated astrocytes form young adult and old mice.

For consistency, the effect of Barium was measure at the same voltage steps as the effect of 4-aminopyridine for three experimental protocols used. Figures 3.9-3.12 present the data collected. Overall, it is clear that the proportion of the potassium current that is conducted via barium-sensitive channels is approximately double than that of the 4-aminopyridine sensitive channel types, constituting up to 40% of the total potassium current.

When measuring the total potassium current, the proportion of the current sensitive to block by barium chloride in young adult mice is greater at lower voltage steps than at higher, 40 and 42 % against 33 and 34 % respectively (see Figure 3.9). Similarly, group III displays the same pattern appears: at lowest voltage steps barium chloride blocks 30-31% and only 22-23% at high voltage steps. There is also a tendency for decrease in the amount of current blocked by barium chloride in group III. However, the comparison of two age groups, as

calculated by the two-sample t test shows that no significant differences were found between the astrocytes from young adult and old mice.

The second protocol was recorded to allow measuring the effect of barium chloride on inwardly rectifying potassium current separately (holding potential -50 mV with 11 voltage steps from -130 mV to +70 mV). The ranges of the blocking effect of barium chloride are 45 - 46 % in lowest and 34 – 35% in highest voltage steps of the protocol in young adult mice, whereas for astrocytes from old mice exhibit the 19 – 20 % in low and only 10 -12 % in high voltage steps (see Figure 3.10). There is a much greater proportion of the overall current in young adult astrocytes that is barium-sensitive, than in cells from old mice. These data show that when comparing Group I and III, young astrocytes display double or even more of the current that can be blocked by barium.

The last protocol was constructed to record only the voltage-gated potassium currents (holding potential -80 mV with a deactivating pre-step of -20 mV and 12 voltage steps starting from -70 up to +40 mV). Overall, the amount of Barium-sensitive current is much lower in this dataset, than it is in protocols that measure total and inwardly rectifying potassium currents. When looking at voltage-gated potassium current, a similar proportion of the rapidly desensitizing and steady state currents are blocked by the bath addition of barium chloride. In the steady state current the ranges of the barium-sensitive currents are 19 – 21 per cent and 14 – 23 per cent in astrocytes from young adult and old mice respectively (see Figure 3.11). Barium block appears to be consistent throughout the voltage steps and does not significantly vary with age (as measured using the two-sample t test). In the rapidly desensitizing portion of the current the ranges of the Barium blockage were as follows (see Figure 3.12): 16 -19 per cent in young adult and 22 – 25 per cent in astrocytes from old mice. Similarly to the steady state current, the effect of Barium was universal across all voltage steps here, as expected for a protocol that

measures a single type of potassium current. However, in astrocytes from old mice the proportion of rapidly desensitizing potassium current that is blocked by the addition of barium chloride was higher than that of the young adult cells, although the two-sample t test showed no significant difference. This lack of significance can be explained by the high error in the experiments with the astrocytes from old mice.

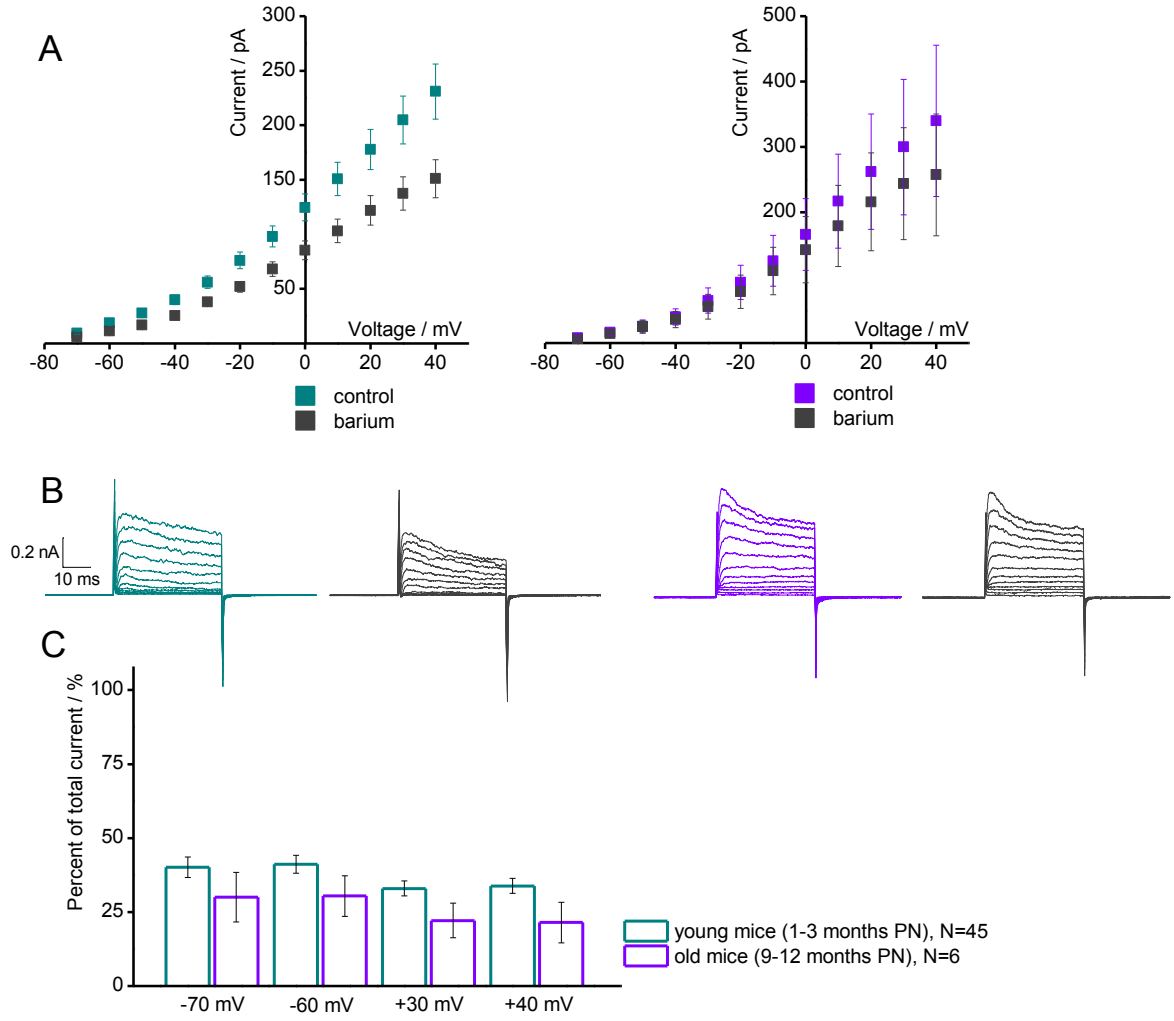

Figure 3.9: **Fractions of the barium chloride sensitive currents in total potassium current do not change with age.** Proportion of the overall current that is susceptible to Barium in young adult and old mice were 40.1±3.5, 41.2±3.0, 32.9±2.5 and 33.9±2.6 and per cent in young mice and 30.0±8.4, 30.4±6.9, 22.2±5.8 and 21.5±6.9 per cent in old mice respectively, with higher fractions of the current consistently blocked at lowest voltage steps. The ratios of barium chloride - sensitive current portion in total potassium current appear to be greater in the first group of astrocytes, i.e. astrocytes from young adult mice.

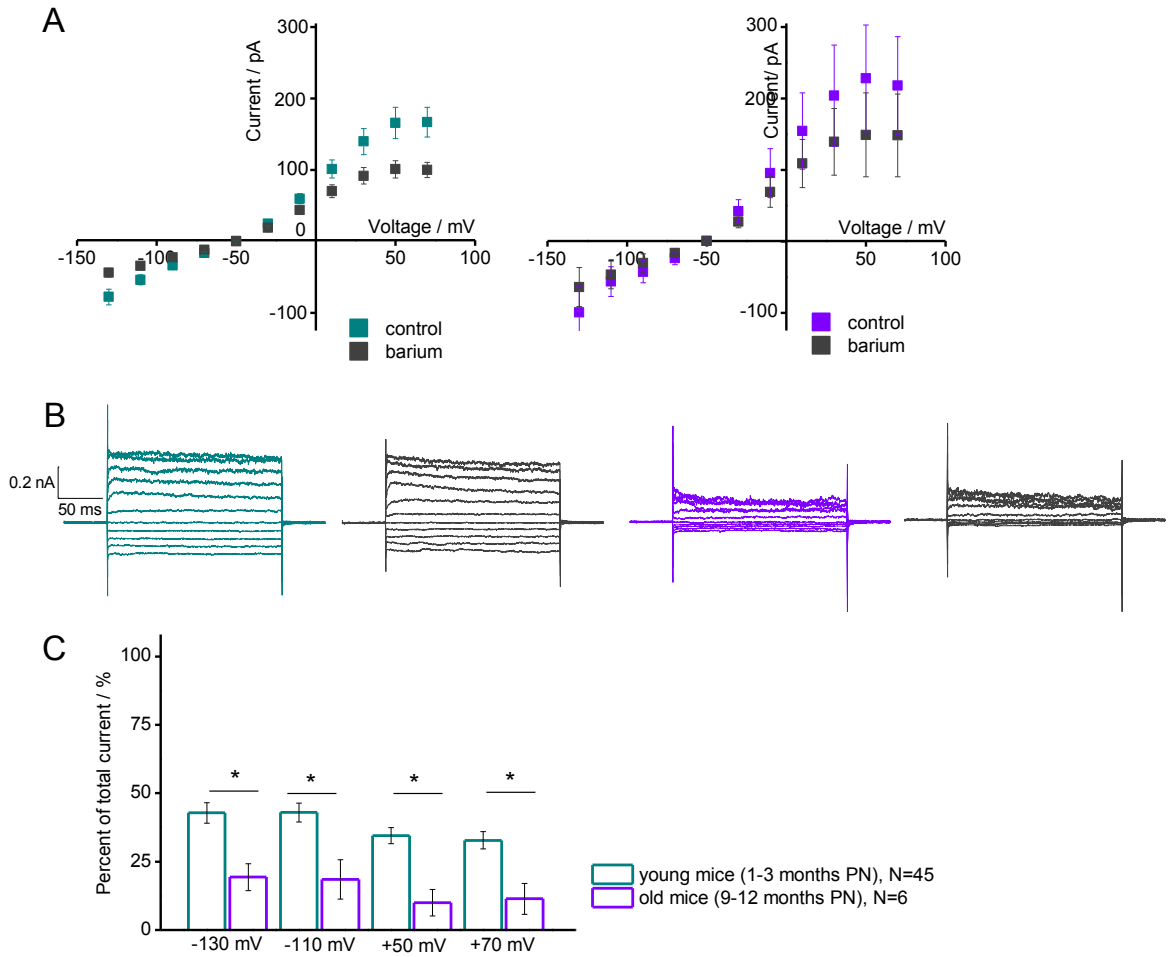

Figure 3.10: **Fractions of the barium chloride sensitive currents in inwardly rectifying and total potassium current decrease in older mice.** Barium-sensitive currents in young adult mice were 42.8±3.8 and 42.9±3.4 for inwardly rectifying potassium current. In Group III the inwardly rectifying potassium currents were 19.3±4.9 and 18.5±7.2 per cent, ($p=0.003$ and $p=0.01$ at -130 mV and -110 mV steps as calculated with two-sample t test). At higher voltage steps barium chloride sensitive currents were 34.7±3.0 and 32.8±3.1 in Group I and in old mice 10.0±4.8 and 11.4±5.6 per cent respectively ($p=0.001$ and $p=0.007$ at +50 mV and +70 mV as calculated with a two-sample t test). The amount of Barium-sensitive current shows a clear decrease in Group III in comparison with Group I. Two-sample t test showed a significant difference between young adult and old mice; * shows $p<0.01$ as calculated with two-sample t test.

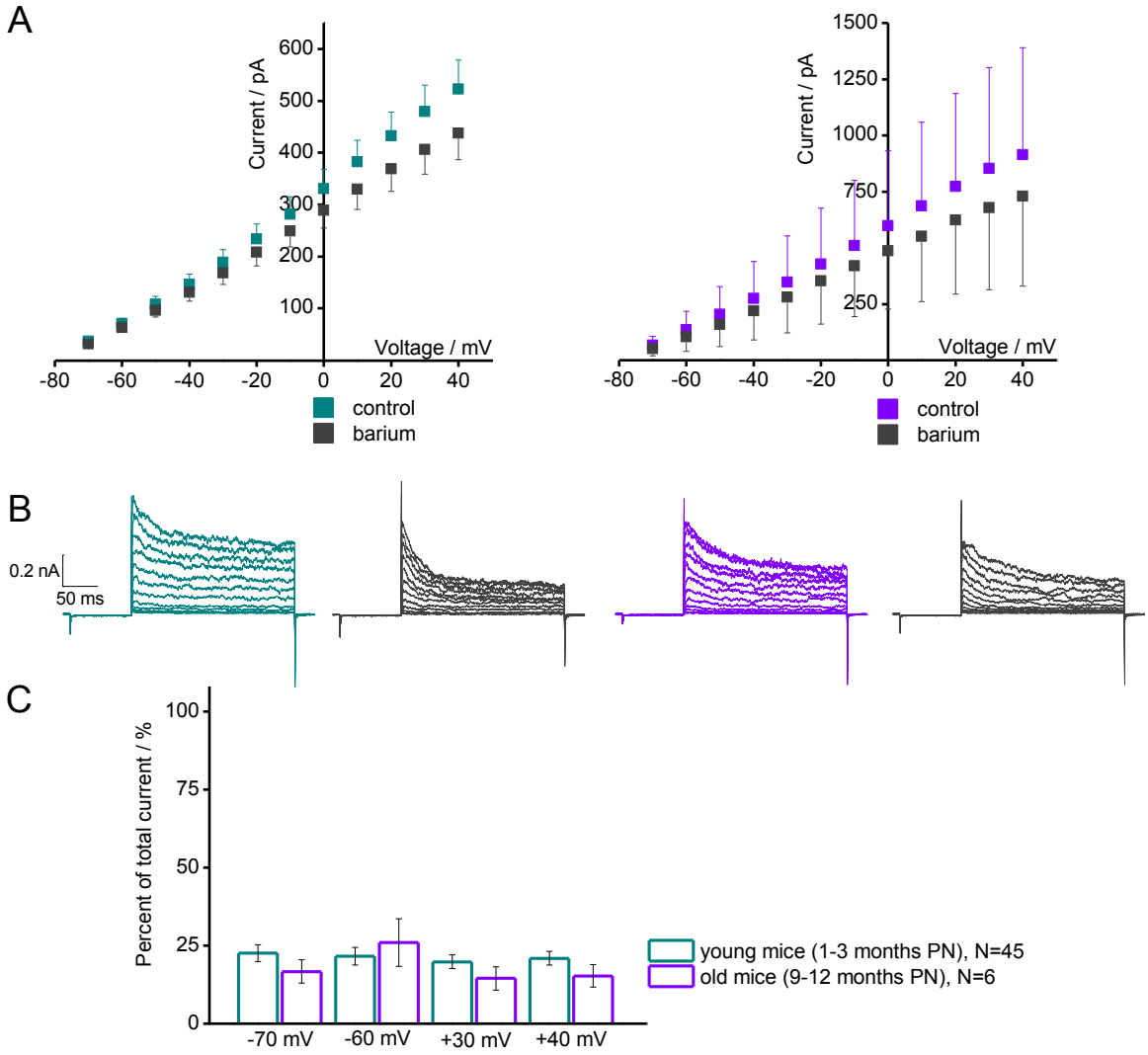

Figure 3.11: **Fractions of the barium chloride sensitive currents in steady state potassium current do not change with age**. The proportion of barium chloride-sensitive current in steady state voltage-gated currents in young adult mice was 22.6±2.6, 21.6±2.8, 19.8±2.2 and 21.0±2.2 per cent of control current; in old mice 16.7±3.7, 26.0±7.6, 14.5±3.8 and 15.3±3.6 per cent of control. The amount of barium-sensitive current shows a small decrease in Group III with the exception of -60 mV voltage step. Two-sample t test showed no significant difference between young adult and old mice.

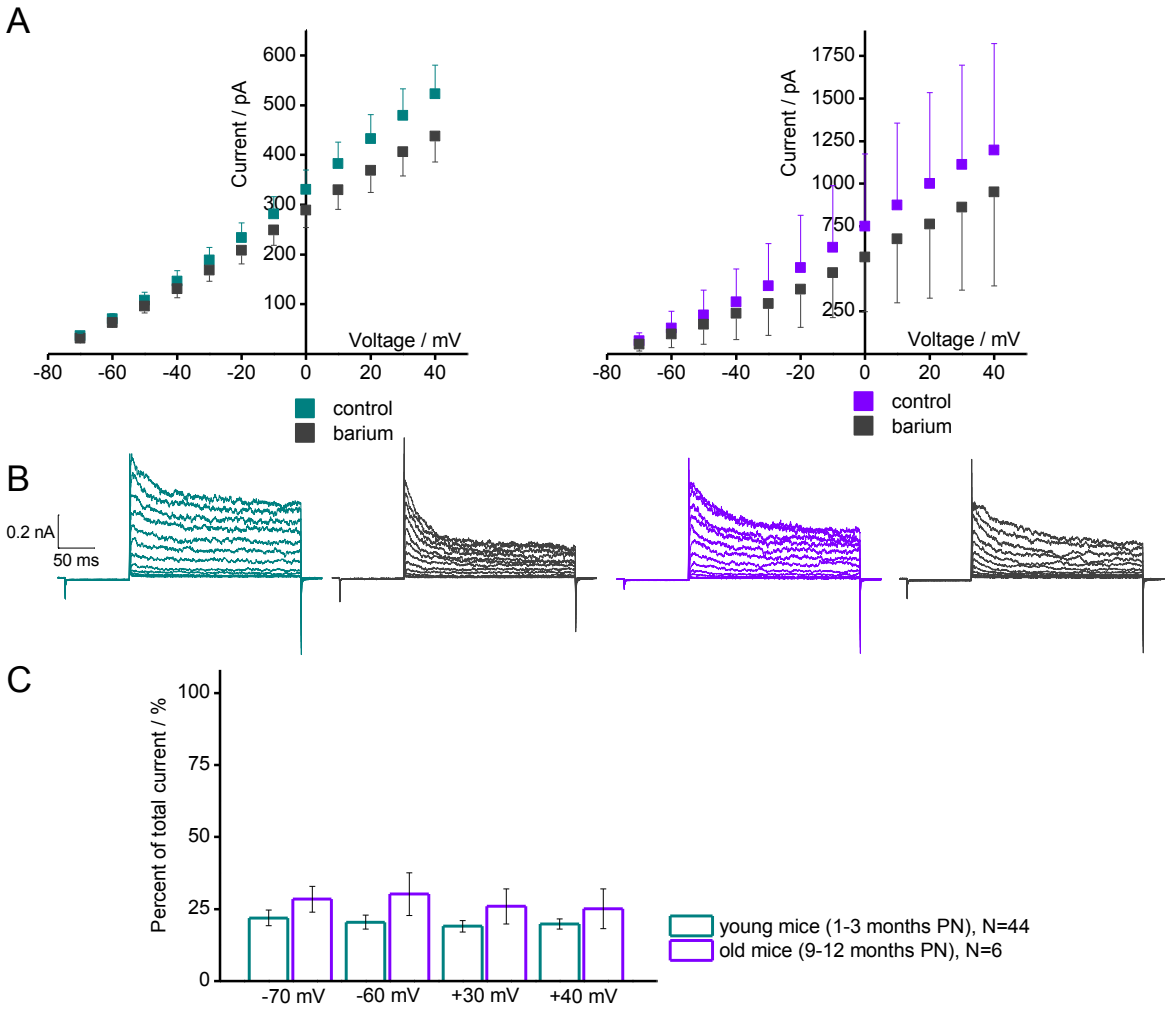

Figure 3.12: **Fractions of the barium chloride sensitive currents in rapidly desensitizing potassium current do not change with age.** Rapidly desensitizing voltage-gated current has a Barium-sensitive fraction. In young adult mice the barium-sensitive fractions were 22.6±2.6, 21.6±2.8, 19.8±2.2 and 21.0±2.2 per cent, and in old mice 16.7±3.7, 26.0±7.6, 14.5±3.8 and 15.3±3.6 per cent. The amount of Barium-sensitive current shows a small increase in Group III, however, the two-sample t test showed no significant difference between young adult and old mice.

3.4.2 Combined effect of blockers

An alternative set of data was collected, using a mix of both blockers, in order to measure the effect of bath addition of both 4-aminopyridine and barium chloride. This was done to investigate whether the individual blockers can affect more than one subtype of potassium current or if there is any interference between their actions that can lead to different results.

Figures 3.13-16 below show the combined effect of both blockers applied in a single experiment. Similarly to data collection for individual blocker addition experiments, three protocols were used for combined blocker effect. In young adult mice the highest voltage steps exhibit higher amount of current blocked by the addition of 40 μM of 4-aminopyridine and 100 μM barium chloride. This is not the case in Group III, which corresponds to astrocytes isolated from old mice. Despite this trend, there is no significant difference between the amounts of current blocked at different voltage steps as checked by the two-sample t test. Similarly, when comparing the groups of astrocytes to each other, there is a trend for increased amount of current that is sensitive to combined blockers effect. This difference was not found significant with a two-sample t test (see Figure 3.13).

The second protocol illustrates the effect of the combined blockers addition on inwardly rectifying and total potassium currents (see Figure 3.14). Here, the fractions of the total current blocked by the addition of both blockers fell in the 38 – 41.2 per cent and 48.6 – 60.8 per cent in astrocytes from young adult and old mice respectively. Group I shows fairly consistent effect on both high and low voltage steps, whereas in Group III the effect of the addition of both 4-aminopyridine and barium chloride is clearly more prominent on high voltage steps of the protocol. However, the difference between the proportions of the current blocked by two blockers at high voltage steps is not significantly different

to that of the lowest voltage steps. When comparing the results from two groups to each other, at higher voltage steps the difference between young adult and old mice is significant with $p<0.01$, unlike the results for the lowest two voltage steps.

The last protocol was used to collect data for voltage gated potassium currents: the steady state and the rapidly desensitizing components of it. In the steady state part of the current the effect of the addition of combined blockers produces a consistent effect throughout all voltage steps: the fractions that are blockers-sensitive reside in 32.9 – 33.6 per cent range of the overall current in young adult mice. There is a greater degree of variability in the data for Group III: the range of the susceptible current is 37.9 – 47.2 per cent of the total current. When the results for two age groups were compared using two-sample t test that there is no significant differences between the proportion of the current that is inhibited by the addition of both 4-aminopyridine and barium chloride.

Rapidly desensitizing voltage-gated potassium currents were compared in isolated astrocytes from young adult and old mice. Similarly to the steady state current, astrocytes in Group I display a consistent amount of current that is inhibited by the addition of two blockers – data fall into the following range 29.4 – 32.3 per cent. Also similar to the steady state data, astrocytes from Group III have a great range of variability: 39.7 – 48.5 per cent of the total current. The comparison of the two age groups against each other show that there is a trend for the increase in the proportion of current that is sensitive to blockers mix, however the difference is not significant on all voltage steps; two of the voltage steps, -70 and +30 mV, are significantly different ($p<0.01$), whereas -60 mV and +40 mV are not significant ($p>0.01$).

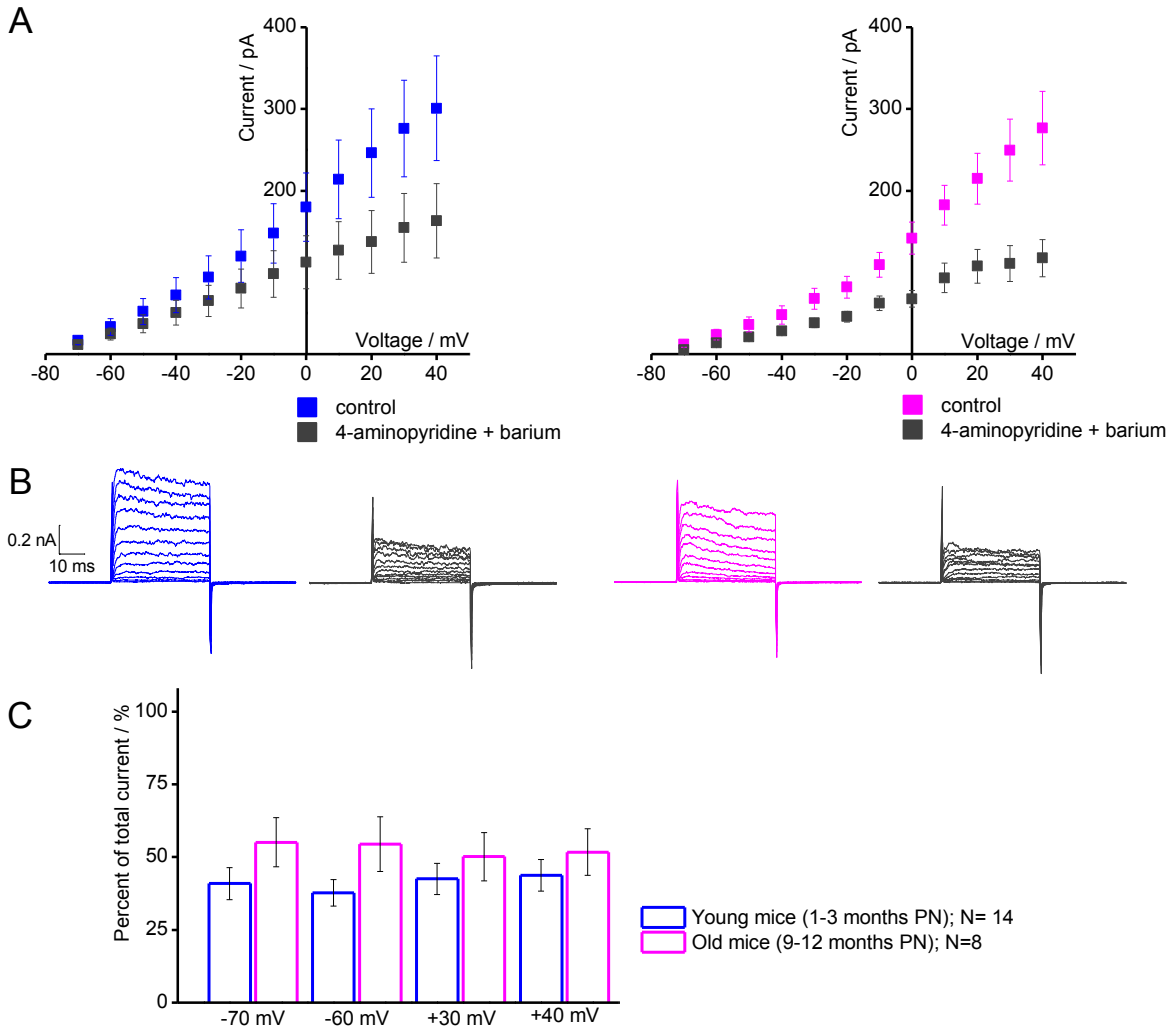

Figure 3.13: **Fraction of current sensitive to combined blockers in total potassium current does not change with age.** Proportions of the overall current that is susceptible to both blockers in young adult mice 40.9±5.5, 37.7±4.5, 42.5±5.4 and 43.7±5.4 per cent of control at voltage steps in order of increase. In Group III the following fractions of current that are sensitive to both blockers were measured: 55.1±8.5, 54.5±9.4, 50.1±8.3 and 51.7±8.0 per cent at respective voltage steps. The fraction of current sensitive to both blockers is greater in group III, but this difference is not significant as calculated with two-sample t test.

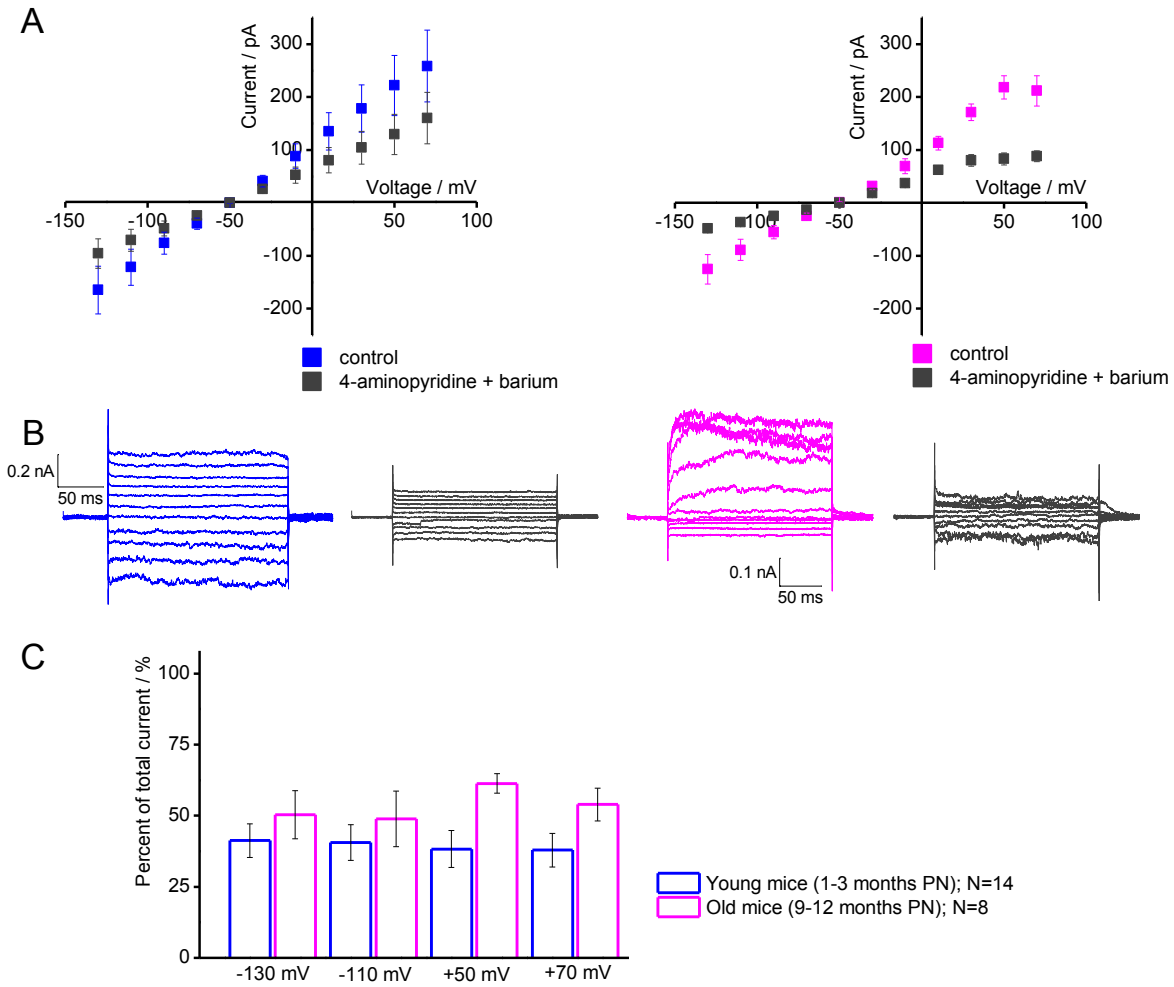

Figure 3.14: **Fraction of current sensitive to combined blockers in total and inwardly rectifying potassium current does not change with age.** Proportions of the overall current that is susceptible to both blockers in young adult mice were 41.3±5.9, 40.6±6.3, 38.3±6.5 and 37.9±5.9 per cent of control. In Group III the proportions of the respective voltage steps were 50.3±8.5, 48.9±9.8, 61.3±3.4 and 53.9±5.8 per cent. The fraction of current sensitive to both blockers is greater in Group III, but this difference is not significant at lowest voltage steps, where inwardly rectifying potassium current is the predominant current. At high voltage steps, however, the difference was significant with $p<0.05$ ($p=0.01$ and $p=0.02$ when comparing Group I and Group III at +50 and +70 mV as calculated with two-sample t test).

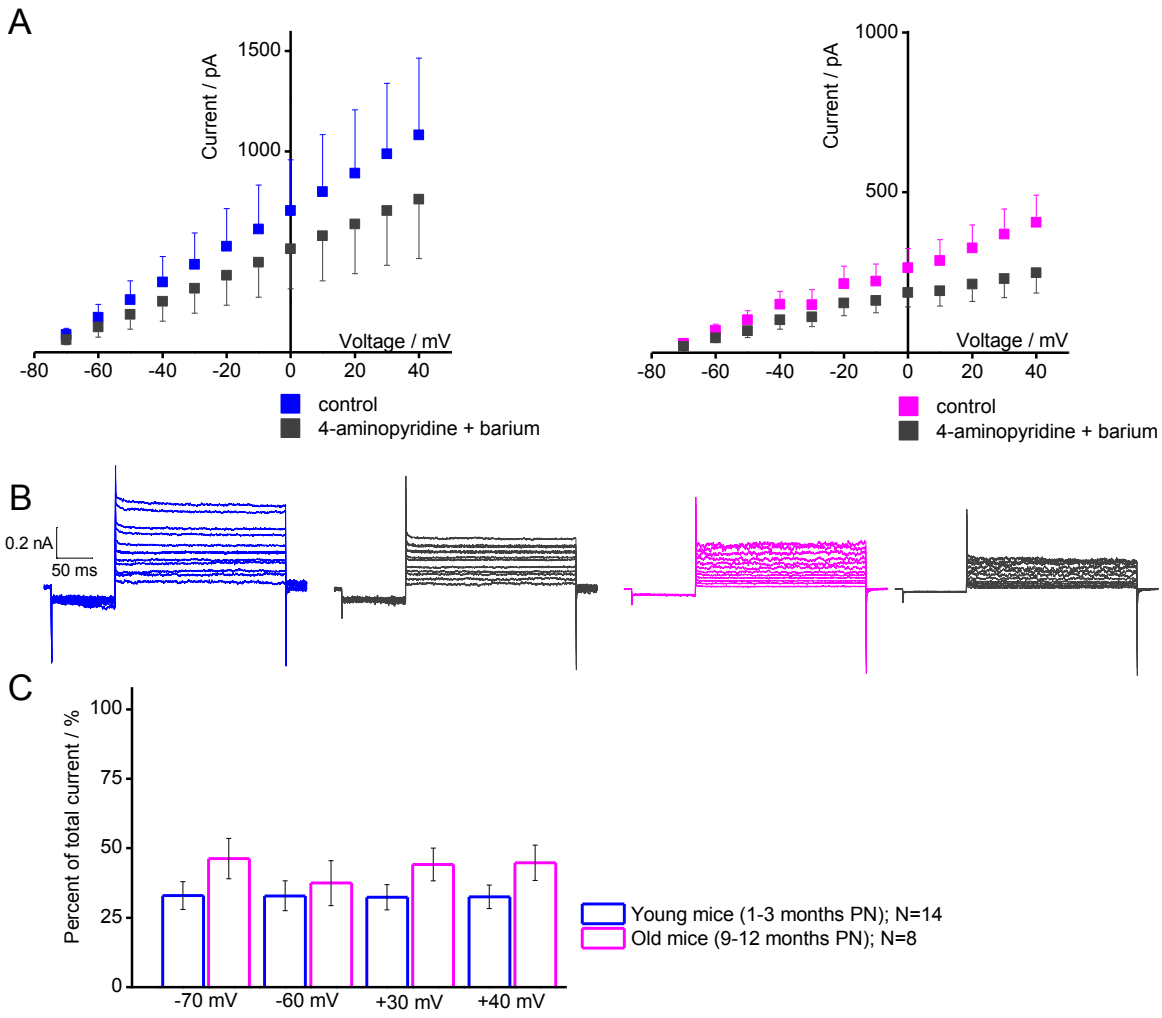

Figure 3.15: **Fraction of current sensitive to combined blockers in steady state potassium current does not change with age**. Proportion of the overall current that is susceptible to both blockers in young adult and old mice varies within 32.9 – 33.6 per cent and 37.9 – 47.2 per cent, respectively. The fraction of current sensitive to both blockers is greater in group III, but this difference is not significant with the two-sample t test.

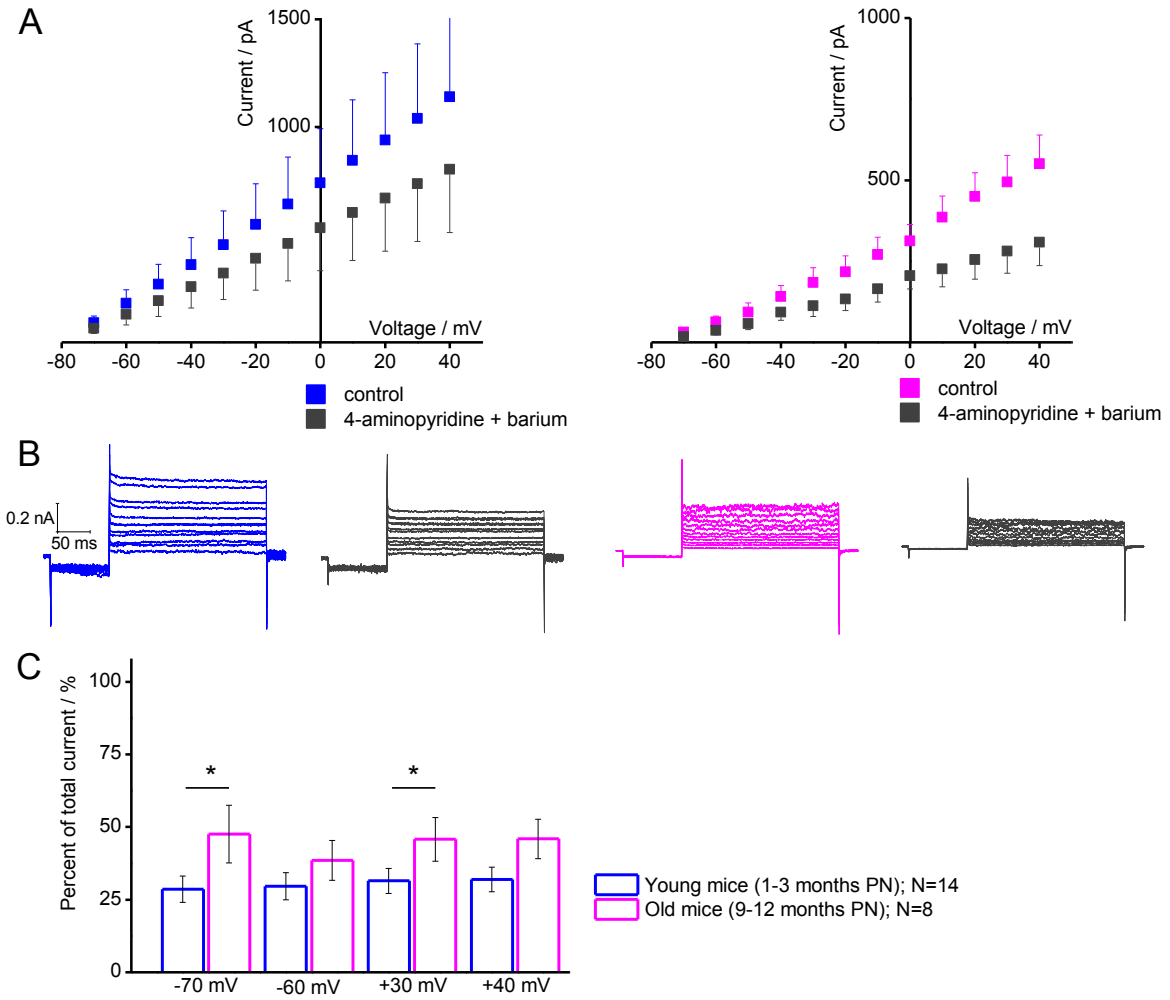

Figure 3.16: **Fraction of current sensitive to combined blockers in rapidly desensitizing potassium current increases with age**. Proportion of the overall current that is susceptible to both blockers in young adult and old mice varies within 29.4 – 32.3 per cent and 39.7 – 48.5 per cent respectively. The fraction of current sensitive to both blockers is greater in group III, but this difference is significant on some of the voltage steps (-70 mV and +30 mV), as measured with the two-sample t test; * shows $p<0.01$.

3.5 Conclusions

This chapter set out to investigate the changes that occur in electrophysiological profiles of cortical astrocytes from somatosensory cortex during the process of non-pathological ageing. Table 2 summarises the results, covered in this chapter.

	Potassium current	Change/effect in aged mice
Cell capacitance		↑
Current density	Total	↑
	K_{ir}	-
	K_D	↑
	K_A	↑
4-aminopyridine block	Total	-
	K_{ir}	-
	K_D	-
	K_A	-
Barium chloride block	Total	-
	K_{ir}	↓
	K_D	-
	K_A	-
Combined block	Total	-
	K_{ir}	-
	K_D	-
	K_A	↑

Table 2: Summary of effects, described in Chapter 3.

Firstly, the size of the cell somas was compared between the two age groups. It was found to be significantly greater in older mice. Since it is known that there is an increase in the GFAP production around the 40 - 44 weeks old mice (Amenta et al. 1998) so the increased capacitance in Group III was expected. Current densities

on average were higher in isolated cells from Group III, when measured with all but one electrophysiological protocol. The exceptions were the data collected for the lowest voltage steps of the protocol for recording inwardly rectifying potassium currents. There was no significant change in the current density of inwardly rectifying potassium current between young mature and old mice. It is possible that this lack of increase in the current density can lead to astrocytes being unable to effectively remove extracellular potassium following action potential (Rossi 2015; Finch 2003). However, it can also be a consequence of ageing as opposed to a cause.

The proportions of currents were described by their blocker-sensitivities. Proportion of current sensitive to both 4-aminopyridine and barium were measured in separate experiments and some experiments were performed using both blockers together. All experiments using 40 μM of 4-aminopyridine showed no significant difference in the proportion of the overall current susceptible to blocker between young mature and old mice. When taken together with the data collected for current density, it can be concluded that the since the current density rises but the proportion of 4-aminopyridine sensitive current remains the same, there is in fact an increase in the proportion of 4-aminopyridine sensitive current from young mature to old mice.

When a blocker for inwardly rectifying potassium current – barium chloride, was applied the isolated astrocytes from young mature mice showed a greater inhibition of the total current than astrocyte isolated from old mice. The proportion of the current that was barium chloride - sensitive at 100 μM was reduced by 50 per cent or more. It appears that the inwardly rectifying potassium channels expression or functioning reduces with non-pathological ageing. These data point to similar processes, underlying non-pathological ageing and various pathological settings, for instance ischemia-like conditions (Pannicke et al. 2000).

However, this reduction was only seen at the protocol aimed for recording the inwardly rectifying potassium current; the trend was similar in other protocols, but high error bars coupled with only a small fraction of this current type at other protocols.

When a cocktail of both blockers at the same concentrations was used, the data appeared in disagreement with the previous experiments. The overall trend displayed an increase in the proportion of current, which was sensitive to both of the blockers. Some of the protocols (namely the protocol for recording total potassium current, negative voltage steps of protocol for recording the inwardly rectifying potassium current and protocol for recording the voltage-gated potassium current) showed no significant difference, whereas the proportion of the total current blocked by the mixture of both blockers increased in some voltage steps, including the most positive voltage steps in the protocol for recording inwardly rectifying potassium current and some of the voltage steps, at which the rapidly desensitizing potassium current was measured. It also appeared that in young mature mice the proportion of the current blocked by the addition of both 4-aminopyridine and barium chloride together was smaller than what was expected from the experiments where the blockers were applied separately. The proportion of the total current that should be blocked by the blocker cocktail was 69 per cent for -70 mV (from holding potential -80 mV) but instead it was only 40 per cent. Therefore it is possible that the simultaneous blockage of multiple potassium channels leads to increased build up of potassium ions inside the patched cells and an increased conductance via the leaky potassium channel types, unaffected by the blockers used (L. Y. Kucheryavykh et al. 2009; Zhou et al. 2009).

In conclusion, it has been shown that in non-pathological ageing prominent changes in cortical astrocyte take place. The capacitance of the cells increase, showing that on average astrocytes increase in size, potentially signifying that the

proportion of reactive astrocytes increases. Current densities of voltage-dependent potassium currents (total, K_D and K_A or slowly deactivating and rapidly desensitizing potassium current types) increase with age, whereas the current density of inwardly rectifying potassium current does not. The fractions of the overall current that are sensitive to 4-aminopyridine blocked (specific blocker for voltage gated potassium currents at the concentration used) (Tse et al. 1992). The Barium-sensitive fraction of the current was significantly diminished in old mice. These changes shift the overall balance from the healthy state towards more reactive and hyperpolarised astrocytes, similar to those brought about by age-related diseases, such as Alzheimer disease.

Chapter 4 – Autocrine current interactions

Interaction of P2X, NMDARs and PAR – 1 channels and potassium currents of astrocytes and neurons

4.1 Aim and Hypothesis

The aim of this chapter was to explore a potential link between one or possibly more channel types of astrocytes and the potassium currents and to identify what types of currents are involved, if any. Firstly, isolated neurons and astrocytes were compared in their responses to bath addition of 10 μM ATP or $\alpha\beta$ – methylene ATP (analogue of ATP) in the presence or absence of intracellular Calcium. It was determined that neuronal and astrocytic responses were different, thus limiting the mechanism in question to astrocytes only. Multiple drugs were used to determine which channels are involved in this mechanism. Secondly, the effect of the addition of 10 μM $\alpha\beta$ – methylene ATP or NMDA under the presence of Calcium chelator EGTA was measured. As mentioned previously, this study focused primarily on the functionality of the potassium currents, thus the following jargon was used: total potassium current refers the full, non-filtered current conducted by the patched cell; inwardly rectifying potassium current was current measured at two lowest voltage steps (repolarising step from -50 mV of holding potential to -130 mV and -110 mV to induce inward potassium current). Voltage-gated potassium currents were split by their components: the steady state (K_D) current, measured between 50-150 ms of voltage step stimulation; the rapidly inactivating (K_A) potassium current refers to sharp peak at the start of the voltage step stimulation. The facilitation effect on potassium currents was further investigated, with the addition of certain potassium channel blockers to find what types of potassium channels may be affected. Lastly, it was tested whether this effect takes place in patched astrocytes in slice. The null hypothesis in this chapter was as follows: **the bath addition of the agonists to $P2X_{1/5}$, NMDARs and PAR-1 receptors should produce no changes in the potassium current measured**. The

data are presented as examples of typical currents and bar charts ± experimental errors. The mean was calculated as follows:

Mean = [K^+ current under the drug] / average [K^+ in control and washout conditions] *100%

Experimental error was calculated as SEM (standard error of mean). Two sample or one-sample t tests were used to calculate significance of the experimental data.

4.2 Results

4.2.1 Effect of addition of ATP or αβ-methylene ATP on isolated neurons

In order to examine whether this mechanism is present in astrocytes only, it was first tested on neurons. Isolated neurons were patched (under the addition of TTX to block the sodium current) and their responses to the addition of ATP or αβ-methylene ATP was measured by recording a protocol where holding potential was -50 mV and a series of voltage steps from -130 mV to +70 mV was measured. The addition of ATP was done in two different conditions: with or without the presence of intracellular Calcium (Ca_i). In the presence of Calcium, the concentration of EGTA used in the patch pipette was 0.1 μM, which allows fluctuations of free calcium inside the cell. In experiments where the patch pipette contained 10 μM of EGTA, any unbound intracellular calcium ions were chelated by the EGTA. This therefore disturbed any potential calcium signals from transducing from outside of the cell. Neither of these conditions yielded any significant increase in the potassium currents of isolated neurons, with ATP addition under the presence of intracellular Calcium produced an average of 97.1±15.3 and 104.5±24.3 per cent at -130 and +70 mV respectively (see figure 4.1). The addition of ATP under the 10 μM of EGTA also did not raise the current significantly at either -130 mV or +70 mV, with average values being 94.1±8.7 and 95±8 per cent respectively.

Under the addition of αβ-methylene ATP the potassium current also did not increase, generating 83.6±5.2 and 96.6±5.4 per cent of the control current in the lowest and highest voltage steps of the protocol. The current in the lowest voltage step appears to diminish slightly, however this effect can be accounted for by the rundown of some of the experiments.

Overall, it was shown that agonists to P2X receptors were not able to induce an increase in the potassium current of the isolated neurons, and therefore it was concluded that they do not have a similar mechanism to that of astrocytes for linking the ionotropic P2 and potassium channels by an intracellular calcium transduction.

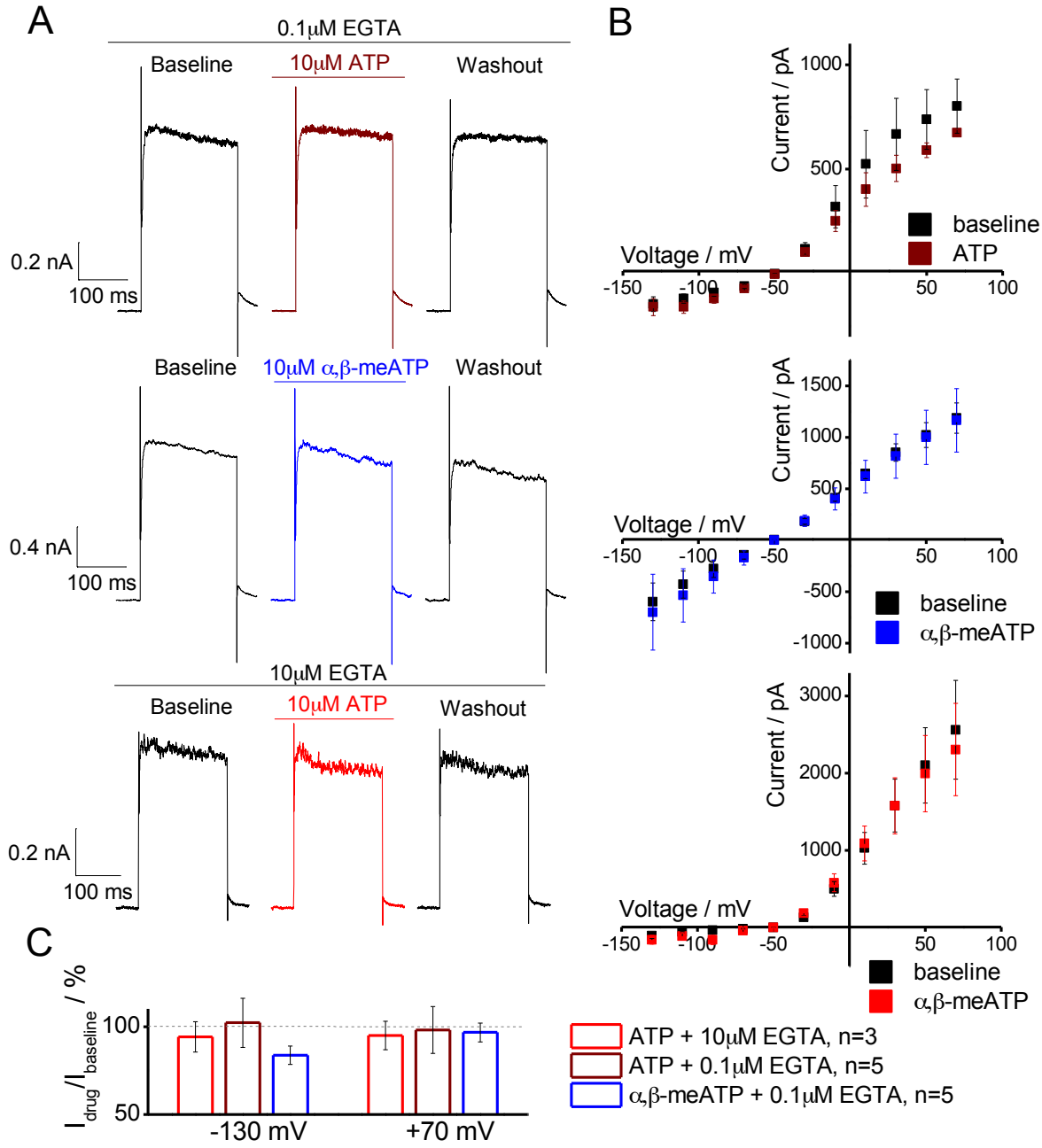

Figure 4.1: **Potassium currents in isolated neurons are not altered upon application of P2X channel agonists**. A – Representative traces of recordings (note the scale change), B – Average I/V relationship graphs for all sets of experiments, C- The average effect of drug applications. Under the absence of intracellular Calcium (achieved by the addition of Calcium chelator 10 μM EGTA into the patch pipette) the current under the ATP was 94.1±8.7 and 95±8 per cent of the control current at -130 and +70mV steps respectively. The addition of ATP under the presence of intracellular Calcium (0.1 μM of EGTA in the patch pipette), the current recorded was 97.1±15.3 and 104.53±24.3 per cent of control respectively. It was measured that the addition of 10 μM αβ-methylene ATP caused the current to be 85 and 96 per cent of control in -130 and +70mV steps. The data did not differ significantly from the control current, as shown by the student t test.

4.2.2 Effect of ATP/ATP under the presence of barium chloride on isolated astrocytes

Similarly to neurons, astrocytes were tested for a response to a bath addition of ATP 0.1 μM EGTA. Astrocytes were isolated using the vibrodissociation technique (see Chapter 2: Methods and Material) from slices of young adult mice 1-3 months postnatal. As can be seen from Figure 4.2, unlike neurons, astrocytes have a response to the addition of ATP. At -130 mV step the average astrocytic potassium current was 106.4±14.4 per cent of the control current. Student t test showed that at this voltage step the application of ATP does not significantly change the current from control. At -130 mV step the conductance is dominated by inwardly rectifying potassium current. Therefore it appears that the inwardly rectifying potassium current is unaffected by the addition of ATP extracellularly. When comparing this result with the data collected for the same voltage step but under the influence of barium chloride blocker, there is a slight increase in the effect of ATP addition. The mean current ratio reaches 109.7±2.8 per cent of control current when the ATP is added after the addition of barium chloride extracellularly. Since barium chloride is a specific blocker for inwardly rectifying potassium current, it shows that when the inwardly rectifying potassium current is removed from the overall potassium current, the extracellular addition of ATP increases the current by 9.6±12.5 per cent. However, the one sample t test used determined that at -130mV the addition of ATP under the influence of barium chloride **does not** cause a significantly different current ($p=0.05$).

At high voltage step (+30mV shown on Figure 4.2) the majority of the current is conducted via the voltage gated potassium channels. The addition of ATP produced a 9.8±12.5 per cent increase, compared to the control current, thus not increasing the current by a significant amount, as calculated by the student t test. However, when barium chloride was applied prior to bath addition of ATP, the

current recorded was 23.5±12.8 per cent higher than the control current, and this difference was significant according to the one sample t test ($p<0.01$).

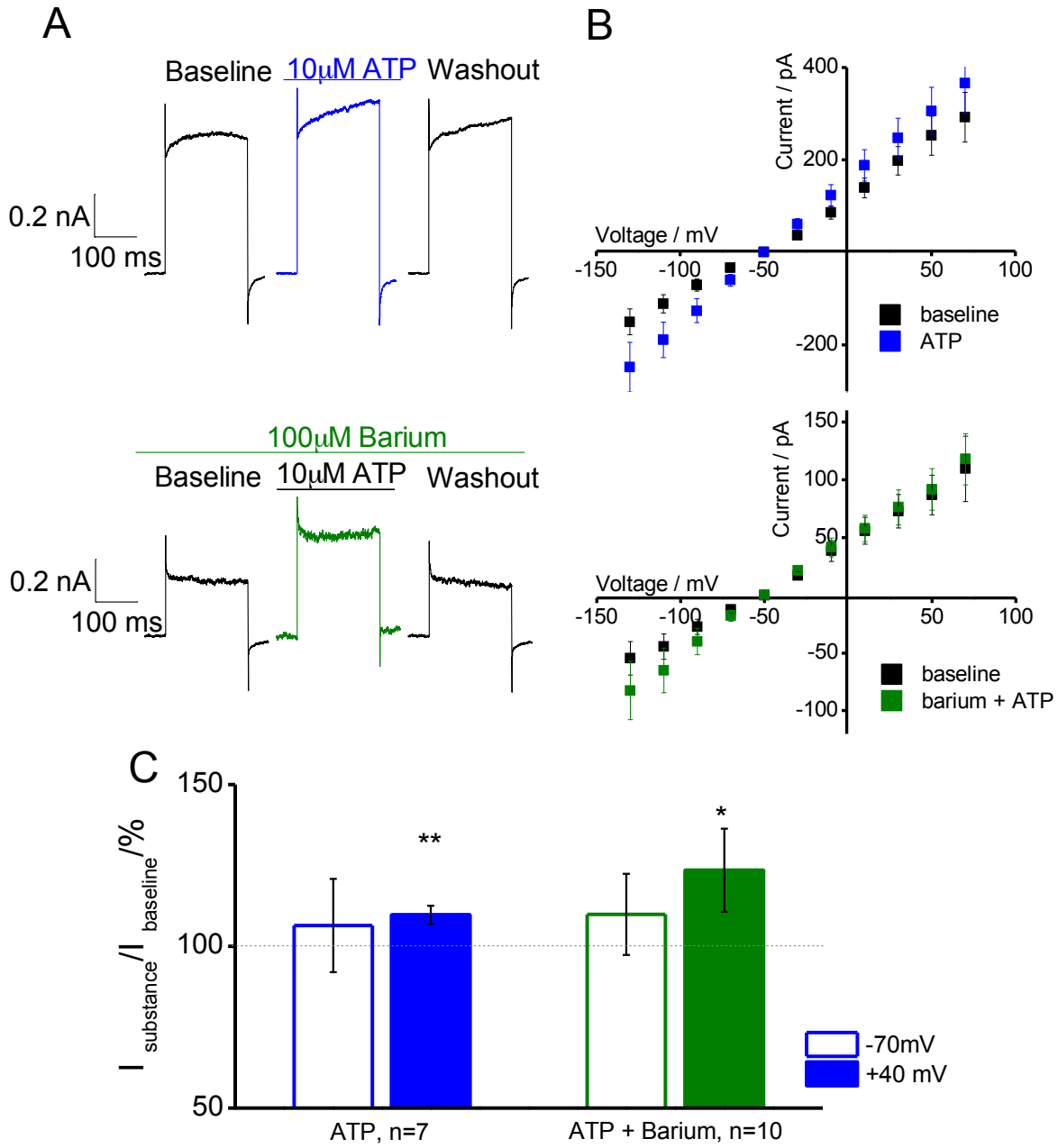

Figure 4.2: **Application of ATP on isolated astrocytes increases the outward potassium conductance.** A – Representative traces of recordings, B – Average I/V relationship graphs, C- The average effect of drug applications. The changes in potassium currents upon activation with 10 μM ATP and ATP under the presence of 100 μM barium chloride were measured. The average current recorded from isolated astrocytes under the 10 μM ATP was 106.4±14.4 and 109.7±2.8 per cent of the control current at -130 and +70mV steps respectively. The addition of ATP under the presence of inwardly rectifying potassium current blocker barium chloride yielded a mean current of 109.8±12.5 and 123.5±12.8 per cent of control current at -130mV and +30mV steps respectively. It was measured that the addition of 10 μM ATP under the presence and absence of barium chloride caused a significant difference at +30mV ($p=0.006$ and $p=0.04$ respectively), but not at -130mV step; ** shows $p<0.01$, * shows $p<0.05$ as measured with one-sample t test.

4.2.3 Effect of addition of $\alpha\beta$-methylene ATP to isolated astrocytes under the presence or absence of intracellular Calcium

In order to investigate the nature of this mechanism, it was decided to test whether this mechanism is Ca-dependent. Calcium signalling is the major type of signal transduction in astrocytes (Corner-Bell et al. 1990). Two conditions were used: with low (0.1 μM) and high (10 μM) EGTA concentrations. If removing intracellular Calcium ions blocks this facilitation of potassium current, then calcium can the link between the P2X and potassium channels. Three protocols were recorded.

Firstly, total potassium currents were measured by a series of voltage steps from -70 to +40 mV from holding potential of -80 mV. Figure 4.3 illustrates the typical currents recorded with this protocol for the +40 mV voltage step as well as the average current ratios ± SEM. Under the presence of intracellular Calcium ions the facilitation of the current upon the addition of $\alpha\beta$-methylene ATP is approximately 20%. A mean increase in current was 15.9±3.7 and 21.8±4.7 per cent compared to the control current in -70 mV and +40 mV respectively. When a high concentration of EGTA (10 μM) was used in the patch pipette, there was no increase in the current when the drug was added to the chamber. Instead the experimental currents were 92.2±3.9 and 91.2±4.7 per cent of control at -70 and +40 mV respectively. A two-sample t test was utilised to assess whether the change in the current was significant: for experiments with intracellular calcium both voltage steps produced a significant change in the current with $p<0.01$.

To test the inwardly rectifying potassium channel, the second protocol was recorded: with holding potential of -50 mV and 11 voltage steps from -130 mV to +70 mV. At the lowest two voltage steps the predominant current type is inwardly rectifying potassium current. Figure 4.4 shows the data for this protocol. At -130 mV voltage step the ratio of current was 104.8±3.0 and 97.7±3.9 per cent under the

presence and absence of intracellular Calcium ions respectively. There is a slight increase in the presence of Calcium, however it is not significant. The inwardly rectifying potassium current does not increase with the addition of extracellular αβ-methylene ATP. The effect on high voltage step is different: the current under the drug application is 116.7±3.7 under 0.1 μM EGTA and 91.2±4.7 per cent of the control current.

Third protocol was recorded with a deactivating pre step of -20mV and 12 voltage steps from -70mV to +40 mV. Two current components were considered separately: the steady state and the rapidly desensitizing currents (Figures 4.5). Under the low concentration of EGTA the current was 118.8±3.7 and 116.9±4.8 per cent of the control current at -70 and +40 mV respectively. Both display a significantly greater current than the control, as tested with the one-sample t test. When high concentration of EGTA was used for patching pipette, the experimental currents were 92.2±6.0 and 96.7±4.1 per cent of the control current. Removing intracellular Calcium ions abolishes this facilitation effect from the bath application of αβ-methylene ATP.

Similar results were obtained for the rapidly desensitizing voltage gated potassium current (Figure 4.5). Under low concentration of EGTA the experimental currents were 111.9±3.2 and 112.6±2.6 per cent of the control current at -70 and +40mV. Both ratios are significantly higher than control currents. When the Calcium chelator is present in high concentration this effect is negated, producing only 90.9±6.2 and 93.9±3.8 per cent of the control current.

Taken together these data clearly suggest that there is a facilitation effect on the potassium current that appears following the application of 10 μM of αβ-methylene ATP. It ranges from a modest 111.9±3.2 to 121.8±4.7 per cent when compared to control current. This effect is prominent on all voltage steps, except

those where inwardly rectifying potassium is the predominant current subtype. The addition of high EGTA to the patch pipette completely abolishes this increase, and even lowers the current by 3 – 13 per cent of control current.

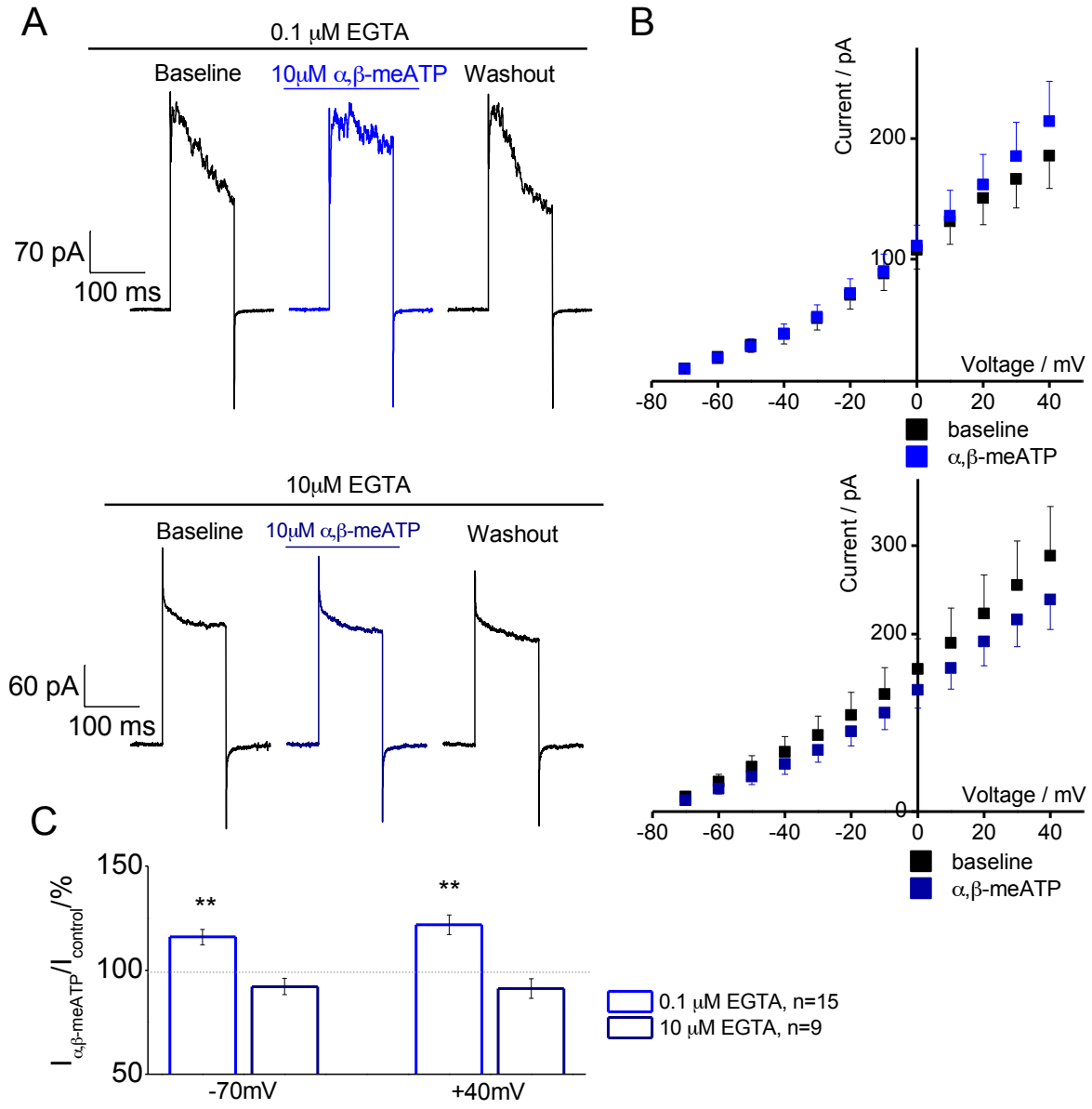

Figure 4.3: **Total potassium current is facilitated by αβ-methylene ATP**. A – Representative traces of recordings, B – Average I/V relationship graphs, C - The average effect of drug applications. The changes in potassium currents upon activation with 10 μM αβ-methylene ATP in cells with 0.1 μM of EGTA and 10 μM EGTA in the patch pipette were measured. The average current recorded from isolated astrocytes activated by 10 μM αβ-methylene ATP in the presence of intracellular Calcium was 115.9±3.7 and 121.8±4.7 per cent of the control current at -70 and +40 mV steps respectively. As calculated with one-sample t test the effect of the addition the analogue of ATP is significantly different from the control current (p=0.0004 and p=0.00007 as calculated with one-sample t test). The addition of αβ-methylene ATP under the presence of Calcium chelator EGTA yielded a mean current of 92.2±3.9 and 91.2±4.7 per cent of control current at -70mV and +40mV steps respectively, failing to increase the potassium current; ** shows p<0.01 with two-sample t test (comparing current ratios under high and low EGTA concentrations). Note scale change.

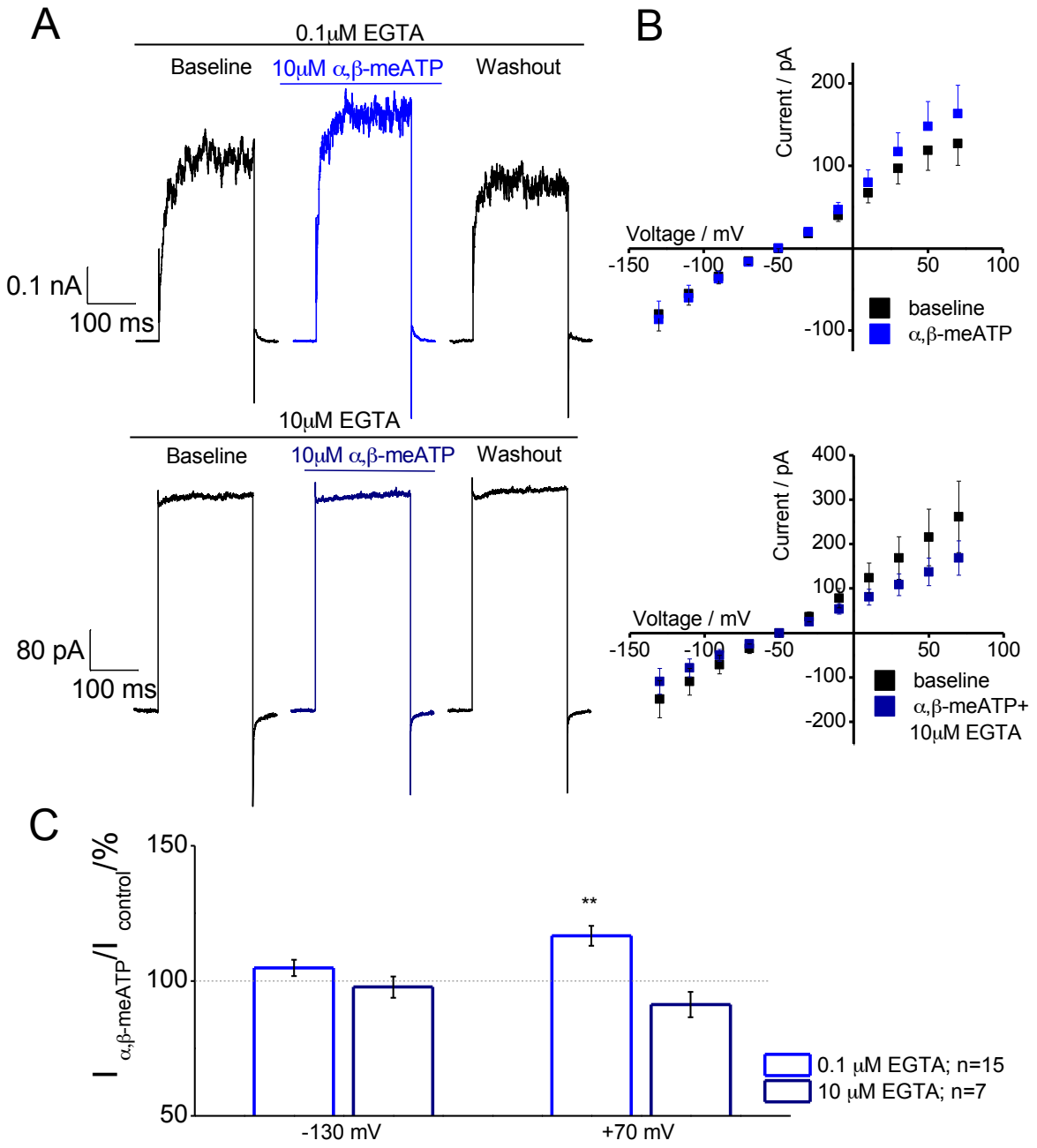

Figure 4.2: **Inwardly rectifying potassium current is not facilitated by αβ-methylene ATP in the presence or absence of intracellular Calcium.** A – Representative traces of recordings, B – Average I/V relationship graphs, C - The average effect of drug applications. The changes in potassium currents upon addition of 10 μM αβ-methylene ATP in cells with 0.1 μM of EGTA and 10 μM EGTA in the patch pipette were measured. The average current recorded from isolated astrocytes activated by 10 μM αβ-methylene ATP in the presence of intracellular Calcium was 104.8±3 and 116.7±3.7 per cent of the control current at -130 and +70 mV steps respectively. As calculated with one-sample t test, the effect of the addition of the analogue of ATP was significant at high voltage steps (p=0.0002), but not at -130mV, where the inwardly rectifying potassium channel dominates the current. The addition of αβ-methylene ATP under the presence of Calcium chelator EGTA yielded a mean current of 97.7±3.9 and 91.2±4.7 per cent of control current at -130mV and +70mV steps respectively, failing to increase the potassium current; ** shows p<0.01 with two-sample t test (p=0.0002, comparing current ratios under high and low EGTA concentrations). Note scale change.

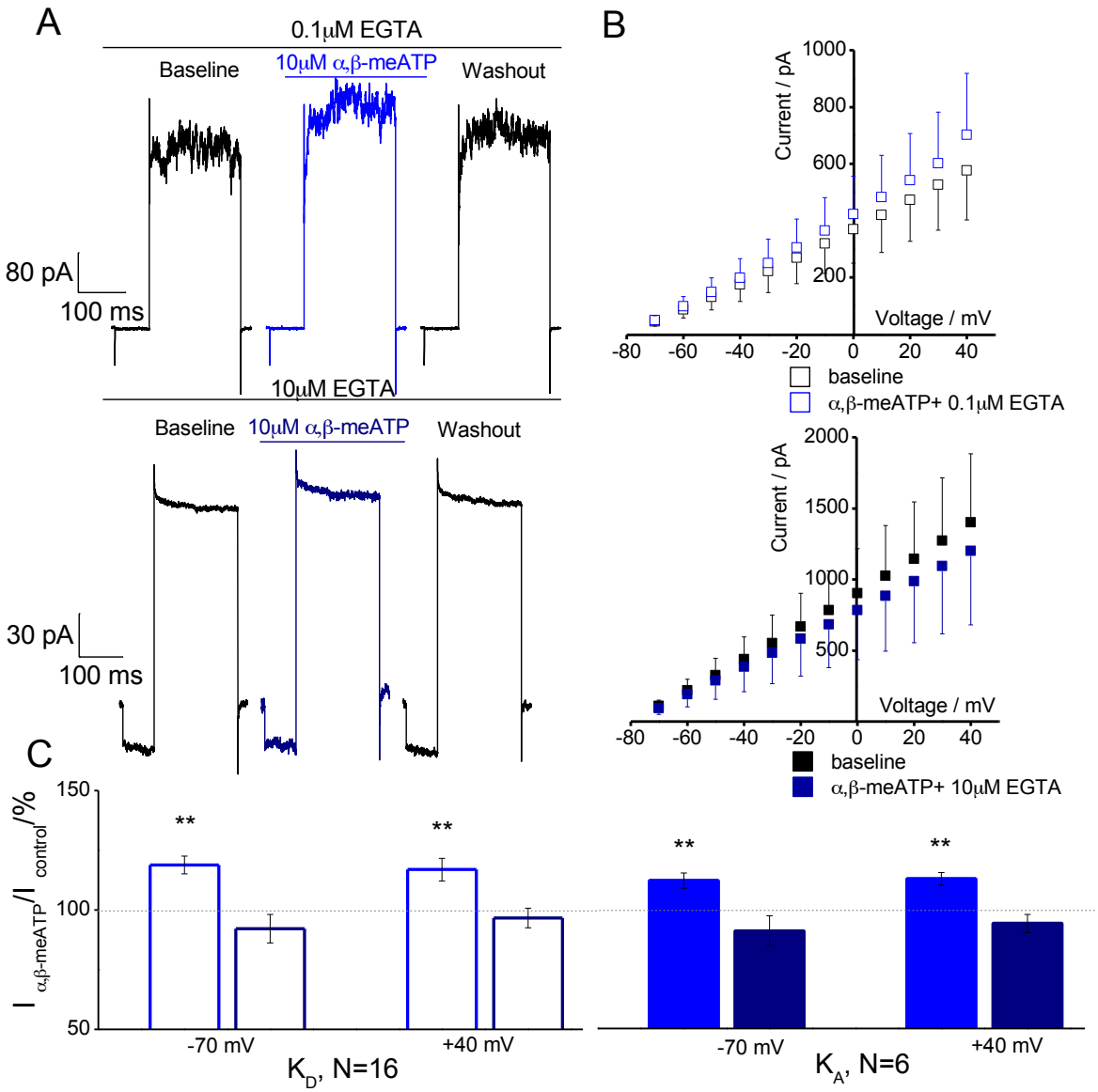

Figure 4.3: **Steady state (K_D) and rapidly inactivating (K_A) potassium currents is facilitated by *αβ*-methylene ATP in the presence of intracellular Ca^{2+}.** A – Representative traces of recordings, B – Average I/V relationship graphs, C - The average effect of drug applications. The changes in potassium currents upon addition of 10 μM *αβ*-methylene ATP in cells with 0.1 μM of EGTA and 10 μM EGTA in the patch pipette were measured. The average current recorded from isolated astrocytes activated by 10 μM *αβ*-methylene ATP in the presence of intracellular Calcium was 118.8±3.7 and 116.9±4.8 per cent (steady state) and 111.9±3.2 and 112.6±2.6 per cent (rapidly inactivating) of the control current at -70 and +40 mV steps respectively. As calculated with one-sample t test both the steady state and rapidly inactivating currents under the addition of the analogue of ATP are significantly greater than the control under the presence of intracellular Calcium (steady state: p=0.00008 and p=0.0007 at low and high voltage steps; rapidly inactivating: p= 0.01 and p=0.002 respectively). ** shows p<0.05 with two-sample t test (p= 0.001 and p=0.002, comparing current ratios under high and low EGTA concentrations). Note scale change.

4.2.4 Effect of addition of NMDA under the presence or absence of intracellular Calcium in isolated astrocytes

It was determined that there was a facilitation effect on the potassium current upon the bath addition of 10 μM of αβ-methylene ATP. This effect was found to be Ca-dependent, since it was abolished by the removal of intracellular Calcium by 10 μM EGTA. It was decided to test whether more than one channel type can be used for this Calcium influx into the astrocytic cell. Since NMDA receptors in glial cells are permeable to Calcium, it was hypothesised that activating NMDARs should elicit the same effect as the activation of P2X receptors.

To activate NMDARs 10 μM of N-methyl-D-aspartate (NMDA) was applied to the recording chamber. Two conditions were used: under the presence of intracellular Calcium ions, and in their absence. Different concentrations of Calcium chelator EGTA, 0.1 and 10 μM were used to make up the respective conditions. In parallel with the αβ-methylene ATP experiments, three protocols were recorded to review the effect of the addition of NMDA on different subtypes of potassium currents. Figures 7-10 show the data collected for these experiments: typical experimental currents observed and averages, presented as mean ± SEM. One sample t test was used to compare the effect observed with the control current and two-sample t test was utilised for comparing the experimental current ratios under the low and high EGTA concentrations.

Figure 4.6 illustrates the data collected for the first protocol: 12 voltage steps starting from -70 mV from the -80 mV holding potential. As can be seen, under the low EGTA concentration, the addition of 10 μM NMDA produces 122.6±5.6 and 123.7±5.3 per cent of control current at the -70 and +40 mV steps respectively. This facilitation effect is significantly different from the control currents and from the 98.2±4.4 and 99.4±4.9 per cent found under 10 μM of EGTA, as calculated with

one-sample and two-sample t tests respectively. Therefore it appears that activation of NMDARs starts the same Ca^{2+} transduction pathway as the activation of P2X receptors in astrocytes, whereby a transient increase in the intracellular calcium can activate the IP_3 channels, located on the ER, which in turn opens internal calcium stores.

Inwardly rectifying potassium current was addressed in the second protocol recorded: holding potential of -50 mV and 11 voltage steps from -130 to +70 mV. At two lowest voltage steps, -130 and -110 mV the inwardly rectifying potassium channel conductance prevails in the current. As can be seen from Figure 4.7, there is a minor increase in current at -130mV (102.8±3.3 compared to 100 % control), however this increase is not significant. At +70mV step, however, this facilitation effect seems to re-appear under the low concentration of EGTA (0.1 μM) – producing 126.2±5.7 per cent of the control current. When the high concentration of Calcium chelator was used the experimental current ratios were 96.5±5.0 and 97.8±4.4 per cent of the control currents. There is no significant difference between the two conditions at -130mV step, but the 28% difference between the current ratios at +70mV is significant with $p<0.01$. This means that the addition of Calcium chelator abolishes the facilitation effect due to the addition of NMDA.

A third protocol was recorded, to measure the voltage-gated potassium currents more closely. The deactivating pre step of -20 mV precedes 12 voltage steps from holding potential of -80 mV starting from -70 mV. Figure 4.8 shows the data collected for the steady state and rapidly desensitizing potassium current components to this protocol. Similarly to the total potassium current, the recordings with low concentrations of EGTA displayed the increase following the addition of the extracellular NMDA. The steady state current had a 121.6±7.6 and 117.0±3.7 per cent of control currents for the -70 and +40 mV steps respectively. When the intracellular Calcium was mopped up by the high concentration of

EGTA this effect did not take place; steady state current yielded 97.6±3.4 and 98.1±3.9 per cent of the control current at lowest and highest voltage steps respectively. A very similar trend was exhibited by the data for the rapidly desensitizing potassium current. Under the presence of intracellular Calcium the lowest and highest voltage steps show 116.6±5.2 and 112.1±4.1 per cent of control, and only 98.1±3.4 and 99.0±3.5 per cent when the 10 μM of EGTA was added to the patch pipette.

These data demonstrated reliably that the effect of the addition of 10 μM of NMDA to the recording chamber is akin to the effect, produced by the addition of the analogue of ATP. Both of these drugs are activators of ionotropic channels that are Calcium permeable in astrocytes. This leads us to believe that the activation of P2X or NMDARs allows an influx of Calcium ions inside the astrocyte soma, where it can subsequently up-regulate the outgoing potassium current.

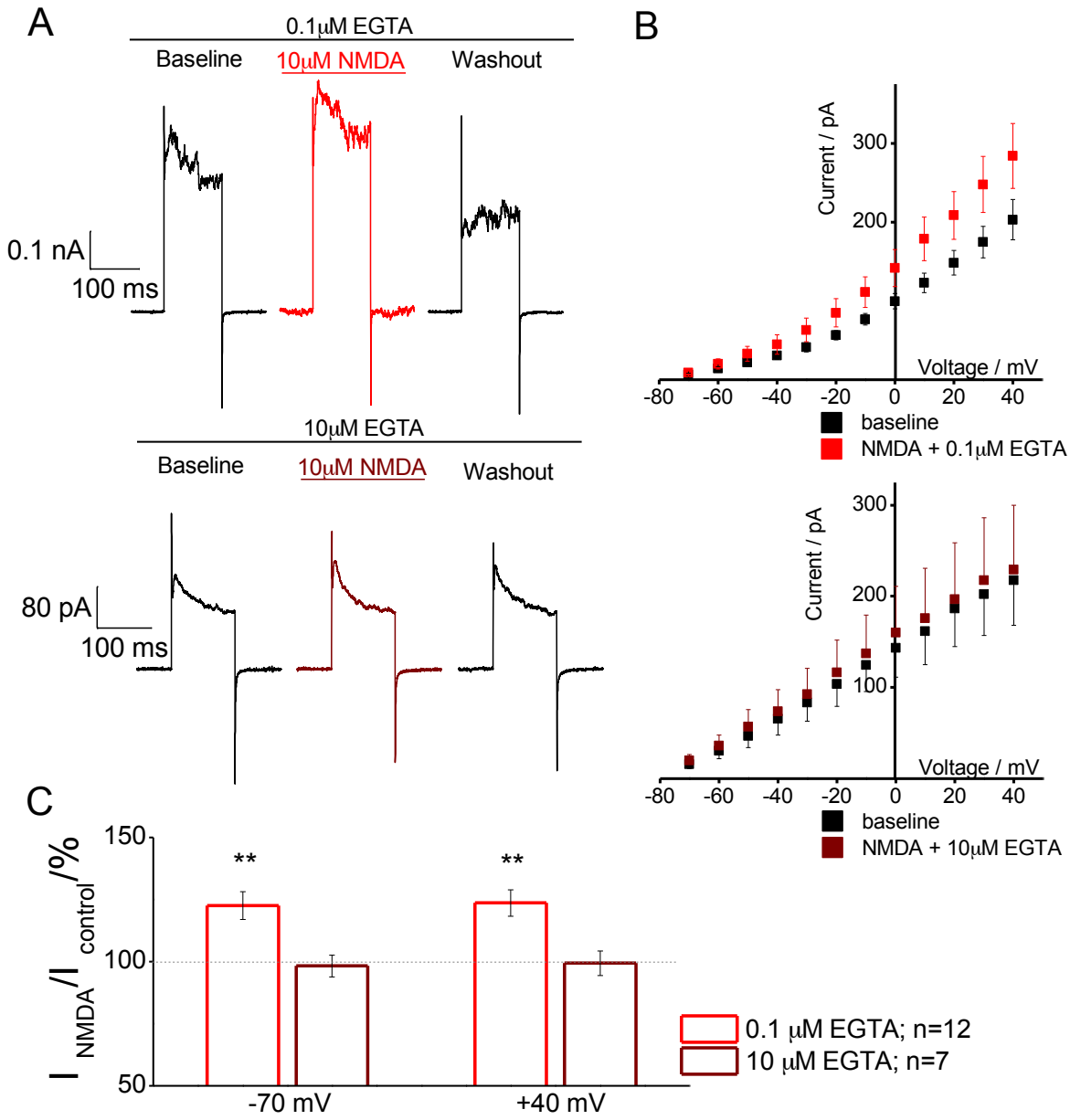

Figure 4.6: **Total potassium current is facilitated by NMDA in the presence of intracellular Ca^{2+}.** A – Representative traces of recordings, B – Average I/V relationship graphs, C - The average effect of drug applications. The changes in potassium currents upon activation with 10 μM NMDA in cells with 0.1 μM of EGTA and 10 μM EGTA in the patch pipette were measured. The average current recorded from isolated astrocytes activated by 10 μM NMDA in the presence of intracellular Calcium was 122.6±5.6 and 123.7±5.3 per cent of the control current at -70 and +40 mV steps respectively. As calculated with one-sample t test the effect of the addition of NMDA was significantly different from the control current (p=0.004 and p=0.0002 at low and high voltage steps respectively). The addition of NMDA under the presence of Calcium chelator EGTA yielded a mean current of 98.2±4.4 and 99.4±4.9 per cent of control current at -70mV and +40 mV steps respectively, failing to increase the potassium current; ** shows p<0.01 with two-sample t test (p=0.003 and p=0.001 at low and high voltage steps, comparing current ratios under high and low EGTA concentrations). Note scale change.

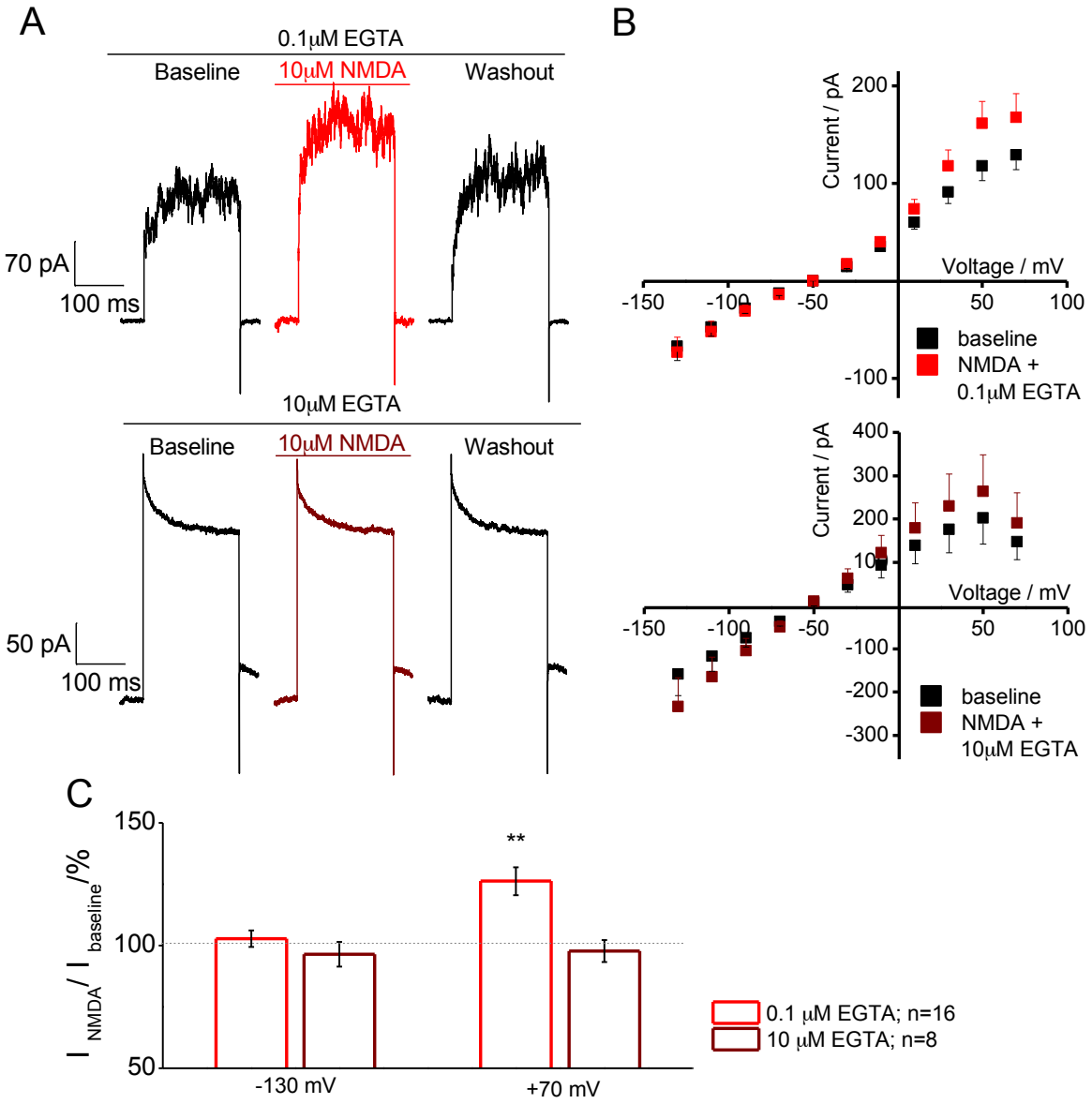

Figure 4.7: **Inwardly rectifying potassium current is not facilitated by NMDA in the presence of intracellular Ca^{2+}.** A – Representative traces of recordings, B – Average I/V relationship graphs, C - The average effect of drug applications. The changes in potassium currents upon activation with 10 μM NMDA in cells with 0.1 μM of EGTA and 10 μM EGTA in the patch pipette were measured. The average current recorded from isolated astrocytes activated by 10 NMDA in the presence of intracellular Calcium was 102.8±3.3 and 126.2±5.7 per cent of the control current at -130 and +70 mV steps respectively. As calculated with one-sample t test, the effect of the addition of NMDA is significant at high voltage step, but not at -130 mV (p=0.0001 for +70 mV step). The addition of NMDA under the presence of Calcium chelator EGTA yielded a mean current of 96.5±5 and 97.8±4.4 per cent of control current at -130 and +70 mV steps respectively, failing to increase the potassium current; ** shows p<0.01 with two-sample t test (p=0.003 at +70 mV, comparing current ratios under high and low EGTA concentrations). Note scale change.

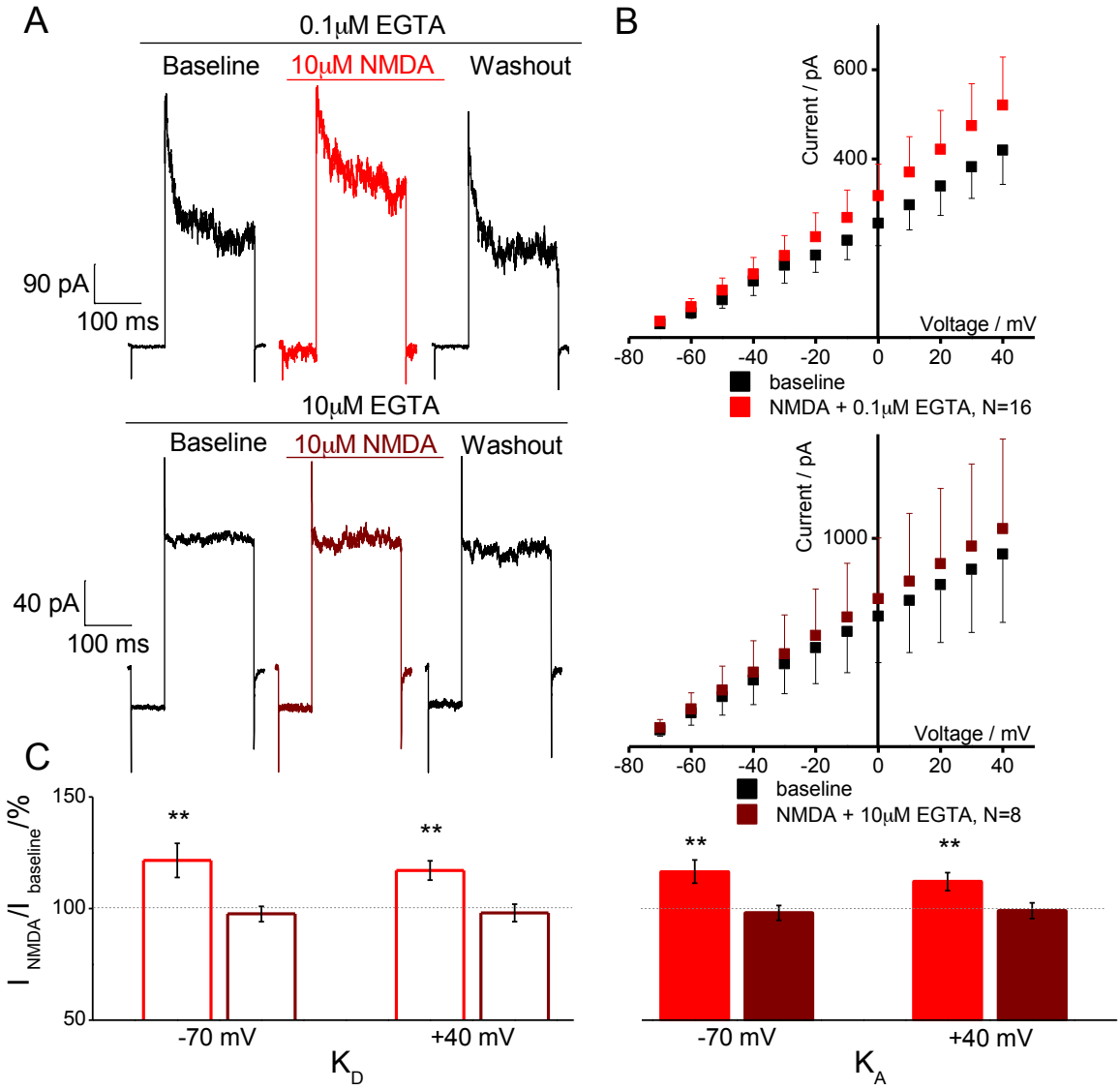

Figure 4.8: **Steady state (KD) and rapidly inactivating (KA) potassium current are facilitated by NMDA in the presence of intracellular** $^{Ca2+}$. A – Representative traces of recordings, B – Average I/V relationship graphs, C - The average effect of drug applications. The changes in potassium currents upon activation with 10 μM NMDA in cells with 0.1 μM of EGTA and 10 μM EGTA in the patch pipette were measured. The average current recorded from isolated astrocytes activated by 10 μM NMDA in the presence of intracellular Calcium was 121.6±7.6 and 117.0±3.7 per cent of the control steady state current at -70 and +40 mV steps respectively. The average rapidly inactivating current recorded from isolated astrocytes activated by 10 μM NMDA in the presence of intracellular Calcium was 116.6±5.2 and 112.1±4.1 per cent of the control current at -70 and +40 mV steps respectively. The addition of NMDA under the 10 μM EGTA yielded a mean steady state current of 97.6±3.4 and 98.1±3.9 per cent and mean rapidly inactivating current of 98.1±3.4 and 99.0±3.5 per cent of control current at -70 and +40 mV steps respectively, failing to increase either steady state or rapidly inactivating potassium currents. As calculated with one-sample t test the effect of the addition of NMDA is significant for both currents under the presence of intracellular Calcium (Steady state: p=0.008 and p=0.001 for -70 and +40 mV; rapidly inactivating: p=0.005 and p=0.007 at -70 and +40 mV respectively); ** shows p<0.01 with two-sample t test (comparing current ratios under high and low EGTA concentrations). Note scale change.

4.2.5 Age-related changes in the link between activation of NMDARs and potassium currents of astrocytes

The effect of ageing on this facilitation of potassium current by the addition of NMDA to the aCSF was investigated. Astrocytes were isolated from mice of Group III (9-12 months old) and patch-clamped, with three protocols being recorded for the control current, current under the application of NMDA and the washout current under the presence of intracellular Calcium ions. Figure 4.9 shows the data collected for these cells.

As calculated with one-sample t test the effect of the addition of NMDA in astrocytes from old mice diminishes compared to their young counter parts. The total potassium current was increased by the addition of NMDA at the lowest voltage steps, producing a mean current ratio of 117.2±9.2 per cent of the control current at -70 mV. However, this increase diminished towards the highest voltage steps; +40 mV step had an average current ratio of 100.7±2.7 per cent of control current.

The protocol for recording inwardly rectifying potassium current collected the data that was very akin to corresponding data collected from young adult mice. At the lowest voltage step, -130 mV, the current ratio is 105.8±3.3, showing only a small insignificant increase, whereas at +70 mV the current reaches 120.0±6.7 per cent of the control current upon the addition of the NMDA.

Voltage-gated potassium currents, both steady state and rapidly desensitizing kinds, seem to be less susceptible to this facilitation effect in astrocyte from Group III mice. Steady state current type reaches 109.9±7.2 per cent at -70 mV and only 104.7±4.0 per cent of control currents and rapidly desensitizing potassium current

shows a smaller effect of NMDA still: 105.8±3.6 and 101.5±1.3 per cent respectively.

The data presented on Figure 4.9 displays that the facilitation that activation of NMDARs causes in young adult mice is less prominent in astrocytes from older mice. Specifically, the voltage-gated potassium currents seem to be less responsive to the addition of 10 μM of NMDA.

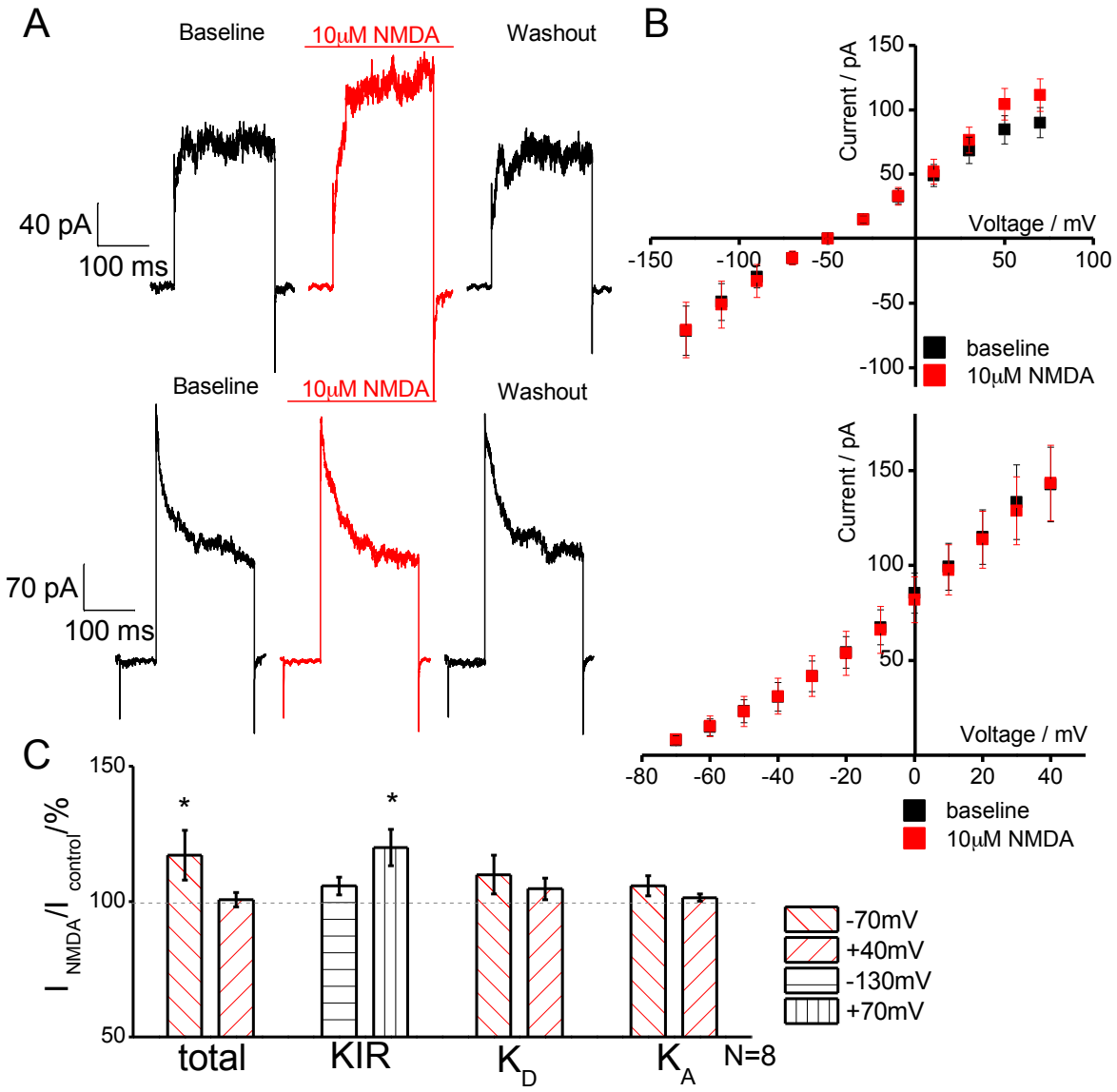

Figure 4.9: **Facilitation of potassium currents by NMDA is less pronounced in old mice**. A – Representative traces of recordings, B – Average I/V relationship graphs, C - The average effect of drug applications. The changes in potassium currents upon activation with 10 μM NMDA in astrocytes from old mice (9-12 months PN) were measured. The average current recorded from isolated astrocytes activated by 10 μM NMDA was 117.2±9.2 and 100.7±2.7 per cent of the control current at -70 and +40 mV in total potassium current. The inwardly rectifying current was 105.8±3.3 and 120.0±6.7 per cent of control at -130 and +70 mV voltage steps respectively. The average steady state current recorded from isolated astrocytes activated by 10 μM NMDA was 109.9±7.2 and 104.7±4.0 per cent of the control current at -70 and +40 mV of total potassium current; rapidly desensitizing current produced current ratios of 105.8±3.6 and 101.5±1.3 at corresponding voltage steps. As calculated with one-sample t test the effect of the addition of NMDA in astrocytes from old mice diminishes compared to their young counter parts, so only the lowest voltage step for the steady state current produces a significant ($p<0.05$) increase when compared to control current; * shows $p<0.05$ with one-sample t test ($p = 0.052$ and $p=0.01$ for -70 mV and +70 mV of total and inwardly rectifying potassium currents respectively). Note scale change.

4.2.6 Distinguishing between affected potassium currents by the bath addition of αβ-methylene ATP under 4-aminopyridine or barium chloride

To further investigate the nature of this facilitation mechanism, two potassium channel blockers were used to determine whether there is a specific subtype of potassium channel that is affected by the extracellular addition of αβ-methylene ATP. The blockers used were 4-aminopyridine and barium chloride, at 40 and 100 μM concentrations respectively.

4-aminopyridine is a voltage-gated potassium channel blocker, which is often used for evoking epileptogenesis (Frenguelli and Wall 2016). Barium chloride is a specific inwardly rectifying potassium channel blocker. The barium ion resides in the pore of the channel, thus prohibiting its' conductive properties(Seifert et al. 2009). Since the hypothesis at work is that adding the αβ-methylene ATP affects the conduction of voltage-gated potassium currents, then blocking the inwardly rectifying potassium current should yield a greater increase in this facilitation effect. It is even possible that blocking the inwardly rectifying potassium current can cause this effect to appear at -130 mV step, despite not being prominent in other experimental conditions.

The electrophysiological protocols used were identical to those in the previous experiments. When the current ratios were calculated in experiments with the addition of the blockers, the current under the blocker was used as a control. This was done specifically to avoid confusion between the effect of the blocker on the control current and the effect of the addition of the αβ-methylene ATP on top of the blocker.

Figures 4.10 – 4.12 illustrate the data collected for these experiments, presented as mean ± SEM in bar charts and displaying typical examples of currents observed during these recordings. Firstly, the total potassium current was measured (see

Figure 4.10), and the differences in them due to addition of αβ-methylene ATP under the influence of 4-aminopyridine or barium chloride. In control condition, where 10 μM αβ-methylene ATP was added without the presence of any blockers, the mean current ratios were 122.6±5.6 and 123.7±5.3 per cent of the control current at -70 and +40 mV steps respectively. The addition of αβ-methylene ATP after the application of 4-aminopyridine yielded the current ratios of only 104.8±5.0 and 102.2±4.1 for the corresponding voltage steps. This means that the addition of 4-aminopyridine effectively blocks the facilitation effect of the addition of αβ-methylene ATP to the aCSF. Therefore, the currents affected by this effect are sensitive to 4-aminopyridine, which is a known voltage-gated potassium channel blocker. When barium chloride was added to the bath prior to the addition of αβ-methylene ATP, the experimental current ratios reached 133.1±17.2 and 117.3±7.7 per cent of control currents at -70 mV and +40 mV respectively. Both sets of current ratios from control condition and under the influence of barium chloride were significantly different from their respectively control currents (as calculated with one-sample t test, $p<0.01$), and also significantly different from the data collected for experiments under the influence of 4-aminopyridine blocker (as calculated with two-sample t test, $p<0.01$).

The data for the protocol, recording inwardly rectifying potassium current (holding potential -50 mV with 11 voltage steps from -130 to +70 mV) are presented on Figure 4.11. The current ratios recorded in the control condition were 102.8±3.3 and 126.2±5.7 per cent of the control current at -130 mV and +70 mV respectively. Current ratios recorded under the presence of 4-aminopyridine showed a mean of 104.0±5.3 and 104.1±4.2 for the same voltage steps, thus not introducing any changes at -130 mV but completely abolishing the facilitation of current at +70 mV. Application of barium chloride prior to the addition of αβ-methylene ATP yielded 109.0±3.8 and 114.7±3.8 per cent of control currents. At 130 mV only the experiments where barium chloride was added demonstrate a

significantly increased current upon the addition of αβ-methylene ATP (as calculated with one-sample t test, $p<0.01$). This means that when the inwardly rectifying potassium current is blocker, the potassium current elevates upon application of 10 μM αβ-methylene ATP. At highest voltage step, the trend is similar to the data collected with the previous protocol. The addition of 4-aminopyridine blocks the effect of the addition of αβ-methylene ATP, whereas barium chloride does not.

Thirdly, the data obtained through protocol for considering voltage-gated potassium current are presented on Figure 4.12. Two distinct components, the steady state and rapidly desensitizing potassium currents were studied separately. The control conditions for steady state voltage-gated potassium current yielded 121.6±7.6 and 117.0±4.4 per cent of control currents at -70 and +40 mV steps respectively. When 4-aminopyridine was applied prior to the addition of αβ-methylene ATP, mean current ratios of 114.1±6.6 and 102.8±6.1 per cent were recorded. Finally, in experiments with addition of barium chloride, the following current ratios were recorded for -70 and +40 mV: 122.5±4.5 and 111.1±3.9 per cent respectively. The addition of 4-aminopyridine blocked the facilitation of potassium current at +40 mV, but only reduced it at -70 mV. Barium chloride, however, did not decrease the effect shown in control condition. At -70 mV all experimental conditions displayed an increase in current upon the addition of αβ-methylene ATP (one-sample t test, $p<0.05$), whereas at +40 mV only the control and experiments under barium chloride are significantly different from their control current ratios.

The data for rapidly desensitizing potassium current appeared more similar to the data for the total potassium current. In control experiments the addition of αβ-methylene ATP evoked 116.6±5.2 and 112.1±4.1 per cent of control currents, at -70 and +40 mV respectively. The experiments where 4-aminopyridine was added

prior to $\alpha\beta$-methylene ATP application these voltage steps displayed 108.7±1.9 and 105.3±2.8 per cent of control current ratios only. Addition of barium chloride yielded 120.5±5.7 and 111.0±3.5 per cent of control current ratios at corresponding voltage steps. Both conditions, the control experiments and with addition of barium chloride, were significantly different from the current ratios calculated for the experiments with the addition of 4-aminopyridine (as calculated with two-sample t test, $p<0.05$).

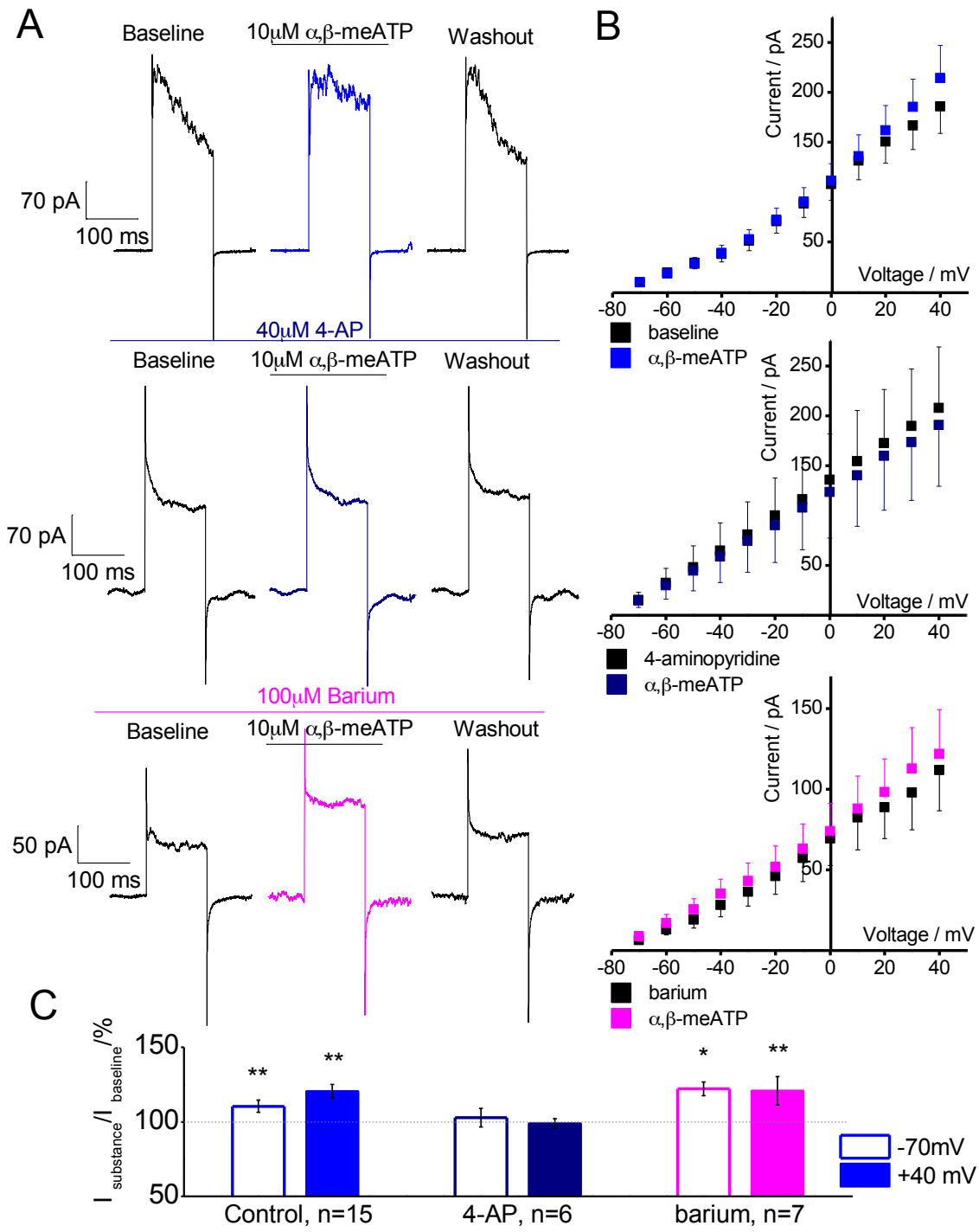

Figure 4.10: **Facilitation of total potassium current by αβ-methylene ATP is blocked by 4-aminopyridine but not barium chloride.** A – Representative traces of recordings, B – Average I/V relationship graphs, C - The average effect of drug applications. The changes in potassium currents upon activation with 10 μM αβ-methylene ATP in cells under the application of 40 μM 4-aminopyridine and 100 μM barium chloride in the aCSF were measured. As calculated with two-sample t test both conditions, control and under the influence of barium, yielded significantly greater currents than experiments with the application of 4-aminopyridine; ** shows $p<0.05$ with two-sample t test ($p=0.02$ and $p=0.005$ at -70 and +40 mV when comparing current ratios in control and 4-aminopyridine conditions $p=0.04$ (at +40 mV step) for barium chloride and 4-aminopyridine experimental conditions); * shows $p<0.05$ as measured with one-sample t test ($p=0.03$ at -70 mV steps in experiments with addition of barium chloride).

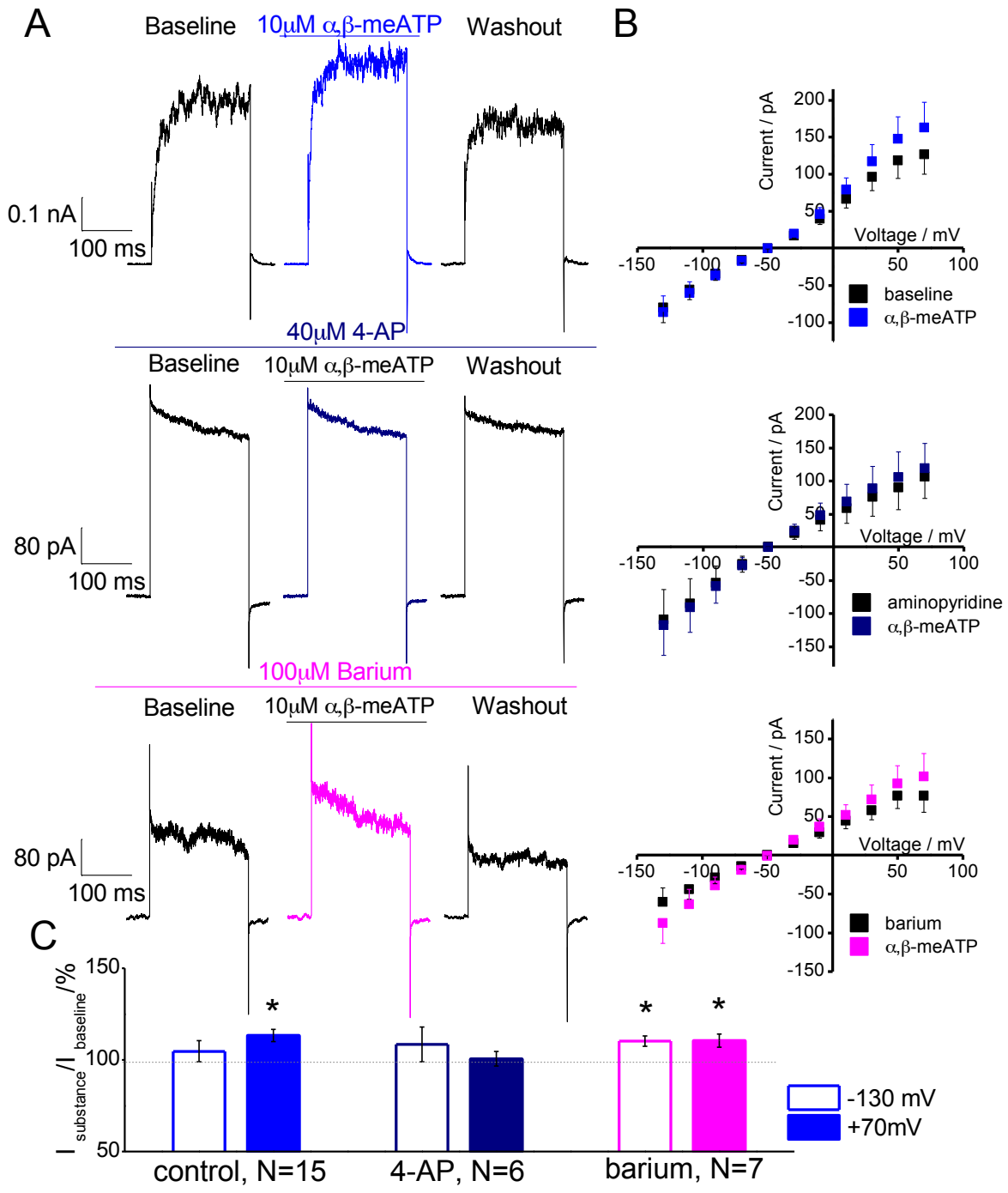

Figure 4.11: **Facilitation of inwardly rectifying potassium currents by αβ-methylene ATP is blocked by 4-AP but not barium chloride.** A – Representative traces of recordings, B – Average I/V relationship graphs, C - The average effect of drug applications. The changes in potassium currents upon activation with 10 μM NMDA in cells under the application of 40 μM 4-aminopyridine and 100 μM barium chloride in the aCSF were measured. As calculated with two-sample t test both conditions, control and under the influence of barium, produced significantly greater currents than those in the experiments with 4-aminopyridine. At -130 mV the addition of barium chloride allowed the increase of the current; * shows $p<0.05$ with two-sample t test (comparing control and barium chloride to 4-aminopyridine conditions respectively). Note scale change.

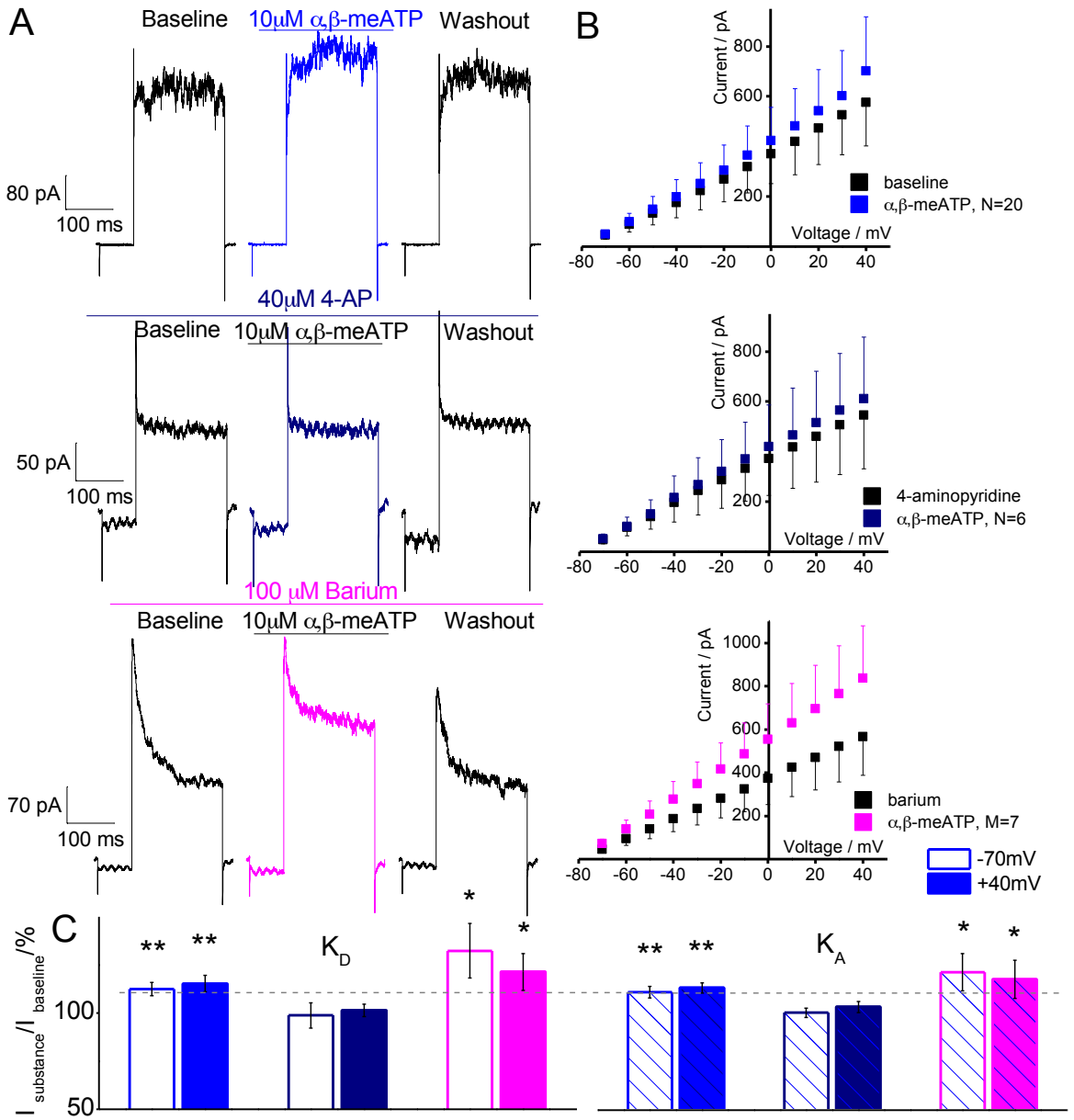

Figure 4.12: **Facilitation of steady state (K_D) and rapidly inactivating (K_A) voltage-gated potassium currents by αβ-methylene ATP is blocked by 4-aminopyridine but not barium chloride.** A – Representative traces of recordings, B – Average I/V relationship graphs, C - The average effect of drug applications. The changes in potassium currents upon activation with 10 μM αβ-methylene ATP in cells under the application of 40 μM 4-aminopyridine and 100 μM barium chloride in the aCSF were measured. As calculated with two-sample t test at +40 mV step both, K_D and K_A, currents were significantly higher in experiments with application of barium chloride; ** shows $p<0.05$ with two-sample t test (steady state current: $p=0.04$ when comparing current ratios in control and experiments with barium chloride with experiments with 4-aminopyridine. Rapidly inactivating current: $p=0.04$ $p=0.02$ respectively); * shows $p<0.05$ as calculated with the one-sample t test ($p=0.0008$ and $p=0.011$ experiments with barium chloride).

4.2.7 Distinguishing between potassium currents affected by the addition of NMDA under 4-aminopyridine or barium chloride

An identical set of experimental conditions was set up for testing whether the bath addition of 10 μM αβ-methylene ATP produced a similar set of data, as did the experiments that used NMDA as an activator of the autocrine mechanism that links NMDARs and P2X receptors in astrocytes with voltage-gated potassium channels. Three protocols were recorded, with four potassium current subtypes being measured. The data is presented below in Figures 4.13 – 4.15 as mean ± SEM and examples of typical currents observed during the recordings.

Total potassium current was considered in the first protocol: 12 voltage steps, starting from -70 to +40 mV, from holding potential of -80 mV. Figure 4.13 displays the data collected for this protocol from three experimental conditions. Control experiments show 110.4±4.1 and 120.5±4.7 per cent current ratios from control current at -70 and +40 mV steps. Addition of 4-aminopyridine prior to the application of NMDA achieved full block of the actions of NMDA: 102.8±6.1 and 98.8±3.4 per cent of control currents. When barium chloride was used in place of 4-Aminopyridine, the facilitation effect of NMDA not only was not blocked, but instead it increased further. The mean current ratios were 122.1±4.7 and 120.8±9.5 per cent of control currents at low and high voltage steps respectively. These data follow the same pattern as the data collected for the experiments with the addition of αβ-methylene ATP.

Second protocol considers both inwardly rectifying and total potassium currents (see Figure 4.14). In control condition the addition of NMDA caused the current to be 104.7±5.8 and 113.3±3.4 per cent of control currents for -130 and +70 mV respectively. The addition of 4-aminopyridine before the application of NMDA did not introduce prominent change at -130 mV step (108.5±9.5), however at +70 mV the increase was completely abolished, with the current staying at 100.6±4.0

per cent of control. Finally, barium chloride did not inhibit the increase that is caused by the addition of NMDA. The current ratios measured in experiment with barium chloride were 110.3±3.4 and 110.6±3.6 per cent at low and high voltage steps respectively. Again, similarly to data for experiments with $\alpha\beta$-methylene ATP, at -130 mV step, the addition of barium chloride allowed the facilitation effect to be seen. At high voltage step in this protocol, the data show very similar trend to the protocol above.

The third protocol, for reflecting the trends in voltage-gated potassium currents, was recorded. The steady state and rapidly desensitizing components of the currents measured by this protocol are considered separately, but are presented on together on Figure 4.15.

The steady state current reaches 112.5±3.4 and 115.3±4.2 per cent of control currents, when recorded without any blockers added. The addition of 4-aminopyridine before the application of NMDA fully blocked any increase in current, with 98.8±6.6 and 101.4±3.2 per cent of control currents at -70 and +40 mV respectively. When barium chloride was used in place of 4-Aminopyridine, the effect of the addition of NMDA became more prominent: 132.3±14.1 and 121.4±9.6 per cent at corresponding voltage steps. These data show that the addition of barium chloride exaggerates the mechanism in question, whereas 4-aminopyridine diminishes the effect of NMDA. From this one can derive that the potassium channels that are affected by this mechanism are of voltage-gated variety, since blocking them inhibits this mechanism.

The patterns presented by rapidly inactivating potassium current are similar to that of the steady state potassium current. Such, the control experiments show the facilitation of current to 110.5±3.0 and 112.6±2.6 per cent at -70 and +40 mV respectively. The addition of 4-aminopyridine removes this intensification effect

and only yields 99.8±2.4 and 102.8±2.9 per cent at corresponding voltage steps. The addition of barium chloride, however, causes the opposite. The current ratios increase to 120.7±9.7 and 117.0±9.9 per cent respectively under the influence of barium chloride.

Taken together, the data gathered for the effect of the addition of NMDA display patterns comparable with those of experiments where $\alpha\beta$-methylene ATP was used in place of NMDA. This means that the mechanism at work is a common one for both of these drugs and the corresponding channels (NMDARs and $P2X_{1/5}$ receptors) are involved in this mechanism in a similar manner.

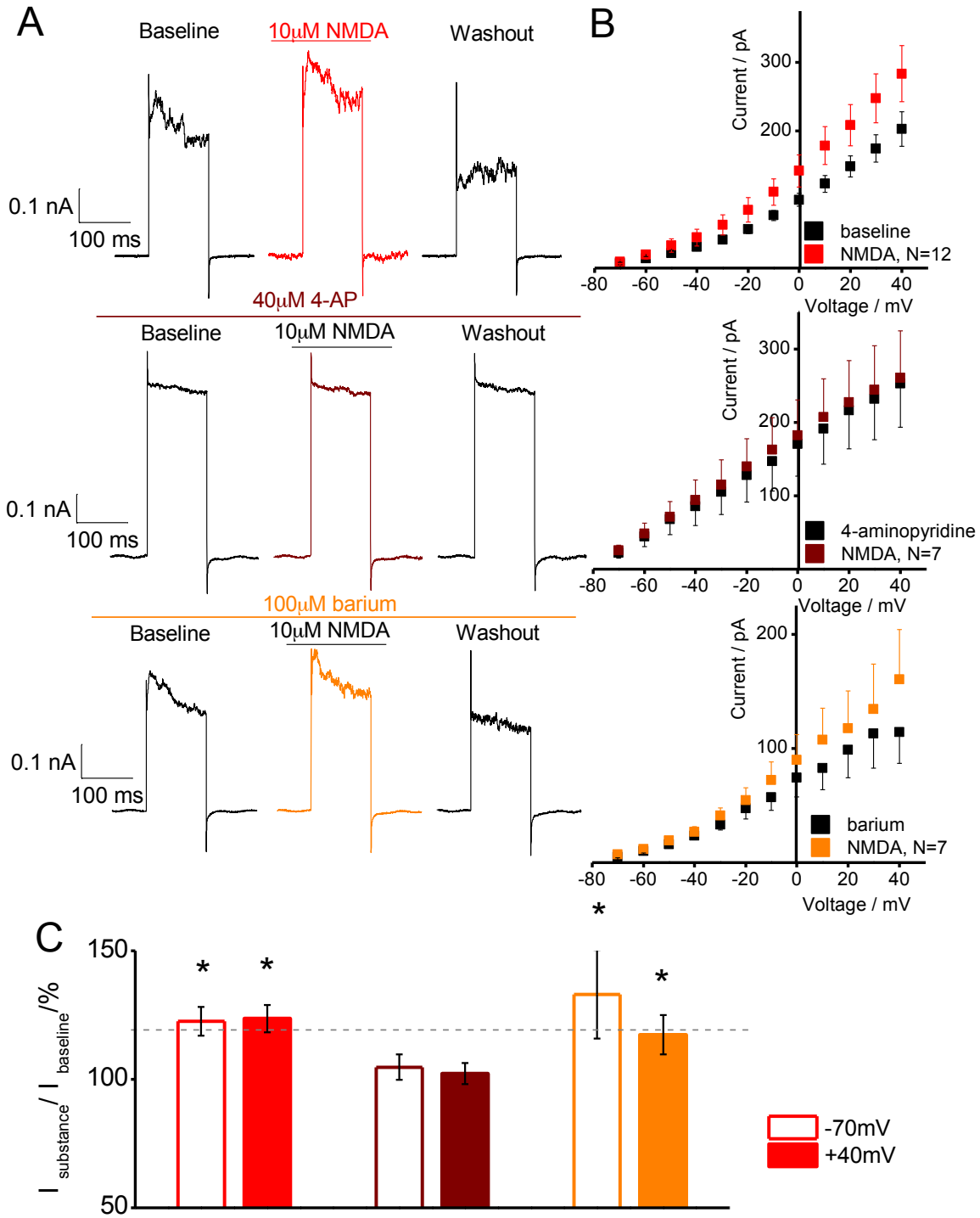

Figure 4.13: **Facilitation of total potassium current by NMDA is blocked by 4-aminopyridine but not barium chloride**. A – Representative traces of recordings, B – Average I/V relationship graphs, C - The average effect of drug applications. The changes in potassium currents upon activation with 10 μM NMDA in cells under the application of 40 μM 4-aminopyridine and 100 μM barium chloride in the aCSF were measured. As calculated with two-sample t test the currents measured in both conditions, control and under the influence of barium, were significantly greater than those from experiments with 4-aminopyridine; * shows $p<0.05$ with two-sample t test (comparing current ratios in different experimental conditions).

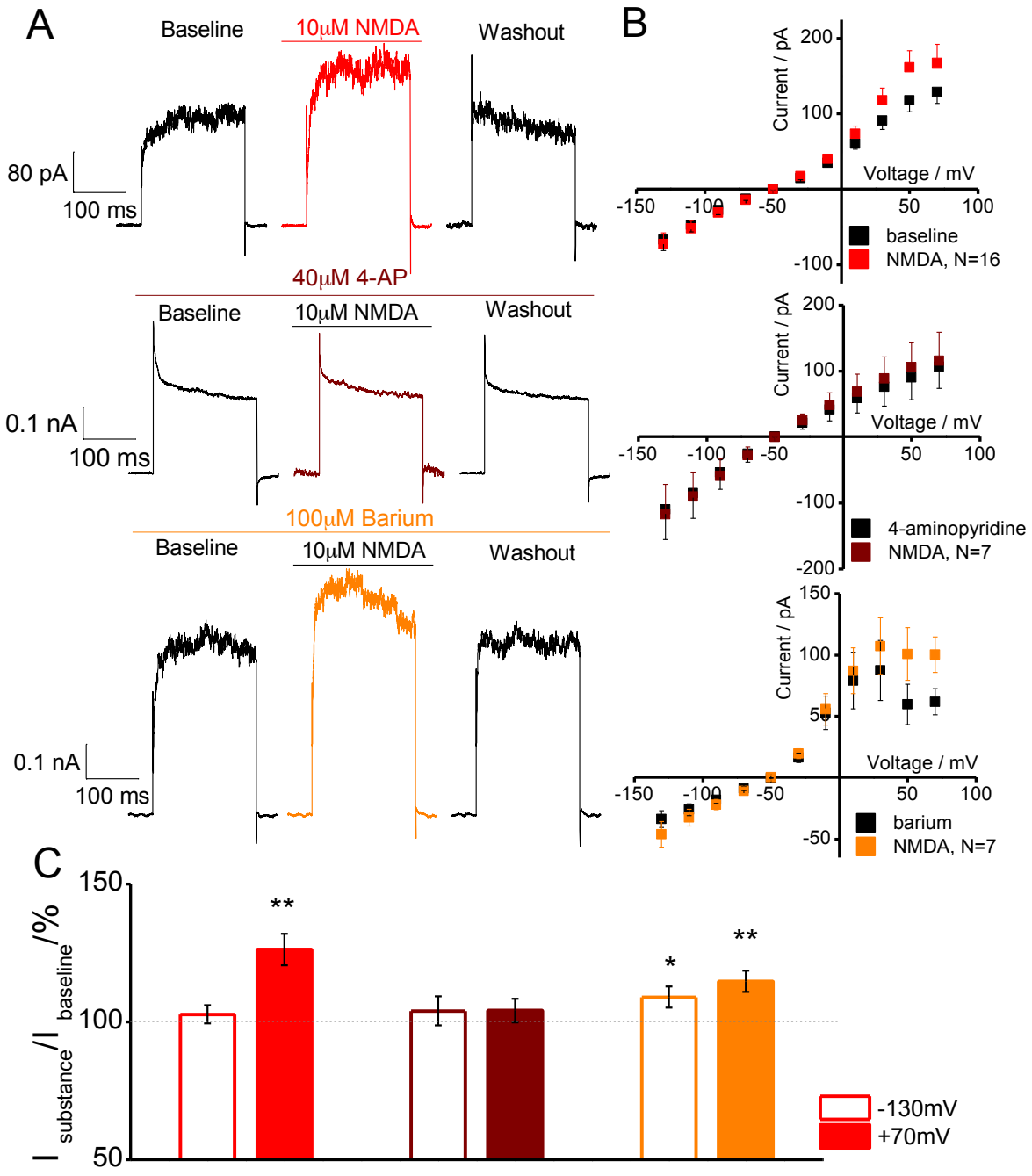

Figure 4.14: **Facilitation of inwardly rectifying potassium current by NMDA is blocked by 4-aminopyridine but not barium chloride**. A – Representative traces of recordings, B – Average I/V relationship graphs, C - The average effect of drug applications. The changes in potassium currents upon activation with 10 μM NMDA in cells under the application of 40 μM 4-aminopyridine and 100 μM barium chloride in the aCSF were measured. As calculated with two-sample t test the currents measured in both conditions, control and under the influence of barium, were significantly greater than those from experiments with the application of 4-aminopyridine at high voltage step. At -130 mV the addition of barium chloride allowed the facilitation effect to take place; ** shows $p<0.05$ with two-sample t test (comparing current ratios in different experimental conditions). Note scale change.

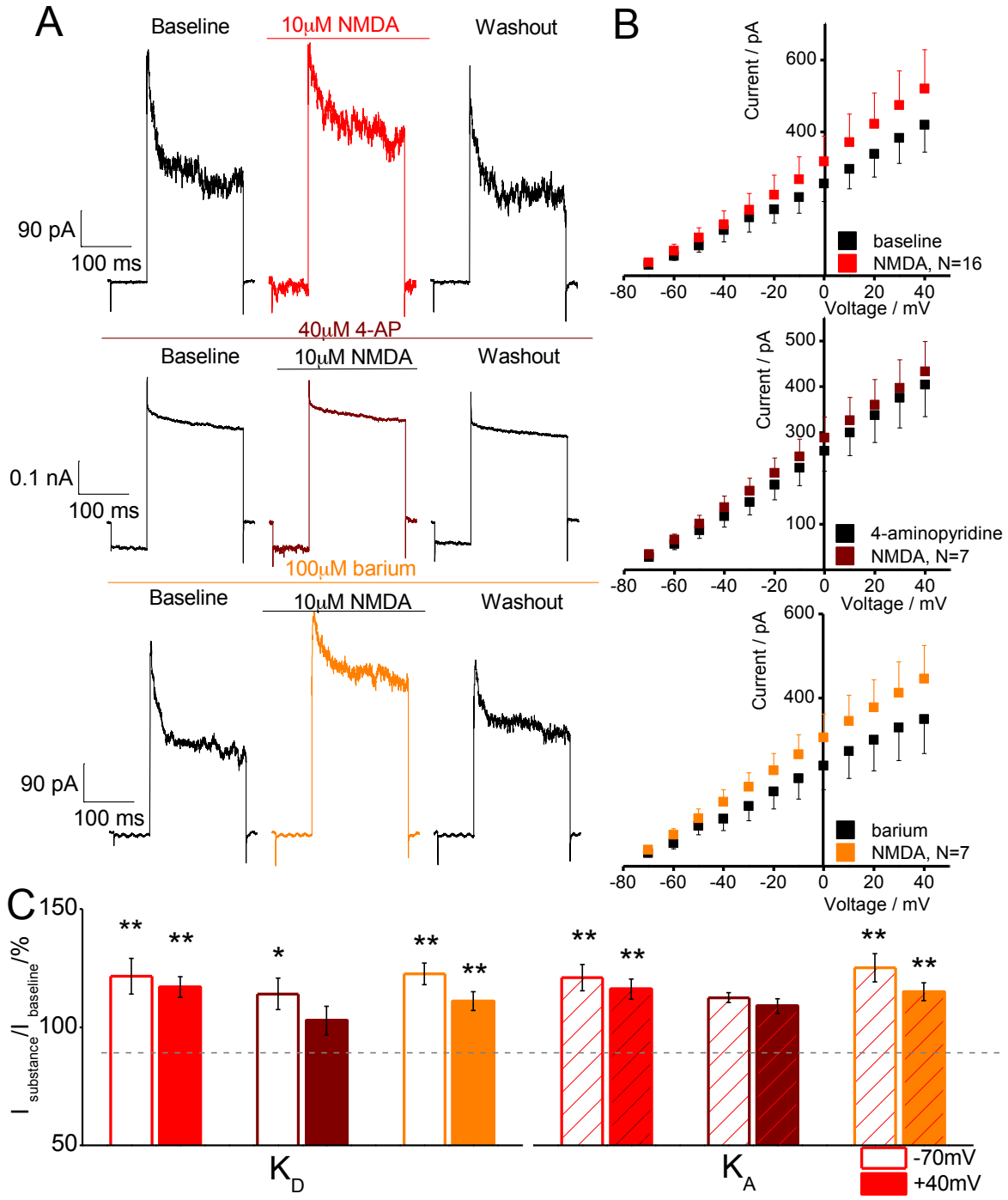

Figure 4.15: **Facilitation of steady state (K_D) and rapidly inactivating (K_A) voltage-gated potassium currents by NMDA is blocked by 4-aminopyridine but not barium chloride**. A – Representative traces of recordings, B – Average I/V relationship graphs, C - The average effect of drug applications. The changes in potassium currents upon activation with 10 μM NMDA in cells under the application of 40 μM 4-aminopyridine and 100 μM barium chloride in the aCSF were measured. As calculated with two-sample t test the currents measured in both conditions, control and barium chloride experiments, were significantly greater than that from experiments with 4-aminopyridine; * shows P<0.05 as calculated with one sample t test; ** shows p<0.05 with two-sample t test. Note scale change.

4.2.8 Distinguishing between potassium currents affected by the addition of TFLLR under 4-aminopyridine or barium chloride

From the data described in sections 4.3.1-4.3.6, it has been shown that there is a cellular mechanism that links the ionotropic channels, namely P2X and NMDARs, and potassium channels in the astrocytic soma. It was determined that the voltage-gated potassium current subtype is affected by the activation of either of these channels. Upon activation of P2X or NMDARs with their agonists the channels open and permit an influx of ions, some of which will be Ca^{2+} ions. This Calcium-driven message will reach the inside of the cell, where it can affect multiple players and elicit a subsequent response, in this case the elevation of voltage-gated potassium current by 10-30 percent. The increase in the potassium out flux can raise the extracellular concentration of K^{+} ions in nearby projections of other astrocytes and trigger responses from other glial cells. An increase in the intracellular Calcium can itself trigger a vast number of molecular cascades, thus making this a mechanism of high functional importance.

If the activation of ionotropic receptors can propagate the Calcium messenger inside the cell, can a stimulation of a metabotropic receptor that raises the intracellular concentration of Calcium, elicit a similar response, causing an increase in potassium current?

PAR-1 is a G-protein coupled receptor that is also known as coagulation factor II (thrombin) receptor. It is present in many types of cells, including astrocytes and neurons. In astrocytes it is expressed specifically in sell body and astrocytic endfeet, which enwrap capillaries in the brain. Activating PAR-1 receptor increases intracellular Ca^{2+} concentration (Junge et al. 2004). This made PAR-1 receptor a perfect testing candidate for testing whether the mechanism in question

has a GPCR connection. A short peptide, TFLLR-NH2 (TFLLR), derived from PAR-1 receptor acts was used as a selective agonist.

The experimental set up was identical to experiments with NMDA and $\alpha\beta$-methylene ATP, with three protocols being recorded. The data collected for experiments with TFLLR are presented on Figures 4.16-4.18 below.

Overall, the pattern displayed by the total potassium current is akin to that shown by the experiments with $\alpha\beta$-methylene ATP and NMDA. At control conditions, the addition of 10 μM TFLLR caused a slight rise of potassium current, 105.6±7.8 and 114.6±4.5 per cent at -70 and +40 mV. The addition of 4-aminopyridine reversed this effect, yielding 90.2±5.3 and 91.1±3.7 per cent of control current ratios. In experiments where barium chloride was applied prior to the addition of TFLLR, the current ratios reached 125.9±7.9 and 114.7±2.9 per cent of control currents. Once again, the addition of 4-aminopyridine before the application of TFLLR blocks any increase in the potassium current, whereas the addition of barium chloride only exaggerates the effect of TFLLR.

The protocol, studying both total and inwardly rectifying potassium current also showed similar trends as the experiments with the addition of ionotropic receptor agonists. Figure 4.17 illustrates the data obtained. In control conditions, the mean current ratios upon the addition of TFLLR were 106.6±4.5 and 111.1±4.0 per cent. At -130 mV there is no prominent increase in the potassium current following the addition of TFLLR. Adding 4-aminopyridine resulted in decrease of the current ratios: 88.9±3.8 and 102.1±6.7 per cent were achieved at -130 and +70 mV respectively. At corresponding voltage steps, the addition of barium chloride caused an increase in the potassium current after the addition of TFLLR up to 119.4±7.4 and 121.2±6.6 per cent respectively. In this protocol application of barium chloride prior to TFLLR aids the increase of the potassium current.

Data collected for the third protocol, consisting of two current components, is presented on Figures 4.18, with steady state and rapidly desensitizing currents respectively. In control conditions, the steady state voltage-gated potassium current reached 113.5±6.8 and 108.9±3.7 upon the addition of TFLLR, very similar to that of rapidly desensitizing potassium current: 110.4±6.5 and 109.0±3.2 per cent of control current ratios at -70 and +40 mV steps respectively. The addition of 4-aminopyridine rectified this facilitation effect of TFLLR: 92.4±6.3 and 90.1±4.7 per cent for the steady state and 91.0±7.9 and 88.7±4.4 per cent for the rapidly desensitizing potassium currents at corresponding voltage steps. When barium chloride was added instead of 4-aminopyridine, the facilitation effect of the application of TFLLR was completely restored and even enhanced. The steady state current achieved 115.2±4.0 and 111.1±2.9 per cent and the rapidly desensitizing potassium current 116.7±3.7 and 112.2±3.0 per cent of control currents at -70 and +40 mV respectively.

Overall, these data show that activation of PAR -1 channel elicits the same effect as the activation of ionotropic NMDA and P2X receptors in isolated astrocytes. Therefore, it can be assumed that the mechanism responsible for link between these receptors and potassium current is unique for ionotropic and metabotropic receptors.

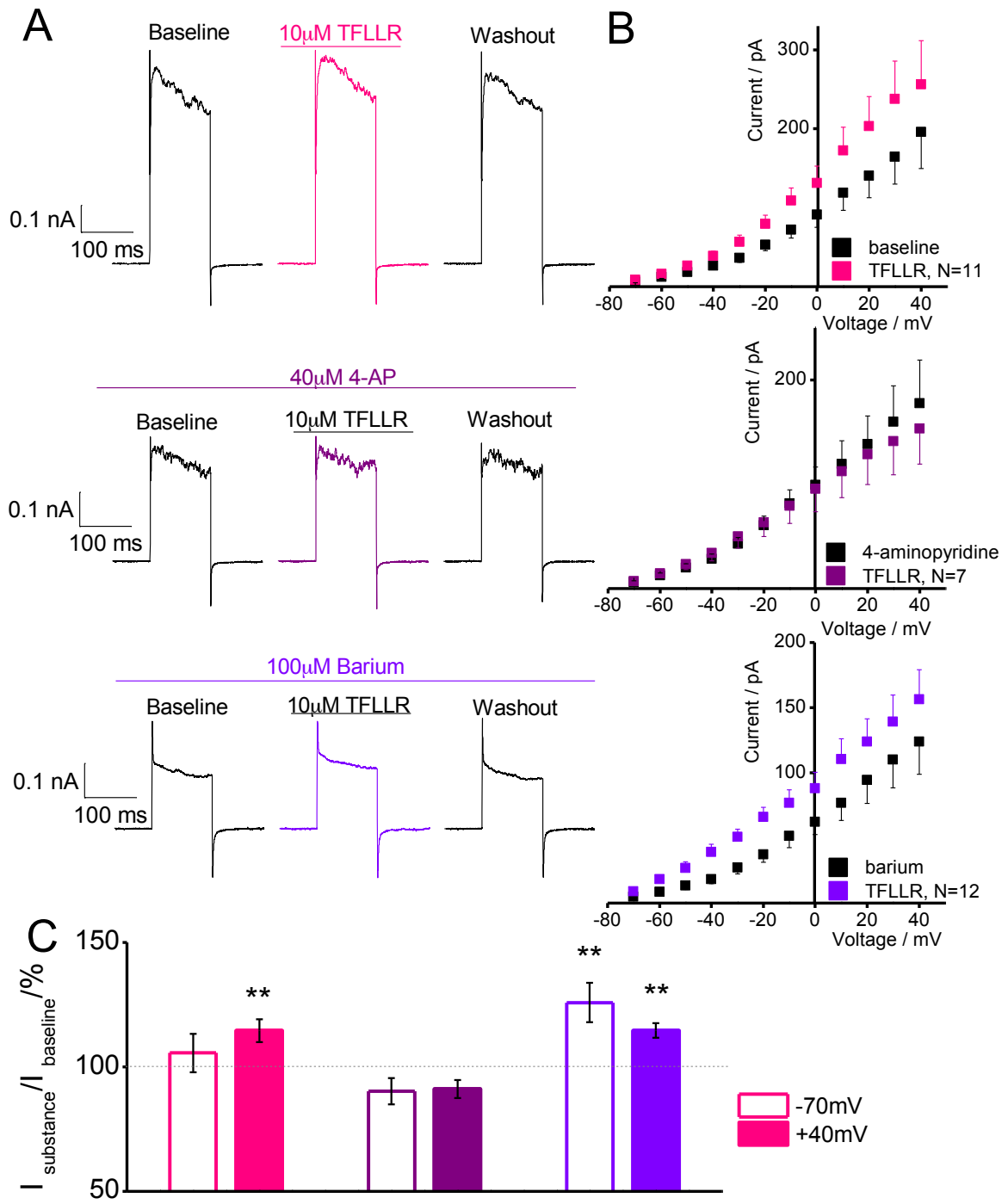

Figure 4.16: **Facilitation of total potassium current by TFLLR is blocked by 4-aminopyridine but not barium chloride**. A – Representative traces of recordings, B – Average I/V relationship graphs, C - The average effect of drug applications. The changes in potassium currents upon activation with 10 μM TFLLR in cells under the application of 40 μM 4-aminopyridine and 100 μM barium chloride in the aCSF were measured. As calculated with two-sample t test the currents measured in both conditions, control and under the influence of barium, were significantly greater than that from experiments with 4-aminopyridine; ** shows $p<0.01$ with two-sample t test (comparing current ratios in different experimental conditions).

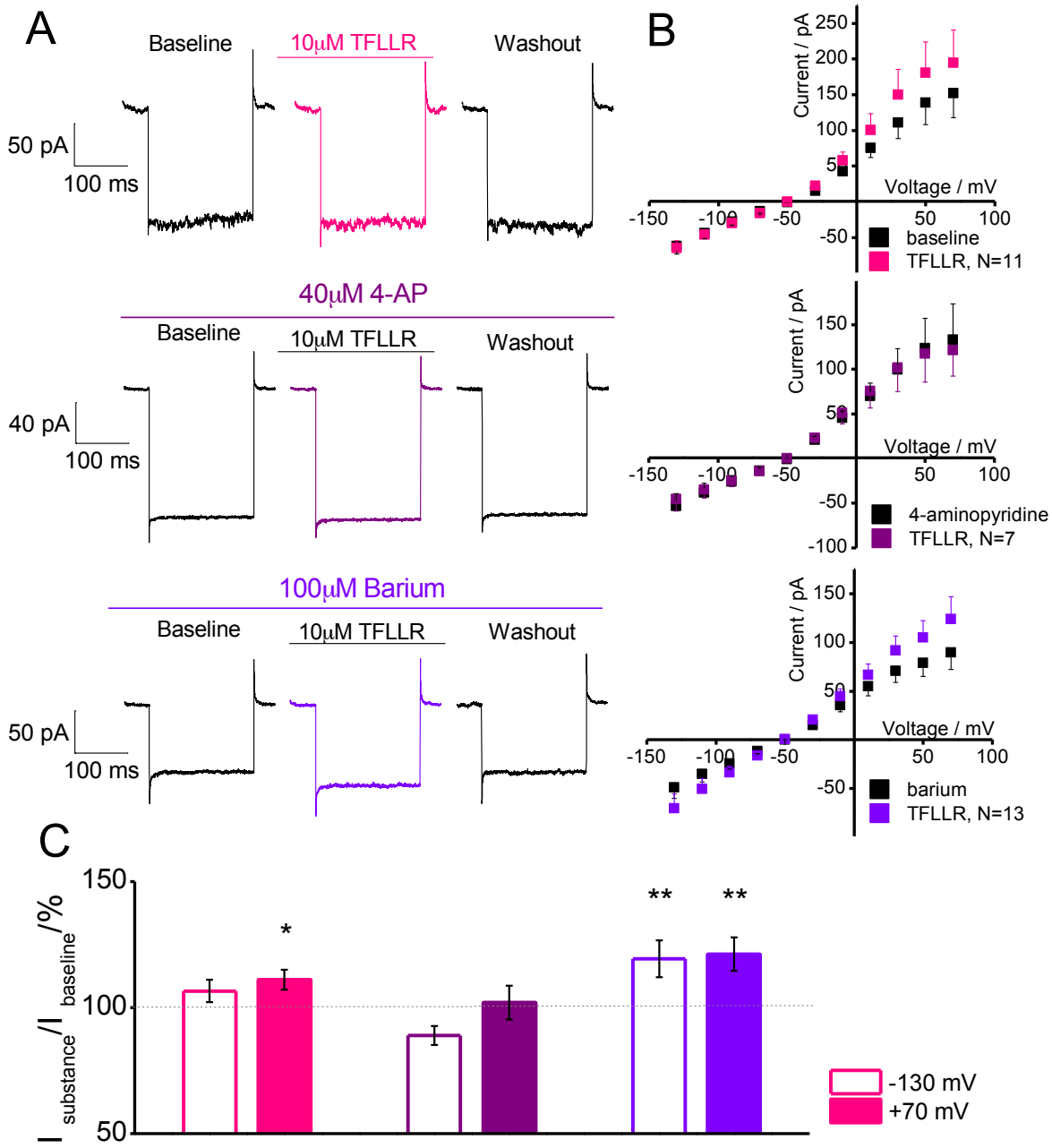

Figure 4.17: **Facilitation of inwardly rectifying potassium current by TFLLR is blocked by 4-aminopyridine but not barium chloride**. A – Representative traces of recordings, B – Average I/V relationship graphs, C - The average effect of drug applications. The changes in potassium currents upon activation with 10 μM TFLLR in cells under the application of 40 μM 4-aminopyridine and 100 μM barium chloride in the aCSF were measured. As calculated with two-sample t test the currents from both conditions, control and under the influence of Barium, were significantly greater than those from experiments with 4-aminopyridine at low voltage steps. At +70 mV the addition of barium chloride allowed the increase of the current; ** shows $p<0.01$ with two-sample t test (comparing current ratios in different experimental conditions); * shows $p<0.01$ as calculated with the one-sample t test. Note scale change.

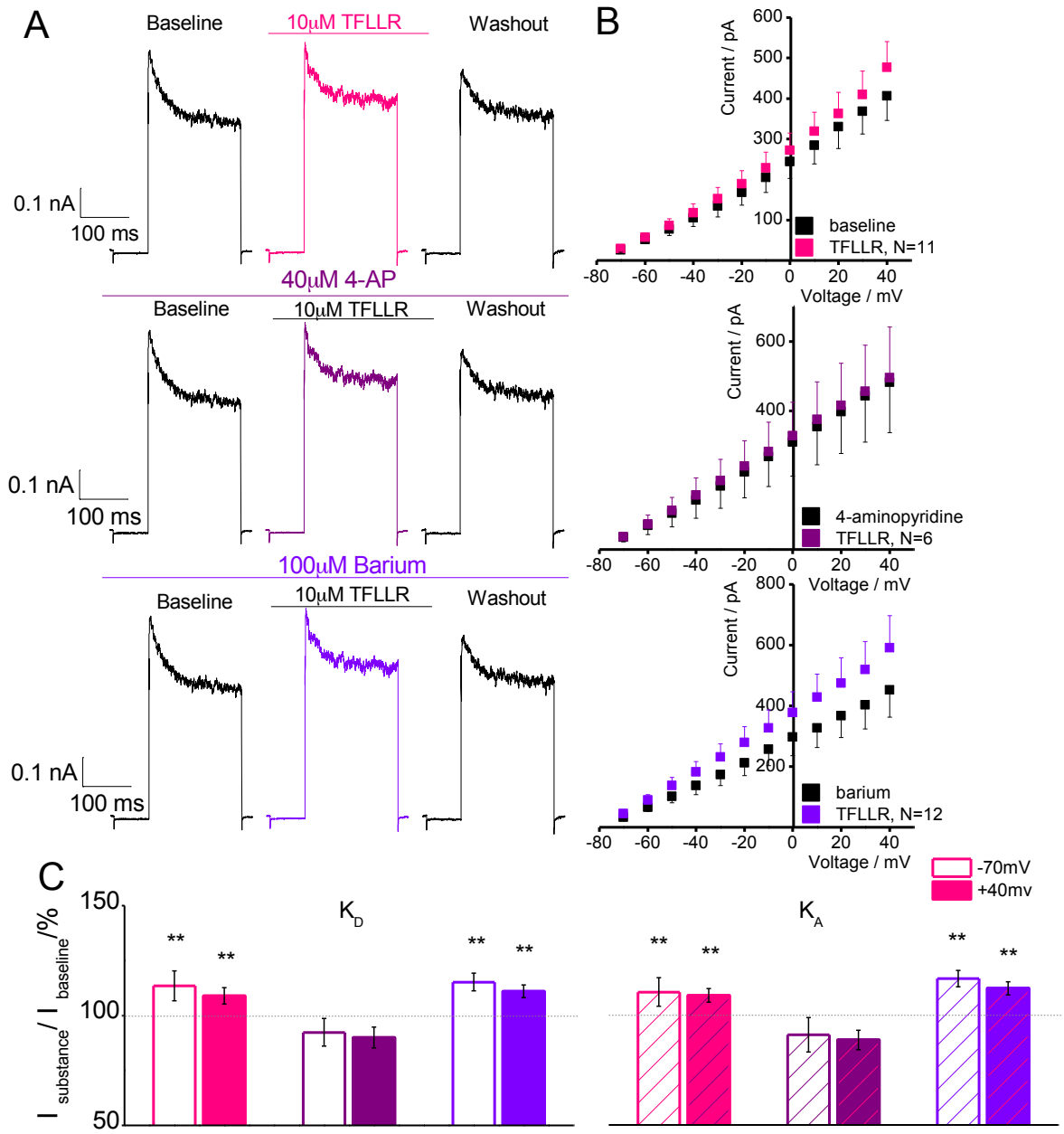

Figure 4.18: **Facilitation of steady state (K_D) and rapidly inactivating (K_A) voltage-gated potassium currents by TFLLR is blocked by 4-aminopyridine but not barium chloride.** A – Representative traces of recordings, B – Average I/V relationship graphs, C - The average effect of drug applications. The changes in potassium currents upon activation with 10 μM TFLLR in cells under the application of 40 μM 4-aminopyridine and 100 μM barium chloride in the aCSF were measured. As calculated with two-sample t test the currents from both control and barium chloride experiments were significantly greater than those recorded in experiments with 4-aminopyridine; ** shows $p<0.01$ with two-sample t test (comparing current ratios in different experimental conditions).

4.2.9 The effect of addition of αβ-methylene ATP in astrocytes in slices

The cells were patched in slices in order to test, whether this mechanism is viable in the presence of other cells, and in intact astrocytes *in situ*, with all the projections of the patched astrocyte (including perisynaptic branchlets and endfeet) are linked to the entire synaptic network in a more or less intact manner. Figures 4.19 and 4.20 display the data collected for whole-cell patched astrocytes in slices.

Firstly, some cells were patched in slice and their potassium currents were recorded overtime to examine the spontaneous fluctuations. These experiments were used as control time courses (Figure 4.19). For experimental conditions, 10 μM αβ-methylene ATP was applied during some recordings (marked with a blue and purple lines) and in other recordings 100 μM barium chloride was added to the aCSF prior to application of αβ-methylene ATP. The facilitation effect is still present in these experiments. Upon the activation of the P2X receptors with the addition of αβ-methylene ATP, the current ratio grew up to 138.3±14.6 per cent. When compared with control experiments, the difference was significant ($p=0.11*10^{(-9)}$ as calculated with the two-sample t test. In experiments with the addition of the drug under the influence of barium chloride blocker the maximal current ratio was 135.8±14.2 ($p=0.14*10^{(-6)}$ per cent of the control current as calculated with the two-sample t test). These data show that the described effect of facilitation of current by the activation P2X receptors is relevant in the context of the entire slice. It can therefore be assumed that this mechanism takes place in the living brain of rodents.

Figure 4.20 shows the data collected for the astrocytes patched in slice in the same format as the data presented above. It compared the control experiments, where no drugs were added (green on Figure 4.20) and two sets of experiments with the

addition of αβ-methylene ATP, with and without the prior treatments with the barium chloride blocker. The protocol for total and inwardly rectifying potassium current was recorded. In control experiments the current ratios were 101.2±2.7 and 100.0±1.6 per cent at corresponding time points as application of drug in other experimental conditions. The addition of αβ-methylene ATP increased the current in both, high and low, voltage steps; the current ratios recorded were 126.2±11.3 and 122.6±7.3 per cent at -130 and +30 mV steps respectively. The addition of barium chloride prior to the application of αβ-methylene ATP did not block this increase, yielding 114.0±6.4 and 121.4±7.1 per cent of control current at corresponding voltage steps. These data show that the facilitation effect, originally demonstrated in isolated astrocytes, is still present in patched astrocytes in slices. When working in slices *in situ*, the application of agonists, such as αβ-methylene ATP, the network effects can provide secondary effects. For instance, the application of an analogue of ATP would activate both P2 and P1 receptors in neurons, which can have downstream effects. These include increased neuronal signalling, transmitter release with increased glutamate and potassium uptake.

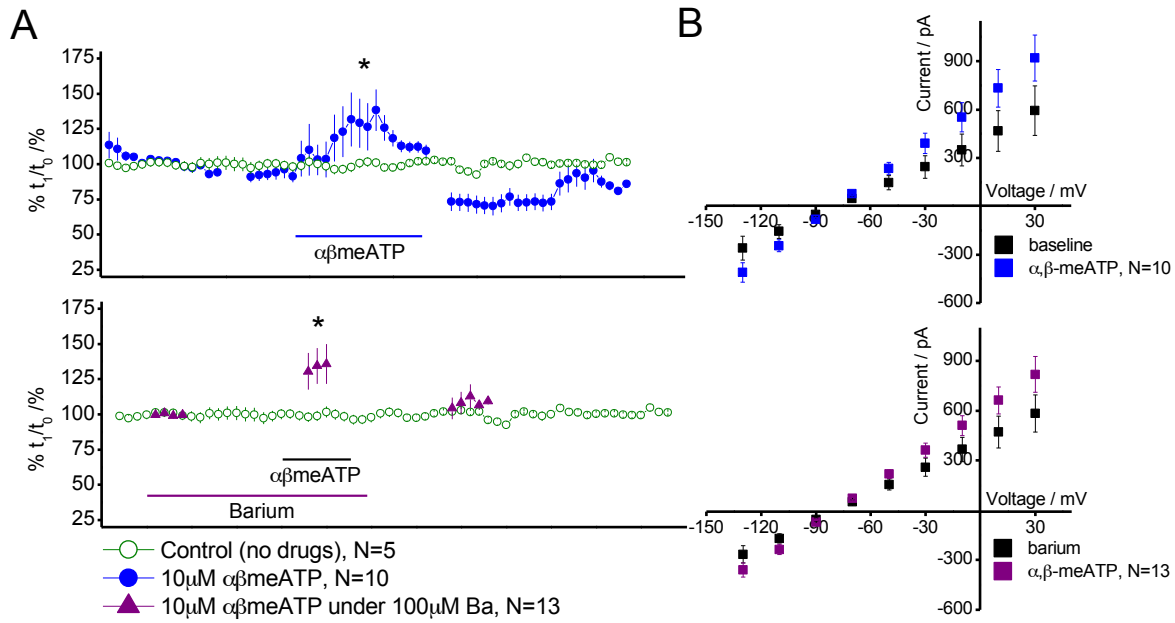

Figure 4.19: **Time course of whole-cell patched clamped astrocytes in slices.** A time course of voltage steps was measured every 30 seconds (resting potential -50mV with voltage steps from -130mV to +30mV), with application of αβ-methylene ATP and addition of barium chloride and subsequent application of αβ-methylene ATP. At its peak, the addition of μM αβ-methylene ATP increases the current by 38.3±14.6 per cent (p=1.17*10^(-8) significantly different as measured with two-sample t test). Upon the washout of the drug the effect was reversible. When barium chloride is added prior to the application of αβ-methylene ATP, the maximal current was 135.8±14.2 per cent (p=1.37*10^(-5) when comparing current ratios recorded in experiments with the addition of αβ-methylene ATP under the presence of barium chloride and control conditions); * shows p<0.05 as calculated with two sample t test.

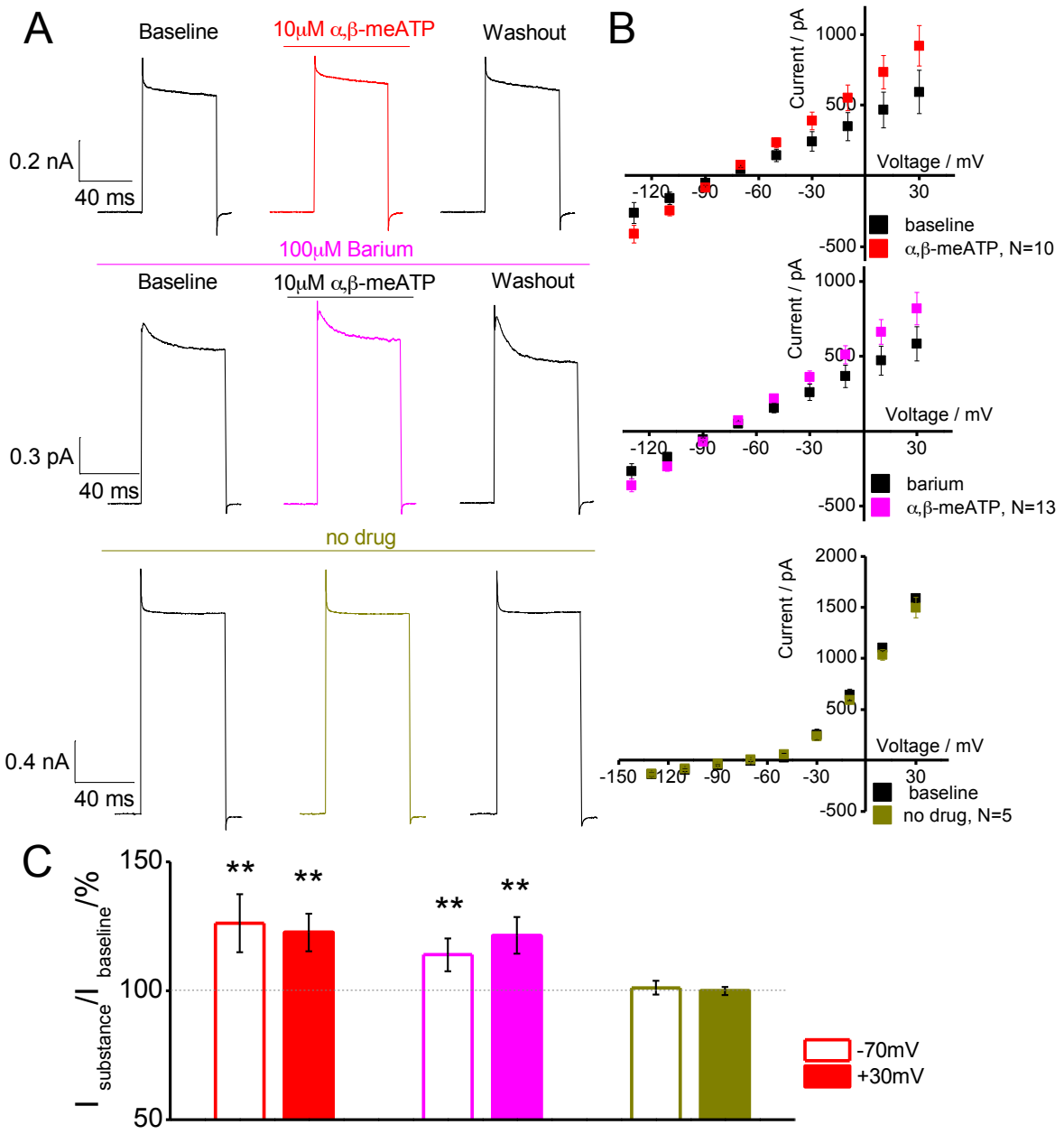

Figure 4.20: **αβ-methylene ATP facilitates potassium conductance in whole-cell patched clamped astrocytes in slice.** The changes in potassium currents upon activation with 10 μM αβ-methylene ATP in cells under the application of 100 μM barium chloride in the aCSF were measured. The average currents recorded from isolated astrocytes activated by 10 μM αβ-methylene ATP in the control conditions were 126.2±11.3 and 122.6±7.3 per cent of the control current at -130 and +30mV steps respectively. The addition of αβ-methylene ATP under the presence of barium chloride yielded a mean current of 114.0±6.4 and 121.4±7.1 per cent of control current at -130mV and +30mV steps respectively, fully prohibiting the increase the potassium current. The control experiments without any drugs added evoked mean current ratios of 101.2±2.7 and 100.0±1.6 per cent of the control current at corresponding voltage steps. As calculated with two-sample t test control and barium chloride experiments were significantly different from experiments with the application of 4-aminopyridine; ** shows $p<0.05$ with two-sample t test. Note scale change.

4.3 Conclusions

This chapter set out to overview the data collected from isolated neurons and astrocytes and astrocytes patched in slice. The null hypothesis stated that the addition of agonists for the following channels: P2X, NMDARs and PAR-1; does not alter the potassium currents conducted by astrocytic cells.

Firstly, it was determined that in isolated neurons the addition of $\alpha\beta$-methylene ATP does not in fact alter the outward potassium current recorded. Therefore the null hypothesis is correct for neurons. When the same experiments were completed with isolated astrocytes, the effect was present (see sections 4.3.2). This link between P2X and potassium currents is a mechanism unique to astrocytes.

The nature of this mechanism was closely studied in isolated astrocytes. It was found that this facilitation effect is Ca-dependent, as it was banished completely by the addition of EGTA – a Calcium chelator. This means that upon the activation of P2X receptors, a small amount of Calcium ions enter the sell and initiate a Calcium cascade that causes an increase in potassium current conductance as a result. Another agonist of a different type of ionotropic ion channel was used – NMDA – to activate NMDARs. This was done because it is known that the astrocytic subtypes of NMDARs are Ca-permeable (Palygin et al. 2010), therefore it was assumed that it can be linked to the same molecular cascade. Indeed, the activation of NMDARs with their selective agonist NMDA caused the same effect in the presence of intracellular Calcium. The removal of Calcium completely abolished the increase of the potassium current, thus showing that this molecular cascade involves the glutamate receptor.

Some experiments with NMDA were also done in astrocytes isolated from mice of age group III (9-12 months post-natal; for more details see Chapter 2). This

facilitation effect diminishes with age, and is seen in higher voltage steps, but not on lower voltage steps (see section 4.3.5). This can be due to potential change in the subunit composition or a post-translational modification of NMDA receptors, making these receptors less permeable to Ca^{2+} ions and thus putting an end to the influx of Calcium ions into the cell. Alternatively, it could be a different disruption of this mechanism downstream of NMDARs.

Further experiments were conducted to see which specific subtypes of potassium channels are involved in this mechanism. Since there are a large number of potassium channel types (Hibino et al. 2010), and multiple ones are expressed in glial cells (Vit et al. 2008; Pannicke et al. 2000; Butt and Kalsi 2006).To determine whether the mechanism described is affecting one or more subtypes of potassium channels, two blockers were used: 4-aminopyridine (voltage-gated potassium current blocker) and barium chloride (inwardly rectifying potassium current). Experiments using either NMDA or $\alpha\beta$-methylene ATP were conducted with the addition of one of the blockers prior to the application of the agonists. The patterns of data collected for two types of channels were very similar: the addition of 4-aminopyridine blocked the increase of the potassium current upon the application of agonists, whereas the addition of barium chloride did not. In some cases, the application of barium chloride blocker at the voltage steps, where the inwardly rectifying potassium current dominates, introduced this facilitation of the current (see sections 4.3.5-4.3.6).

It was hypothesised that if the activation of ionotropic receptors can cause an influx of Calcium into the cell and a consequent increase in the potassium current, then it is possible that activation of a metabotropic receptor that is part of the cascade should cause the same result. PAR-1 receptor was chosen as a metabotropic receptor, because it is present in astrocytes, especially on the soma and the endfeet enwrapping the blood vessels (Junge et al. 2004). The activation of

PAR-1 receptor initiates astrocytic Ca2+ signalling (Lalo et al. 2014). As section 4.3.7 demonstrates, the application of TFLLR – an agonist of PAR-1 receptor evoked the same response as the agonists of ionotropic receptors. Under the addition of TFLLR without the influence of the blockers, the potassium current increases. This increase was blocked by the addition of 4-aminopyridine, but not of barium chloride. Therefore it can be assumed that both ionotropic and metabotropic channels (P2X, NMDARs and PAR-1) are part of the same molecular mechanism, that connects the agonists from the aCSF and the outward potassium currents, elicited by the astrocytic cell.

Lastly, section 4.3.8 covers the data collected during patching the astrocytes in slices. The effect is persistent as long as the agonist is present at the aCSF. The facilitation effect takes place in slices as well as in isolated cells. However, unlike in isolated cell, the increase in potassium current appears at -130 mV voltage step (where current is mainly conducted via the inwardly rectifying potassium channel).

Overall, the data presented in this chapter suggest that there is a molecular mechanism that links the P2X, NMDARs and PAR-1 receptors on one hand and voltage-gated potassium current on the other. It has been shown that this mechanism is Calcium-dependent, and involves voltage-gated potassium currents, but not inwardly rectifying potassium currents. This mechanism provides a link between ionotropic and metabotropic receptors, expressed in astrocytes and the outward potassium current. There is no relationship between the activation of astrocyte (by influx of Calcium ions) and the inwardly rectifying potassium current. Therefore it could be proposed that the neurotransmitters, spilled at the synapse activate astrocyte and cause an increased of outward potassium current. Alternatively, the extracellular potassium concentration could be driven up by neuronal activity. It is possible that the increased outward potassium current

triggers the potassium buffering process, but more experiments are needed before any conclusions can be drawn. This mechanism could be an assistant method of recruiting nearby astrocytic branches, by increasing the outward potassium conductance, which would initiate the process of potassium buffering in these astrocytic projections.

Chapter 5 – Light transmission and tissue swelling

Astrocytes participation in potassium buffering measured as changes in Light Transmittance

5.1 Aim and hypothesis

The aim of this chapter is to put the mechanism, described in Chapter 4 into a physiological context, e.g. *ex vivo* brain slice. Activation of a number of astrocytic channels was shown to increase the outward, but not inward potassium currents. However, does this mechanism take place in an intact slice; and if so, what is the significance of this autocrine regulation for the signalling and potassium buffering processes of the cortex?

It was assumed, that potassium currents should best be studied via considering their involvement in tissue swelling and potassium buffering (Kofuji and Newman 2004; Song and Gunnarson 2012; Anděrová et al. 2014; Chvátal, Anděrová, and Syková 2004). A method chosen for this chapter was experiments where light transmittance of the tissue slices was measured (Kreisman et al. 1995). It is known that the when using light microscope for electrophysiological recordings, the tissue slice refracts the light in a certain pattern. Changes in relative proportions of extra-cellular matrix and somas will affect this refractory pattern. This can be measured by taking a series of pictures and consecutive comparison of those (see Chapter 2 for more details). The current scientific doctrine agrees that during the process of potassium buffering astrocytes take up the extracellular potassium and water molecules, simultaneously or otherwise (Kofuji and Newman 2004; Nagelhus, Mathiisen, and Ottersen 2004). This in turn causes the shrinkage of the extracellular space, which can be measured by the light transmittance experiments as an increase in the signal.

A set of experiments was performed, using stimulation of different strengths to study how the activity of slices influences the tissue swelling. A number of agents were used to activate or block the mechanism, described previously and any changes in the light transmittance signals of the slices. The tissue slices were derived from young adult (1-3 months postnatal) and older mice (5-8 months postnatal). This was done in order to test whether the light transmittance signals and their alterations due to activity would be different in slices from distinct age groups. For some of the experiments data collected through field recordings were compared to light transmittance data, to provide comparison between data collected by the laboratory previous and in due course of this project.

5.2 Application of hypo-osmotic aCSF

To ensure that the data that can be gathered by this method can be compared to the published values, certain control experiments were performed. Firstly, the addition of hypo-osmotic aCSF was tested for its effect on the transmittance of light in the brain slice. Similarly to Stroman et al. (2008) addition of hypo-osmotic aCSF increased the Light Transmittance (LT) of the cortical slices used by a little under 4% of the control signal (See Figure 5.1).

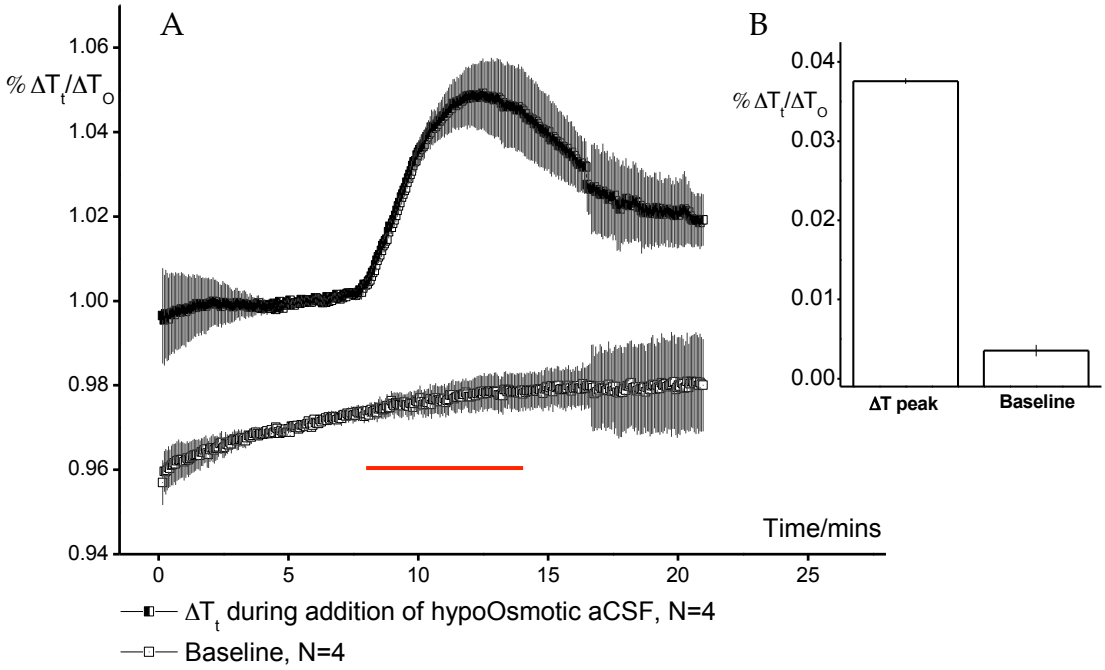

Figure 5.1: **Response to hypo-osmotic aCSF application**. A – Time course of LT (black) where red line shows the application of the hypo-osmotic aCSF. Baseline (grey) shows experiments where the hypo-osmotic aCSF was not added to bath. B – Peaks of LT (ΔT/average of control and washout LT) of baseline and experiment with hypo-osmotic aCSF addition. The application of hypo-osmotic aCSF produced a peak of 1.038±3.6*10^-4, whereas the baseline experiment showed no significant increase in the signal.

5.3 Measuring activity-dependent tissue swelling

Tissue swelling in response to activity was measured. In order to determine the relationship between the extent of tissue swelling and the activity of the tissue the following experiments were conducted. Since the typical activity mimicking stimulation of the cortex is Theta Burst stimulation (Larson and Munkácsy 2015), experiments with 1, 2 and 5 Theta bursts were performed. The stimulus strength for the fEPSP was set around 30-50 percent of the maximal, to ensure that the network was not over-activated. Figure 5.2 shows time courses for experiments with 1, 2 and 5 Theta Bursts (TBS1, 2 and 5 respectively) stimulations. No significant difference was found between the sizes of the peaks produced by various amounts of stimulations: the maximal peak responses measured were $0.011\pm7.1*10^{-4}$, $0.01\pm3.8*10^{-4}$ and $0.011\pm1.3*10^{-4}$ for one, two and five Theta Bursts respectively (Section B, Figure 5.2). However, it was noticed that the time delay between the onset of activity and the peak of the response increased with greater strength and duration of stimulation. Figure 5.3 illustrates a close up of the average peaks (section A) and the time delays between the stimulation and the highest peak of the response reached in different conditions (section B). It appears that at higher stimulation, the TBS5, the peak is less acute, and takes longer time to reach maximum: just under one minute whereas it takes 13 seconds to reach the peak response in experiments with only one Theta Burst stimulation. Another difference is the decay of the LT signal following the peak. In experiments with TBS5 stimulation the recovery of the signal is slower, showing that although the size of the peak and therefore the extent of the tissue swelling does not vary significantly, the time it takes to restore the resting state volumes of the extra-cellular matrix (ECM) and the astrocytic syncytium is greater in experiments with TBS5.

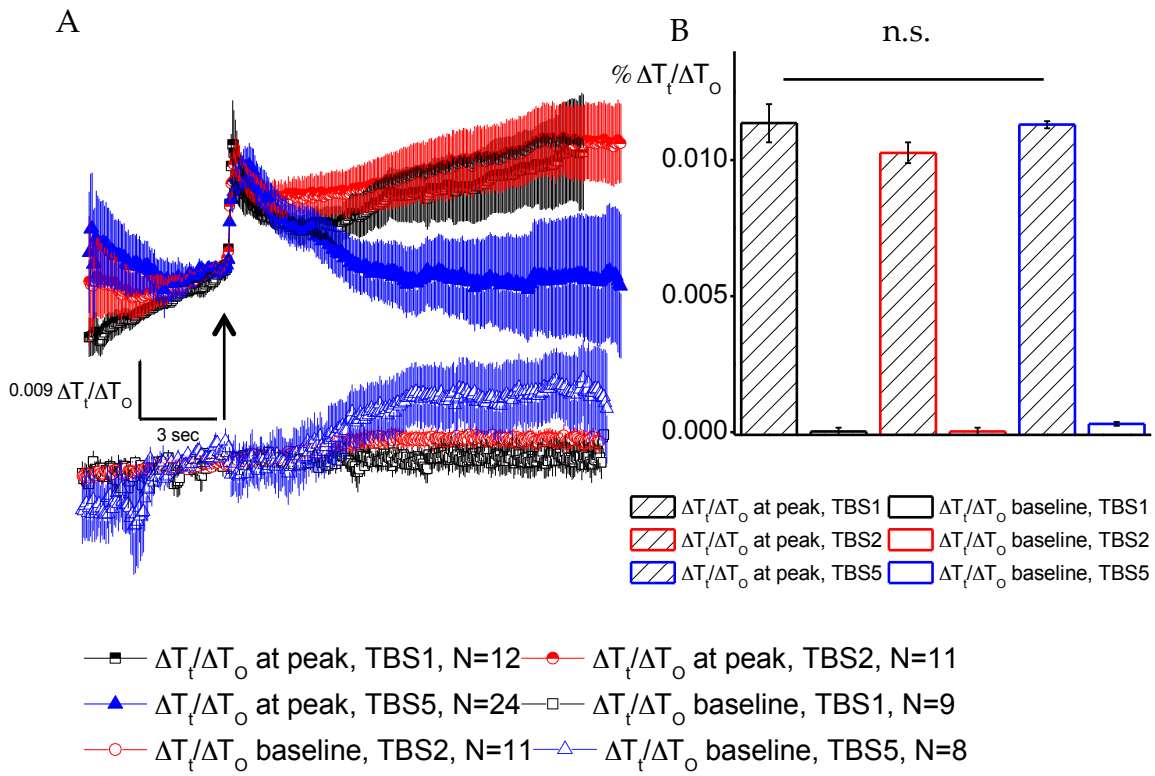

Figure 5. 2: **Responses to different stimulation strengths**. A – time course of LT experiments where 1 (black), 2 (red) and 5 (blue) Theta Bursts were given to the slice. B – peak values; the stimulation yielded 0.011±7.1*10^-4, 0.01±3.8*10^-4 and 0.011±1.3*10^-4 respectively. The peaks were not significantly different from each other (as tested with two-sample t test).

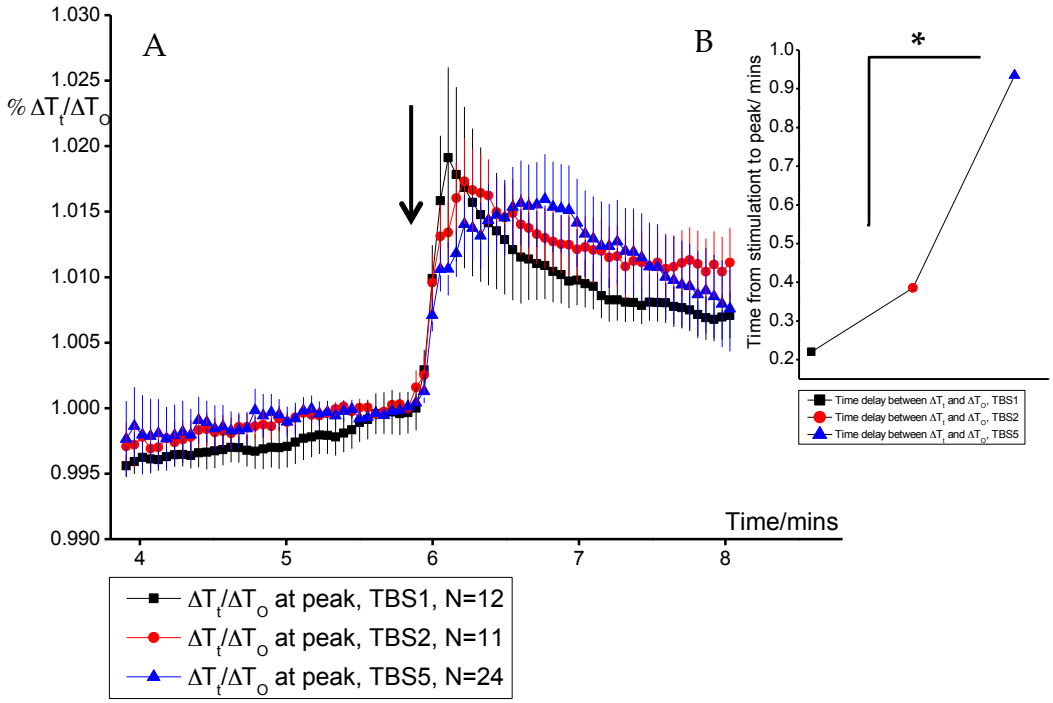

Figure 5.3: **The peaks of responses to various stimulation strengths**. A – peaks of LT responses to TBS1, TBS2 and TBS5. B – time delay between stimulation and peak in experiments with 1, 2 and 5 Theta Bursts stimulations; * p<0.01 as calculated with two-sample t test.

5.4 Tissue swelling in response to 1 TBS

The minimal stimulation (1 Theta Burst Stimulation) was applied to test whether at this level of activity any changes to the LT signal can be introduced either by pharmacological agents or if slices from group II mice (6-9 months Postnatal) show any difference in the response to 1 TBS. Firstly, the effect of the addition of 10 μM of TFLLR to experiments with slices from young adult and older mice. The strengths of responses to a single Theta Burst Stimulation were compared in slices from young adult and older mice. A solution of high potassium (10 mM) was also applied as a control.

5.4.1 Tissue swelling in young adult (1-3 months PN) and older (5-8 months PN) mice in response to 1TBS

A single Theta Burst stimulation was applied to slices from young adult and older mice, in order to investigate whether there is a differential effect of activity on the Light Transmittance signal in slices of different ages. It was hypothesised that there would be a difference in the response profile to the same stimulation, because astrocytes are thought to start loosing the efficiency of their potassium buffering function (Sofroniew and Vinters 2009). As can be seen from Figure 5.4, the response of the slice to a Theta Burst stimulation reduces in group II mice: the peak becomes less prominent and the rate of restoration of the signal is lower in experiments with older mice. The experiments using the young adult mice had a maximal response peak of $0.012 \pm 2.4 * 10^{-3}$, whereas the peak reached in the slices from older mice was $0.007 \pm 4.5 * 10^{-4}$ ΔT. This can be explained by two factors, perhaps working individually or in synergy. Since it is much harder to elicit an electrophysiological response to stimulation in older mice, for example the LTP (Long-Term Potentiation) requires a much stronger stimulus than in young mice (Lynch et al. 2008), the lower LT peak in mice of group II can be due to the same phenomenon. Alternatively, the potassium buffering could already be starting to decline from group II (6-9 months old) onwards.

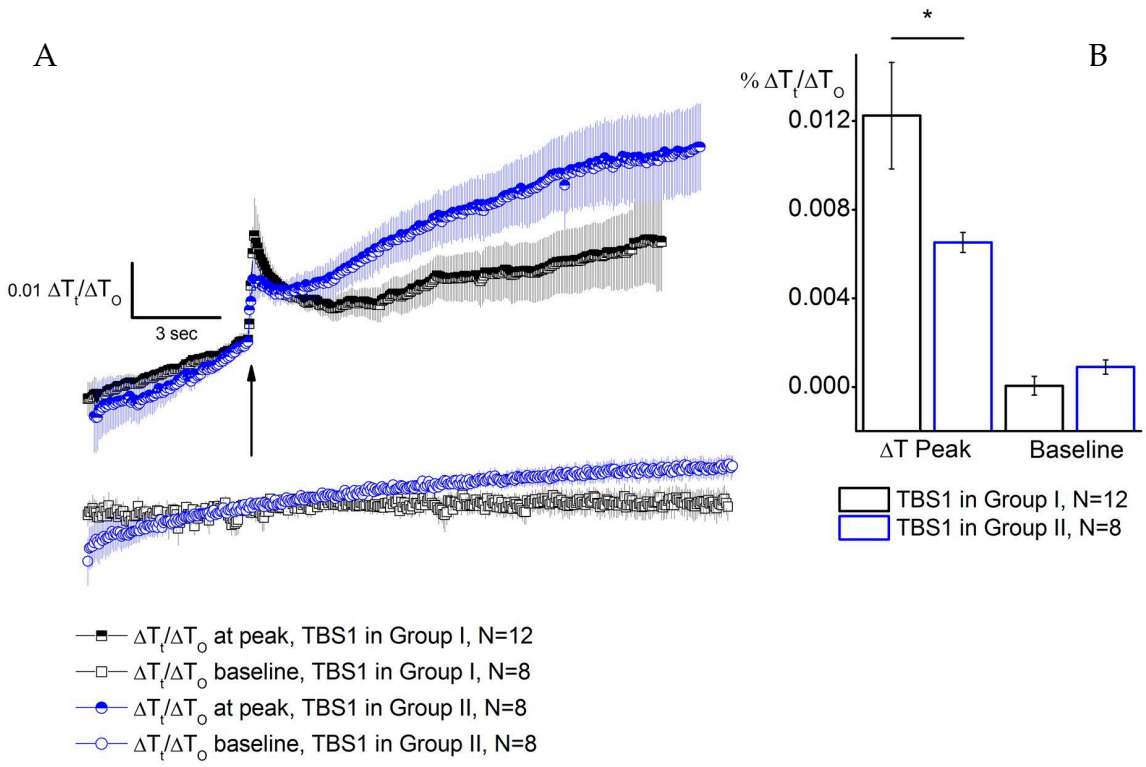

Figure 5.4: **Comparing response to 1 TBS in young adult and older mice.** A – time course of experiments with TBS1 stimulation in young adult (1-3 months) and older (5-8 months) mice. Arrow shows the onset of stimulation. B – Bar chart representation of peaks and baselines of responses. The maximal response peaks recorded for slices from young adult mice were 0.012±2.4*10^-3, and peak for experiments with older mice were 0.007±4.5*10^-4 ΔT. The responses measured in young adult mice were significantly greater than that of the older mice, as calculated with two-sample t test; * - p<0.05.

5.4.2 The effect of TFLLR on tissue swelling in young adult mice

A single Theta Burst stimulation was used to evoke a light transmittance signal in coronal slices from young adult mice. In order to test whether activation of PAR-1 receptor on astrocytes can influence the process of potassium buffering via the mechanism described in Chapter 4. Figure 5.5 illustrates the data gathered for these experiments – there is no significant difference in the size of the response or its duration in experiments with the addition of the TFLLR, although there is a trend for an increase in the size of the peak. The maximal peak reached by the control experiments was $0.011 \pm 7.8*10^{-4}$ and the experiments with the addition of TFLLR yielded $0.013 \pm 9.36*10^{-4}$ peak of light transmittance. It was proposed that with a small stimulation, such as a single Theta Burst stimulation, it was possible that the possible effect might not be seen.

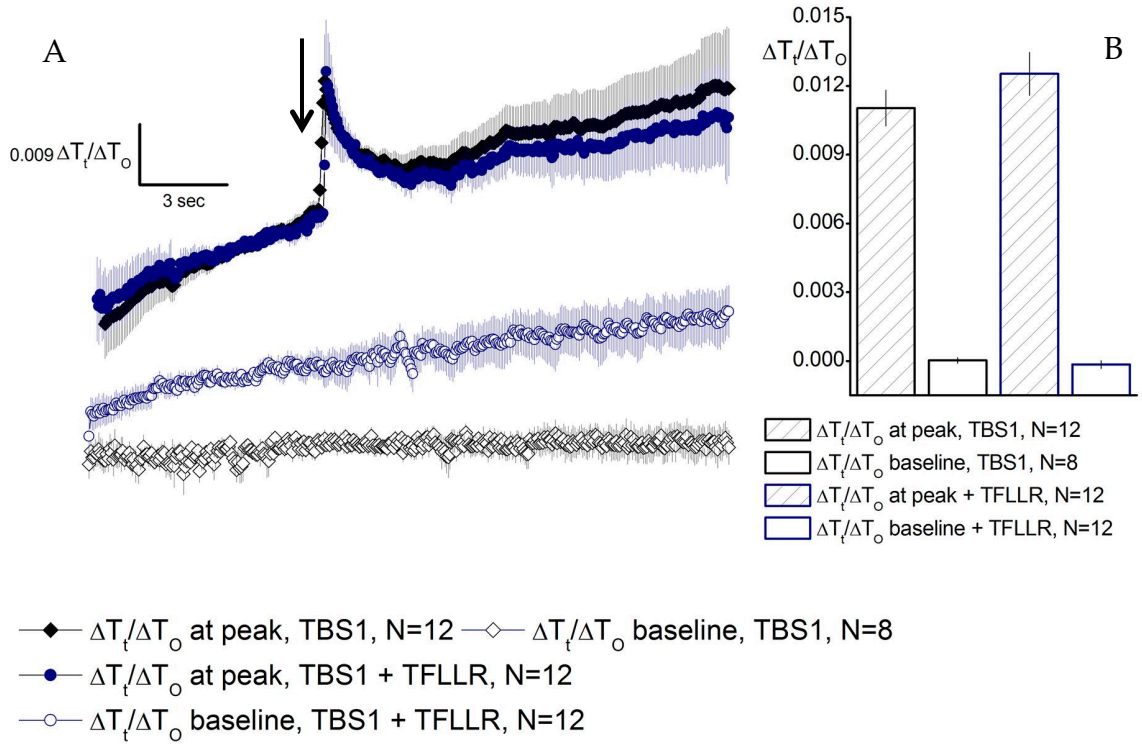

Figure 5.5: **Addition of TFLLR to slices from young adult mice undergoing 1TBS**. A – time course of control (black) and experiments with the addition of TFLLR (blue) with the application of 1 TBS. B – peak size in control (black) and experiments with TFLLR (blue). Black arrow illustrates the onset of the stimulation. The maximal response reached 0.011±7.8*10^-4 in control experiments, and 0.013±9.36*10^-4 in the experiments with the addition of TFLLR. Responses were not significantly different, as calculated with two-sample t test.

5.4.3 Tissue swelling in response to single TBS and TFLLR application in group II mice

Similarly to comparing the effect of the addition of TFLLR in young adult mice, these experiments were repeated again using slices derived from group II mice. It was done in order to check whether in older mice application of TFFLR – agonist to PAR-1 receptor, has the same effect to the response of the slice to a single Theta Burst stimulation.

Figure 5.6 illustrates the data gathered for group II. When 10 μM TFLLR was added to bath, the peak of the response was smaller than the maximal response peak generated in control experiments, 0.0065±1.4*10^-4 and 0.0034±5.4*10^-4 respectively. Due to the method for data analysis (the peak is compared to the average between control and washout levels of Light Transmittance), the peak appears even smaller in the experiments with TFLLR addition, since the rate of restoration of the signal back to pre-stimulation levels is much slower than in control experiments. It can be assumed that the activation of PAR-1 receptors sets off the molecular mechanism described in Chapter 4. As a result of the activation of this mechanism the outward potassium current of astrocytes is increased, thus increasing the amount of potassium ions in the extracellular space. It is possible that the presence of TFLLR prevents the astrocytes from being able to fully execute the buffering of potassium due to increased outward potassium current, which is seen in the course of the experiment as a slower rate of recovery of the light transmittance signal.

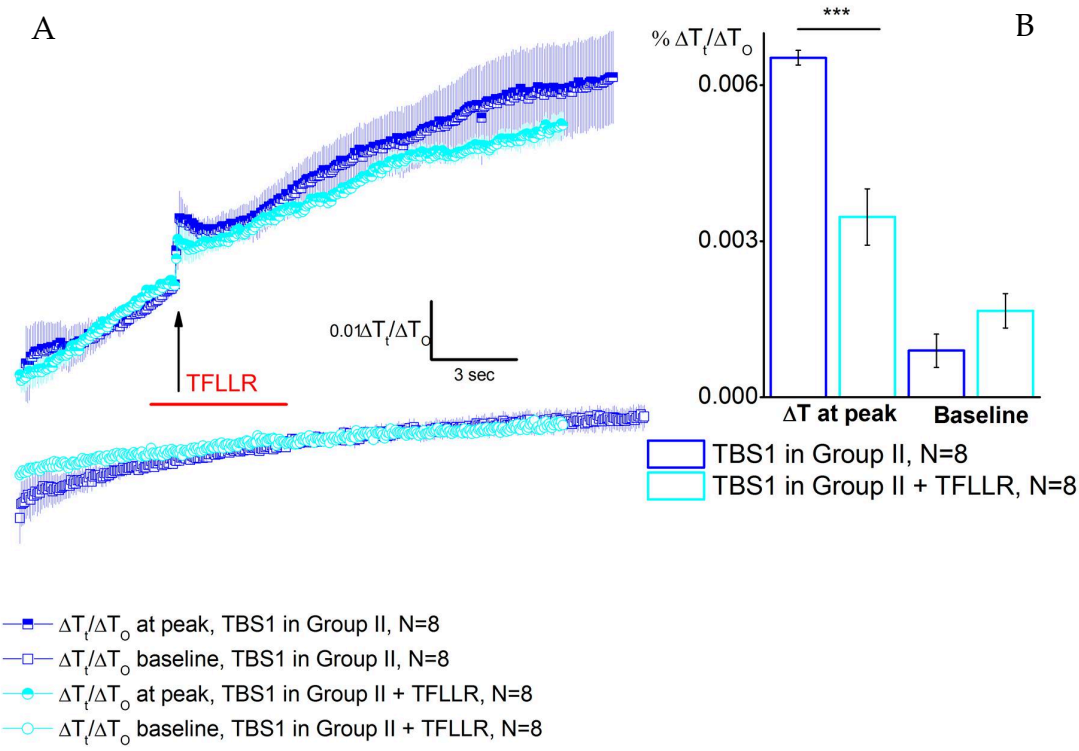

Figure 5.6: **Addition of TFLLR to slices from young adult mice undergoing 1TBS**. A – time course of control (black) and experiments with the addition of TFLLR (blue) with the application of 1 TBS. B – peak size in control (black) and experiments with TFLLR (blue). Black arrow illustrates the onset of stimulation, red line shows the application of 10 μM TFLLR. The maximal response reached 0.0065±1.4*10^-4 in control experiments, and 0.0034±5.4*10^-4 in the experiments with the addition of TFLLR; *** shows $p<0.0001$, as calculated with two-sample t test.

5.4.4 Tissue swelling in response to single TBS and α, β methylene-ATP application in group I mice

Analogously to the experiments with the addition of TFLLR (see sections 5.4.2 and 5.4.3) some experiments where the agonist of $P2X_{1/5}$ receptors was used. In the previous chapter of this study it was shown that the application of α, β methylene-ATP raises the outward potassium current. Figure 5.7 illustrates the data for these experiments. The baseline of the experiments with the addition of α, β methylene-ATP rise a lot more than the control experiments, and does not restore to the pre-stimulation levels after the maximal response peak, reaching a plateau around 102.6 per cent of the control signal. The maximal peak yielded by the stimulation in the control experiments was $0.011\pm7.8*10^{-4}$ and $0.009\pm6*10^{-4}$ in the experiments with the addition of α, β methylene-ATP. However, because the signal in the experiments with the addition of α, β methylene-ATP does not recover fully, an alternative data analysis was performed. When the maximal response was normalised to the control signal only, the maximal peak was calculated to be $0.031\pm6.7*10^{-4}$.

So the activation of the mechanism described in the previous chapter by α, β methylene-ATP increase the extent of the tissue swelling in these experiments and also reduced the rate of recovery following the stimulation of the slice. It can therefore be proposed that this mechanism in can play a significant role in both the activity of the slice and consecutive tissue swelling.

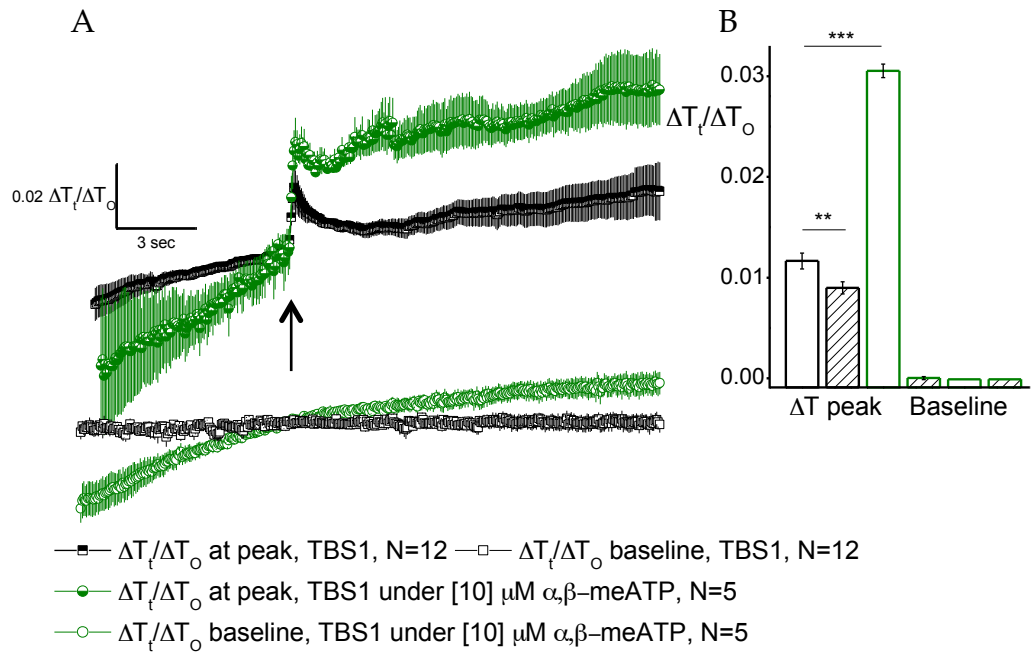

Figure 5.7: **Addition of α, β methylene-ATP to slices from young adult mice undergoing 1 TBS**. A – time course of control (black) and experiments with the addition of α, β methylene-ATP (green) with the application of 1 TBS. B – peak size in control (black) and experiments with α, β methylene-ATP (green). Black arrow illustrates the onset of stimulation, red line shows the application of 10 μM α, β methylene-ATP. The maximal response reached 0.011±7.8*10^-4 in control experiments, and 0.009±6*10^-4 in the experiments with the addition of α, β methylene-ATP. When the maximal response was normalised to the control signal only, the maximal peak was calculated to be 0.031±6.7*10^-4; ** shows p< 0.001, *** shows p<0.0001 as calculated with two-sample t test.

5.4.5 Tissue swelling in response to single TBS and addition of high KCL

As a control measure, some experiments were performed where a solution containing high concentration of potassium chloride (10 mM) was applied and a single Theta Burst stimulation was given (see Figure 5.8). The peak signal reached upon the addition of the high potassium aCSF was approximately 4 times greater than the peak from the Theta Burst stimulation, 4.26±1.17*10^-4 per cent increase was seen in the Light Transmittance of the experiments when the aCSF with high potassium was added. The peaks recorded from the stimulation were 1.1±7.77*10^-4 and 0.98±1.31*10^-4 per cent increase in the light transmittance signal in control and high KCL experiments respectively. The peaks corresponding to stimulation were not significantly different from each other, as calculated with two-sample t test.

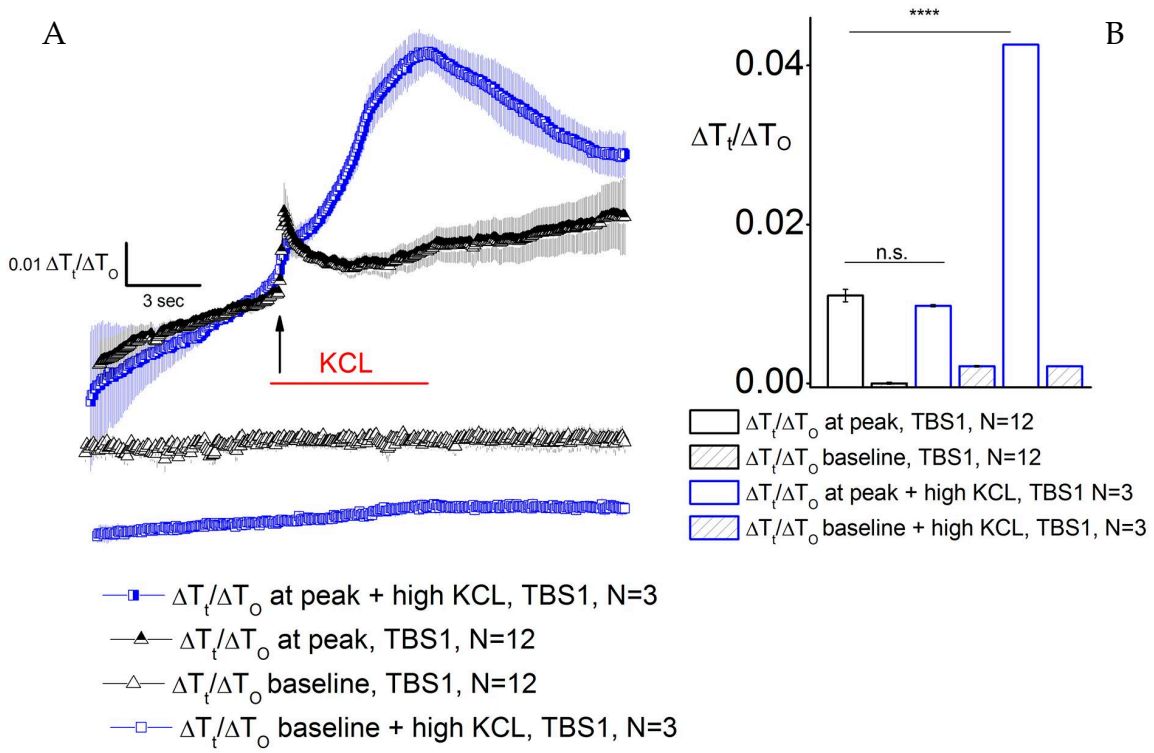

Figure 5.8: **Addition of 10 mM KCL solution to slices from young adult mice undergoing 1 TBS**. A – time course of control (black) and experiments with the addition of aCSF with high potassium (blue) with the application of 1 TBS. B – peak size in control (black) and experiments with high KCL (blue). Black arrow illustrates the onset of stimulation; red line shows the application of aCSF with 10 mM KCL. The maximal peak reached 0.011±7.8*10^-4 in control experiments, and 0.009±1.3*10^-4 in the experiments with the addition of aCSF containing high potassium. The maximal response to the high potassium solution was calculated to be 0.043±1.1*10^-4; n.s. – no significant difference, * - p< 0.00001 as calculated with two-sample t test.

5.5 Tissue swelling in response to 2 TBS2

It was proposed that in order to study the activity of the tissue a greater stimulation might be required still. In the cortex, to reach the Long-Term Potentiation a much greater stimulus is required compared to hippocampus for example (Malenka 1994; Kuo and Dringenberg 2012). For this reason some of the experiments were performed using two or five (see Section 5.6) Theta Burst stimulation. In this section the data gathered for the experiments with two Theta Bursts stimulations are described. Both time courses of experiments and bar charts representing the peak responses and baselines are presented as averages and standard error of means.

5.5.1 Comparing the response to 2 TBS of slices derived from young adult and older mice (groups I and II respectively)

The response to 5 TBS was recorded for slices derived from the young adult and older mice (groups I and II respectively). The maximal peaks of response were compared as well as the rate of decay of these peaks. The data gathered for these experiments are summarised in Figure 5.9. The maximal peaks of the response to stimulation were not significantly different in experiments with two age groups: $0.009 \pm 1.3 * 10^{-3}$ and $0.011 \pm 7.4 * 10^{-4}$ for groups I and II respectively, although the trend shows the increase of the response in older mice. Also, in the experiments with slices from group II mice the rate of decay of the signal is slower and the signal remains significantly higher than in the control experiments. The same effect was found when comparing the responses to a single Theta Burst stimulation in experiments with different ages of mice. This consistency leads to believe that it might be an important difference, that is apparent between groups I and II already.

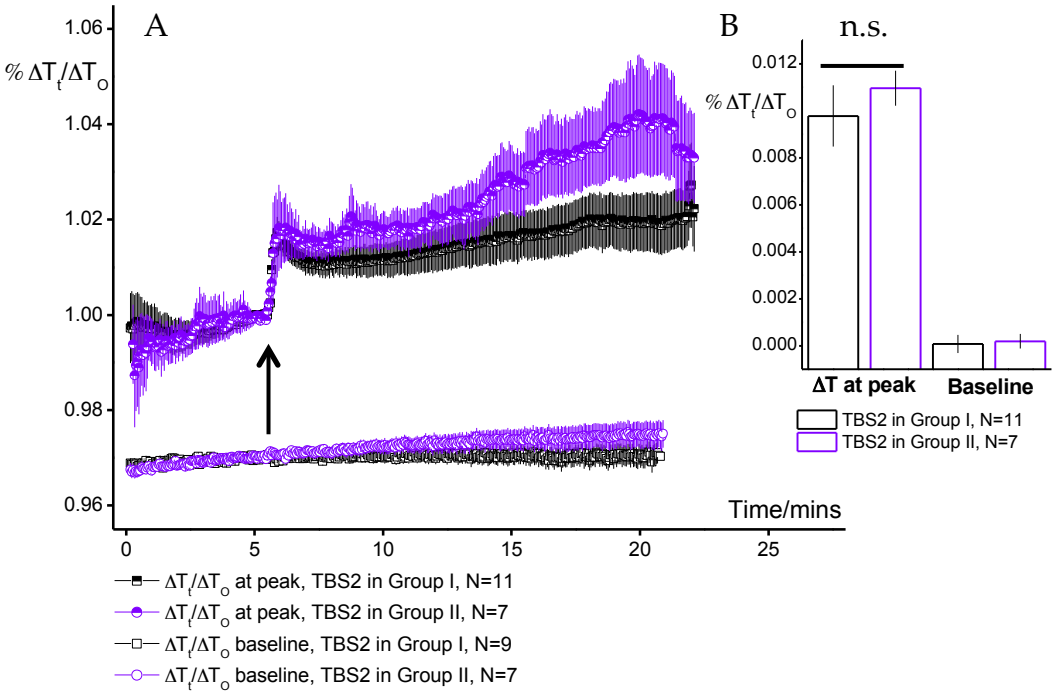

Figure 5.9: **Responses to 2 TBS in young adult and older mice.** A – time course of experiments with TBS2 stimulation in young adult and older mice. Arrow shows stimulation. B – Bar chart representation of peaks and baselines of responses. The maximal peaks were recorded to be 0.009±1.3*10^-3 and 0.011±7.4*10^-4 for groups I and II respectively. No significant difference was determined between the maximal peak, as calculated with two-sample t test; n.s. – no significant difference.

5.5.2 The effect of the addition of TFLLR to the experiments with 2 TBS in slices from young adult mice

The experiments with the addition of TFLLR in young adult mice were repeated with two Theta Bursts stimulations. Figure 5.9 summarises the data gathered. Under the addition of TFLLR the maximal response upon the stimulation is much smaller than that of the control experiments. The shape of the peak response was different from that of the control experiment, as well as the speed of restoration of the signal. However, no significant difference was measured in the signal following the response to the stimulation.

The effect of the addition of TFLLR in experiments with 1 Theta Burst stimulation yielded a response that was not significantly different from the control. In fact, the trend the data display shows a decrease in the maximal peak size in the experiments with a single stimulation. The data displayed on Figure 5.9 show a similar trend: the peak size of the maximal response is smaller than that of control experiments, $0.004 \pm 1.6 * 10^{-4}$ against $0.009 \pm 6.2 * 10^{-4}$. However, due to the lack of recovery in the signal, following the stimulations, the data analysis shows the difference in the peak size as a significant result. It is argued that if the maximal responses were only compared to T0 (the last time point prior to stimulation), then the difference between the experiments with the addition of drug and without would disappear. Indeed, this alternative method of analysis produced an average peak value of $0.014 \pm 1.37 * 10^{-4}$ for experiments with the addition of TFLLR and $0.014 \pm 6.43 * 10^{-4}$ for the control experiments. No significant difference was detected when using the two-sample t test.

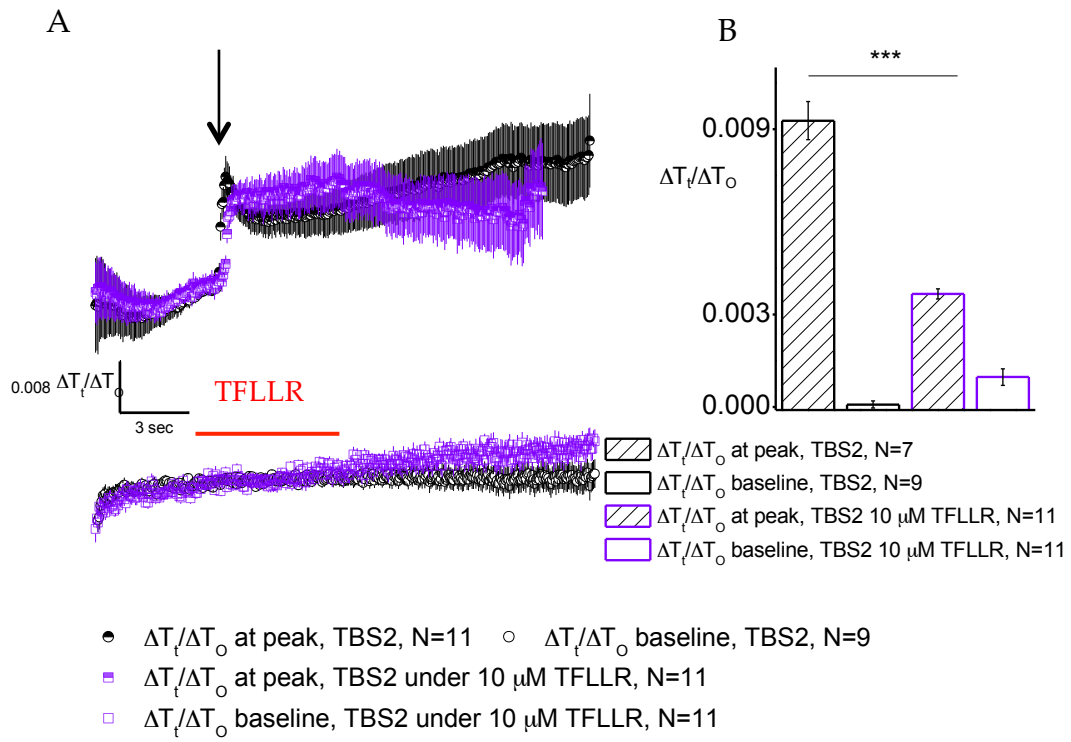

Figure 5.10: **Addition of TFLLR to slices from young adult mice undergoing 2 TBS**. A – time course of control (black) and experiments with the addition of TFLLR (purple) with the application of 2 TBS. B – peak size in control (black) and experiments with TFLLR (purple). Black arrow illustrates the onset of stimulation; red line shows the application of 10 μM of TFLLR. The maximal peak reached 0.009±6.2*10^-4 in control experiments, and 0.004±1.6*10^-4 in the experiments with the addition of TFLLR. When the maximal response was normalised to the control signal only, the maximal peak was calculated to be 0.014±6.43*10^-4 in the control and 0.014±1.37*10^-4 in experiments with the addition of the drug; *** - p< 0.0001 as calculated with two-sample t test.

5.5.3 The effect of the addition of TFLLR to the experiments with 2 TBS in slices from group II mice

Similarly to experiments with the addition of TFLLR to slices cut from young adult mice (1-3 months postnatal) some experiments were performed using the slices derived from mice from group II (6-9 months postnatal). This was done to investigate whether the effect of the drug application is different in older mice with a stronger stimulation. As can be seen from Figure 5.10, the responses recorded for two conditions were fairly similar in shape, but not in peak size. Application of 10 μM TFLLR caused a decrease in the maximal response size, yielding only $0.007 \pm 1.1 * 10^{-4}$ increase whereas control experiments had an increase in the light transmittance of $0.011 \pm 2.24 * 10^{-4}$. The data collected for experiments with TFLLR with young adult and older mice demonstrates a similar trend for decrease of the peak size when compared to respective control experiments.

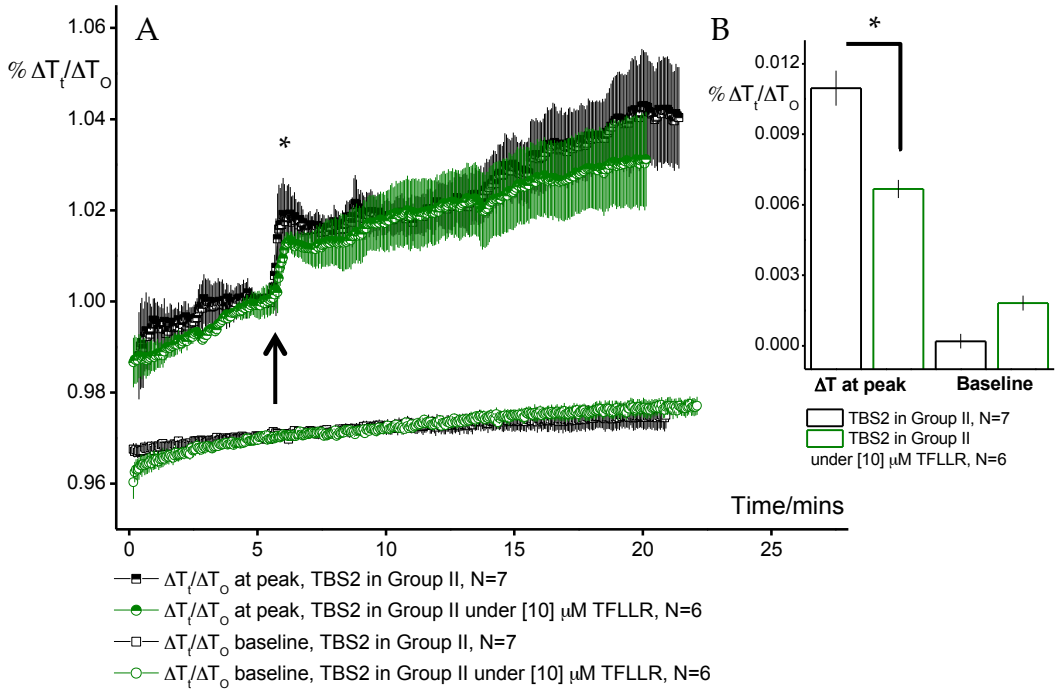

Figure 5.11: **Addition of TFLLR to experiments with 2 TBS in group II mice**. A – time course of experiments with TBS2 stimulation showing control experiments (black) and experiments with TFLLR application (green). Arrow shows the onset of stimulation. B – Bar chart representation of peaks and baselines of responses. The maximal peak of the experiments with TFLLR application was 0.007±1.1*10^-4 whereas control experiments had an increase in the light transmittance of 0.011±2.24*10^-4. The peak in control experiments was significantly greater than that of experiments with the addition of TFLLR, as calculated with two-sample t test; * – $p<0.0001$.

5.5.4 The effect of the addition of α, β methylene-ATP to the experiments with 2 TBS in slices derived from group I mice

Experiments with the addition of α, β methylene-ATP were performed using 2 Theta Burst stimulations, in order to investigate whether the effect of the drug application varies with the stronger stimulus. In experiments with a single stimulation the addition of α, β methylene-ATP yielded a diminished maximal peak response to the stimulation. When comparing those data with experiments where two Theta Burst stimulations were applied (see Figure 5.11), the trend appears to stay the same. Here the peak response measured was slightly lower than that of control experiments: $0.009 \pm 6.2 * 10^{-4}$ against $0.008 \pm 3.32 * 10^{-4}$. However, due to an increase in the baseline and the data analysis method (the peak was normalised to the average between control and washout signals), these averages do not seem to reflect the true pattern. When the peaks were normalised to the control signal only, the maximal responses were $0.013 \pm 1.58 * 10^{-4}$ in control and $0.022 \pm 1.81 * 10^{-4}$ in experiments with α, β methylene-ATP. The peaks evoked by stimulation in experiments with α, β methylene-ATP were significantly greater than those of control experiments, as calculated with the two-sample t test ($p<0.0001$).

Following this inconclusiveness of the data it was decided to repeat the experiments with the addition of α, β methylene-ATP using 5 Theta Burst stimulations as well to examine the role of the stimulation strength for this effect. The data are summarised in section 5.6.4.

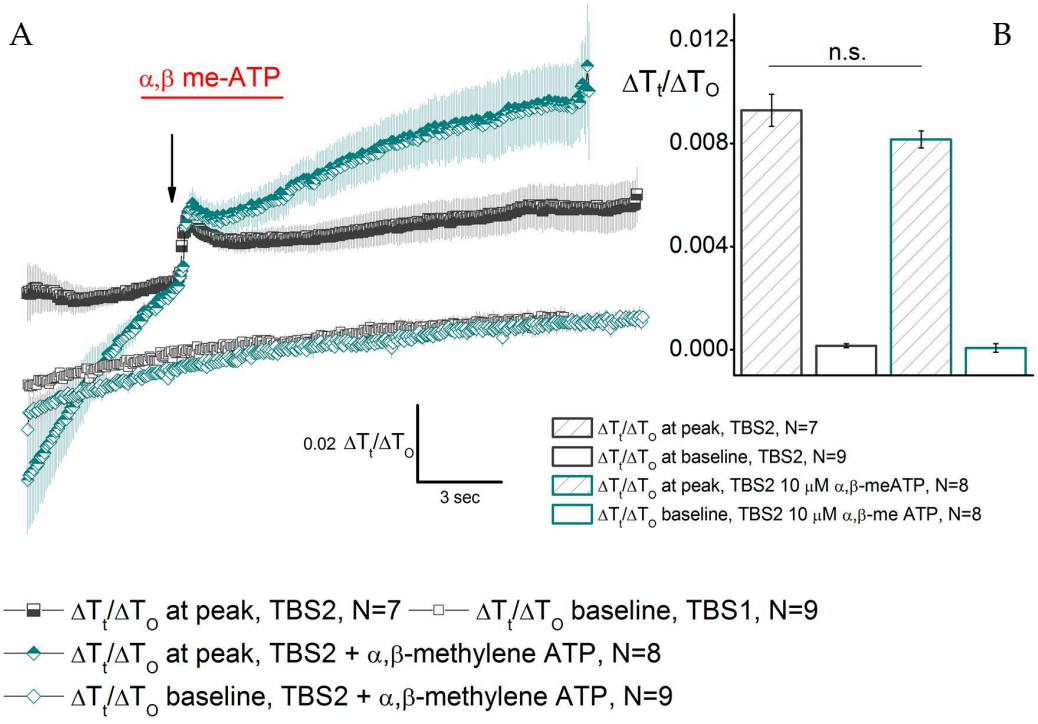

Figure 5.12: **Addition of α, β methylene-ATP to experiments with 2 TBS in group I mice.** A – time course of experiments with TBS2 stimulation showing control experiments (dark grey) and experiments with α, β methylene-ATP application (dark cyan). Arrow shows the onset of stimulation. B – Bar chart representation of peaks and baselines of responses. The maximal peak of the experiments with α, β methylene-ATP application was 0.008±3.32*10^-4 whereas control experiments had an increase in the light transmittance of 0.009±6.2*10^-4. When the peaks were normalised to the control signal only, the maximal responses were 0.013±1.58*10^-4 in control and 0.022±1.81*10^-4 in experiments with α, β methylene-ATP .The peak in control experiments was significantly greater than that of experiments with the addition of α, β methylene-ATP, as calculated with two-sample t test; n.s. – not significant, as calculated with two-sample t test.

5.5.5 The effect of the addition of TFLLR to the experiments with 2 TBS and addition of high KCL in slices from group I mice

The reaction to bath application of high KCL aCSF was measured in experiments with two Theta Burst stimulations under the control and application of 10 μM TFLLR experiments. It was hypothesised that the application of TFLLR should decrease the extent of tissue swelling upon the Theta Burst stimulations, similarly to the results obtained in the experiments with two Theta Burst stimulations. Since the addition of TFLLR reduced the maximal response of the light transmittance, it was also assumed that the addition of high KCL aCSF would yield a similar data pattern. Figure 5.12 shows the data collected for these experiments. Two Theta Burst stimulations yielded a peak $0.0130\pm2.0*10^{-4}$ compared with $0.0128\pm4.2*10^{-4}$ increase in light transmittance produced by two Theta Burst stimulations in the presence of TFLLR. As in the previous experiments the addition of TFLLR lightly reduced the size of the peak in the response, although in this case the difference was not significant, as calculated with two-sample t test. This was not the case for the peak generated by the application of high KCL. The presence of 10 μM TFLLR increased the size of the light transmittance by $0.0676\pm1.2*10^{-4}$ compared to $0.0569\pm1.0*10^{-4}$ ΔT increase in control experiments. This increase in the signal response to high KCL solution is significantly greater in experiments with TFLLR, as calculated with two-sample t test. It is possible that the application of TFLLR activates the mechanism, described in Chapter 4 Results, which in turn causes an increased tissue swelling, producing a greater change in the light transmittance signal of the tissue upon the second depolarisation achieved with high KCL aCSF.

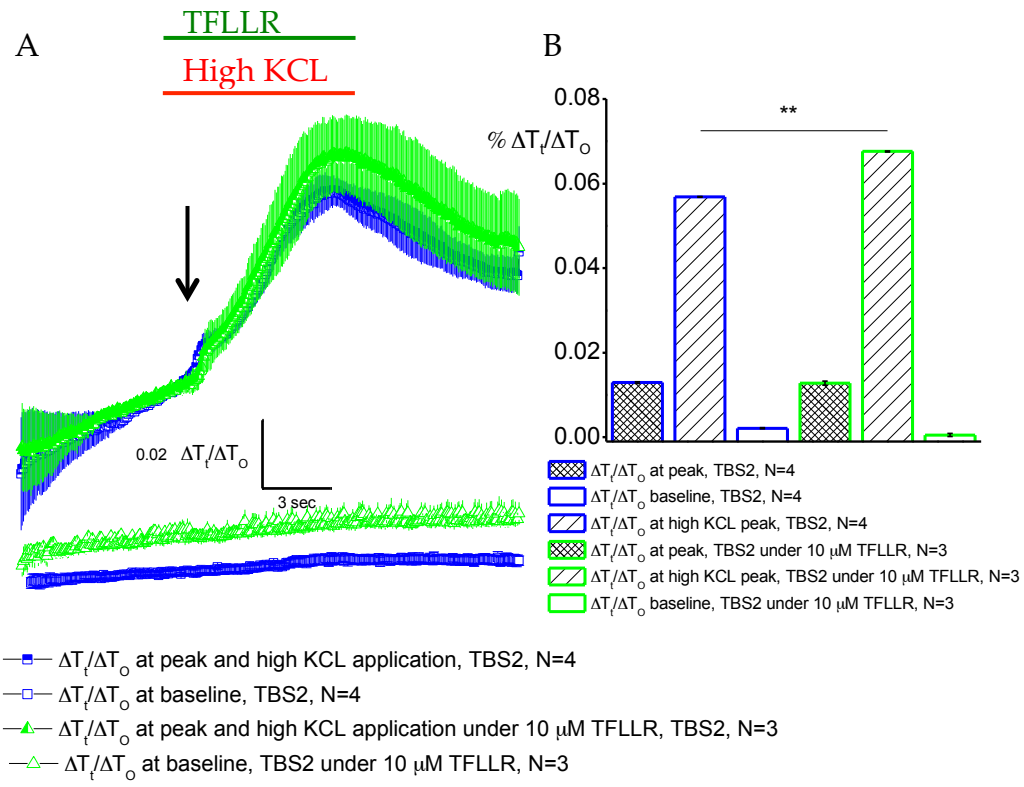

Figure 5.13: **Addition of high KCL solution to slices from young adult mice undergoing 2 TBS with and without the application of TFLLR**. A – time course of control (blue) and experiments with the addition of aCSF with high potassium (green) with the application of 2 TBS. B – peak size in control (blue) and experiments with high KCL (green). Black arrow illustrates the onset of stimulation; red line shows the application of aCSF with 10 mM KCL and the green line shows the application of 10 μM TFLLR. The maximal peak reached 0.0130±2.0*10^-4 in control experiments (blue bar with dense fill), and 0.0128±4.2*10^-4 in the experiments with the addition of TFLLR (green bar with dense fill). The peaks reached by the addition of aCSF containing high potassium were 0.0569±1.0*10^-4 in control (blue bar with medium fill) and 0.0676±1.2*10^-4 in experiments with the addition of TFLLR (green bar with dense fill); ** - p< 0.0001 as calculated with two-sample t test.

5.6 Tissue swelling in response to 5 TBS

All of the experiments were repeated with 5 Theta Burst stimulations, in order to study the STP and LTP (Short-Term and Long-Term Potentiation respectively). Five Theta Bursts stimulation are a sufficient stimulus for evoking LTP (Rasooli-Nejad et al. 2014). Both time courses of experiments and bar charts representing the peak responses and baselines are presented as averages and standard error of means.

5.6.1 Comparing the response in light transmittance signal to 5 TBS of slices from young adult and older mice (groups I and II respectively)

Similarly to experiments with one and two Theta Burst stimulations, the changes in light transmittance of the slices of different age groups were compared, but this time a stronger stimulation was used. Figure 5.13 summarises the data collected for these experiments. The data points show a familiar trend: in experiments with older mice the change in the light transmittance and therefore the extent of tissue swelling does not fully return back to baseline level but instead the swelling reaches a plateau after a small decrease. Due to the fact that the peak is measured by comparing the maximal response to the average between the control and the washout signals, the peak size does not appear to be greater in experiments with mice of group II as oppose to young adult mice. Experiments with group I yielded a $0.0147 \pm 1.6 * 10^{-4}$ increase, whereas the signal in experiments with group II mice only raised the signal by $0.0131 \pm 2.6 * 10^{-4}$ per cent. However, if the washout reading was taken out of the account, then the maximal responses were $0.0152 \pm 2.0 * 10^{-4}$ and $0.0187 \pm 2.5 * 10^{-4}$ for groups I and II respectively.

It was also noted that in the experiments with 5 TBS stimulation, the difference in the signal at the end of the experiment (15-20 minutes from the start) were significantly different in the age groups used. Following the stimulation, the slices

that originated from group II mice retained a higher light transmittance signal than before the stimulation. This means that the older slices performed less effective potassium buffering and therefore had a greater tissue swelling and depolarisation of the tissue. This phenomenon could be the reason for the decreased likelihood of LTP generation in older slices.

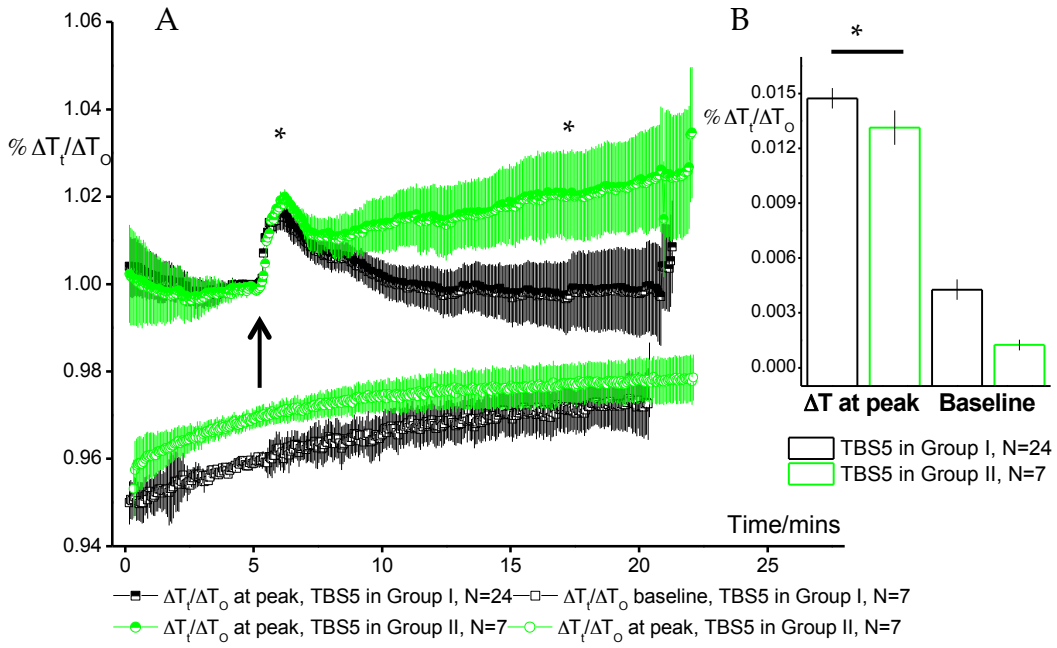

Figure 5.14: **Responses to 5 Theta Bursts stimulations in young adult and older mice**. A – time course of experiments with TBS5 stimulation in young adult (black) and older (green) mice. Black arrow shows the onset of stimulation. B – Bar chart representation of peaks and baselines of responses. The maximal peak responses recorded upon the stimulation were 0.0147±1.6*10^-4 in young and 0.0131±2.6*10^-4 in older mice. The difference between peaks was significant as calculated with two-sample t test ($p<1.8*10^{-5}$). The difference in light transmittance signal 10 minutes after the onset of stimulation was also significant. When alternative analysis method was used, where the peak sizes were normalised to control signal only, the peaks yielded were 0.0152±2.0*10^-4 in young and 0.0187±2.5*10^-4 older mice; n.s. – no significant difference, * - $p < 0.0001$.

5.6.2 The effect of the addition of TFLLR to the experiments with 5 TBS in slices from young adult mice

As stated above, the experiments with addition of 10 μM TFLLR were also repeated with five Theta Bursts stimulations. In regular Long-Term Potentiation experiments, 5 TBS stimulus consistently produces LTP in cortex(Lalo et al. 2014). Figure 5.13 illustrates the data collected for these experiments. The application of 10 μM TFLLR prior, during and just after the onset of stimulation causes a large increase in the maximal peak of the light transmittance signal. In these experiments with slices from young adult mice the control experiments experienced a $0.0147 \pm 1.61 * 10^{-4}$ increase in the signal, whereas the experiments with the addition of TFLLR had $0.0475 \pm 9.4 * 10^{-4}$ peak upon the stimulation. Not only the peak size increased by the addition of the drug. The rate at which the signal fell after the stimulation was significantly greater in experiments with TFLLR, although it did not quite restore back to the resting levels completely, thus keeping the washout part of the signal still higher than that of the control experiments. This increase did not take place in any previous experiments, possibly due to insufficient stimulation strength. In fact, in experiments with weaker stimuli (see Sections 5.4.2-5.4.3 and 5.5.2-5.5.3) the addition of 10 μM TFLLR reduced the swelling of the tissue. It can be concluded that the presence of TFLLR in the experiments with 5TBS stimulation increased the extent of the tissue swelling by roughly a factor of 3. Since the assumption is that this PAR-1 agonist caused an increase in the outward potassium current, this increase in the tissue swelling can be attributed to the outflow of potassium from the astrocytes. However, an increase in the rate of decay of the signal was also seen, which is assumed to be due to an increase in the potassium buffering by astrocytes. It is possible then to speculate that there can be a two-step mechanism for switching on this potassium buffering function of the syncytium.

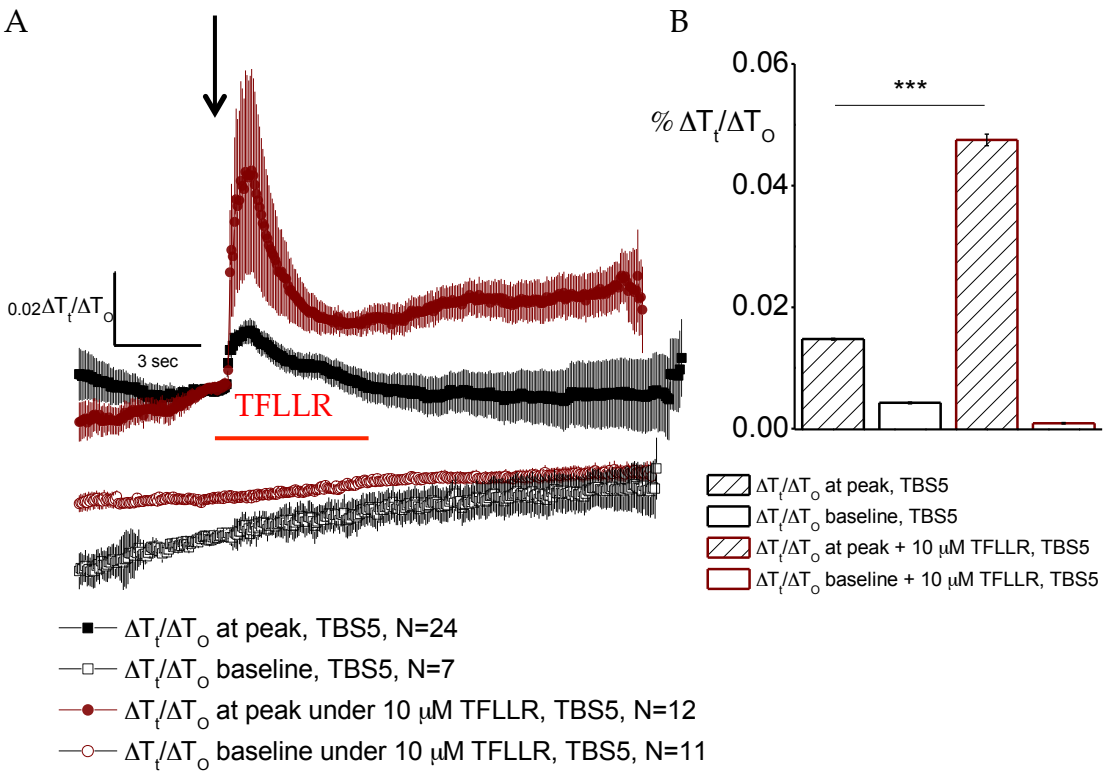

Figure 5.15: **Addition of TFLLR to experiments with 5 TBS in group I mice (1-3 months old)**. A – time course of experiments with TBS5 stimulation showing control experiments (black) and experiments with TFLLR application (burgundy). Black arrow shows the onset of stimulation, and the red lines shows the application of TFLLR in experiments where the drug was applied. B – Bar chart representation of peaks and baselines of responses, normalised to the average between the control (T_0) and washout signals (T_{15}). The maximal peak of the experiments with TFLLR application was 0.0475±9.4*10^-4 whereas control experiments had an increase in the light transmittance of 0.0147±1.61*10^-4 ΔT. The peak in control experiments was significantly smaller than that of experiments with the addition of TFLLR, as calculated with two-sample t test; *** – $p<0.0001$ ($p=6.0*10^{-21}$).

5.6.3 The effect of the addition of TFLLR to the experiments with 5 TBS in slices from group II mice

In order to study the effect of age, experiments with 5 Theta Burst stimulations and the application of TFLLR were repeated, this time with slices derived from older mice. The data collected for these experiments are summarised in Figure 5.14. The data are visibly different from those collected using young adult mice. In experiments where 5-8 months old mice were used, there was no greater increase in the maximal response to the stimulation in the experiments with TFLLR application than in the control ones. Both the amplitude of the response and the speed of recovery of the signal appeared largely similar to those of the control experiments. It is surprising that the effect of the addition of TFLLR to young adult slices diminishes to this extent by age group II.

The maximal increase of the response reached by the control experiments was $0.0131 \pm 2.6 * 10^{-4}$ ΔT whereas the experiments with the addition of TFLLR yielded a peak of $0.0145 \pm 3.3 * 10^{-4}$, which was significantly greater than the control peak, as calculated with the two-sample t test. However, the facilitation effect of TFLLR addition was greatly diminished in older mice of group II. This once more leads to believe that there is a mechanism at work that starts to fade from middle age already.

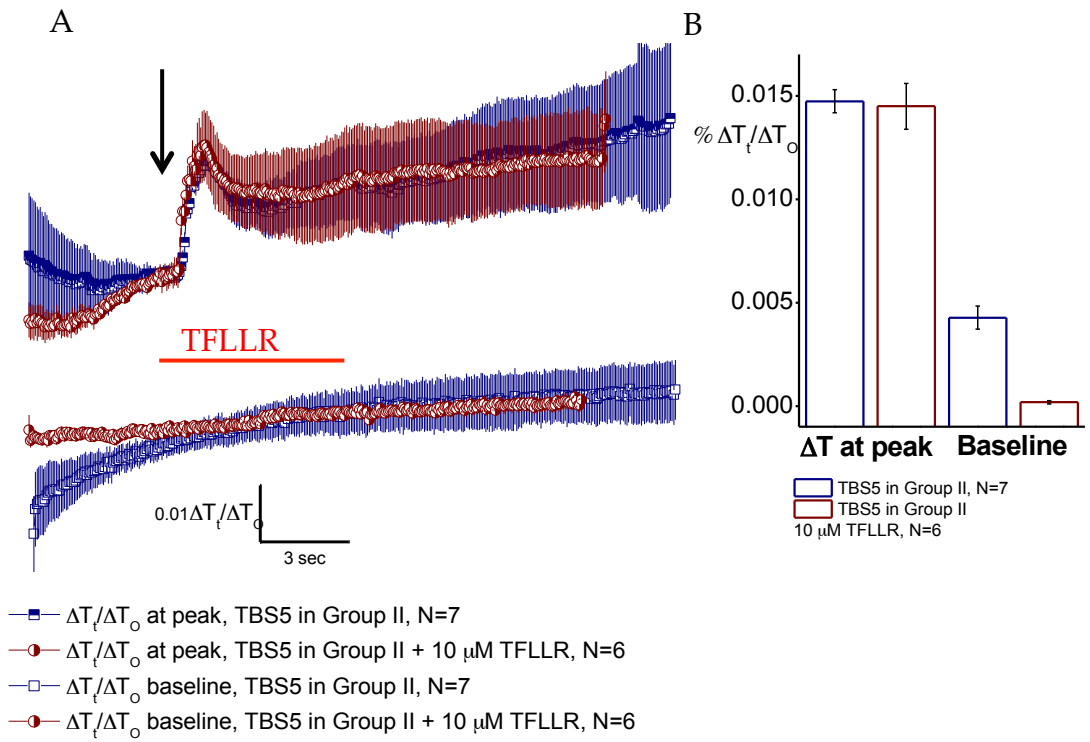

Figure 5.16: **Addition of TFLLR to experiments with 5 TBS in group II mice (5-8 months postnatal).** A – time course of experiments with TBS5 stimulation showing control experiments (navy) and experiments with TFLLR application (burgundy). Black arrow shows the onset of stimulation, and the red lines shows the application of TFLLR in experiments where the drug was applied. B – Bar chart representation of peaks and baselines of responses, normalised to the average between the control (T_0) and washout signals (T_{15}). The maximal peak of the control experiments was 0.0145±3.3*10^-4 whereas experiments with TFLLR application had an increase in the light transmittance of 0.0131±2.6*10^-4 ΔT. The peaks were not significantly different, as calculated with two-sample t test.

5.6.4 The effect of the addition of α, β methylene-ATP to the experiments with 5 TBS in slices from young adult mice

The experiments with five Theta Bursts stimulations and the application of 10 μM α, β methylene-ATP were performed to compare the effect of the addition of this drug in the experiments with a stronger stimulation. The data collected for these experiments is presented on Figure 5.15. The control experiments showed the maximal response of 0.0147±1.6*10^-4, whereas the addition of 10 μM α, β methylene-ATP yielded a peak of 0.0260±7.3*10^-4. This difference was significant, as calculated with two-sample t test. Similarly to the pattern, displayed by the experiments with TFLLR application, both the size of the peak of the response as well as the speed of the recovery of the light transmittance signal is increased when compared to control experiments.

Another similarity of the data collected for α, β methylene-ATP and TFLLR experiments is that the plateau reached by the signal after recovering from the stimulation is significantly greater than the washout portion of the signal of the control experiments. As can be seen from Figure 5.14, between 15 and 20 minutes after the start of the experiment the average signal in the experiments with the addition of the drug was measured to be 1.04±8.2*10^-4, and this was significantly greater than 99.8±6.9*10^-3 per cent light transmittance signal that was measured in control experiments. The consistency of these data patterns increases the reliability of the hypothesis that the mechanism described in the previous chapter is linked to potassium buffering function of astrocytes.

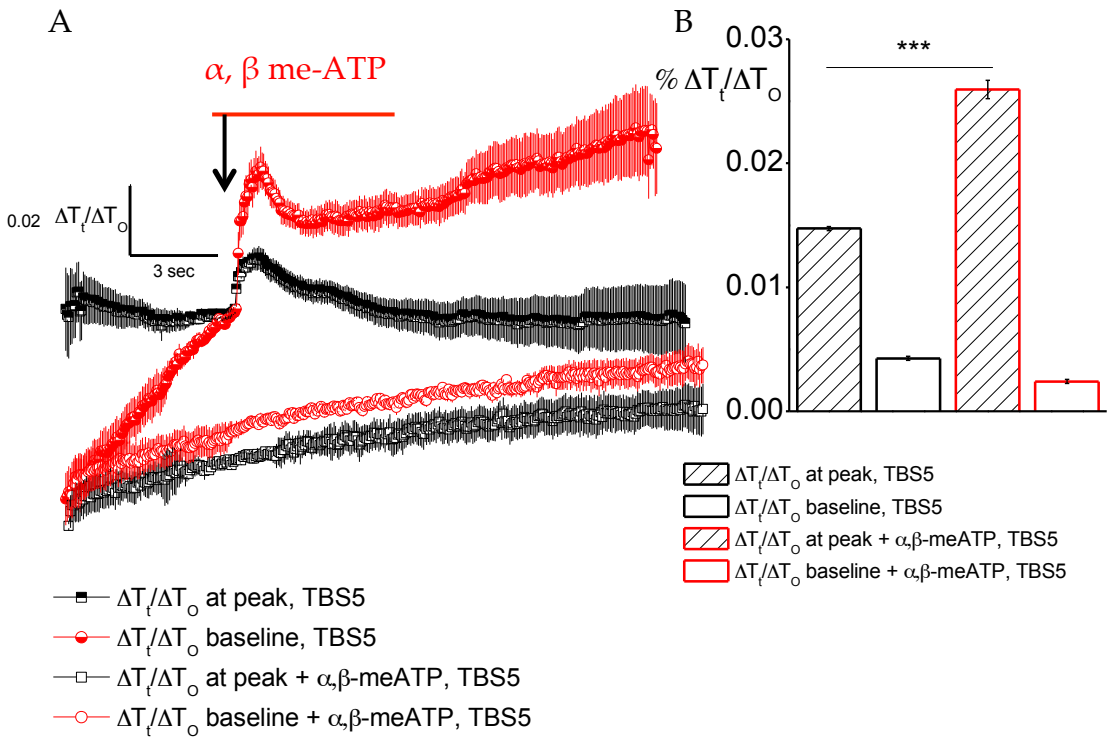

Figure 5.17: **Addition of α, β methylene-ATP to experiments with 5 TBS in group I mice (1-3 months postnatal).** A – time course of experiments with TBS5 stimulation showing control experiments (black) and experiments with α, β methylene-ATP application (red). Black arrow shows the onset of stimulation, and the red line shows the application of α, β methylene-ATP in experiments where the drug was applied. B – Bar chart representation of peaks and baselines of responses, normalised to the average between the control (T_0) and washout signals (T_{15}). The maximal peak in the experiments with α, β methylene-ATP application was 0.0147±1.6*10^-4 whereas control experiments had an increase in the light transmittance of 0.0260±7.3*10^-4 ΔT. The peak in control experiments was significantly smaller than that of experiments with the addition of α, β methylene-ATP, as calculated with two-sample t test; *** – p<0.0001.

5.6.5 The effect of the addition of memantine to the experiments with 5 TBS in slices from young adult mice

Another drug was applied to the experiments with 5 Theta Bursts stimulation – memantine. Memantine is a drug used currently used for treatment of dementia, and specifically as part of the combinational therapy in Alzheimer's disease (J. Ma, Mufti, and Leung 2015). At low concentrations, such as 3 μM memantine preferentially binds to NMDA receptors on glial cells (Talantova et al. 2013). Since memantine acts on glial NMDARs it was assumed that it could also have an effect on the mechanism linking stimulation of various ionic channels of glial with increased outward potassium current. The results collected for these experiments are presented on Figure 5.16 below. As can be seen, the maximal peak of the response was not altered significantly by the addition of memantine. The increase measured in the control experiments was $0.0147 \pm 1.6 * 10^{-4}$ whereas in experiments with the addition of memantine the increase was only $0.010 \pm 1.2 * 10^{-4}$ ΔT. Due to the nature of the data analysis used, the amplitude of the peak, normalised to the average of control and washout light transmittance signal, appears to be smaller in experiments with the addition of memantine. When the alternative analysis method was used, the maximal peaks reached by the control and memantine experiments were $0.0152 \pm 2.0 * 10^{-4}$ and $0.0158 \pm 1.1 * 10^{-4}$ respectively. Another peculiarity was the rate of the recovery of the peak - it was much slower in the experiments where the drug was applied. Overall, following the peak of the response to 5 Theta Bursts, the signal in recording with memantine does not fall significantly until the end of the experiment, thus meaning that the initial tissue swelling that was achieved by the stimulation was not reversed completely by potassium buffering. It is possible that by blocking astrocytic NMDARs, memantine prevents the triggering of the mechanism that would otherwise set off the process of potassium buffering.

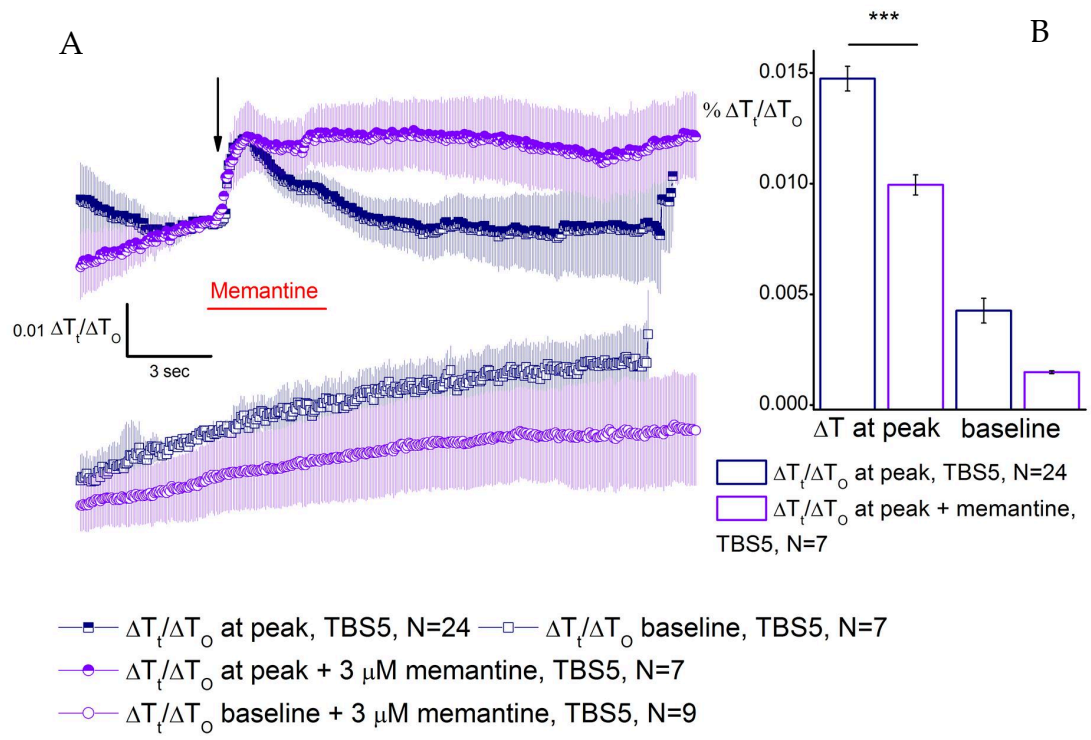

Figure 5.18: **Addition of memantine to experiments with 5 TBS in group I mice (1-3 months postnatal).** A – time course of experiments with TBS5 stimulation showing control experiments (navy) and experiments with memantine application (purple). Black arrow shows the onset of stimulation, and the red line shows the application of memantine in experiments where the drug was applied. B – Bar chart representation of peaks and baselines of responses, normalised to the average between the control (T_0) and washout signals (T_{15}). The maximal peak in the experiments with memantine application was 0.010±1.2*10^-4 whereas control experiments had an increase in the light transmittance of 0.0147±1.6*10^-4 ΔT. The peak in experiments with the addition of memantine was significantly smaller than that of control experiments, as calculated with two-sample t test; *** shows $p<0.0001$.

5.7 Simultaneous tissue swelling and LTP recordings

Some of the experiments were continued for a longer duration. This was done in order to collect and compare data for both light transmittance and LTP alike. In this section the data collected for these longer experiments are presented. Similarly to the data described previously, the time courses of average experiments, both light transmittance and electrophysiological ones are presented as well as bar charts of peak amplitudes, signals at 20-22 minutes and slopes of fEPSP. All data are presented as averages with standard error of mean, unless otherwise stated.

5.7.1 The effect of the addition of TFLLR to the experiments with 2 TBS in slices from young adult mice

Experiments with two Theta Burst stimulations and TFLLR application were recorded for longer durations, to measure both the light transmittance signal and the fEPSP slope. Figure 5.17 illustrates data collected for both the light transmittance signals and electrophysiological recordings made for both experimental conditions. Two Theta Burst stimulations normally do not provide a sufficient stimulation for the onset for LTP, and so the addition of 10 μM TFLLR was hypothesised to rectify this.

The light transmittance signals were not significantly different in experiments with the addition of 10 μM TFLLR, with the maximal peak responses reaching $0.0080 \pm 2.99 * 10^{-4}$ and $0.0083 \pm 2.04 * 10^{-4}$ ΔT respectively. As explained above the analysis method diminishes the effect of the addition of TFLLR on the maximal response to the stimulation and therefore appears to be not altered, however when the peaks were normalised to control signals only it was clearer that the addition of TFLLR increases the peak. The data also did not display differential patterns in the second half of the recordings, with the control experiments reaching

1.011±1.29*10^-4 ΔT and experiments with TFLLR 0.009±2.5*10^-4 ΔT signal between 20 and 22 minutes after the start of the experiment.

The data collected through electrophysiological recordings from the slices revealed a different pattern. Here, similarly to the light transmittance signal both conditions displayed similar fEPSP slope at the end of the recordings (50-55 minutes measurements that correspond to early phase LTP readings) with the control experiments reaching only 102.1±3.77 per cent of the control slope and the experiments with the addition of TFLLR reached 114.1±2.66 per cent of control. These readings were not significantly different as calculated with two-sample t test.

However, the short-term potentiation, normally measured around 20-30 minutes after the stimulation of the tissue proved to vary in two experimental conditions. In experiments without the addition of TFLLR the slope of the fEPSP reduced to 83.5±3.07 per cent of control before recovering later in the recordings. In those slices where 10 μM TFLLR was added there was no reduction in the slope of the EPSP; instead a potentiation was measured of 123.8±1.77 per cent of control slope measurement. These data were significantly different with $p<0.0001$.

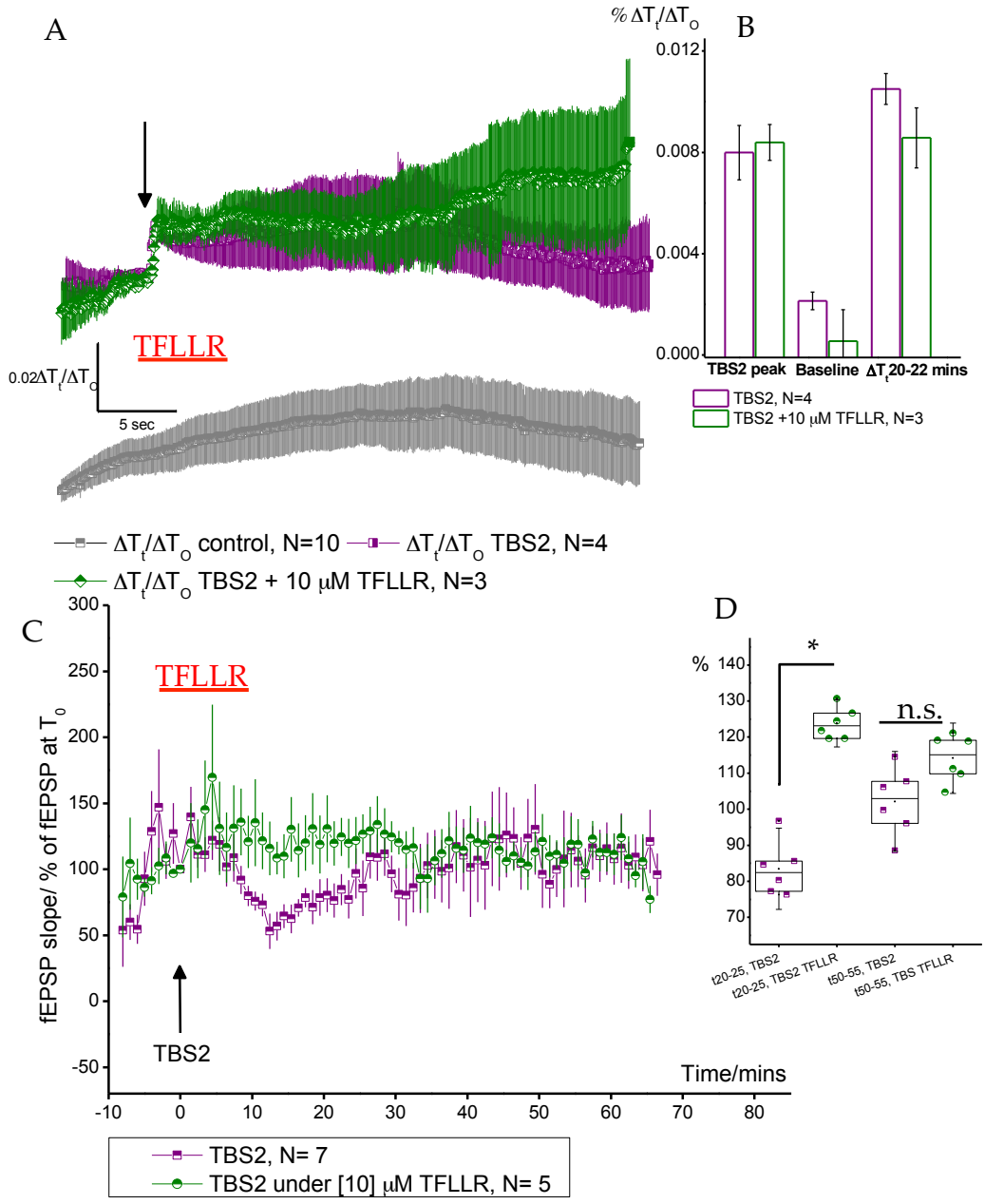

Figure 5.19: **Addition of TFLLR to experiments with 5 TBS in group I mice (1-3 months postnatal).** A – time course of experiments with TBS5 stimulation showing control experiments (purple) and experiments with TFLLR application (green). Black arrow shows the onset of stimulation, and the red line shows the application of TFLLR in experiments where the drug was applied. B – Bar chart representation of peaks and baselines of responses, normalised to the average between the control (T_0) and washout signals (T_{15}). The maximal peak in the experiments with TFLLR application was 0.014±6.43*10^-4 whereas control experiments had an increase in the light transmittance of 0.014±6.43*10^-4 ΔT. There were no significant differences detected between the light transmittance signals of two experimental conditions. C – Time course showing the slopes of fEPSPs, purple shows control experiments and green – the experiments with TFLLR. D – Box charts, illustrating the comparison between the peak responses to stimulation and fEPSP between 20-22 minutes after the stimulation. Boxes show mean and SEM and whiskers show SD. The slopes of control and experiments with TFLLR were not significantly different at 50-55 minutes, as calculated with two-sample t test, but the slopes of fEPSPs at 20-22 minutes after the stimulation were significantly increased in experiments with TFLLR; * – $p<0.0001$.

5.7.2 The effect of the addition of α, β methylene-ATP to the experiments with 5 TBS in slices from young adult mice

Similar to experiments described in section 5.7.1 some experiments with five Theta Burst stimulations and addition of 10 μM α, β methylene-ATP were performed with both the light transmittance and electrophysiological recordings being made simultaneously. It was hypothesised that since the addition of 10 μM α, β methylene-ATP to short experiments increased the amplitude of the maximal response to the peak the same effect should be achieved in these experiments. Since ATP can activate glial cells, it can be used for enhancing LTP and so it was also hypothesised that the slope of fEPSP would be increased around 50-55 minutes of the electrophysiological recording.

The data gathered for these experiments with the addition of 10 μM α, β methylene-ATP are displayed on Figure 5.18. The light transmittance signals in experiments with 10 μM α, β methylene-ATP did not show a decrease back to control levels following the five Theta Burst stimulations, which was the pattern displayed by the control experiments. On the contrary, after the response to the stimulation, the signal in experiments with the drug application slightly restored back to resting levels for a short period of time before increasing for the rest of the recording. At 20-22 minutes of the recording the signal of the control experiments was measured to be 0.022±2.6*10^-4 whereas the experiments with α, β methylene-ATP had an average light transmittance signal of 0.078±7.2*10^-4 ΔT. This difference was calculated to be significant with the $p<0.0001$.

Sections C and D on Figure 5.18 display the data collected for the field recordings of both experimental conditions. Two time points were used to compare the slopes of the fEPSPs: 20-22 and 50-55 minutes after the stimulation. These time points correspond to short-term and early long-term potentiation times. The average

slope measured in experiments with the addition of α, β methylene-ATP was not significantly different from the slopes in control experiments at both time points. Control experiments yielded a short-term potentiation of 121.9±1.9 per cent, whereas the average slope increase in experiments with α, β methylene-ATP was 117.1±5.8 per cent. At 50-55 minutes control experiments showed 22.8±2.1 per cent increase in slope, experiments with the drug addition –26.4±7.0 per cent. Comparing both sets of data revealed no significant difference.

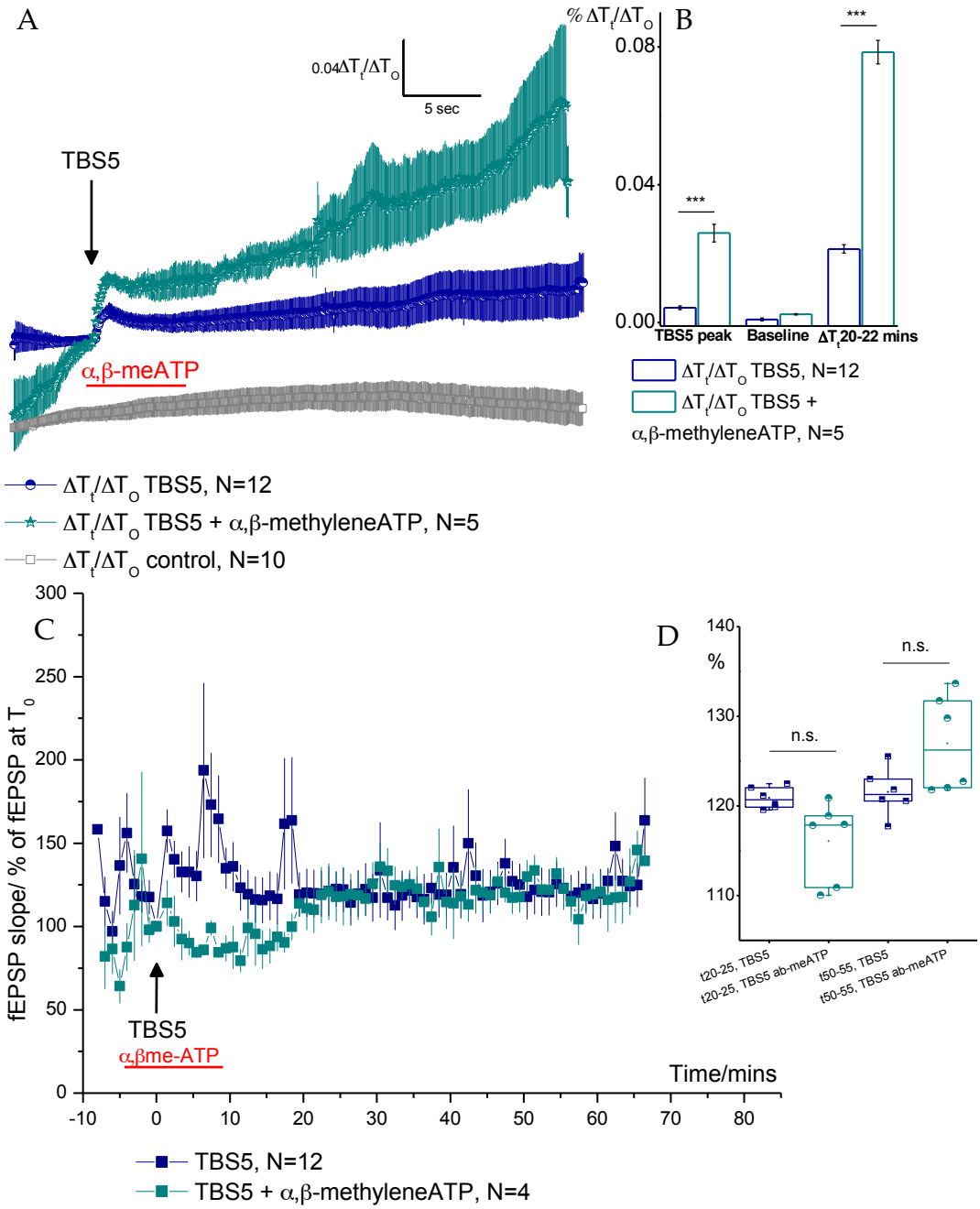

Figure 5.20: **Addition of α, β methylene-ATP to experiments with 5 TBS in group I mice (1-3 months postnatal).** A – time course of experiments with TBS5 stimulation showing control experiments (navy) and experiments with α, β methylene-ATP application (green). Black arrow shows the onset of stimulation, the red line shows the application of α, β methylene-ATP in experiments where the drug was applied. B – Bar chart representation of peaks and baselines of responses normalised to average signal ($T_0 + T_{15}/2$). The maximal peak in the experiments with α, β methylene-ATP application was 0.0260±7.32*10^-4, whereas control experiments had an increase in the light transmittance of 0.0147±1.61*10^-4 ΔT. C – Time course showing the slopes of fEPSPs. D – Box charts, illustrating the comparison between the peak responses to stimulation and fEPSP between 20-22 minutes after the stimulation. Boxes show mean±SEM, whiskers - SD. At 20-22 minutes control experiments showed 121.9±1.9 % and experiments with α, β methylene-ATP – 117.1±5.8 % of baseline. LTP (50-55 minutes) in control experiments showed 22.8±2.1 per cent increase in slope, experiments with the drug addition – 26.4±7.0 per cent; *** shows p<0.001, n.s. – no significant difference.

5.7.3 The effect of the addition of memantine to the experiments with 5 TBS in slices from young adult mice

Finally, the long experiments with simultaneous field and light transmittance recordings were repeated with five Theta Burst stimulations and the addition of memantine. As explained previously, memantine is NMDA receptor blocker, which at low concentrations (such as 3 μM) acts as a specific blocker to glial NMDARs (Ahmed et al. 2004). It can therefore be used to block one of the pathways of the mechanism, described in Chapter 4. Figure 5.19 below summarises the data collected for these experiments.

As can be seen from sections A and B of Figure 5 the application of 3 μM of memantine reduced the light transmittance signal, with both the maximal response to the stimulation as well as the signal at 20-22 minutes. In the experiments with the addition of this drug the maximal peak of the signal was $0.010\pm4.5*10^{-4}$ and the average signal, measured between 20-22 minutes was $0.016\pm3.9*10^{-4}$. Both of these measurements were significantly smaller than the corresponding data in the control experiments. It was concluded that the application of memantine reduced the amount of tissue swelling by selectively blocking the glial NMDA receptors.

Data collected through field recordings are presented in sections C and D of Figure 5.19. It was found that the application of memantine to the recording chamber reduced the slope of the fEPSP after the five Theta Burst stimulations. In control experiments both short-term and long-term potentiation was established upon the stimulation: 136.9±0.9 and 141.8±2.1 per cent respectively. The addition of memantine reversed this potentiation and the slope of the fEPSP was measured to be 72.4±2.5 and 71.0±1.8 per cent of the control measurement at 20-22 and 50-55

minutes respectively. Comparing datasets collected for two experimental conditions revealed a significant difference at both time points ($p<0.0001$).

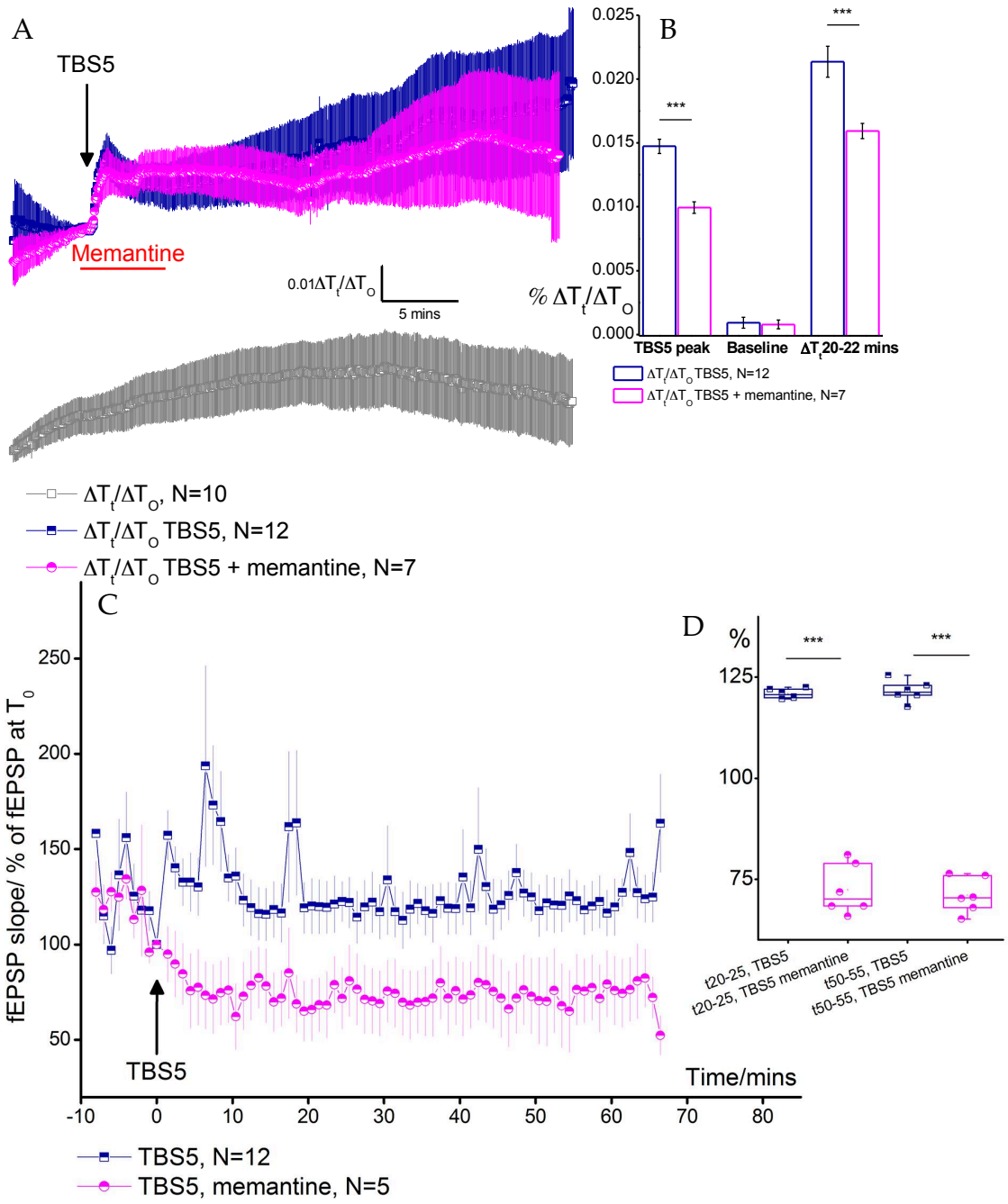

Figure 5.21: **Addition of memantine to experiments with 5 TBS in group I mice (1-3 months postnatal).** A – time course of experiments with TBS5 stimulation showing control experiments (navy) and experiments with memantine application (pink). Black arrow shows the onset of stimulation, and the red line shows the application of memantine in experiments where the drug was applied. B – Bar chart representation of peaks and baselines of responses. The maximal peak in the experiments with memantine application was 0.010±4.5*10^-4, whereas control experiments had an increase in the light transmittance of 0.0147±1.61*10^-4 ΔT. C – Time course showing the slopes of fEPSPs. Both averages are normalised to T_0 (the last reading prior to the stimulation). D – Box charts, illustrating the comparison between the peak responses to stimulation and fEPSP between 20-22 minutes after the stimulation. Boxes show mean±SEM and whiskers show SD. At 20-22 minutes the control experiments showed 121.9±1.9 % and experiments with memantine – 72.4±2.5 % of control slope. LTP (50-55 minutes) in control experiments showed 22.8±2.1 % increase in slope, experiments with the drug addition had a decrease of signal to 71.0±1.8 %; *** – p<0.001.

5.7.4 Comparing the response to 5 TBS of slices from young adult and older mice (groups I and II respectively)

In order to study the effect of age the long experiments were conducted with slices cut from young adult and older mice. The light transmittance signals were compared in experiments with two age groups. The data collected for these experiments are presented below on Figure 5.20. It was very clear that there are no drastic differences between the responses to five Theta Burst stimulations in young adult and older mice. Slices form group I had a maximal peak of $0.0133 \pm 8.09 * 10^{-4}$ whereas experiments with group II mice had an increase in the light transmittance of $0.0136 \pm 2.89 * 10^{-4}$. The overall trend displayed by the data was towards the increase of the overall tissue swelling following the stimulation and a shorter and less efficient recovery period. For example, at 20-22 minutes the average signal measured from young mice was 0.0214±2.61*10^-4 and in older mice it was $0.019 \pm 4.7 * 10^{-4}$. However, due to quite strong variability of the signal these differences were not found to be significant. Overall, it was seen that with higher stimulations the differences in response of the two age groups were diminishing. It is possible that this trend can explain the lack of differences found when long-term potentiation is measured, as it would normally be evoked by a strong stimulus such as 5TBS or above.

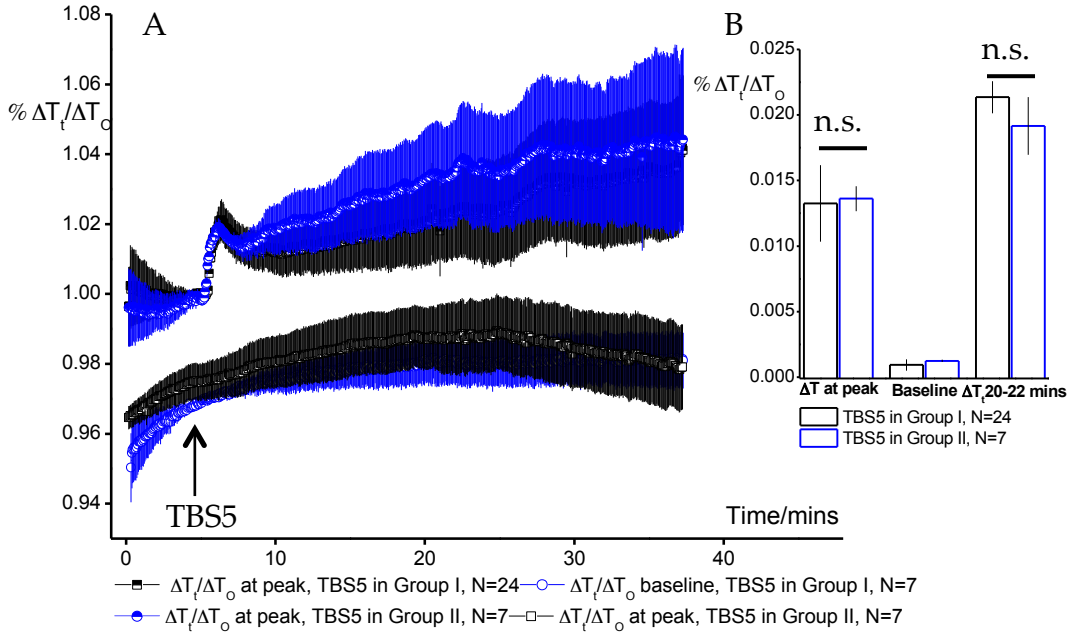

Figure 5.22: **Responses to 5 TBS in group I (1-3 months postnatal) and group II (5-8 months postnatal) mice.** A – time course of experiments with TBS5 stimulation showing experiments with young adult (black) and experiments with older (blue) mice. Black arrow shows the onset of stimulation. B – Bar chart representation of peaks and baselines of responses, normalised to the average between the control (T_0) and washout signals (T_{15}). The maximal peak in the experiments with mice from group I was 0.0133±8.09*10^-4 whereas experiments with group II mice had an increase in the light transmittance of 0.0136±2.89*10^-4 ΔT. The response to stimulation in light transmittance signals were not significant different in two age groups as calculated with two-sample t test. When signals were compared at 20-22 minutes the experiments with older slices showed a higher extent of swelling, although this difference was not found significant with the two-sample t test.

5.8 Conclusions

This chapter set out to study the molecular mechanism, linking a number of astrocytic channels with their voltage-gated potassium currents on an integrated network level. Once the nature of this mechanism was established at the level of isolated astrocytes, the next step naturally was to consider this mechanism and its' implications on the whole network. This was done in slices, so the whole astrocytic syncytium was intact as well as the connections between the neural and astrocytic components of the cortex.

Firstly, it was shown that the method chosen for the light transmittance experiments collects similar data to published values. For example, the application of hypo-osmotic increases the light transmittance signal, similarly to literature in the field. Another control experiment involved the application of high concentration KCL aCSF. The light transmittance increased as a result of this addition, similarly to previously published data (Syková and Chvátal 2000). Stimuli of various strengths were applied and the responses in light transmittance were compared (see Figures 5.2 and 5.3). In order to consider the age-related differences, that can potentially influence the extent or pattern of tissue swelling, slices were cut from mice of two age groups – young adult mice (1-3 months postnatal) and older mice (5-8 months postnatal). It was found that the slices from older mice on average show a weaker response to the stimulation. This pattern was the same in experiments with single Theta Burst stimulation and 5TBS. However, the baseline of the older slices had a greater tendency towards swelling, often failing to restore its' signal to pre-stimulation levels.

A number of pharmacological agents were applied in an attempt to affect the molecular mechanism, linking some astrocytic channels and outwards potassium conductance. To activate this mechanism, TFLLR and α, β methylene-ATP were

applied at 10 μM concentration. When a single Theta Burst stimulation was applied, the addition of TFLLR caused no change to the light transmittance signal in young adult mice. Older slices, however, demonstrated a decrease in their response to stimulation when TFLLR was applied. The addition of α, β methylene-ATP generated different data. The average maximal peak of the response following the stimulation was increased by the addition of this analogue of ATP.

These experiments were repeated with a stronger stimulation of two Theta Burst stimulations. Here the slices from older mice showed an increase in their light transmittance responses compared to slices derived from younger mice. The addition of TFLLR in both groups showed a slight decrease of the response to the stimulus, and the addition of α, β methylene-ATP caused an increase in this signal. These data were similar to those collected for the experiments with a single Theta Burst stimulation. Another set of experiments with two Theta Burst stimulations and TFLLR application was conducted. Here, a solution of high KCL concentration (10 mM) was applied after the stimulation. In experiments where TFLLR was present the secondary response to the changes in light transmittance was greater than that of the control.

Finally, experiments with five Theta Burst stimulations were performed. It was found that the response to the stimulation in slices derived from older mice was weaker. Both sets of experiments with the additions of TFLLR and α, β methylene-ATP caused a great increase in the response peak to the stimulation. It was concluded that the strength of stimulus plays an important role in the effect of these drugs. Memantine was used to inhibit the mechanism, described in the previous chapter. Experiments with five Theta Burst stimulations showed that application of memantine reduces the signal response to the stimulation.

Some longer experiments were conducted where the light transmittance signals were compared the slopes of EPSPs. When two age groups were compared in their light transmittance, little change was measured. TFLLR was applied to experiments with two Theta Burst stimulations. The light transmittance signal showed little difference over the peak size and the signal level at 20-22 minutes of the recording. Short-term potentiation was increased in the experiments with TFLLR, but the long-term potentiation was not significantly changed. It is possible that the effects of the addition of TFLLR might be different if a stronger stimulation was applied. When α, β methylene-ATP was applied to experiments with 5TBS stimulation, the light transmittance signal was increased at both time points: in response to the stimulation and at 20-22 minutes of the recording. The application of this drug did not significantly increase either short or long-term potentiation. Finally, the addition of memantine produced significant alterations to both light transmittance signal and the slope of EPSP. In experiments with memantine both the response to the stimulation and the signal at 20-22 minutes of the recording was diminished. The slope of EPSP was decreased by the application of memantine and the plasticity was reversed: short and long term depressions were achieved instead of potentiation.

Overall, this chapter set out to investigate the effects of potentiating or inhibiting the mechanism that was described in chapter 4 on the network level. It was shown that the effect of the application of TFLLR, α, β methylene-ATP and memantine produced distinct results. The strength of the stimulus was very important as the data collected for experiments with weak stimulation showed different effects of the addition of TFLLR. The potential link between all of the results described above and the implications of this mechanism on the functioning and plasticity of the cortex are evaluated in the Discussion chapter.

Chapter 6 – Discussion and conclusion

6.1 Overview of conclusions

The aim of this study was to investigate a possible molecular mechanism, linking various astrocytic channels ($P2X_{1/5}$, NMDARs and PAR-1) with potassium conductance of isolated cortical astrocytes; and to explore whether this modulation takes place in slice, and carries importance in the process of potassium buffering and the shrinkage of extracellular space.

Firstly, it was investigated whether age alters the conductance of potassium current subtypes in neocortical astrocytes from layers 2/3 of somatosensory cortex. To do so, the currents measured in young (1-3 months old) and old (9-12 months old) were compared with the fractions of the overall potassium current that were susceptible to 4-aminopyridine or barium chloride or both. It was found that the capacitance of astrocytes significantly increased in size from young adult to older mice, meaning that the cells, or at least the cell somas increase in size, as the animal grows older. This conforms to the current understanding of astrocytic age-related changes: increased number of astrocytes expresses GFAP and show increased soma size – factors that can later on lead to astrogliosis (Goss, Finch, and Morgan 1990; Correa-Cerro and Mandell 2007).

When current densities were compared, it was found that the inwardly rectifying potassium channel conductance does not increase with age, unlike voltage-dependent potassium currents. Since Kir4.1 channels have been implicated in potassium buffering, this lack of increase in density in old age can mean that astrocytes may be less effective at clearing the extracellular potassium ions following action potentials; this could potentially lead to neuroinflammation and astrogliosis(Rossi 2015; Salminen et al. 2011; Pekny and Nilsson 2005; Pekny and

Pekna 2014). Alternatively, this observation could be a consequence of ageing as opposed to a cause.

The proportions of current sensitive to 4-aminopyridine and barium were compared in young and old mice. The 4-aminopyridine sensitive fraction of the current did not increase with age, unlike the fraction of the current that was sensitive to barium chloride – young mice displayed a much higher barium sensitivity. The current density of voltage-gated potassium channel increases with age (meaning there are more voltage-gated potassium channels expressed on the soma), but 4-aminopyridine-sensitive fraction of the potassium current does not rise significantly. This is the opposite of the inwardly rectifying potassium current – it showed no change in the current density but a significant decrease in the fraction of the current that is sensitive to barium chloride. Since the greatest difference was measured at very negative voltage steps of the protocol, aimed at measuring the inwardly rectifying potassium channel, the vast majority of the current should be conducted via the Kir4.1 channels. This decrease shows a dramatic change in the electrophysiological characteristic of cortical astrocytes, as a decreased conductance of inwardly rectifying channel could have large implications for potassium clearance and water homeostasis (Seifert et al. 2009; Nagelhus, Mathiisen, and Ottersen 2004).

The addition of both blockers together showed blockage of a smaller proportion of the generic current than the application of blockers separately. Comparison between young and older mice showed an increase in proportion of the current that is sensitive to both blockers. Most of the voltage steps across three protocols used showed no significant difference, with the exception of highest voltage steps in the protocol for recording inwardly rectifying potassium current (+50 and +70mV). This could be explained by a great degree of depolarization of astrocytes at these voltage steps, which may produce an artefact. It was also noticed that in

older mice more patched cells experienced the so-called rundown, which, although filtered where possible (experiments with a clear rundown were excluded from analysis), could have introduced an error.

In chapter 4 the link between channels of astrocytes and the potassium currents was investigated. Firstly, the same experiments were performed on neurons to ensure that this is an astrocytic specific mechanism. It was expected that if an astrocyte detects signs of activity, e.g. ATP or it's analogues, it would increase the inwardly rectifying potassium current in order to instigate the process of potassium buffering. However, it was found that the inwardly rectifying potassium channel conductance was unaffected by the addition of agonists to $P2X_{1/5}$, NMDARs or PAR-1 receptors. Instead it was determined that applying an agonist to any of the aforementioned channels causes an elevation in the outward potassium current. This mechanism was Calcium-dependent, as it is known that all three of the channels are able to pass through calcium ions (or in the case of PAR-1 channel cause a release of intracellular calcium store as a secondary messenger). This effect was also reliably blocked by the addition of high EGTA. It was also determined that this mechanism is far less prominent in older cells, thus indicating at a potential neuroprotective role it may play in young animals.

To further dissect this mechanism, 4-aminopyridine and barium chloride blockers were used. It was found that the increased current is susceptible to the former but not latter blocker, thus once again proving that it is not the inwardly rectifying potassium channel being involved. On the contrary, in some experiments with the addition of barium blocker the facilitation effect of adding an agonist was increased in size. The following hypothesis was built on the basis of the data collected: activation of ionotropic ($P2X_{1/5}$ and NMDARs) or metabotropic (PAR-1) receptors can cause an influx of calcium ions into the cell and a consecutive increase in the potassium current (via the intracellular calcium stores). This is in

line with previous findings from our laboratory, showing that activation of PAR-1 receptors initiates calcium signalling (Lalo et al. 2014), and that $P2X_{1/5}$ and NMDARs are permeable to calcium in astrocytes (Palygin et al. 2010). Whereas in experiments with activation of P2X and NMDA receptors secondary effects, arising from activating neuronal receptors could introduce variability into data, PAR-1 receptors are primarily expressed in astrocytes, thus making it possible to compare these data sets. Since the effects seen in all three data sets are similar, it can be assumed that the effects seen in experiments with P2X and NMDARs are due to experimental stimulus and not secondary effects. The significance of this mechanism is unclear. It appears that similar to neurons, astrocytes can respond to activation of their receptors with increased outward potassium current. It is possible that this is a necessary first step for the process of potassium buffering, but further investigation is required. Alternatively, this mechanism could be an auxiliary pathway to recruit more astrocytic branches to the task of potassium uptake. During neuronal activity, there spill of glutamate and other neurotransmitters initiates the process of glutamate buffering. This is done through transporter channels, which utilise energy from the exchange of Na^+, K^+ and H^+. As a result, the local concentration of potassium outside the astrocytic branch increases further. Perhaps the mechanism, discussed in Chapter 4, mimics this local rise in potassium current and thus starts the process of potassium uptake in nearby astrocytic projections.

Lastly, Chapter 5 attempted to explore the significance of the mechanism discovered on isolated cells. A model for studying tissue swelling and potassium buffering during activity was chosen in order to test whether this mechanism affects the process of potassium clearance (Kreisman et al. 1995; Syková and Chvátal 2000). Various stimulations were utilised and it seemed that the highest stimulation used - 5 TBS showed the most prominent results, as well as highest effect of the drugs. It was found that α, β methylene-ATP and TFLLR yielded a

significant increase in the extent of tissue swelling. It can be concluded that the activating the mechanism, described in chapter 4, increases the extent of tissue swelling as well as the rate of recovery of the signal. This means that the mechanism is involved in the process of potassium buffering, making the voltage-gated potassium channels important in this astrocytic function. However, it was also shown that the current density of voltage gated potassium channels increases with age, but (in the case for experiments with NMDARs) this facilitation is greatly diminished in mice of age group III. These findings, taken together, lead to the following conclusions: firstly, voltage-gated potassium channels are implicated in the process of potassium buffering by astrocytes; secondly, activating astrocytes by agonist applications to P2X, NMDARs or PAR-1 channels (the channels that have been tested in this study, but it's perfectly possible for others to be involved too) increases both the ''depolarisation'' of astrocytes and consecutive potassium clearance. Lastly, this mechanism rapidly diminishes with non-pathological ageing, and it almost completely non-functional in group III, therefore the loss of function takes place between 1-3 and 9-12 months old. This happens despite the increase of density of voltage-gated potassium channels in older mice.

Overall, it can be said that slices from older mice exhibited a greater extent of decline in the baseline signal, showing that they are less viable than the younger slices. Most of the responses to activity recorded in older mice were weaker, and so were the effects of the addition of agonists to P2X or PAR-1 receptors. Chapter 5 also covered the experiments that recorded the LTP and LT experiments simultaneously. Here, the application of TFLLR with 2 TBS did not manage to increase the LT signal of the slice nor the size of the slope of fEPSP significantly at 50 minutes, but a slight increase in the short-term potentiation was measured. At higher stimulations, the addition of α, β methylene-ATP has increased the LT signal, but failed to significantly change the slope of the fEPSP. It is possible that

more experiments are needed to see a more prominent increase in the synaptic plasticity upon the addition of this analogue of ATP, as it has been shown before that application of non-hydrolysable analogues of ATP can rescue the LTP (Rasooli-Nejad et al. 2014). Lastly, the addition of memantine was expected to reduce the signal (via selective inhibition of glial NMDARs at concentration used), which indeed took place. The slope of EPSP was decreased plasticity was reversed: short and long term depressions were achieved instead of potentiation.

There are limitations to the method chosen to monitor the clearance of potassium from the extracellular space. Since potassium concentration outside the cells is linked with glutamate uptake, the measured increase in the signal can be partially attributed to glutamate transport into the cell, as well as the influx of potassium ions. However, the light transmission experiments were performed to investigate, if the mechanism, described previously, is relevant *in situ*. The most prominent result was achieved with the application TFLLR, which should have no secondary network effects. The extent of tissue swelling in experiments with activation P2X and NMDA receptors may be concealed by the neuronal responses to the addition of corresponding agonists. It is therefore considered that for the purpose of testing the relevance of the molecular mechanism, described in Chapter 4, this method was sufficient. However, for any further investigations perhaps a different approach might prove to yield more concrete data.

This project set out to investigate the link between various functions of astrocytes by studying the connection of multiple channels expressed in astrocytes and whether these connections are a subject to age-related alterations. Understanding how astrocytes participate in the signalling and mediate synaptic plasticity as well as carrying out the homeostatic functions such as potassium clearance. The approach utilised in this study was to start with a single cell and then progress into *ex vivo* models that are more representable of physiological conditions. The

data obtained in the due course of this project points toward voltage-gated potassium channels as an important player in potassium clearance, the mechanism of which remains unknown. Further investigations are needed to shed light on exact mechanisms of connectivity of various astrocytic channels with voltage-gated potassium channels and potassium buffering.

6.2 Discussion

6.2.1 NG2 vs astrocytes

A study by Bernardinelli et al. (2008) reports two distinct electrophysiological profiles of astrocytes. The authors term these ''naïve'' and ''complex'' astrocytes. Naïve astrocytes were found to have a passive electrophysiological conductance with little of voltage-dependency shown; whereas the complex astrocytes were seen to have a distinct K_A and K_D voltage-gated currents. In the study animals used were 15-21 days old rats. The authors report the majority of the astrocytes to be naïve (71%) (Bernardinelli and Chatton 2008). The young adult group used in this project consisted of mice that were 3-5 months old, thus making it a higher developmental stage.

Interestingly, Wallraff et al. describe similar types of glial cells based on their junction coupling in a mouse hippocampus (Wallraff et al. 2004). These authors denote complex astrocytes as GluR cells and naïve – GluT. The former cell types appears to have little to no junction coupling, whereas GluT cells form a large astrocytic network. Both cell types were identified by expression of EGFP, however morphological differences are reported in: such, GluT cells are described as having oval somata with multiple primary branches and a rich network of tiny projections radiating from these projections. GluR cells, however, are said to have a smaller and more round somatic body as well as fewer primary branches. The distinction in the amount of coupling was striking: no weak or intermediate amount of coupling was found (Wallraff et al. 2004). The electrophysiological

profile of the GluT cells reported above is similar to the current recorded in this study.

Following a relatively short period of uncertainty about their identity and distinction from astrocytes, the GluR cells were renamed as NG2 cells, and at present these cells are considered to be the fourth biggest subclass of glial cells (Nishiyama, Yang, and Butt 2005). NG2 glial cells have been shown to possess a long list of ion channels and neurotransmitter receptors that provide them with complex electrophysiological and antigenic profiles(V. A. Larson, Zhang, and Bergles 2016). They are present in developmental and mature CNS. This glial cell types can also proliferate into oligodendrocytes, which makes they a crucial player in remyelination process following injury or disease (Richardson et al. 2011). For experimental purposes it is important to be able to confidently distinguish between the true astrocytes and the NG2 cells. Despite a range of commonly expressed markers, there are enough distinctive differences. Such, NG2 were never shown to express GFAP or glutamine synthase – typical astrocytic markers; whereas sodium channels are expressed on NG2 cells unlike astrocytes(V. A. Larson, Zhang, and Bergles 2016). Electrophysiologically, NG2 glial cells are expected to display smaller currents with very little inward conductance as well as a smaller somatic size and higher input resistance. These differences are sufficient to allow discrimination between these cell types when conducting experiments. In the recent years many new studies have addressed the regional differences in glial cells, their expression patterns and functional variations. The field of glial heterogeneity promises some exciting discoveries in the near future.

6.2.2 Cellular senescence

It has been shown that density of outward voltage-gated potassium channels is increased in microglial cells of aged mice (Schilling and Eder 2014), and in pyramidal cells of layer 5 of the cortex at least one alpha subunit of delayer

rectifying potassium channels (Kv9.1) are up-regulated in aged humans and primates (Luebke and Chang 2007; Erraji-Benchekroun et al. 2005). Together with findings of this study, it can be proposed that there is an importance of this increased numbers of voltage-gated potassium channels in multiple cell types in the brain. Since it has also been shown that outward (but not inwardly rectifying) potassium current can be induced in microglial cells by the addition of β-amyloid peptide, it can be proposed that this increased potassium current is a consequence of the deposition of senile plaques (S. Chung et al. 2001). Another potential factor, affecting potassium channels in physiological ageing is the accumulation of ROS (reactive oxygen species), which has been shown to affect multiple subunits of potassium channels and modify their functioning (Sesti, Liu, and Cai 2010). It is argued that the AP (action potential) amplitude, as well as after hyperpolarisation (AHP) in sub-populations of neurons are altered during ageing and these changes arise from the different expression patterns of K^+ channels. If the alteration of the expression comes from accumulation of ROS, astrocytic potassium channels should also be subjected to these changes. However, more studies are required to investigate glial-specific expression patterns in aged animals (Puthanveettil 2014).

An increase in some outward potassium channels has been reported in pathological states. Such, in glioblastoma, a large-conductance BK channels have been demonstrated to have an increased sensitivity to Calcium ions. This sensitivity can allow malignant cells to remain active even at typical resting potential states in response to small peaks in intracellular Calcium ions (Ransom, Liu, and Sontheimer 2002). Although the levels of expression of inwardly rectifying potassium channels were found to not be much different from normal brain tissue, the inwardly rectifying current in glioblastoma was greatly reduced. It was determined that Kir channels in glioblastoma are mislocalised, and targeted to cell nucleus instead of the plasma membrane, thus contributing to decreased current density of inward potassium current (Molenaar 2011). Glioblastoma most

often develops in individuals of 40 years old and above, it is likely that some changes in potassium channel expression or post-translational modifications that occur prior to the oncogenic shift are identical in the process of non-pathological ageing.

Astrocytes appear to act as hubs for convergence of signals from multiple pathways as well as filters for plaques and ROS. For instance, it was shown that astrocytes collect Aβ42 protein and build up amyloid plaques inside, leading to enlarged endosomes and as a consequence – a greater proportion of reactive astrocytes. These plaque depositions are not destroyed but persist, thus bring about the apoptotic events for both astrocytes and neurons alike (Nagele et al. 2003; Söllvander et al. 2016). Amyloid plaques are just one example from many other risk factors, increasing the likelihood of development of disease. It is also likely then that astrocytes accumulate these stresses and become more likely to enter cellular senescence state and express senescence – associated secretory phenotype. This includes an increased expression of GFAP and vimentin filaments, some pro-inflammatory cytokines as well as accumulation of toxic aggregates (Salminen et al. 2011). It is believed that once the senescence state has been achieved by the astrocytes, they can enhance the speed of neurodegeneration and as a consequence the deterioration of functional capacity of the brain. In this study we have seen a steady increase in the size of the somata of astrocytes from layers 2/3 of somatosensory cortex as well as density of voltage-gated potassium currents from young adult to older age. This could be a marker for the accumulation of various stresses, leading to the onset of cellular senescence.

6.2.3 Potassium buffering and Kir channels

The overview of potassium buffering by astrocytes can be found in the Introduction chapter. However, it is important to point out that most of the glial studies on this topic focus on Kir4.1 channel – the most highly expressed inwardly

rectifying potassium channel subtype in astrocytes. It's specific subcellular location: increased density near the perisynaptic endfeet and co-expression with Aquaporin 4 hint at the importance of these channels in the clearance of potassium(Nagelhus, Mathiisen, and Ottersen 2004; Kofuji et al. 2002). It is considered that the synapse is the major source of K+ ions. It has been shown that neuronal activity can induce slow inward potassium current that is susceptible to the application of Barium (Rouach 2013). It is not, however, clear what is the signal that initiates the inward flux of Kir channels. We have shown that voltage-gated potassium currents, present in cortical astrocytes are affected by a list of neuro- and gliotransmitters in both isolated and in slice set-ups. Facilitation these currents introduced changes in the patterns of tissue swelling and therefore potassium buffering of slices. It is possible that this may be a way of modulation of the buffering process. This facilitation of potassium current was not a necessary signal for inducing the buffering, since a response was also seen in control experiments. However, when working in an intact slice it is not possible to dissect whether there was endogenous stimulation of this mechanism by neuronal or glial transmitters. Since the mechanism was measured in isolated cells, primarily consisting of cell bodies, it cannot be said whether the same process takes place in branches of astrocytes, and in the finest of projections. Nevertheless, it can be suggested that facilitation of outward potassium current following the activation of $P2X_{1/5}$, NMDARs or PAR-1 receptors may be a way of propagating the buffering of potassium onto other branches of the same astrocytes. Such, the cell body of the astrocyte would expel more potassium into the extracellular matrix, thus providing a stimulus to initiate the process of buffering in nearby astrocytic processes.

There are however, clear limitations of using patch clamping technique in isolated cells to study potassium buffering. Firstly, as pointed out above, the density of Kir4.1 channels is highest on the projections of astrocytes, especially the endfeet

that enwrap the blood vessels. Electrophysiological recordings are by and large maid by patching the cell body of the cell, therefore leaving out the finer projections, as it is hard to control the voltage of small outgrowths with high resistance and low volume. It is therefore hard to be sure what voltage/current perturbations can take place in the branches of astrocytes. Since astrocytes can depolarise in response to neuronal activity and subsequent influx of potassium, both voltage and current clamp conditions do not truly reflect the parameters of the cell. Such, when evoked inward current is measured in astrocyte in slice it represents the current imposed onto the cell by having a set resting voltage potential. Similarly, current clamp mode fails to show K^+ buffering because the equilibrium potential (E_K) of potassium can change depending on neuronal activity. Rouach et al. suggests that simultaneously with an electrophysiological recording the extracellular concentrations of potassium should be measured (2013).

6.2.4. Plasticity of glia

Another important field that arose since the discovery of the tripartite synapse (Araque et al. 1999) is the plasticity of glia, and their interactions with neurons. To date multiple types of glial plasticity have been reported. Structural changes, such as increased coverage of the tripartite synapse by perisynaptic astrocytic processes (PAPS) in various brain regions (Genoud et al. 2006; Bernardinelli et al. 2014), as well as alterations in calcium signalling (Sibille et al. 2015) and as a consequence – synaptic strength (Pannasch et al. 2011). There is also a body of literature that reports both short- and long-term plasticity of astrocytic clearance of potassium and glutamate (for a recent review see (Cheung et al. 2015)).

The data presented in Chapter 4 of this project provides an example of such plasticity in response to extracellular transmitter application. It is proposed that

the link between $P2X_{1/5}$, NMDARs and PAR-1 receptors, located on the plasma membrane of astrocytes and the outward potassium currents is the alterations in the intracellular calcium concentrations. Since these changes of intracellular calcium can remain extremely local within distinct compartments of a single astrocyte (Rusakov 2015), calcium ions appear to be the master regulator of multiple astrocytic functions. As suggested above, the increase in the outward conductance of potassium is the result of influx of calcium into the cell and potentially signal amplification through the IP_3 pathway. The measured increase in the potassium current could not be attributed to calcium-activated potassium channels in astrocytes. This is because the calcium-activated potassium channels that are expressed in astrocytes are primarily located on the perisynaptic endfeet (Price et al. 2002; Girouard et al. 2010). However, the secondary processes were lost during the isolation process, and therefore only the channels, expressed on the cell bodies constituted to recordings. The voltage-gated potassium channels, such as those responsible for K_D and K_A type currents, are the most likely candidates to be responsible for this facilitation effect. It was shown in the course of this project that astrocytes respond with plasticity to certain stimuli, similarly to neurons, albeit the mechanisms of plasticity of astrocytes as well as the downstream effects remain somewhat elusive.

6.2.5 Non-excitable cells

Astrocytes are often referred to as non-excitable cells, however this name may well be mistaken. A whole variety of channels and transporter that are voltage-dependent are expressed in astrocytes, such as Na+/K+ ATPases and Na+/HCO3-transporters, GLTs and some potassium channels(Xue et al. 2010; Florence, Baillie, and Mulligan 2012; Bekar 2004; Smart, Bosma, and Tempel 1997). The expression of such a number of channels that are affected by voltage fluctuations suggests that astrocytes are indeed a subject to depolarisation.

Previously, it has been shown in our laboratory that astrocytes respond rapidly to a group of chemical transmitters (Lalo, Pankratov, et al. 2011). This project has added the changes in the outward potassium current to this list of astrocytic responses. In Chapter 5 the effect of the facilitation of outward potassium current on the process of tissue swelling (as a marker of potassium buffering) was addressed. At higher stimulation the tissue showed a greatly increased extent of swelling in experiments where PAR-1 or $P2X_{1/5}$ receptors were activated. This result links the outward potassium currents in astrocytes with the process of buffering. As proposed above, it is possible that the outward potassium current on the cell some may act a propagator of the buffering by initiating the process of potassium uptake in more distal astrocytic processes. Naturally, more experiments would be needed to test this hypothesis. However, the existence of this mechanism and it's evolution with age are clear, thus proposing an importance of this molecular link in the process of ageing.

6.3 Future directions

Further experiments to collect complementary data to this project would benefit from would employ molecular biological techniques and imaging. To identify the specific subtypes of potassium channel, immunocytochemistry could be employed to test which voltage-gated potassium channel subtypes are most prominent in soma bodies of the astrocytes isolated form layers 2/3 of somatosensory cortex. Experiments in the intact slices with simultaneous recordings of intracellular calcium levels and astrocytic currents may provide an insight the amount of calcium allowed into the cell and how wide spread the elevations are. Tissue swelling experiments with a simultaneous monitoring of extracellular potassium concentration could be beneficial when comparing the effect of the mechanism in question. Overall, this project has delivered another potential player in the process of potassium buffering and the interplay of various astrocytic functions.

Bibliography:

Abbracchio, Maria P, Geoffrey Burnstock, Alexei Verkhratsky, and Herbert Zimmermann. 2009. "Purinergic Signalling in the Nervous System: an Overview." *Trends in Neurosciences* 32 (1): 19–29.

Agulhon, Cendra, Jeremy Petravicz, Allison B McMullen, Elizabeth J Sweger, Suzanne K Minton, Sarah R Taves, Kristen B Casper, Todd A Fiacco, and Ken D McCarthy. 2008. "What Is the Role of Astrocyte Calcium in Neurophysiology?." *Neuron* 59 (6): 932–46.

Ahmed, M M, H Hoshino, T Chikuma, M Yamada, and T Kato. 2004. "Effect of Memantine on the Levels of Glial Cells, Neuropeptides, and Peptide-Degrading Enzymes in Rat Brain Regions of Ibotenic Acid-Treated Alzheimer's Disease Model." *Neuroscience* 126 (3): 639–49.

Allen, Nicola J, and Ben A Barres. 2005. "Signaling Between Glia and Neurons: Focus on Synaptic Plasticity." *Current Opinion in Neurobiology* 15 (5): 542–48.

Amenta, Francesco, Elena Bronzetti, Maurizio Sabbatini, and Jose Antonio Vega. 1998. "Astrocyte Changes in Aging Cerebral Cortex and Hippocampus: a Quantitative Immunohistochemical Study." *Miscroscopy Research and Technique* 43 (October): 29–33.

Amiry-Moghaddam, M, D S Frydenlund, and O P Ottersen. 2004. "Anchoring of Aquaporin-4 in Brain: Molecular Mechanisms and Implications for the Physiology and Pathophysiology of Water Transport." *Neuroscience* 129 (4): 997–1008.

Anděrová, Miroslava, Jana Benesova, Michaela Mikesova, David Dzamba, Pavel Honsa, Jan Kriska, Olena Butenko, et al. 2014. "Altered Astrocytic Swelling in the Cortex of A-Syntrophin-Negative GFAP/EGFP Mice." Edited by Giuseppe Biagini. *PLoS ONE* 9 (11): e113444–34.

Angulo, Ester, Veronique Noe, Vicent Casado, Josefa Mallol, Teresa Gomez-Isla, Carmen Lluis, Isidre Ferrer, Carlos J Ciudad, and Rafael Franco. 2004. "Up-Regulation of the Kv3.4 Potassium Channel Subunit in Early Stages of Alzheimer's Disease." *Journal of Neurochemistry* 91 (3): 547–57.

Araque, Alfonso, Giorgio Carmignoto, Philip G Haydon, Stéphane H R Oliet, Richard Robitaille, and Andrea Volterra. 2014. "Gliotransmitters Travel in Time and Space." *Neuron* 81 (4). Elsevier Inc.: 728–39.

Araque, Alfonso, Vladimir Parpura, Rita P Sanzgiri, and Philip G Haydon. 1999. "Tripartite Synapses:Glia, the Unacknowledged Partner." *Trends in Neurosciences* 22 (5): 1–8.

Armstead, W M. 2005. "Heat Shock Protein Modulation of KATP and KCa Channel Cerebrovasodilation After Brain Injury." *AJP: Heart and Circulatory Physiology* 289 (3): H1184–90.

Attwell, David, Alastair M Buchan, Serge Charpak, Martin Lauritzen, Brian A

Macvicar, and Eric A Newman. 2010. “Glial and Neuronal Control of Brain Blood Flow.” *Nature* 468 (7321): 232–43.

Avoli, Massimo, and John G R Jefferys. 2016. “Models of Drug-Induced Epileptiform Synchronization in Vitro.” *Journal of Neuroscience Methods* 260 (February). Elsevier B.V.: 26–32.

Barres, Barbara A, Walter J Koroshetz, Linda L Y Chun, and David P Corey. 1990. “Ion Channel Expression by White Matter Clia: the Type-L Astrocyte.” *Neuron* 5: 527–44.

Bekar, L K. 2004. “Complex Expression and Localization of Inactivating Kv Channels in Cultured Hippocampal Astrocytes.” *Journal of Neurophysiology* 93 (3): 1699–1709.

Benz, B, G Grima, and K Q Do. 2004. “Glutamate-Induced Homocysteic Acid Release From Astrocytes: Possible Implication in Glia-Neuron Signaling.” *Neuroscience* 124 (2): 377–86.

Bernardinelli, Yann, and Jean-Yves Chatton. 2008. “Differential Effects of Glutamate Transporter Inhibitors on the Global Electrophysiological Response of Astrocytes to Neuronal Stimulation.” *Brain Research* 1240 (November): 47–53.

Bernardinelli, Yann, Jerome Randall, Elia Janett, Irina Nikonenko, Stéphane König, Emma Victoria Jones, Carmen E Flores, et al. 2014. “Activity-Dependent Structural Plasticity of Perisynaptic Astrocytic Domains Promotes Excitatory Synapse Stability.” *Current Biology* 24 (15). Elsevier Ltd: 1679–88.

Bezzi, Paola, and Andrea Volterra. 2001. “A Neuron–Glia Signalling Network in the Active Brain.” *Current Opinion in Neurobiology* 11: 387–94.

Bezzi, Paola, Giorgio Carmignoto, Lucia Pasti, Sabino Vesce, Daniela Rossi, Barbara Lodi Rizzini, Tullio Pozzan, and Andrea Volterra. 1998. “Prostaglandins Stimulate Calcium-Dependent Glutamate Release in Astrocytes.” *Nature* 391 (January): 1–5.

Blaine, Judith, Michel Chonchol, and Moshe Levi. 2015. “Renal Control of Calcium, Phosphate, and Magnesium Homeostasis..” *Clinical Journal of the American Society of Nephrology : CJASN* 10 (7). American Society of Nephrology: 1257–72.

Bordey, Angelique, and Harald Sontheimer. 1999. “Differential Inhibition of Glial K+ Currents by 4-AP.” *American Journal of Physiology - Renal Physiology*, December, 1–12.

Boyden, Edward S, Feng Zhang, Ernst Bamberg, Georg Nagel, and Karl Deisseroth. 2005. “Millisecond-Timescale, Genetically Targeted Optical Control of Neural Activity.” *Nature Neuroscience* 8 (9): 1263–68.

Bradley, Sophie J, and R A John Challiss. 2012. “G Protein-Coupled Receptor Signalling in Astrocytes in Health and Disease: a Focus on Metabotropic Glutamate Receptors.” *Biochemical Pharmacology* 84 (3).

Brown, D A, B H Gahwiler, W H Griffith, and J V Halliwell. 1990. “Membrane Currents in Hippocampal Neurons.” *Progress in Brain Research* 83: 141–60.

Brunso-Bechtold, J K, M C Linville, and W E Sonntag. 2000. "Age-Related Synaptic Changes in Sensorimotor Cortex of the Brown Norway X Fischer 344 Rat." *Brain Research* 872: 125–33.

Bushong, Eric A, Maryann E Martone, Ying Z Jones, and Mark H Ellisman. 2002. "Protoplasmic Astrocytes in CA1 Stratum Radiatum Occupy Separate Anatomical Domains." *Journal of Neuroscience* 22 (January): 183–92.

Butt, Arthur M., and Amanpreet Kalsi. 2006. "Inwardly Rectifying Potassium Channels (Kir) in Central Nervous System Glia: a Special Role for Kir4.1 in Glial Functions." *Journal of Cellular and Molecular Medicine* 10 (1): 33–44.

Cahoy, J D, B Emery, A Kaushal, L C Foo, J L Zamanian, K S Christopherson, Y Xing, et al. 2008. "A Transcriptome Database for Astrocytes, Neurons, and Oligodendrocytes: a New Resource for Understanding Brain Development and Function." *Journal of Neuroscience* 28 (1): 264–78.

Carlson, Bruce A. 2014. "A Fast BK-Type KCa Current Acts as a Postsynaptic Modulator of Temporal Selectivity for Communication Signals," September, 1–16.

Chen, J, and H B Zhao. 2014. "The Role of an Inwardly Rectifying K+ Channel (Kir4.1) in the Inner Ear and Hearing Loss." *Neuroscience* 265 (April): 137–46.

Cheung, Giselle, Jérémie Sibille, Jonathan Zapata, and Nathalie Rouach. 2015. "Activity-Dependent Plasticity of Astroglial Potassium and Glutamate Clearance." *Neural Plasticity* 2015 (6): 1–16.

Chever, O, B Djukic, K D McCarthy, and F Amzica. 2010. "Implication of Kir4.1 Channel in Excess Potassium Clearance: an in Vivo Study on Anesthetized Glial-Conditional Kir4.1 Knock-Out Mice." *Journal of Neuroscience* 30 (47): 15769–77.

Christie, M J, R A North, P B Osborne, J Douglass, and J P Adelman. 1990. "Heteropolymeric Potassium Channels Expressed in Xenopus Oocytes From Cloned Subunits." *Neuron* 4 (3).

Chung, Hee Jung, Xiang Qian, Melissa Ehlers, Yuh Nung Jan, and Lily Yeh Jan. 2009. "Neuronal Activity Regulates Phosphorylation- Dependent Surface Delivery of G Protein-Activated Inwardly Rectifying Potassium Channels." *Proceedings of the National Academy of Sciences* 106 (January): 629–34.

Chung, Sungkwon, Jungsun Lee, Eun-Hye Joe, and Dae-Yong Uhm. 2001. "Beta-Amyloid Peptide Induces the Expression of Voltage Dependent Outward Rectifying K+ Channels in Rat Microglia." *Neuroscience Letters* 300: 67–70.

Chvátal, Alexandr, Miroslava Anděrová, and Eva Syková. 2004. "Analysis of K +Accumulation Reveals Privileged Extracellular Region in the Vicinity of Glial Cells in Situ." *Journal of Neuroscience Research* 78 (5): 668–82.

Coco, S, F Calegari, E Pravettoni, D Pozzi, E Taverna, P Rosa, M Matteoli, and C Verderio. 2003. "Storage and Release of ATP From Astrocytes in Culture." *Journal of Biological Chemistry* 278 (2): 1354–62.

Coetzee, William A, Yimy Amarillo, Joanna Chiu, Alan Chow, David Lau, Tom McCormack, Herman Moreno, et al. 2002. "Molecular Diversity of K+

Channels." *Annals of the New York Academy of Sciences*, January, 1–53.
Conti, Fiorenzo, Andrea Minelli, Silvia DeBiasi, and Marcello Melone. 1997. "Neuronal and Giiai Localization of NMDA Receptors in the Cerebral Cortex." *Molecular Neurobiology* 14: 1–18.
Corner-Bell, A H, S M Finkbeiner, M S Cooper, and S J Smith. 1990. "Glutamate Induces Calcium Waves in Cultured Astrocytes: Long-Range Glial Signaling. ." *Science* 247 (4941): 470–73.
Correa-Cerro, Lina S, and James W Mandell. 2007. "Molecular Mechanisms of Astrogliosis: New Approaches with Mouse Genetics." *Journal of Neuropathology and Experimental Neurology* 66 (March): 169–76.
Covelo, A, and A Araque. 2016. "Lateral Regulation of Synaptic Transmission by Astrocytes." *Neuroscience* 323 (May): 62–66.
Critchley, Macdonald. 1931. "The Neurology of Old Age." *The Lancet*, 1–7.
D'Adamo, Maria Cristina, Luigi Catacuzzeno, Giuseppe Di Giovanni, Fabio Francolini, and Mauro Pessia. 2013. "K+ Channelepsy: Progress in the Neurobiology of Potassium Channels and Epilepsy." *Frontiers in Cellular Neuroscience*, September, 1–21.
Danbolt, N C. 2001. "Glutamate Uptake." *Progress in Neurobiology* 65 (March): 1–105.
De Backer, Ivan, Sufyan S Hussain, Stephen R Bloom, and James V Gardiner. 2016. "Insights Into the Role of Neuronal Glucokinase." *American Journal of Physiology - Renal Physiology*, May.
Derst, Christian, Frank Doring, Regina Preisig-Muller, Jurgen Daut, Andreas Karschin, Nicola Jeck, Stefanie Weber, Hartmut Engel, and Karl-Heinz Grzeschik. 1998. "Partial Gene Structure and Assignment to Chromosome 2q37 of the Human Inwardly Rectifying K+ Channel (Kir7.1) Gene (KCNJ13)." *Genomics* 54 (December): 560–63.
Diniz, Daniel G, César A R Foro, Carla M D Rego, David A Gloria, Fabio R R De Oliveira, Juliana M P Paes, Aline A De Sousa, et al. 2010. "Environmental Impoverishment and Aging Alter Object Recognition, Spatial Learning, and Dentate Gyrus Astrocytes." *European Journal of Neuroscience* 32 (3): 509–19.
Djukic, B, K B Casper, B D Philpot, L S Chin, and K D McCarthy. 2007. "Conditional Knock-Out of Kir4.1 Leads to Glial Membrane Depolarization, Inhibition of Potassium and Glutamate Uptake, and Enhanced Short-Term Synaptic Potentiation." *Journal of Neuroscience* 27 (42): 11354–65.
Edvinsson, Johan M, Anish J Shah, and Lawrence G Palmer. 2011. "Kir4.1 K+ Channels Are Regulated by External Cations" 5 (3): 269–79.
Erraji-Benchekroun, Loubna, Mark D Underwood, Victoria Arango, Hanga Galfalvy, Paul Pavlidis, Peggy Smyrniotopoulos, J John Mann, and Etienne Sibille. 2005. "Molecular Aging in Human Prefrontal Cortex Is Selective and Continuous Throughout Adult Life." *Biological Psychiatry* 57 (5): 549–58.
Feetham, C H, N Nunn, R Lewis, C Dart, and R Barrett-Jolley. 2015. "TRPV4 and K Caion Channels Functionally Couple as Osmosensors in the Paraventricular

Nucleus." *British Journal of Pharmacology* 172 (7): 1753–68.
Fields, R D. 2008. "Oligodendrocytes Changing the Rules: Action Potentials in Glia and Oligodendrocytes Controlling Action Potentials." *The Neuroscientist* 14 (6): 540–43.
Finch, Caleb E. 2003. "Neurons, Glia, and Plasticity in Normal Brain Aging." *Neurobiology of Aging* 24 (May): S123–27.
Fink, Michel, Fabrice Duprat, Florian Lesage, Catherine Heurteaux, and Michel Lazdunski. 1996. "Cloning, Functional Expression and Brain Localization of a Novel Unconventional Outward Rectifier K+ Channel." *The European Molecular Biology Journal* 15: 6854–62.
Florence, Clare M, Landon D Baillie, and Sean J Mulligan. 2012. "Dynamic Volume Changes in Astrocytes Are an Intrinsic Phenomenon Mediated by Bicarbonate Ion Flux." Edited by Alexander A Mongin. *PLoS ONE* 7 (11): e51124.
Frenguelli, Bruno G, and Mark J Wall. 2016. "Combined Electrophysiological and Biosensor Approaches to Study Purinergic Regulation of Epileptiform Activity in Cortical Tissue." *Journal of Neuroscience Methods* 260 (February). Elsevier B.V.: 202–14.
Garcia-Lopez. 2010. "The Histological Slides and Drawings of Cajal." *Frontiers in Neuroanatomy*, 1–16.
Genoud, Christel, Charles Quairiaux, Pascal Steiner, Harald Hirling, Egbert Welker, and Graham W Knott. 2006. "Plasticity of Astrocytic Coverage and Glutamate Transporter Expression in Adult Mouse Cortex." Edited by Charles Stevens. *PLoS Biology* 4 (11): e343–48.
Girouard, H, A D Bonev, R M Hannah, A Meredith, R W Aldrich, and M T Nelson. 2010. "Astrocytic Endfoot Ca2+ and BK Channels Determine Both Arteriolar Dilation and Constriction." *Proceedings of the National Academy of Sciences* 107 (8): 3811–16.
Goldstein, Steve A N, Detlef Bockenhauer, Ita OKelly, and Noam Zilberberg. 2001. "Potassium Leak Channels and the Kcnk Family of Two-P-Domain Subunits." *Nature Reviews Neuroscience* 2 (March): 1–10.
Goldstein, Steve A N, Laura A Price, David N Rosenthal, and Mark H Pausch. 1998. "ORK1, a Potassium-Selective Leak Channel with Two Pore Domains Cloned From *Drosophila Melanogaster* By Expression in *Saccharomyces Cerevisiae*." *Proceedings of the National Academy of Sciences* 93 (November): 13256–61.
Gordon, Thomas R, Jeffery D Kocsis, and Stephen G Waxman. 1988. "Evidence for the Presence of Two Types of Potassium Channels in the Rat Optic Nerve." *Brain Research* 447: 1–9.
Goss, James R, Caleb E Finch, and David G Morgan. 1990. "Age-Related Changes in Glial Fibrillary Acidic Protein mRNA in the Mouse Brain." *Neurobiology of Aging* 12 (July): 165–70.
Grosse, Gisela, Dirk Eulitz, Theodor Thiele, Ingrid Pahner, Sascha Schröter, Shigeo Takamori, Johannes Grosse, et al. 2003. "Axonal Sorting of Kir3.3 Defines a

GABA-Containing Neuron in the CA3 Region of Rodent Hippocampus." *Molecular and Cellular Neuroscience* 24 (3): 709–24.

Guo, Donglin, Yajamana Ramu, Angela M Klem, and Zhe Lu. 2003. "Mechanism of Rectification in Inward-Rectifier K +Channels." *The Journal of General Physiology* 121 (4): 261–76.

Hablitz, J J, H Sontheimer, A Bordey, and A Lyons. 2000. "Electrophysiological Characteristics of Reactive Astrocytes in Experimental Cortical Dysplasia." *American Journal of Physiology - Renal Physiology*, 1–13.

Haj-Yasein, N N, G F Vindedal, M Eilert-Olsen, G A Gundersen, O Skare, P Laake, A Klungland, et al. 2011. "Glial-Conditional Deletion of Aquaporin-4 (Aqp4) Reduces Blood-Brain Water Uptake and Confers Barrier Function on Perivascular Astrocyte Endfeet." *Proceedings of the National Academy of Sciences* 108 (43): 17815–20.

Halassa, Michael M, Tommaso Fellin, and Philip G Haydon. 2007. "The Tripartite Synapse: Roles for Gliotransmission in Health and Disease." *Trends in Molecular Medicine* 13 (2): 54–63.

Hatton, G I. 2004. "Dynamic Neuronal-Glial Interactions: an Overview 20 Years Later." *Peptides* 25: 403–11.

Hayakawa, Natsumi, Hironori Yokoyama, Hiroyuki Kato, and Tsutomu Araki. 2008. "Age-Related Alterations of Oxidative Stress Markers in the Mouse Hippocampal CA1 Sector." *Experimental and Molecular Pathology* 85 (2): 135–40.

Hayakawa, Natsumi, Hiroyuki Kato, and Tsutomu Araki. 2007. "Age-Related Changes of Astorocytes, Oligodendrocytes and Microglia in the Mouse Hippocampal CA1 Sector." *Mechanisms of Ageing and Development* 128 (4): 311–16.

Henn, Fritz A, Hengo Haljamae, and Anders Hamberger. 1972. "Glial Cell Function: Active Control of Extracellular K+ Concentration." *Brain Research* 43: 437–43.

Herculano-Houzel, Suzana. 2014. "The Glia/Neuron Ratio: How It Varies Uniformly Across Brain Structures and Species and What That Means for Brain Physiology and Evolution." *Glia* 62 (9): 1377–91.

Hertz, L. 1965. "Possible Role of Neuroglia: a Potassium-Mediated Neuronal-Neuroglial-Neuronal Impulse Transmission System." *Nature* 12 (June).

Hibino, H, A Fujita, K Iwai, M Yamada, and Y Kurachi. 2004. "Differential Assembly of Inwardly Rectifying K+ Channel Subunits, Kir4.1 and Kir5.1, in Brain Astrocytes." *Journal of Biological Chemistry* 279 (42): 44065–73.

Hibino, H, A Inanobe, K Furutani, S Murakami, I Findlay, and Y Kurachi. 2010. "Inwardly Rectifying Potassium Channels: Their Structure, Function, and Physiological Roles." *Physiological Reviews* 90 (1): 291–366.

Hibino, H, Y Horio, A Ianobe, K Doi, T Gotow, Y Uchiyama, T Kubo, and Y Kurachi. 1999. "Expression of an Inwardly Rectifying K+ Channel, Kir4.1, in Satellite Cells of Rat Cochlear Ganglia.." *American Journal of Physiology - Renal Physiology* 277 (October): 638–44.

Hibino, Hiroshi, Kayoko Higashi-Shingai, Akikazu Fujita, Kaori Iwai, Masaru Ishii, and Yoshihisa Kurachi. 2004. "Expression of an Inwardly Rectifying K+ Channel, Kir5.1, in Specific Types of Fibrocytes in the Cochlear Later Wall Suggests Its Functional Importance in the Establishment of Endocochlear Potential." *European Journal of Neuroscience* 19: 76–84.

Higashi, Kayoko, Akikazu Fujita, Atsushi Inanobe, Masayuki Tanemoto, Katsumi Doi, Takeshi Kubo, and Yoshihisa Kurachi. 2001. "An Inwardly Rectifying K+ Channel, Kir4.1, Expressed Inastrocytes Surrounds Synapses and Blood Vessels in Brain." *American Journal of Physiology - Renal Physiology* 281 (July): 922–31.

Hirase, Hajime. 2005. "A Multi-Photon Window Onto Neuronal–Glial–Vascular Communication." *Trends in Neurosciences* 28 (5): 217–19.

Hodgkin, A L, and A F Huxley. 1952. "A Quantitative Description of Membrane Current and Its Application to Conduction and Excitation in Nerve." *The Journal of Physiology* 117: 500–544.

Huang, Y, Y Zhou, W Yang, R Butters, H W Lee, S Li, A Castiblanco, E M Brown, and J J Yang. 2007. "Identification and Dissection of Ca2+-Binding Sites in the Extracellular Domain of Ca2+-Sensing Receptor." *Journal of Biological Chemistry* 282 (26): 19000–19010.

Iizuka, M, I Tsunenari, Y Momota, I Akiba, and T Kono. 1997. "Localization of G-Protein-Coupled Inwardly Rectifying K+ Channel, CIR, in the Rat Brain." *Neuroscience* 77 (February): 1–13.

Inanobe, Atsushi, Yukiko Yoshimoto, Yoshiyuki Horio, Ken-Ichiro Morishige, Hiroshi Hibino, Shigeto Matsumoto, Yoshimitsu Tokunaga, et al. 1999. "Characterization of G-Protein-Gated K+ Channels Composed of Kir3.2 Subunits in Dopaminergic Neurons of the Substantia Nigra." *The Journal of Neuroscience : the Official Journal of the Society for Neuroscience* 19 (February): 1006–17.

Inoue, Isao, Nideki Nagase, Kuki Kishi, and Tomihiko Higuti. 1991. "ATP-Sensitive K+ Channel in the Mitochondrial Inner Membrane." *Nature* 352 (July): 1–4.

Ishii, Masaru, Akikazu Fujita, Kaori Iwai, Shunji Kusaka, Kayoko Higashi, Atsushi Inanobe, Hiroshi Hibino, and Yoshihisa Kurachi. 2003. "Differential Expression and Distribution of Kir5.1 and Kir4.1 Inwardly Rectifying K+ Channels in Retina.." *AJP: Cell Physiology* 285 (2). American Physiological Society: C260–67.

Ishii, Takahiro M, Christopher Silvia, Birgit Hirschberg, Chris T Bond, John P Adelman, and James Maylie. 1997. "A Human Intermediate Conductance Calcium-Activated Potassium Channel." *Proceedings of the National Academy of Sciences* 94 (October): 11651–56.

Jalenques, I, E Albuisson, G Despres, and R Romand. 1995. "Distribution of Glial Fibrillary Acidic Protein (GFAP) in the Cochlear Nucleus of Adult and Aged Rats." *Brain Research* 686: 223–32.

Jan, Lily Yeh, and Yuh Nung Yan. 1994. “Potassium Channels and Their Evolving Gates.” *Nature* 371 (September).

Jelacic, T M, M E Kennedy, K Wickman, and D E Clapham. 2000. “Functional and Biochemical Evidence for G-Protein-Gated Inwardly Rectifying K+ (GIRK) Channels Composed of GIRK2 and GIRK3.” *Journal of Biological Chemistry* 275 (46): 36211–16.

Jelacic, T M, S M Sims, and D E Clapham. 1999. “Functional Expression and Chracterization of G-Protein-Gated Inwardly Rectifying K+ Channels Containing GIRK3.” *Journal of Membrane Biology* 169: 123–39.

Jiang, Lin-Hua, Miran Kim, Valeria Spelta, Xuenong Bo, Annmarie Surprenant, and R Alan North. 2003. “Subunit Arrangement in P2X Receptors.” *The Journal of Neuroscience : the Official Journal of the Society for Neuroscience* 23 (October): 8903–10.

Junge, Candice E, C Justin Lee, Katherine B Hubbard, Zhoabin Zhang, Jeffrey J Olson, John R Hepler, Daniel J Brat, and Stephen F Traynelis. 2004. “Protease-Activated Receptor-1 in Human Brain: Localization and Functional Expression in Astrocytes.” *Experimental Neurology* 188 (1): 94–103.

Kaiser, Melanie, Iris Maletzki, Swen Hülsmann, Bettina Holtmann, Walter Schulz-Schaeffer, Frank Kirchhoff, Mathias Bähr, and Clemens Neusch. 2006. “Progressive Loss of a Glial Potassium Channel (KCNJ10) in the Spinal Cord of the SOD1 (G93A) Transgenic Mouse Model of Amyotrophic Lateral Sclerosis.” *Journal of Neurochemistry* 99 (3): 900–912.

Kamphuis, Willem, Jinte Middeldorp, Lieneke Kooijman, Jacqueline A Sluijs, Evert-Jan Kooi, Martina Moeton, Michel Freriks, Mark R Mizee, and Elly M Hol. 2014. “Glial Fibrillary Acidic Protein Isoform Expression in Plaque Related Astrogliosis in Alzheimer's Disease.” *Nba* 35 (3). Elsevier Ltd: 492–510.

Karnani, Mahesh, and Denis Burdakov. 2011. “Multiple Hypothalamic Circuits Sense and Regulate Glucose Levels.” *American Journal of Physiology - Renal Physiology* 300 (January).

Karschin, Christine, Elke Dissmann, Walter Stuhmer, and Andreas Karschin. 1996. “IRK(L-3) and GIRK(L-4) Inwardly Rectifying K+ Channel mRNAs Are Differentially Expressed in the Adult Rat Brain.” *The Journal of Neuroscience : the Official Journal of the Society for Neuroscience* 16 (June): 3559–70.

Kenna, S, J Roper, K Ho, S Hebert, S J Ashcroft, and F M Ashcroft. 1994. “Differential Expression of the Inwardly-Rectifying K-Channel ROMK1 in Rat Brain..” *Molecular Brain Research* 24: 353.

Kettenmann, H, K H Backus, and M Schachner. 1984. “Aspartate, Glutamate and Gamma-Aminobutyric Acid Depolarize Cultured Astrocytes.” *Neuroscience Letters* 52: 25–29.

Kettenmann, Helmut, and Alexei Verkhratsky. 2008. “Neuroglia: the 150 Years After.” *Trends in Neurosciences* 31 (12): 653–59.

Kimelberg, Harold K, and Maiken Nedergaard. 2010. “Functions of Astrocytes and Their Potential as Therapeutic Targets.” *Neurotherapautics the Journal of the*

American Society for Experimental NeuroTherapeutics 7 (October): 338–53.
Kofuji, P, and E A Newman. 2004. "Potassium Buffering in the Central Nervous System." *Neuroscience* 129 (4): 1043–54.
Kofuji, Paulo, Bernd Biedermann, Venkatraman Siddharthan, Maik Raap, Ian Iandiev, Ivan Milenkovic, Achim Thomzig, R diger W Veh, Andreas Bringmann, and Andreas Reichenbach. 2002. "Kir Potassium Channel Subunit Expression in Retinal Glial Cells: Implications for Spatial Potassium Buffering." *Glia* 39 (3): 292–303.
Krapivinsky, Grigory, Igor Medina, Lily Eng, Luba Krapivinsky, Yinhai Yang, and David E Clapham. 1998. "A Novel Inward Rectifier K+ Channel with Unique Pore Properties." *Neuron* 20 (May): 995–1005.
Kreisman, Norman R, Joseph C LaManna, Shih-Chu Liao, Edwin R Yeh, and J Ricardo Alcala. 1995. "Light Transmittance as an Index of Cell Volume in Hippocampal Slices: Optical Differences of Interfaced and Submerged Positions." *Brain Research* 693: 179–86.
Kremsky, Isaac, Todd E Morgan, Xiaogang Hou, Lei Li, and Caleb E Finch. 2012. "Age-Changes in Gene Expression in Primary Mixed Glia Cultures From Young vs. Old Rat Cerebral Cortex Are Modified by Interactions with Neurons." *Brain, Behavior, and Immunity* 26 (5): 797–802.
Krzan, Mojca, Matjaz Stenovec, Marko Kreft, Tina Pangršič, Sonja Grilc, Philip G Haydon, and Robert Zorec. 2003. "Calcium-Dependent Exocytosis of Atrial Natriuretic Peptide From Astrocytes." *The Journal of Neuroscience : the Official Journal of the Society for Neuroscience* 23 (5): 1580–83.
Kubo, Yoshihiro, Timothy J Baldwin, Lily Y Jan, and Yuh Nung Jan. 1993. "Primary Structure and Functional Expression of a Mouse Inward Rectifier Potassium Channel." *Nature* 362 (March): 1–7.
Kucheryavykh, Lilia Y, Yuriy V Kucheryavykh, Mikhail Inyushin, Yaroslav M Shuba, Priscila Sanabria, Luis A Cubano, Serguei N Skatchkov, and Misty J Eaton. 2009. "Ischemia Increases TREK-2 Channel Expression in Astrocytes: Relevance to Glutamate Clearance." *The Open Neuroscience Journal* 3 (1): 40–47.
Kucheryavykh, Y V, L Y Kucheryavykh, C G Nichols, H M Maldonado, K Baksi, A Reichenbach, S N Skatchkov, and M J Eaton. 2006. "Downregulation of Kir4.1 Inward Rectifying Potassium Channel Subunits by RNAi Impairs Potassium Transfer and Glutamate Uptake by Cultured Cortical Astrocytes." *Glia* 55 (3): 274–81.
Kuffler, S W, J G Nicholls, and R K Orkand. 1966. "Physiological Properties of Glial Cells in the Central Nervous System of Amphibia." *Journal of Neurophysiology* 29: 768–87.
Kuo, Min-Ching, and Hans C Dringenberg. 2012. "Comparison of Long-Term Potentiation (LTP) in the Medial (Monocular) and Lateral (Binocular) Rat Primary Visual Cortex." *Brain Research* 1488 (C). Elsevier: 51–59.
Kusaka, Shuji, Atsushi Inanobe, Akikazu Fujita, Yasunaka Makino, Masayuki Tanemoto, Kenji Matsushita, Yasuo Tano, and Yoshihisa Kurachi. 2001.

"Functional Kir7.1 Channels Localized at the Root of Apical Processes in Rat Retinal Pigment Epithelium." *The Journal of Physiology* 531 (February): 27–36.
Lacza, Z. 2003. "Heart Mitochondria Contain Functional ATP-Dependent K+ Channels." *Journal of Molecular and Cellular Cardiology* 35 (11): 1339–47.
Lacza, Zsombor, James A Snipes, Béla Kis, Csaba Szabó, Gary Grover, and David W Busija. 2003. "Investigation of the Subunit Composition and the Pharmacology of the Mitochondrial ATP-Dependent K+ Channel in the Brain." *Brain Research* 994 (1): 27–36.
Lalo, U, Y Pankratov, S P Wichert, M J Rossner, R A North, F Kirchhoff, and A Verkhratsky. 2008. "P2X1 and P2X5 Subunits Form the Functional P2X Receptor in Mouse Cortical Astrocytes." *Journal of Neuroscience* 28 (21): 5473–80.
Lalo, U, Yuri Pankratov, Frank Kirchhoff, R Alan North, and Alexei Verkhratsky. 2006. "NMDA Receptors Mediate Neuron-to-Glia Signaling in Mouse Cortical Astrocytes." *Journal of Neuroscience* 26 (10): 2673–83.
Lalo, Ulyana, Oleg Palygin, Richard Alan North, Alexei Verkhratsky, and Yuriy Pankratov. 2011. "Age-Dependent Remodelling of Ionotropic Signalling in Cortical Astroglia." *Aging Cell* 10 (3): 392–402.
Lalo, Ulyana, Oleg Palygin, Seyed Rasooli-Nejad, Jemma Andrew, Philip G Haydon, and Yuriy Pankratov. 2014. "Exocytosis of ATP From Astrocytes Modulates Phasic and Tonic Inhibition in the Neocortex." Edited by Alberto Bacci. *PLoS Biology* 12 (1): e1001747–21.
Lalo, Ulyana, Yuriy Pankratov, Vladimir Parpura, and Alexei Verkhratsky. 2011. "Ionotropic Receptors in Neuronal–Astroglial Signalling: What Is the Role of 'Excitable' Molecules in Non-Excitable Cells." *Biochimica Et Biophysica Acta (BBA) - Molecular Cell Research* 1813 (5): 992–1002.
Larson, John, and Erin Munkácsy. 2014. "Theta-Burst LTP." *Brain Research*, November. Elsevier, 1–13.
Larson, John, and Erin Munkácsy. 2015. "Theta-Burst LTP." *Brain Research* 1621 (C). Elsevier: 38–50.
Larson, Valerie A, Ye Zhang, and Dwight E Bergles. 2016. "Electrophysiological Properties of NG2+ Cells: Matching Physiological Studies with Gene Expression Profiles." *Brain Research* 1638 (May): 138–60.
Le Prince, Ghislaine, Pia Delaere, Christiane Fages, Charles Duyckaerts, Jean-Jacques Hauw, and Marcienne Tardy. 1993. "Alterations of Glial Fibrillary Acidic Protein mRNA Level in the Aging Brain and in Senile Dementia of the Alzheimer Type." *Neuroscience Letters* 151: 71–73.
Lee, Cheol-Koo, Richard Weindruch, and Tomas A Prolla. 2000. "Gene-Expression Profile of the Ageing Brain in Mice." *Nature Genetics* 25 (July): 1–4.
Lehmann, Claudia, Stefanie Bette, and Jürgen Engele. 2009. "High Extracellular Glutamate Modulates Expression of Glutamate Transporters and Glutamine Synthetase in Cultured Astrocytes." *Brain Research* 1297 (C). Elsevier B.V.: 1–8.
Lesage, Florian, Eric Guillemare, Michel Fink, Fabrice Duprat, Catherine

Heurteaux, Michel Fosset, Georges Romey, Jacques Barhanin, and Michel Lazdunski. 1995. “Molecular Properties of Neuronal G-Protein-Activated Inwardly Rectifying K.” *The Journal of Biological Chemistry* 270 (December): 28660–67.

Lesage, Florian, Roberto Reyes, Michel Fink, Fabrice Duprat, Eric Guillemare, and Michel Lazdunski. 1996. “Dimerization of TWIK-1 K+ Channel Subunits via a Disulfide Bridge.” *The European Molecular Biology Journal* 15: 6400–6407.

Li, Dongdong, Karine Hérault, Kätlin Silm, Alexis Evrard, Sonja Wojcik, Martin Oheim, Etienne Herzog, and Nicole Ropert. 2013. “Lack of Evidence for Vesicular Glutamate Transporter Expression in Mouse Astrocytes..” *The Journal of Neuroscience : the Official Journal of the Society for Neuroscience* 33 (10). Society for Neuroscience: 4434–55.

Li, Dongliang, Bin Huang, Jiangdong Liu, Liang Li, and Xingang Li. 2013. “Decreased Brain KATP Channel Contributes to Exacerbating Ischemic Brain Injury and the Failure of Neuroprotection by Sevoflurane Post-Conditioning in Diabetic Rats.” Edited by Ken Arai. *PLoS ONE* 8 (8). Public Library of Science: e73334–12.

Liévens, J C, B Woodman, A Mahal, O Spasic-Boscovic, D Samuel, L Kerkerian-Le Goff, and G P Bates. 2001. “Impaired Glutamate Uptake in the R6 Huntington's Disease Transgenic Mice.” *Neurobiology of Disease* 8 (5): 807–21.

Liu, Wang Min. 2013. “Potassium Ion Channels in Retinal Ganglion Cells (Review).” *Molecular Medicine Reports*, June, 1–9.

Luebke, J I, and Y M Chang. 2007. “Effects of Aging on the Electrophysiological Properties of Layer 5 Pyramidal Cells in the Monkey Prefrontal Cortex.” *Neuroscience* 150 (3): 556–62.

Luscher, Christian, Lily Y Jan, Markus Stoffel, Robert C Malenka, and Roger A Nicoll. 1997. “G Protein-Coupled Inwardly Rectifying K+ Channels (GIRKs) Mediate Postsynaptic but Not Presynaptic Transmitter Actions in Hippocampal Neurons.” *Neuron* 19 (September): 687–95.

Lynch, Gary, Christopher S Rex, Lulu Y Chen, and Christine M Gall. 2008. “The Substrates of Memory: Defects, Treatments, and Enhancement.” *European Journal of Pharmacology* 585 (1): 2–13.

Ma, D, N Zerangue, Y F Lin, A Colins, M Yu, Y N Jan, and L Y Jan. 2001. “Role of ER Export Signals in Controlling Surface Potassium Channel Numbers.” *Science* 291: 316–19.

Ma, Jingyi, Asfandyar Mufti, and L Stan Leung. 2015. “Effects of Memantine on Hippocampal Long-Term Potentiation, Gamma Activity, and Sensorimotor Gating in Freely Moving Rats.” *Nba* 36 (9). Elsevier Inc: 2544–54.

MacAulay, Nanna, and Thomas Zeuthen. 2012. “Glial K+ Clearance and Cell Swelling: Key Roles for Cotransporters and Pumps.” *Neurochemical Research* 37 (11): 2299–2309.

MacKinnon, Roderick. 2003. “Potassium Channels.” *FEBS Letters* 555 (1): 62–65.

Malenka, Robert C. 1994. “Synaptic Plasticity in the Hippocampus: LTP and LTD.”

Cell 78: 535–38.
Marcus, D C, T Wu, P Wangemann, and P Kofuji. 2002. "KCNJ10 (Kir4.1) Potassium Channel Knockout Abolishes Endocochlear Potential." *AJP: Cell Physiology* 282 (2): C403–7.
Martin, Andrew J, Karl J Friston, James G Colebatch, and Richard S J Frackowiak. 1991. "Decreases in Regional Cerebral Blood Flow with Normal Aging." *Journal of Cerebral Blood Flow & Metabolism* 11: 684–89.
Martin, Jane, and Michelle Gorenstein. 2010. *Chapter 28 - Normal Cognitive Aging*. *Brocklehurst's Textbook of Geriatric Medicine and Gerontology*. Seventh Edition. Elsevier Inc.
Matyash, Vitali, and Helmut Kettenmann. 2010. "Heterogeneity in Astrocyte Morphology and Physiology." *Brain Research Reviews* 63 (1-2). Elsevier B.V.: 2–10.
Meltzer, Carolyn Cidis, Michael N Cantwell, Phil J Creer, Doron Ben-Eliezer, Gwenn Smith, Guido Frank, Walter H Kaye, Patricia R Houck, and Julie C Price. 2000. "Does Cerebral Blood Flow Decline in Healthy Aging? a PET Study with Partial-Volume Correction." *Journal of Nuclear Medicine* 41: 1–8.
Mi, Huaiyu, Thomas J Deerinck, Maggie Jones, Mark H Ellisman, and Thomas L Schwartz. 1996. "Inwardly Rectifying K+ Channels That May Participate in K+ Buffering Are Localized in Microvilli of Schwann Cells." *The Journal of Neuroscience : the Official Journal of the Society for Neuroscience* 16 (April): 2421–29.
Miller, Christopher. 2000. "An Overview of the Potassium Channel Family." *Genome Biology* 1 (October): 1–5.
Minami, Kohtaro, Takashi Miki, Takashi Kadowaki, and Susumu Seino. 2004. "Roles of ATP-Sensitive K+ Channels as Metabolic Sensors." *Diabetes* 53 (December): 1–5.
Molenaar, Remco J. 2011. "Ion Channels in Glioblastoma." *ISRN Neurology* 2011 (21): 1–7.
Mongin, A A. 2004. "ATP Regulates Anion-Channel Mediated Organic Osmolyte Release From Cultured Rat Astrocytes via Multiple Ca2+-Sensitive Mechanisms." *AJP: Cell Physiology*, September.
Montana, V. 2004. "Vesicular Glutamate Transporter-Dependent Glutamate Release From Astrocytes." *Journal of Neuroscience* 24 (11): 2633–42.
Morrison, John H, and Mark G Baxter. 2012. "The Ageing Cortical Synapse: Hallmarks and Implications for Cognitive Decline." *Nature Reviews Neuroscience*, March, 1–27.
Mostany, R, J E Anstey, K L Crump, B Maco, G Knott, and C Portera-Cailliau. 2013. "Altered Synaptic Dynamics During Normal Brain Aging." *Journal of Neuroscience* 33 (9): 4094–4104.
Mothet, Jean-Pierre, Angele T Parent, Herman Wolosker, David J Linden, Jr Roscoe O Brady, Christopher D Ferris, Michael A Rogawski, and Solomon H Snyder. 2000. "D-Serine Is an Endogenous Ligand for the Glycine Site of the N-

Methyl-D-Aspartate Receptor." *Proceedings of the National Academy of Sciences* 97 (9): 4926–31.
Muller, W, and U Misgeld. 1989. "Carbachol Reduces IK, Baclofen, but Not IK, GABA in Guinea Pig Hippocampal Slices." *Neuroscience Letters* 102 (July): 229–34.
Nagele, Robert G, Michael R DAndrea, H Lee, Venkateswar Venkatar, and Hoau-Yan Wang. 2003. "Astrocytes Accumulate Ab42 and Give Rise to Astrocytic Amyloid Plaques in Alzheimer Disease Brains." *Brain Research* 971: 197–209.
Nagelhus, E A, T M Mathiisen, and O P Ottersen. 2004. "Aquaporin-4 in the Central Nervous System: Cellular and Subcellular Distribution and Coexpression with KIR4.1." *Neuroscience* 129 (4): 905–13.
Nakai, Junichi, Masamichi Ohkura, and Keiji Imoto. 2001. "A High Signal-to-Noise Ca2+ Probe Composed of a Single Green Fluorescent Protein." *Nature Biotechnology* 19 (February): 1–5.
Nakamura, Nobuhiro, Yoshiro Suzuki, Hidenari Sakuta, Kayoko Ookata, Katsumasa Kawahara, and Shigehisa Hirose. 1999. "Inwardly Rectifying K+ Channel Kir7.1 Is Highly Expressed in Thyroid Follicular Cells, Intestinal Epithelial Cells and Choroid Plexus Epithelial Cells: Implication for a Functional Coupling with Na+,K+-ATPase." *Biochemical Journal* 342: 329–36.
Nedergaard, Maiken, and Alexei Verkhratsky. 2012. "Artifact Versus Reality-How Astrocytes Contribute to Synaptic Events." *Glia* 60 (7): 1013–23.
Neusch, C. 2006. "Lack of the Kir4.1 Channel Subunit Abolishes K+ Buffering Properties of Astrocytes in the Ventral Respiratory Group: Impact on Extracellular K+ Regulation." *Journal of Neurophysiology* 95 (3): 1843–52.
Neusch, Clemens, Nora Rozengurt, Russell E Jacobs, Henry A Lester, and Paulo Kofuji. 2001. "Kir4.1 Potassium Channel Subunit Is Crucial for Oligodendrocyte Development and *In Vivo* Myelination." *The Journal of Neuroscience : the Official Journal of the Society for Neuroscience* 21 (August): 5429–38.
Nichols, N R, J R Day, N J Laping, S A Johnson, and C E Finch. 1993. "GFAP mRNA Increases with Age in Rat and Human Brain." *Neurobiology of Aging* 14: 421–29.
Nishiyama, Akiko, Zhongshu Yang, and Arthur Butt. 2005. "Astrocytes and NG2-Glia: What's in a Name?." *Journal of Anatomy* 207 (6): 687–93.
Nolte, Christiane, Marina Matyash, Tatyana Pivneva, Carola G Schipke, Carsten Ohlemeyer, Uwe-Karsten Hanisch, Frank Kirchhoff, and Helmut Kettenmann. 2001. "GFAP Promoter-Controlled EGFP- Expressing Transgenic Mice: a Tool to Visualize Astrocytes and Astrogliosis in Living Brain Tissue." *Glia*, no. 33: 72–86.
Norenberg, M D, and A Martinez-Hernandez. 1979. "Fine Structural Localization of Glutamine Synthetase in Astrocytes of Rat Brain. ." *Brain Research* 161 (2): 303–10.
North, R Alan. 2002. "Molecular Physiology of P2X Receptors.." *Physiological*

Reviews 82 (4). American Physiological Society: 1013–67.
Oberheim, Nancy Ann, Steven A Goldman, and Maiken Nedergaard. 2011. "Heterogeneity of Astrocytic Form and Function." In *Astrocytes*, 814:23–45. Methods in Molecular Biology. Totowa, NJ: Humana Press.
Ogawa, S, T M Lee, A R Kay, and D W Tank. 1990. "Brain Magnetic Resonance Imaging with Contrast Dependent." *Proceedings of the National Academy of Sciences* 87 (December): 9868–72.
Okami, Toyokazu, Akitsugu Yamamoto, Koichiro Omori, Tatsuyoshi Takada, Masanobu Uyama, and Yutaka Tashiro. 1990. "Immunocytochemical Localization of Na+, K+-ATPase in Rat Retinal Pigment Epithelial Cells." *The Journal of Histochemistry and Cytochemistry* 38: 1267–75.
Olsen, M L, S L Campbell, and H Sontheimer. 2007. "Differential Distribution of Kir4.1 in Spinal Cord Astrocytes Suggests Regional Differences in K+ Homeostasis." *Journal of Neurophysiology* 98 (2): 786–93.
Palygin, Oleg, Ulyana Lalo, Alexei Verkhratsky, and Yuriy Pankratov. 2010. "Ionotropic NMDA and P2X1/5 Receptors Mediate Synaptically Induced Ca2+ Signalling in Cortical Astrocytes." *Cell Calcium* 48 (4): 225–31.
Pankratov, Y, U Lalo, A Verkhratsky, and R A North. 2007. "Quantal Release of ATP in Mouse Cortex." *The Journal of General Physiology* 129 (3): 257–65.
Pankratov, Y, U Lalo, O A Krishtal, and A Verkhratsky. 2009. "P2X Receptors and Synaptic Plasticity." *Neuroscience* 158 (1): 137–48.
Pannasch, Ulrike, Lýdia Vargová, Jurgen Reingruber, Pascal Ezan, David Holcman, Eva Syková, and Nathalie Rouach. 2011. "Astroglial Networks Scale Synaptic Activity and Plasticity." *Proceedings of the National Academy of Sciences* 108 (May): 8467–72.
Pannicke, Thomas, Frank Faude, Andreas Reickenbach, and Winfried Reichelt. 2000. "A Function of Delayed Rectifier Potassium Channels in Glial Cells: Maintenance of an Auxiliary Membrane Potential Under Pathological Conditions." *Brain Research* 826 (April): 187–93.
Parpura, Vladimir, and Alexei Verkhratsky. 2012. "The Astrocyte Excitability Brief: From Receptors to Gliotransmission." *Neurochemistry International* 61 (4). Elsevier Ltd: 610–21.
Parpura, Vladimir, and Robert Zorec. 2010. "Gliotransmission: Exocytotic Release From Astrocytes." *Brain Research Reviews* 63 (1-2). Elsevier B.V.: 83–92.
Parpura, Vladimir, Trent A Basarsky, Fang Liu, Ksenija Jeftinija, Srdija Jeftinija, and Phillip G Haydon. 1994. "Glutamate-Mediated Astrocyte-Neuron Signalling." *Nature* 369: 1–4.
Partiseti, Michel, Vincent Collura, Magali Agnel, Jean-Michel Culouscou, and David Graham. 1998. "Cloning and Characterization of a Novel Human Inwardly Rectifying Potassium Channel Predominantly Expressed in Small Intestine." *FEBS Letters* 434: 171–76.
Pathak, Dhruba, Dongxu Guan, and Robert C Foehring. 2016. "Roles of Specific Kv Channel Types in Repolarization of the Action Potential in Genetically

Identified Subclasses of Pyramidal Neurons in Mouse Neocortex." *Journal of Neurophysiology* 115 (May): 2317–29.
Pearson, Wade L, Michelle Dourado, Matthew Schreiber, Lawrence Salkoff, and Colin G Nichols. 1999. "Expression of a Functional Kir4 Family Inward Rectifier K¤ Channel From a Gene Cloned From Mouse Liver." *The Journal of Physiology* 514: 639–53.
Pearson, Wade L, Michelle Dourado, Matthew Schreiber, Lawrence Salkoff, and Colin G Nichols. 2004. "Expression of a Functional Kir4 Family Inward Rectifier K +Channel From a Gene Cloned From Mouse Liver." *The Journal of Physiology* 514 (3): 639–53.
Pekny, M, and M Pekna. 2014. "Astrocyte Reactivity and Reactive Astrogliosis: Costs and Benefits." *Physiological Reviews* 94 (4): 1077–98.
Pekny, Milos, and Michael Nilsson. 2005. "Astrocyte Activation and Reactive Gliosis." *Glia* 50 (4): 427–34.
Pelvig, D P, H Pakkenberg, A K Stark, and B Pakkenberg. 2008. "Neocortical Glial Cell Numbers in Human Brains." *Neurobiology of Aging* 29 (11): 1754–62.
Perea, Gertrudis, and Alfonso Araque. 2010. "GLIA Modulates Synaptic Transmission." *Brain Research Reviews* 63 (1-2): 93–102.
Pessia, Mauro, Paola Imbrici, Maria Cristina D'Adamo, Lorena Salvatore, and Stephen J Tucker. 2001. "Differential pH Sensitivity of Kir4.1 and Kir4.2 Potassium Channels and Their Modulation by Heteropolymerisation with Kir5.1." *The Journal of Physiology* 532 (2): 359–67.
Petralia, Ronald S, Mark P Mattson, and Pamela J Yao. 2014. "Communication Breakdown: the Impact of Ageing on Synapse Structure." *Ageing Research Reviews* 14 (March). Elsevier B.V.: 31–42.
Petryszak, Robert, Maria Keays, Y Amy Tang, Nuno A Fonseca, Elisabet Barrera, Tony Burdett, Anja Füllgrabe, et al. 2016. "Expression Atlas Update—an Integrated Database of Gene and Protein Expression in Humans, Animals and Plants." *Nucleic Acids Research* 44 (D1): D746–52.
Philip, Shaji, and William M Armstead. 2004. "NMDA Dilates Pial Arteries by KATP and Kca Channel Activation." *Brain Research Bulletin* 63 (2): 127–31.
Preisig-Muller, Regina, Gunter Schlichthorl, Tobias Goerge, Steffen Heinen, Andrea Bruggemann, Sindhu Rajan, Christian Derst, Rudiger W Yeh, and Jurgen Daut. 2002. "Heteromerization of Kir2.X Potassium Channels Contributes to the Phenotype of Andersen's Syndrome." *Proceedings of the National Academy of Sciences of the United States of America* 99 (May).
Price, Diana L, Jeffrey W Ludwig, Huaiyu Mi, Thomas L Schwarz, and Mark H Ellisman. 2002. "Distribution of rSlo Ca2+-Activated K+ Channels in Rat Astrocyte Perivascular Endfeet." *Brain Research* 956 (November): 183–93.
Prüss, Harald, Christian Derst, Reinhard Lommel, and Rüdiger W Veh. 2005. "Differential Distribution of Individual Subunits of Strongly Inwardly Rectifying Potassium Channels (Kir2 Family) in Rat Brain." *Molecular Brain Research* 139 (1): 63–79.

Puthanveettil, Sathyanarayanan V. 2014. “Dissecting Mechanisms of Brain Aging by Studying the Intrinsic Excitability of Neurons,” December, 1–9.

Ransom, Christopher B, Xiaojin Liu, and Harald Sontheimer. 2002. “BK Channels in Human Glioma Cells Have Enhanced Calcium Sensitivity.” *Glia* 38 (4): 281–91.

Rasooli-Nejad, S, O Palygin, U Lalo, and Y Pankratov. 2014. “Cannabinoid Receptors Contribute to Astroglial Ca2+-Signalling and Control of Synaptic Plasticity in the Neocortex.” *Philosophical Transactions of the Royal Society B: Biological Sciences* 369 (1654): 20140077–77.

Richardson, William D, Kaylene M Young, Richa B Tripathi, and Ian McKenzie. 2011. “NG2-Glia as Multipotent Neural Stem Cells: Fact or Fantasy?.” *Neuron* 70 (4): 661–73.

Rivera-Aponte, D E, M P Méndez-González, A F Rivera-Pagán, Y V Kucheryavykh, L Y Kucheryavykh, S N Skatchkov, and M J Eaton. 2015. “Hyperglycemia Reduces Functional Expression of Astrocytic Kir4.1 Channels and Glial Glutamate Uptake.” *Neuroscience* 310 (December): 216–23.

Rose, Christine R, and Frank Kirchhoff. 2015. “Glial Heterogeneity: the Increasing Complexity of the Brain.” *E-Neuroforum* 6 (3): 59–62.

Rossi, Daniela. 2015. “Astrocyte Physiopathology: at the Crossroads of Intercellular Networking, Inflammation and Cell Death.” *Progress in Neurobiology*, May. Elsevier Ltd, 1–35. doi:10.1016/j.pneurobio.2015.04.003.

Rouach, Nathalie. 2013. “How Do Astrocytes Shape Synaptic Transmission? Insights From Electrophysiology,” September, 1–19.

Rusakov, Dmitri A. 2015. “Disentangling Calcium-Driven Astrocyte Physiology.” *Nature Publishing Group* 16 (4). Nature Publishing Group: 226–33.

Rusakov, Dmitri A, Lucie Bard, Michael G Stewart, and Christian Henneberger. 2014. “Diversity of Astroglial Functions Alludes to Subcellular Specialisation.” *Trends in Neurosciences* 37 (4). Elsevier Ltd: 228–42.

Salminen, Antero, Johanna Ojala, Kai Kaarniranta, Annakaisa Haapasalo, Mikko Hiltunen, and Hilkka Soininen. 2011. “Astrocytes in the Aging Brain Express Characteristics of Senescence-Associated Secretory Phenotype.” *European Journal of Neuroscience* 34 (1): 3–11.

Schafer, J A, and S L Troutman. 1987. “Potassium Transport in Cortical Collecting Tubules From Mineralocorticoid-Treated Rat.” *American Journal of Physiology - Renal Physiology* 253 (July).

Scheibel, Madge E, Robert D Lindsay, Uwamie Tomiyasu, and Arnold B Scheibel. 1975. “Progressive Dendritic Changes in Aging Human Cortex.” *Experimental Neurology* 47: 392–403.

Schewe, Marcus, Ehsan Nematian-Ardestani, Han Sun, Marianne Musinszki, Sönke Cordeiro, Giovanna Bucci, Bert L de Groot, Stephen J Tucker, Markus Rapedius, and Thomas Baukrowitz. 2016. “A Non-Canonical Voltage-Sensing Mechanism Controls Gating in K2P K+ Channels.” *Cell* 164 (5). Elsevier: 937–49.

Schielke, Gerald P, Hylan C Moises, and A Lorris Betz. 1990. “Potassium Activation of the Na,K-Pump in Isolated Brain Microvessels and Synaptosomes.” *Brain Research* 524: 291–96.

Schilling, Tom, and Claudia Eder. 2014. “Microglial K +Channel Expression in Young Adult and Aged Mice.” *Glia* 63 (4): 664–72.

Schipke, C G, C Ohlemeyer, M Matyash, C Nolte, H Kettenmann, and F Kirchhoff. 2001. “Astrocytes of the Mouse Neocortex Express Functional N-Methyl-D-Aspartate Receptors.” *Federation for American Society of Experimental Biology* 15: 1270–72.

Schipper, Hyman M, ed. 1998. ***Neuroscience Intelligence Unit*** . R.G. LANDES COMPANY.

Schram, Gernot, Peter Melnyk, Marc Pourrier, Zhiguo Wang, and Stanley Nattel. 2004. “Kir2.4 and Kir2.1 K +Channel Subunits Co-Assemble: a Potential New Contributor to Inward Rectifier Current Heterogeneity.” *The Journal of Physiology* 544 (2). Blackwell Publishing Ltd: 337–49.

Scott, H A, F M Gebhardt, A D Mitrovic, R J Vandenberg, and P R Dodd. 2011. “Glutamate Transporter Variants Reduce Glutamate Uptake in Alzheimer's Disease.” *Nba* 32 (3). Elsevier Inc.: 553.e1–553.e11.

Seifert, Gerald, Kerstin Hüttmann, Devin K Binder, Christian Hartmann, Alexandra Wyczynski, Clemens Neusch, and Christian Steinhäuser. 2009. “Analysis of Astroglial K+ Channel Expression in the Developing Hippocampus Reveals a Predominant Role of the Kir4.1 Subunit..” *The Journal of Neuroscience : the Official Journal of the Society for Neuroscience* 29 (23). Society for Neuroscience: 7474–88.

Sesti, Federico, Shuang Liu, and Shi-Qing Cai. 2010. “Oxidation of Potassium Channels by ROS: a General Mechanism of Aging and Neurodegeneration?.” *Trends in Cell Biology* 20 (1): 45–51.

Shahidullah, Mohammad, Naoto Hoshi, Shigeru Yokoyama, Tetsuro Kawamura, and Haruhiro Higashida. 1995. “Slow Inactivation Conserved in Heteromultimeric Voltage-Dependent K+ Channels Between *Shaker* (Kv1) and *Shaw* (Kv3) Subfamilies.” *FEBS Letters* 371: 307–10.

Shimada, A, M Tsuzuki, H Keino, M Satoh, Y Chiba, Y Saitoh, and M Hosokawa. 2006. “Apical Vulnerability to Dendritic Retraction in Prefrontal Neurones of Ageing SAMP10 Mouse: a Model of Cerebral Degeneration.” *Neuropathology and Applied Neurobiology* 32 (1): 1–14.

Sibille, Jeremie, Jonathan Zapata, Jeremie Teillon, and Nathalie Rouach. 2015. “Astroglial Calcium Signaling Displays Short-Term Plasticity and Adjusts Synaptic Efficacy.” *Frontiers in Cellular Neuroscience* 9 (May): 1250–10.

Signorini, Stefano, Y Joyce Liao, Stephen A Duncan, Lilya Y Jan, and Markus Stofel. 1997. “Normal Cerebellar Development but Susceptibility to Seizures in Mice Lacking G Protein-Coupled, Inwardly Rectifying K+ Channel GIRK2.” *Proceedings of the National Academy of Sciences* 94 (February): 923–27.

Silver, Margery H, Kathy Newell, Christopher Brady, Tessa Hedley-White, and

Thomas T Perls. 2002. “Distinguishing Between Neurodegenerative Disease and Disease-Free Aging: Correlating Neuropsychological Evaluations and Neuropathological Studies in Centenarians.” *Psychosomatic Medicine* 64 (May): 493–501.

Simons, Cas, Lachlan D Rash, Joanna Crawford, Linlin Ma, Ben Cristofori-Armstrong, David Miller, Kelin Ru, et al. 2014. “Mutations in the Voltage-Gated Potassium Channel Gene KCNH1 Cause Temple-Baraitser Syndrome and Epilepsy.” *Nature Genetics* 47 (1): 73–77.

Sloane, Jacob A, William Hollander, Douglas L Rosene, Mark B Moss, Thomas Kemper, and Carmela R Abraham. 2000. “Astrocytic Hypertrophy and Altered GFAP Degradation with Age Insubcortical White Matter of the Rhesus Monkey.” *Brain Research* 862: 1–10.

Smart, S L, M M Bosma, and B L Tempel. 1997. “Identification of the Delayed Rectifier Potassium Channel, Kv1.6, in Cultured Astrocytes.” *Glia* 20 (June): 127–34.

Smith, Dean O, Julie L Rosenheimer, and Ronald E Kalil. 2008. “Delayed Rectifier and a-Type Potassium Channels Associated with Kv 2.1 and Kv 4.3 Expression in Embryonic Rat Neural Progenitor Cells.” Edited by Brian McCabe. *PLoS ONE* 3 (2): e1604–9.

Sofroniew, Michael V, and Harry V Vinters. 2009. “Astrocytes: Biology and Pathology.” *Acta Neuropathologica* 119 (1): 7–35.

Song, Yutong, and Eli Gunnarson. 2012. “Potassium Dependent Regulation of Astrocyte Water Permeability Is Mediated by cAMP Signaling.” Edited by Steven Barnes. *PLoS ONE* 7 (4): e34936.

Söllvander, Sofia, Elisabeth Nikitidou, Robin Brolin, Linda Söderberg, Dag Sehlin, Lars Lannfelt, and Anna Erlandsson. 2016. “Accumulation of Amyloid-B by Astrocytes Result in Enlarged Endosomes and Microvesicle-Induced Apoptosis of Neurons.” *Molecular Neurodegeneration*, May. Molecular Neurodegeneration, 1–19.

Staff, Roger T, Alison D Murray, Ian J Deary, and Lawrence J Whalley. 2006. “Generality and Specificity in Cognitive Aging: a Volumetric Brain Analysis.” *NeuroImage* 30 (4): 1433–40.

Steinhäuser, Christian, and Vittorio Gallo. 1996. “News on Glutamate Receptors in Glial Cells.” *Glia* 19: 339–45.

Stephens, Michelle L, Jorge E Quintero, Francois Pomerleau, Peter Huettl, and Greg A Gerhardt. 2011. “Age-Related Changes in Glutamate Release in the CA3 and Dentate Gyrus of the Rat Hippocampus.” *Neurobiology of Aging* 32 (5): 811–20.

stroke.org.uk. 2016. *State of the Nation*.

Stroman, P W, A S Lee, K K Pitchers, and R D Andrew. 2008. “Magnetic Resonance Imaging of Neuronal and Glial Swelling as an Indicator of Function in Cerebral Tissue Slices.” *Magnetic Resonance in Medicine* 59 (4): 700–706.

Sun, H S, Z P Feng, P A Barber, A M Buchan, and R J French. 2007. “Kir6.2-

Containing ATP-Sensitive Potassium Channels Protect Cortical Neurons From Ischemic/Anoxic Injury in Vitro and in Vivo." *Neuroscience* 144 (4): 1509–15.
Surprenant, Annmarie, and R Alan North. 2009. "Signaling at Purinergic P2X Receptors." *Annual Review of Physiology* 71 (1): 333–59.
Syková, Eva, and Alexandr Chvátal. 2000. "Glial Cells and Volume Transmission in the CNS." *Neurochemistry International* 36: 397–409.
Takahashi, Tomoyuki. 1990. "Inward Rectification in Neonatal Rat Spinal Motorneurones." *The Journal of Physiology* 423: 47–62.
Takumi, Toru, Takahiro Ishii, Yoshiyuki Horio, Ken-Ichirou Morishige, Naohiko Takahashi, Mitsuhiko Yamada, Takeshi Yamashita, et al. 1995. "A Novel ATP-Dependent Inward Rectifier Potassium Channel Predominantly Expressed by Glial Cells." *The Journal of Biological Chemistry* 270 (July): 16339–46.
Talantova, Maria, Sara Sanz-Blasco, Xiaofei Zhang, Peng Xia, Mohd Waseem Akhtar, Shu-ichi Okamoto, Gustavo Dziewczapolski, et al. 2013. "Aβ Induces Astrocytic Glutamate Release, Extrasynaptic NMDA Receptor Activation, and Synaptic Loss." *Proceedings of the National Academy of Sciences of the United States of America* 110 (27). National Academy of Sciences: E2518–10.
Taylor, Edward Wyllys. 1895. "A Contribution to the Study of Human Neuroglia." *The Journal of Experimental Medicine* II: 1–28.
Thompson, Scott M, and Beat H Gahwiller. 1992. "Comparison of the Actions of Baclofen at Pre- and Postsynaptic Receptors in the Rat Hippocampus in Vitro." *The Journal of Physiology* 451: 329–45.
Tinker, Andrew, Yuh Nung Jan, and Lily Yeh Jan. 1996. "Regions Responsible for the Assembly of Inwardly Rectifying Potassium Channels." *Cell* 87 (November): 857–66.
Tokimasa, Takayuki, and Toshihiko Nishimura. 2013. "Actions of Barium on Rapidly Inactivating Potassium Current in Bullfrog Sympathetic Neurons." *Neuroscience Letters*, April, 1–4.
Topert, Christoph, Frank Doring, Erhard Wischmeyer, Christine Karschin, Johannes Brockhaus, Klaus Ballanyi, Christian Derst, and Andreas Karschin. 1998. "Kir2.4: a Novel K+ Inward Rectifier Channel Associated with Motorneurons of Cranial Nerve Nuclei." *The Journal of Neuroscience : the Official Journal of the Society for Neuroscience* 18 (June): 4096–4105.
Traynelis, S F, and J Trejo. 2007. "Protease-Activated Receptor Signalling: New Roles and Regulatory Mechanisms." *Current Opinion in Hematology* 14.
Trimmer, James S. 2015. "Subcellular Localization of K+ Channels in Mammalian Brain Neurons: Remarkable Precision in the Midst of Extraordinary Complexity." *Neuron* 85 (2). Elsevier Inc.: 238–56.
Tse, Frederick W, Douglas D Fraser, Steven Duffy, and Brian A. MacVicar. 1992. "Voltage-Activated K+ Currents in Acutely Isolated Hippocampal Astrocytes." *Journal of Neuroscience* 12 (5): 1781–88.
Turner, Kathryn L, Avinash Honasoge, Stephanie M Robert, Michael M McFerrin, and Harald Sontheimer. 2014. "A Proinvasive Role for the Ca 2+-Activated K

+Channel KCa3.1 in Malignant Glioma." *Glia* 62 (6): 971–81.
United Nations. 2015. *Demographic Yearbook 2014*.
Vacher, H, D P Mohapatra, and J S Trimmer. 2008. "Localization and Targeting of Voltage-Dependent Ion Channels in Mammalian Central Neurons." *Physiological Reviews* 88 (4): 1407–47.
Vandenberg, Robert J, and Renae M Ryan. 2013. "Mechanisms of Glutamate Transport.." *Physiological Reviews* 93 (4). American Physiological Society: 1621–57.
VanGuilder, Heather D, Han Yan, Julie A Farley, William E Sonntag, and Willard M Freeman. 2010. "Aging Alters the Expression of Neurotransmission-Regulating Proteins in the Hippocampal Synaptoproteome." *Journal of Neurochemistry* 113 (6).
Ventura, Rachel, and Kristen M Harris. 1999. "Three-Dimensional Relationships Between Hippocampal Synapses and Astrocytes." *The Journal of Neuroscience : the Official Journal of the Society for Neuroscience* 19 (August): 6897–6906.
Verkhrasky, Alexei, Oleg A Krishtal, and Geoffrey Burnstock. 2009. "Purinoceptors on Neuroglia." *Molecular Neurobiology* 39 (3): 190–208.
Verkhratsky, A, and E C Toescu. 2008. "Neuronal-Glial Networks as Substrate for CNS Integration." *Journal of Cellular and Molecular Medicine* 10 (4): 869–79.
Verkhratsky, Alexei, and Christian Steinhäuser. 2000. "Ion Channels in Glial Cells." *Brain Research Reviews* 32 (March): 380–412.
Verkhratsky, Alexei, O A Krishtal, and Ole H Petersen. 2006. "From Galvani to Patch Clamp: the Development of Electrophysiology." *Pflügers Archiv - European Journal of Physiology* 453 (3): 233–47.
Verkhratsky, Alexei, Yuri Pankratov, Ulyana Lalo, and Maiken Nedergaard. 2012. "P2X Receptors in Neuroglia." *Wiley Interdisciplinary Reviews: Membrane Transport and Signaling* 1 (2): 151–61.
Vit, J P, P T Ohara, A Bhargava, K Kelley, and L Jasmin. 2008. "Silencing the Kir4.1 Potassium Channel Subunit in Satellite Glial Cells of the Rat Trigeminal Ganglion Results in Pain-Like Behavior in the Absence of Nerve Injury." *Journal of Neuroscience* 28 (16): 4161–71.
Vivier, Delphine, Khalil Bennis, Florian Lesage, and Sylvie Ducki. 2016. "Perspectives on the Two-Pore Domain Potassium Channel TREK-1 (TWIK-Related K +Channel 1). a Novel Therapeutic Target?." *Journal of Medicinal Chemistry* 59 (11): 5149–57
Volterra, Andrea, and Jacopo Meldolesi. 2005. "Astrocytes, From Brain Glue to Communication Elements: the Revolution Continues." *Nature Reviews Neuroscience* 6 (8): 626–40.
Volterra, Andrea, Nicolas Liaudet, and Iaroslav Savtchouk. 2014. "Astrocyte Ca2+ Signalling: an Unexpected Complexity." *Nature Publishing Group* 15 (5). Nature Publishing Group: 327–35.
Vorobjev, Vladimir. 1991. "Vibrodissociation of Sliced Mammalian Nervous Tissue." *Journal of Neuroscience Methods* 38: 145–50.

Wallraff, Anke, Benjamin Odermatt, Klaus Willecke, and Christian Steinhäuser. 2004. “Distinct Types of Astroglial Cells in the Hippocampus Differ in Gap Junction Coupling.” *Glia* 48 (1): 36–43.

Walls, Anne B, Helle S Waagepetersen, Lasse K Bak, Arne Schousboe, and Ursula Sonnewald. 2014. “The Glutamine–Glutamate/GABA Cycle: Function, Regional Differences in Glutamate and GABA Production and Effects of Interference with GABA Metabolism.” *Neurochemical Research* 40 (2): 402–9.

Walz, Wolfgang. 2000. “Role of Astrocytes in the Clearance of Excess Extracellular Potassium.” *Neurochemistry International* 36 (4-5): 291–300.

Wang, Hao, Dennis D Kunkel, Troy M Martin, Philip A Schwartzkroin, and Bruce L Tempel. 1993. “Heteromultimeric K+ Channels in Terminal and Juxtaparanodal Regions of Neurons.” *Nature* 365 (September): 1–5.

Wang, R, X Liu, S T Hentges, A A Dunn-Meynell, B E Levin, W Wang, and V H Routh. 2004. “The Regulation of Glucose-Excited Neurons in the Hypothalamic Arcuate Nucleus by Glucose and Feeding-Relevant Peptides.” *Diabetes* 53: 1–7.

Wickman, Kevin, Christine Karschin, Andreas Karschin, Marina R Picciotto, and David E Clapham. 2000. “Brain Localization and Behavioral Impact of the G-Protein-Gated K+ Channel Subunit GIRK4.” *The Journal of Neuroscience : the Official Journal of the Society for Neuroscience* 20 (August): 5608–15.

Wilson, G F, and S Y Chiu. 1990. “Potassium Channel Regulation in Schwann Cells During Early Developmental Myelinogenesis.” *The Journal of Neuroscience : the Official Journal of the Society for Neuroscience* 10 (May): 1615–25.

Xue, Zhanxia, Baoman Li, Li Gu, Xiaoling Hu, Min Li, Roger F Butterworth, and Liang Peng. 2010. “Increased Na, K-ATPase Î±2 Isoform Gene Expression by Ammonia in Astrocytes and in Brain in Vivo.” *Neurochemistry International* 57 (4). Elsevier Ltd: 395–403.

Yang, Zhenjiang, Haoxing Xu, Ningren Cui, Zhiqiang Qu, Sengthong Chanchevalap, Wangzhen Shen, and Chun Jiang. 2000. “Biophysical and Molecular Mechanisms Underlying the Modulation of Heteromeric Kir4.1–Kir5.1 Channels by CO2 and pH.” *The Journal of General Physiology* 116 (July): 1–13.

Yellen, Gary. 2002. “The Voltage-Gated Potassium Channels and Their Relatives.” *Nature Review* 419 (September): 1–8.

Zheng, Kaiyu, Lucie Bard, James P Reynolds, Claire King, Thomas P Jensen, Alexander V Gourine, and Dmitri A Rusakov. 2015. “Time-Resolved Imaging Reveals Heterogeneous Landscapes of Nanomolar Ca2+ in Neurons and Astroglia.” *Neuron* 88 (2). The Authors: 277–88.

Zhou, M, G Xu, M Xie, X Zhang, G P Schools, L Ma, H K Kimelberg, and H Chen. 2009. “TWIK-1 and TREK-1 Are Potassium Channels Contributing Significantly to Astrocyte Passive Conductance in Rat Hippocampal Slices.” *Journal of Neuroscience* 29 (26): 8551–64.

1989. *Code of Practice*.